A Dissertation

entitled

**Electrocatalytic Enzyme Sensors for Selective and Sensitive Detection of Biologically Important Molecules**

by

Jhindan Mukherjee

Submitted as partial fulfillment of the requirements for the

Doctor of Philosophy degree in Chemistry

_____

Advisor: Dr. Jon R. Kirchhoff

_____

Graduate School

The University of Toledo

December 2008

An Abstract of

Electrocatalytic Enzyme Sensors for Selective and Sensitive Detection of Biologically Important Molecules

Jhindan Mukherjee

Submitted as partial fulfillment of the requirements for the

Doctor of Philisophy degree in Chemistry

The University of Toledo

December 2008

Cholinergic neurons play a vital role in cognition and memory. Changes in the cholinergic system are associated with severe neurodegenerative disorders such as Alzheimer's disease (AD) and dementia. Hence, it is important to develop analytical strategies that can elucidate mechanisms of such selective cholinergic degradation and also be able to monitor the subtle changes that occur. Biomolecules that can selectively interact with disease specific biomarkers have potential applications in the development of biosensors. These biocatalysts, when integrated with conductive supports produce transducing signals leading to selective detection of the biomarkers. A key to such effective bioelectronic transduction is integration of various biointerfaces and their efficient electronic communication with the underlying conducting support.

The primary focus of the work has been the separation and quantification of cholinergic metabolites using capillary electrophoresis (CE) coupled with electrochemical detection (EC). CE allowed efficient separation of nL sample volumes while enzyme modified microelectrodes (MEs) enabled selective amperometric detection of choline (Ch) and acetylcholine (ACh). This method was used to study the rate of Ch uptake by the High Affinity Choline Uptake transporter protein (CHT) in mouse synaptosomes. The Michaelis-Menten constant of CHT was determined to be 0.79 μM. Further, a cholinomimetic bis-catechol hexamethonium analogue (DTH) was examined for its ability to selectively inhibit Ch uptake by CHT. The $IC_{50}$ value of DTH was determined to be 76 μM. $K_I$ of this inhibitor determined by Dixon plots was calculated as 73 μM. DTH inhibited CHT via a mixed inhibition mode. The results obtained were in logical conclusion with established studies regarding structural aspects and affinity of CHT.

Furthermore, ME techniques were employed to develop two amperometric enzyme microsensor systems as detectors for CE for monitoring low micromolar concentrations of Ch and ACh. The first system was comprised of a trienzyme Au ME incorporating the enzymes acetylcholinesterase (AChE), choline oxidase (ChO) and horseradish peroxidase bound with a redox hydrogel polymer (HRP). Methods for enzyme immobilization onto the ME surface were studied and optimized. Efficient separation and selective amperometric detection of Ch and ACh were achieved at a low detection potential of +0.10 V vs Ag/AgCl. The high selectivity of the enzyme modified ME coupled with extraordinary sensitivity offered by CE enabled low mass detection limits of 38 amol for Ch and ACh. The method exhibited an excellent linear response from 2 – 2000 μM for both Ch and ACh.

An alternative approach involved integration of Prussian Blue (PB), an artificial peroxidase with AChE and ChO on Pt MEs for detection of Ch and ACh. Thermal and electrochemical deposition methods for PB were developed and optimized. PB incorporated enzyme MEs allowed detection of Ch and ACh at a low potential of -0.10 V vs Ag/AgCl. In spite of remarkably different stability conditions of the inorganic catalyst and biomacromolecules, synergistic effects between these systems were achieved to obtain excellent linearity from 10 – 2000 μM for Ch and ACh and operational stability of more than 60 electrophoretic runs.

The power of biomolecular catalysts was further exploited through development of a pyrroloquinoline quinone (PQQ) based glassy carbon (GC) amperometric sensor for real time detection of thiocholine (SCh). PQQ was efficiently incorporated within a conducting polypyrrole matrix that prevented its leaching from the electrode surface. PQQ effectively catalysed the oxidation of SCh and well defined current peaks with fast response times ranging from 11 to 27 s were obtained for various concentrations of hydrolyzed acetylthiocholine (ASCh). The versatility of the assay allowed real time detection of SCh, by addition of AChE into an electrolyte solution containing ASCh. In addition to real time monitoring of ASCh hydrolysis, the inhibition of this hydrolysis process was also observed by addition of carbofuran, an inhibitor of AChE. The extent of inhibition of AChE was sensitive to the amount of carbofuran allowing sensitive detection of potential neurotoxins. The versatility of this sensor seemed promising for further development of various bioassays.

## ACKNOWLEDGEMENTS

I would like to thank my research advisor, Dr. Jon R. Kirchhoff for his tremendous support, advice and graduate education throughout the years. I am grateful to him for allowing me to work in the laboratory with freedom which has enabled me to think independently and develop as a scientist. He has always been there like a true mentor and has guided me in every step of this arduous path. Without his guidance it would be impossible for me to conceive where I stand today.

I would also like to thank my committee members Dr. Katherine A. Wall, Dr. Richard A. Hudson and Dr. Timothy C. Mueser for their time and valuable suggestions. Their scientific input has made my research work more cohesive. Additionally I would like to thank Dr. L. M. V. Tillekeratne for his ardent help.

I would like to extend my sincere gratitude to Charlene Hansen and Pam Samples at the Chemistry Department office, Tom Kina and Yao Ming in the electronics shop and Steve at the glass shop.

I gratefully acknowledge the support of my current and previous lab members, Kristi, Maria, Claire, Jessie, Tatyana, Shontell, Isabel and Claudine who all have made my time of working in the lab more fun.

I am grateful the Department of Chemistry and Graduate School of The University of Toledo for financial assistantship.

Special thanks go to my family members who have played a decisive role in my career. I would like to thank my dear husband Sumanta, for his constant comfort, care, understanding and encouragement; my parents Sridhar and Dipti for bringing me into this world and giving me the opportunity to do all the wonderful things; my sister and best friend, Bidisha; my dearest uncle Damodar, who has been like a father to me and lastly my uncle and aunt Pinaki and Kalpana who have been my constant support.

## TABLE OF CONTENTS

## LIST OF FIGURES

### Chapter 1



### Chapter 2

**Chapter 3**

**Chapter 4**

**Chapter 5**

## LIST OF TABLES

**Chapter 2**



**Chapter 4**



**Chapter 5**

# Chapter 1

# Introduction

## 1.1. Introduction

Cholinergic neurons play a vital role in cognition and memory. Changes in the cholinergic system results in severe neurodegenerative disorders such as Alzheimer's disease (AD) and dementia.[1] These disorders are associated with loss of cognitive functions, memory impairment, disorientation, hallucinations and paranoia. The changes in the cholinergic system are subtle and gradual making it difficult to diagnose such disorders at an early stage. Therefore, it is critical to understand both the mechanism of such selective cholinergic degradation and also to be able to monitor the subtle changes that occur. Hence, it is important to develop analytical separation and detection strategies that will enable quantitative determination of cholinergic neurotransmitters for understanding and improving therapeutic strategies for such diseases.

Biomolecules that can selectively interact with molecules established as specific disease biomarkers have potential applications in the field of biosensors and bioelectronics. These biocatalysts, when integrated with conductive supports produce transducing signals leading to selective detection of such biomarkers. Systems employing enzymes provide a common platform for development of biosensors where the high turnover rates of enzymes produce amplified signals leading to sensitive detection methods. Analytical detection strategies can be further enhanced by using combinations of artificial and natural transducers. Development of bioelectronic transducers involves selective integration of various biointerfaces and their effective electronic communication with the conducting support. The effectiveness of such integrated assemblies can be achieved by employing conducting polymers and redox relay units. Systematic organization of integrated biosystems offers exciting perspectives to yield novel sensing

systems.

### 1.2. Alzheimer's Disease and the Cholinergic System

Neurotransmitters are chemicals used for transmission of signals between a neuron and another cell. The neurological system that uses acetylcholine (ACh) as its neurotransmitter is termed as the cholinergic system. ACh was discovered by Otto Lowei and Sir Henry Dale and together they shared the Nobel Prize in Medicine in 1936. ACh is an important neurotransmitter of both the central and the peripheral nervous system and functions by stimulating numerous muscarinic and nicotinic receptors.[2] It plays an important role in attention, memory, sleep, arousal, motor function and autonomic regulation.[3]

Alzheimers disease is an irreversible progressive brain disorder associated with impaired cholinergic transmission. Common symptoms include dementia, disorientation, loss of cognitive and language skills, hallucinations, etc. The classical markers of AD include overall shrinkage of the brain, accumulation of fragments of amyloid proteins in the brain, formation of insoluble twisted fibers comprising of tau protein known as neurofibrillary tangles, and degradation of neurons.[4] These pathological changes predominantly occur in the cerebral cortex and hippocampus of the brain which are associated with the cholinergic system. Since AD is synonymous with marked decrease in ACh concentration, it was suggested that some of the symptoms of the disease could be attenuated by using drugs that could partially restore the functions of the cholinergic system.[5] Several drugs namely tacrine, donepezil and rivastigmine have been developed which are all acetylcholinesterase (AChE) inhibitors, and function by inhibiting the

hydrolysis of ACh and increasing the level of ACh in the brain.[6] These drugs have shown to improve cognitive skills and delay the symptomatic progression of the disease. In addition to AChE inhibitors, several compounds that act as muscarinic agonists, nicotinic agonists, high affinity choline uptake enhancers and ACh releasers have also been examined as potential drugs for AD.[6]

### 1.3. Choline and Acetylcholine

Figure 1-1 represents the chemical structure of ACh and its precursor molecule choline (Ch). Although ACh has quaternary amine functionality in its chemical structure, it does not belong to the amino acid class of neurotransmitter and is neither derived from an amino acid.

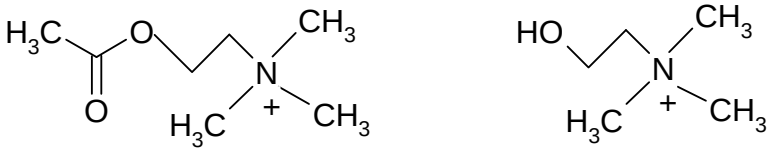


Acetylcholine Choline

**Figure 1-1.** Structure of ACh and Ch.

The cholinergic cycle is represented in Figure 1-2. ACh is synthesized inside the neurons from the precursor molecules Ch and Acetyl-coenzyme A (AcCoA) by choline acetyltransferase (ChAT). Ch however, is not synthesized in the neurons and is transported from the synaptic cleft into the presynaptic terminal. The newly synthesized ACh is transported by a vescicular acetylcholine transporter (VAChT) and loaded into synaptic vescicles inside the neurons. ACh release is $K^+$ dependent and following

depolarization, ACh is released into the synaptic cleft by fusion of the synaptic vescicles with the plasma membrane. The released ACh then activates its receptors and is rapidly hydrolysed by acetylcholinesterase (AChE) to form Ch and acetate ions. [7,8]

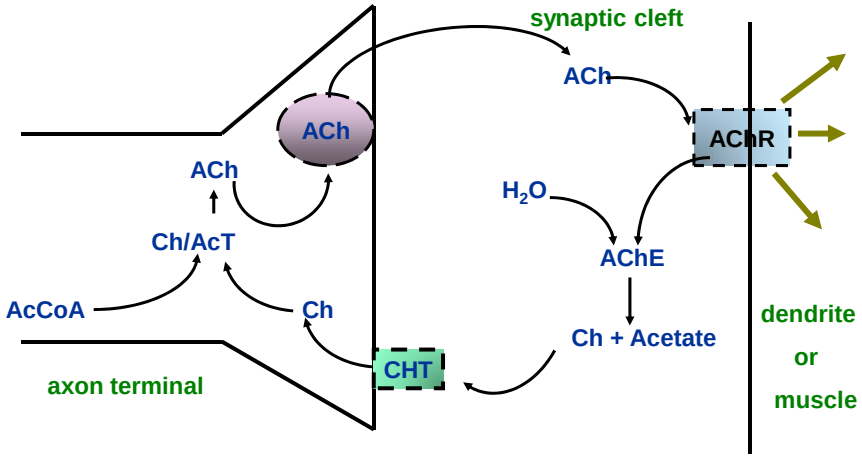


**Figure 1-2.** Schematic of the cholinergic cycle.

### 1.4. Choline Uptake Transporter Proteins

Since the turnover rate for ACh is very high in spite of its concentration being maintained within narrow limits in the mammalian brain, the transport of Ch into presynaptic terminal has been a subject of great interest for several decades.[9] Ch is a long known nutrient and plasma concentrations vary from 5-10 μM depending upon the dietary intake. Substantial sources of Ch for neural activities comes from the diet and reducing Ch concentration in the diet results in reduced ACh sysnthesis.[10, 11] As Ch is a positively charged hydrophilic ion, it cannot diffuse passively across the plasma membrane at physiological pH. There are membrane transport proteins present for this

function. Ch transport in neurons is described by two transport activities- a low affinity choline uptake transport system (LACHT) and a high affinity choline uptake transport system (CHT).

Haga demonstrated that synaptosomes incubated with low concentrations (1-5 μM) of [$^{14}$C]-Ch formed [$^{14}$C]-ACh, and the amount of [$^{14}$C]-ACh synthesized was proportional to the concentration of $Na^+$ ions present in the incubation medium.[12] [$^{14}$C]-Ch uptake into the synaptosomes was also dependent on the concentration of [$^{14}$C]-Ch present in the medium.[12] Ch uptake by this mechanism was attributed to the CHT. Simon and Kuhar also exhibited a $Na^+$ dependent uptake of Ch by varying the composition of Kreb's-Ringer media salt in rat hippocampal synaptosomal preparations. This uptake was also shown to be energy and $Cl^-$ ion dependent.[13] In this system the formation of ACh from Ch was more efficient at lower Ch concentrations.[12] Hence, CHT takes in Ch at a higher affinity and is responsible for selective Ch accumulation by cholinergic neurons exclusively for ACh synthesis.[14] Ch transported by this system into the presynaptic terminals is $Na^+$ dependent. Ch uptake by this process is thought to be the limiting step in ACh synthesis.[15] CHT is present specifically in the cholinergic system.[16] Ch uptake by CHT may be possibly regulated by cytoplasmic ACh concentrations. Raiteri et. al have demonstrated that CHT and AChE are in close proximity to each other and have suggested possibilities of their functional coupling.[17] There has been evidence of decrease in maximum rate ($V_{max}$) of Ch uptake upon addition of selective AChE inhibitors.[18] However, there is still an existing controversy as to whether CHT functions independently or is coupled to ChAT, or AChE. CHT function is also believed to be strongly regulated by various neuronal activities. Its activity is proposed to be modulated

not only by neurotransmitters, but also by secondary messengers such as cAMP (cyclic adenosine monophosphate) and $Ca^{2+}$ ions. [19] The Michaelis constant ($K_m$) of Ch uptake by CHT < 10 μM .[20]

Ch transport by LACHT is linearly dependent on the concentration of Ch and independent of $Na^+$ ions.[20] It has a lower capacity for Ch uptake and negligible ability for ACh synthesis. Ch uptake by LACHT is mostly for phosphatidylcholine synthesis, a major constituent of the eukaryotic cell membrane. Contrary to CHT that are selectively located in presynaptic cholinergic terminals, LACHT can be found in various tissues such as hepatocytes, enterocytes, mitochondria, placental tissue as well as synaptosomes.[20-22] Although LACHT transport have mostly been attributed as a $Na^+$ independent, Ch dependent, passive diffusion some studies have revealed that this low affinity transporter maybe carrier mediated. Ferguson et al. have used chiral methyl-cholines to evaluate the stereospecificity of CHT and LACHT in rat synaptosomes. They showed that R-(+)-α-methylcholine and S-(+)-β-methylcholine could be transported by the CHT. Studies extended on LACHT revealed that only R-(+)-α-methylcholine and not S-(-)-α-methylcholine could be transported across the membrane and that LACHT did not show any selectivity for β-methylcholine.[23] Hence both the transport systems exhibit substrate selectivity with different stereospecificities. The $K_m$ of Ch uptake by LACHT > 20-30 μM and is a saturable process.[20]

### 1.5. Structural Aspects of the High Affinity Choline Uptake Transporter Protein

CHT is mainly expressed by cholinergic neurons. Many research groups have attempted to characterize the structure of CHT, but to date the structural aspects of the

protein responsible for high affinity Ch uptake have not been elucidated. The genes of the CHT proteins cloned from various species have revealed that the proteins belong to the $Na^+$-dependent glucose transporter family. These proteins showed 20-26% sequence similarity with this family but were not homologous to other neurotransmitter transporter proteins. [7,24]

As Ch transporters have affinity for Ch there are two primary characteristics of molecular transport recognition. First, there is specific interaction between a cation binding site on the proteins and the quaternary nitrogen group. Secondly, as Ch and ACh both share this functionality, and Ch uptake is very specific, additional molecular recognition is provided by the hydroxyl functionality present in Ch but absent in ACh.

Deves and Krupka have utilized several methyl, ethyl and propyl quaternary ammonium derivatives of Ch to determine structure affinity relationship in Ch carrier erythrocytes.[25] Their studies suggest that there are very specific binding sites on the protein for interactions with the cationic quaternary nitrogen atom and the hydroxyl group. It is suggested that when a substrate interacts with the protein, its hydroxyl moiety and quaternary nitrogen functionality assumes a fixed position because of these specific interactions. In addition there are specific subsites present on the cationic binding site of the protein for interaction with the three alkyl groups of the quaternary nitrogen.[25] Two of these subsites have severe restrictions, while the third is comparatively flexible. This is supported by the fact that the $K_m$ values of dimethylethyl and diethylmethyl ammonium derivatives were comparable, but there was a six fold increase in $K_m$ value of the corresponding triethyl analogue. Hence, for a substrate with varying lengths of alkyl groups on its quaternary nitrogen atom, the smaller groups would interact with the

restricted sites, while the largest of them would occupy the third relatively unhindered position with its alkyl chain projecting upwards. Interestingly, an increase in the length of the third alkyl group beyond propyl functionality, lead to a steady increase in the binding affinity. This observation has emphasized the presence of a non-polar lipophilic domain, immediately adjacent to the Ch binding site that enabled varying degrees of non specific hydrophobic interactions with the alkyl chains. The distance between the nitrogen-oxygen atoms is also a very crucial factor for affinity binding, the optimal distance being approximately 3.26 to 3.30 Å.[26]

Unlike the binding affinity, which increases with an increase in alkyl chain length, the rate of transport is very sensitive to the size of substrate and a slight increase in size results in a great reduction in transport activity.[25] Hence an increase in size may cause an increase or decrease in binding affinity, but always results in decrease or loss in transport activity. On the other hand, a decrease in substrate dimension results in decrease in binding affinity, but causes negligible change in rate of transport. This is supported by the fact that the rate of transport of tetramethylammonium and Ch were comparable, but binding affinity of the former was 30 times lower than Ch.[25] This also indicates that the hydroxyl group is important for substrate binding but not relevant for subsequent translocation. Hence kinetic studies on binding affinity suggested that a substrate bound to the carrier protein is partially enclosed on the outer side of the membrane and free to protrude out of the binding site.[25] Since studies on kinetics of substrate transport revealed severe size restriction, it indicated that once the substrate is within the membrane it is completely surrounded by the protein in a size and shape selective fashion and has no room for outward projection.

Deves and Krupka have also proposed a mechanism of Ch transport, where they have suggested that binding of a substrate to the carrier protein results in a change in conformation of the protein which enables transport of the substrate across the membrane.[27,28] Utilizing human erythrocytes they have shown that the Ch uptake transporter exists in mainly two distinguishable conformations, the inward-facing conformation and the outward-facing conformation. The carrier alternates between these two conformations. In addition, the inward-facing conformation had two forms, the free carrier and a substrate-bound complex. These forms could be altered by addition of a ligand, suggesting Ch transport across erythrocyte protein carrier via a reciprocating gated channel that allows both influx and efflux of the substrate.[27, 28]

### 1.6. Choline and Acetylcholine Detection

The accurate quantitative analysis of small molecules and ions in complex matrixes requires sensitive and selective detection strategies. The detection of ACh and Ch is challenging as neither molecule is UV-active, electroactive nor fluorescent. Earlier experiments for ACh and Ch analysis have been primarily based on radioassays which were not very specific or sensitive.[29,30] Mass spectroscopy has also been used as a detection technique in combination with gas chromatography (GC), high performance liquid chromatography (HPLC) and capillary electrophoresis (CE).[31,32] The possibility of using an enzyme modified electrode has been exploited as an alternative approach for ACh and Ch detection. The power of enzyme based electrochemical analyses is that enzymes selectively catalyze the conversion of the substrate into electroactive species without interference from other molecules present in the sample. The ACh and Ch

detection strategies described in the current work are based on indirect amperometric detection using chemically modified electrodes as described in Scheme 1-1.

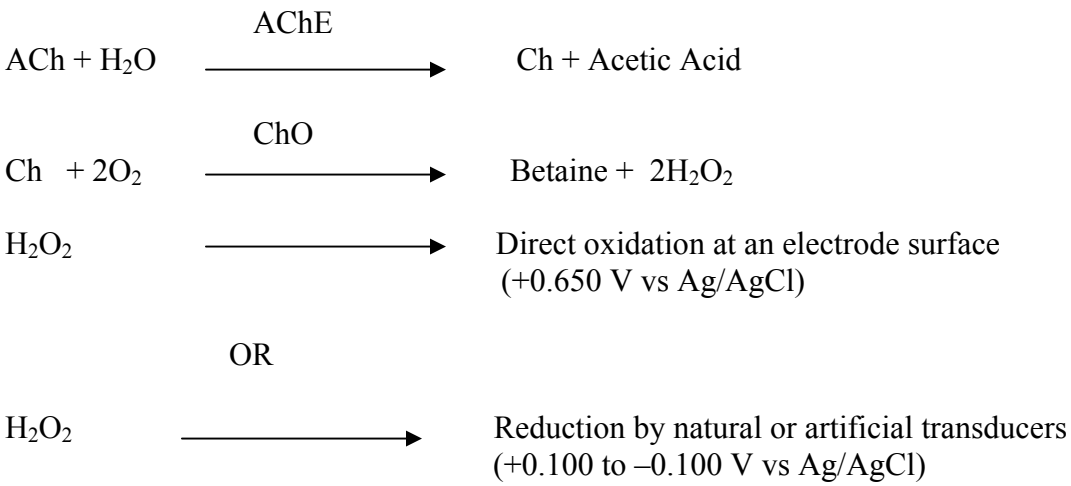


**Scheme 1-1.** Principle of ACh and Ch detection.

ACh and Ch can be electrochemically detected by indirect methods through their conversion into an electroactive molecule, namely hydrogen peroxide ($H_2O_2$) by catalysis via enzymes. In cholinergic neurotransmitters, ACh is enzymatically hydrolysed by AChE to produce Ch and acetic acid. In biological systems, Ch is catalytically oxidized by choline oxidase (ChO) to form betaine and 2 molecules of $H_2O_2$. Hence AChE and ChO integrated on electrode surfaces can generate $H_2O_2$ in response to catalytic conversion of ACh and Ch. $H_2O_2$ generated in the reaction can be detected by its direct oxidation onto an electrode surface at +0.650 V vs Ag/AgCl. Alternately it can be detected by further catalytic reduction at lower potentials (+0.100 to –0.100 V vs. Ag/AgCl). The current produced by either oxidation or reduction of $H_2O_2$ can be

can be quantified and directly related to the concentrations of Ch and ACh.

### 1.7. Mechanistic Aspects of Acetylcholinesterase and Choline Oxidase

Esterases are a class of enzymes that cleave ester bonds through hydrolysis. AChE is a key enzyme present in cholinergic synapses and the neuromuscular junctions. Its function is to hydrolyse ACh with great rapidity for termination of nerve impulse transmission. AChE is one of the fastest enzymes known with a turnover rate >1x $10^5$ molecules of ACh per second and its rate of hydrolysis approaches the maximum possible rate i.e., the diffusion control limit.[33] AChE has been the subject of various enzymological studies because of its impressive rate of catalysis.[34] The International Union of Biochemistry and Molecular Biology (IUBMB) had classified enzymes into six major categories based on the type of reaction they catalyze.[35] However this system of classification has its limitation as some enzymes can catalyze a wide variety of reactions and act on a number of different substrates. Aldrige and Rimon have classified esterase enzymes into three different categories namely Type A, Type B and Type C based on their substrate specificity.[36,37] Type A esterases are not inhibited by organophosphates, but they hydrolyse them. Type B esterases are inhibited by organophosphates due to formation of an irreversible covalent bond. This chemistry has formed the basis of various analytical assays for detection of organophosphorous pesticides and fertilizers.[38] Type C esterases are neither inhibited by organophosphates, nor do they catalyse them. Crystal structure and site directed mutagenesis studies of Type A esterases have revealed that the catalytic site of such enzymes contain a $Ca^{2+}$ ion, a phosphate ion and a His-His dyad.[39] Enzymes such as AChE and butyrylcholinesterase (BuChE) belong to the class B

type of carboxylesterase of the α/β-hydrolase fold family comprising of about 550 amino acid residues. Class B esterases are also referred to as the serine esterases as serine is essential for their catalytic activity.[39] In these enzymes a serine residue ($Ser_{203}$), a glutamate ($Glu_{335}$) and histidine ($His_{448}$) form a catalytic triad. Unlike Type A, Type B esterases do not require any inorganic cofactor. Their mechanism of action involves the activation of the oxygen of the serine group by the histidine residue, followed by a nucleophilic attack of the activated serine hydroxyl on the carbonyl carbon atom of the substrate resulting in the formation of an acyl-enzyme intermediate. In the second step the histidine moiety activates a molecule of water, which attacks the carbonyl carbon atom of the substrate leading to cleavage of the serine ester bond and formation of the product. The reason for the tremendous catalytic power of AChE is not yet fully understood, however the fast reaction rate has been attributed to transition-state stabilization. Several thermodynamic factors such as entropy, strain, solvation effects and electrostatic effects have been stated to contribute to the decrease in free energy in the transition state of the reaction.[40,41]

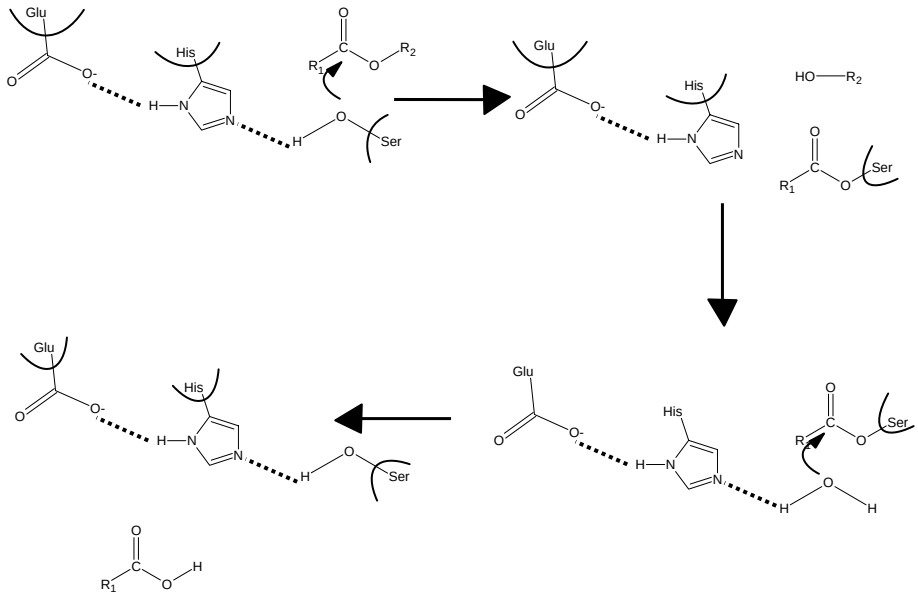


**Figure 1-3.** Mechanism of catalysis of AChE.

Although AChE acts on certain amides, esters and anilides it is much more specific compared to other Type B esterases such as human carboxylesterase 1. This is because AChE has a smaller catalytic site and limited non-specific hydrophobic interactions. Berman et al. have noted that the active site of AChE is buried in the center of the molecule at the bottom of a narrow channel. Hence the mechanism of non-competitive inhibition principally involves binding of the inhibitors at the rim of the channel and consequent blocking of the entrance of the channel leading to the active site.[42] Although the principle function of AChE is hydrolysis of ACh at the neuromuscular junction, it also plays a key role in various other physiological functions such as cell proliferation and differentiation.[43]

The oxidation of alcohols is a key step for a number of biochemical

pathways. The various enzymes employed to catalyze such reactions have been shown to utilize three essential co-factors namely pyrroloquinoline quinone (PQQ), zinc metal centers and flavins.[44] ChO belongs to the class of flavin dependent enzymes known as the GMC enzyme superfamily. This class is comprised of oxidoreductase enzymes that have a highly conserved catalytic site and they catalyse unpolarized alcohols. Other important enzymes of this category include glucose oxidase, cholesterol oxidase, methanol oxidase and choline dehydrogenase. ChO catalyses the oxidation of Ch to glycine betaine via a two step four electron process. In the first step Ch is converted to betaine aldehyde.[44] In the second step of the oxidation reaction, the enzyme bound intermediate betaine aldehyde is converted to glycine. The specific mechanism of ChO has been elucidated based on various kinetic isotope studies. The first step involves the transfer of a hydride ion from α-C of activated Ch to the enzyme bound flavin molecule. It has been proposed that the active site residue has a $pK_a$ of ~ 7.5 which acts as a base to extract the hydride ion to yield the activated alkoxide species. This transient step is stabilized via electrostatic interaction of the alkoxide with an imidazolium moiety from a histidine backbone.[44] The second step involving the conversion of betaine aldehyde to betaine also requires substrate activation. It is proposed that this activation can occur either via the formation of an acyl substrate as in the mechanism of NAD dependent enzymes such as aldehyde dehydrogenase. Alternately substrate activation may also occur by reaction with a water molecule to form a gem-diol as in the case of histidinol dehydrogenase. However evidence gathered from various NMR, kinetic and spectrophotometric data strongly suggest that a hydrated form of betaine aldehyde is required for the second step, which is consistent with the gem-diol mechanism.[45]

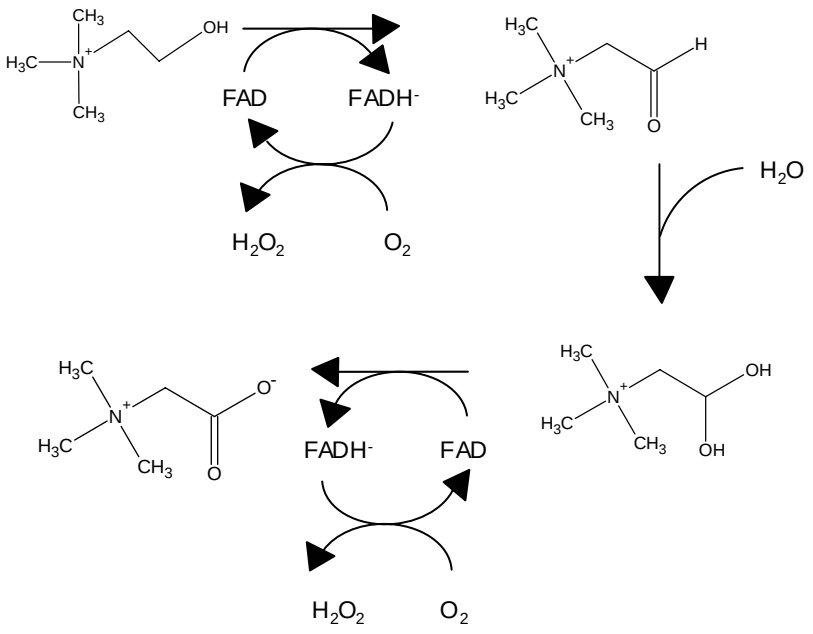


**Figure 1-4.** Mechanism of catalysis of ChO.

### 1.8. Choline and Acetylcholine Separation

Since Ch and ACh generate the same electrical signal upon enzymatic conversion to $H_2O_2$, a separation technique needs to be implemented for separation and analysis of these molecules. Capillary zone electrophoresis (CE) is an analytical technique ideally suited for separation of small quantities of charged hydrophilic molecules.

Capillary Electrophoresis is a broad term encompassing various separation modes such as CE, capillary gel electrophoresis (CGE), capillary isoelectric focusing (CIEF), isotacophoresis (ITP), electrokinetic chromatography (EKC), micellar electrokinetic capillary chromatography (MEKC), microemulsion electrokinetic chromatography (MEEKC), non-aqueous capillary electrophoresis (NACE) and capillary electrochromatography (CEC). CE can be used to separate a wide variety of molecules

with high efficiency such as charged ions, neutral species and even chiral enantiomers. CE is especially well suited for analysis of low volume samples like biomolecules and pharmaceutics as the total volume of the capillary itself is in the range of microliters.

### 1.8.1 Capillary Zone Electrophoresis

As biological samples are associated with complex sample matrices and are available in small quantities, microcolumn separation techniques are best suited for their analysis. CE is an attractive analytical technique especially useful for the separation and analysis of biomolecules. CE is the simplest mode of capliiary electrophoresis and its fundamental principle is separation of molecules based on their charge to size ratio. Typically narrow bore fused silica capillaries (25-200 μm) are used for such separation. The capillaries are filled with a suitable buffer. Three principle method of injection are used for sample introduction into the capillary, namely gravity injection, pressure injection and electrokinetic injection. In gravity injection a difference of height created between the sample reservoir and buffer reservoir causes the sample to flow into the capillary. In pressure injection, external pressure is applied to the sample vial causing the sample to flow into the capillary. Alternately a vacuum is applied in the opposite end of the capillary which creates suction and allows the sample to be drawn into the capillary. In electrokinetic injection a high voltage is applied to the sample via an electrode. After each type of injection, the sample vial is replaced by a buffer reservoir. Very high electric field strengths (15-25 kV) are applied across the capillary for separation of the analytes. Analyte separation in CE is primarily based on a combination of two forces; the electrophoretic velocity of the analyte and the electrosmotic flow (EOF) generated by the

silanol groups of the fused silica capillaries. Application of high separation voltage results in movement of positively charged analytes towards the cathode and negatively charged analytes (anions) towards the anode. Hence separation of ions is based on their charge and velocity differences in the electric filed, termed as electrophoretic mobility ($\mu_{ep}$) of an ion. The inner walls of the capillary bear a negative charge at pH > 3 because of the ionization of silanol groups making up the bare silica capillary. The positively charged ions of the buffer are electrostatically attracted to the negatively charged wall resulting in the formation of an electrical double layer. A potential difference is created in the double layer known as the zeta potential. Upon application of voltage the positively charged buffer ions move towards the cathode and being heavily solvated they drag the buffer solution with them. This type of bulk flow along the capillary is referred as the EOF. The migration of an analyte along the capillary is the sum of its electrophoretic and electroosmotic velocity. The electrosmotic velocity is much more substantial than the electrophoretic velocity of the ions; hence the net result is the movement of all species towards the cathode. Thus positively charged species migrate first, followed by neutral, and then negatively charged species of the same size. The separated components are detected at the cathode.

$$\nu = (\mu_{ep} + \mu_{eo})\, E \qquad (1\text{-}1)$$

Where $\nu$ = net velocity of the analyte, $\mu_{eo}$ = mobility of electroosmotic flow,

and E = electric field strength.

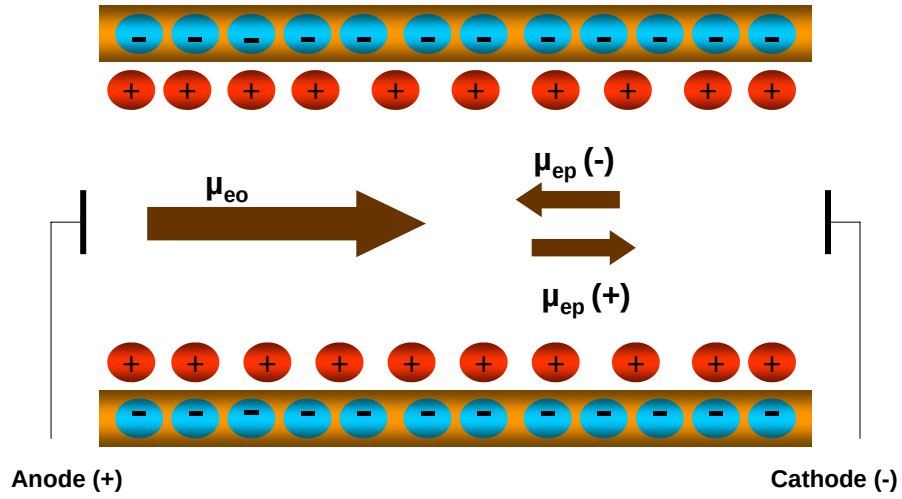


**Figure 1-5**. Schematic of electrosmotic and electrophoretic flow in CE.

There are certain parameters critical for efficient separation by CE. The choice of buffer is crucial as ionic strength of the buffer has a direct effect on the zeta potential and hence the EOF. The pH of the buffer is also a crucial factor as the analytes need to be in a charged state. Hence a high pH buffer is suitable for acidic analytes while a low pH buffer is suitable for separation of basic analytes. EOF is also strongly dependent on the buffer pH i.e., magnitude of EOF is decreased at low pH and increased at high pH. Hence altering the pH of the run buffer is usually the most convenient method to control the EOF. The EOF is also proportional to the electric field or separation voltage applied. While a large value of applied voltage results in fast and efficient separation of the analytes due to an increase in EOF, too high voltages may result in reduction of separation time and lead to decrease in resolution. High electric fields may also result in

substantial joule heating. Joule heating results in unequal heating along the capillary resulting in laminar flow.

The high separation efficiency of CE is mainly due to a constant velocity gradient across the entire capillary cross section resulting in a plug –flow profile as opposed to pressure driven flow in HPLC where frictional forces result in a drop in velocity of the mobile phase near the column walls and creates a parabolic flow. Parabolic flow results in broadening of solute zones and decrease in resolution.

CE offers the advantage of small sample volume, efficient separation, quantification of the analytes, and use of small volumes of reagent. CE techniques have emerged as a powerful tool for the separation of biomolecules in the last decade and offer great advantage in the determination of pharmaceuticals and drug impurities.[46] CE has also been used in the analysis of proteins and peptides, DNA, carbohydrates and lipids.[47-50]

### 1.8.2. CE with Electrochemical Detection

The detection methods primarily used for CE are UV/vis absorption, mass spectrometry and laser induced fluorescence. Although electrochemical detection (EC) method is still not used for routine analysis, it has certain distinct advantages. Three major EC detection modes are generally used with CE, namely conductometric detection, potentiometric detection and amperometric detection. In conductometric detection, conductivity between indicator electrodes are measured upon the application of a small constant alternating current. Conductometric measurement is a universal technique and is particularly advantageous for molecules that are not UV active. Potentiometric detection involves the measurement of the difference in potential between an indicator electrode

and a reference electrode. Amperometric detection is a very sensitive detection technique where a change in current is monitored as the analyte undergoes electrochemical oxidation or reduction at the electrode surface.

EC with amperometric detection offers good selectivity towards electroactive compounds and high sensitivity that is not limited by the short optical path length of the capillary.[50] In addition, the dimensions of microelectrodes (MEs) are ideally suited for use with CE. EC is cost effective and MEs have the advantage of reduced ohmic drop and high current densitiy enabling the possibility of achieving low detection limits. However one major challenge in coupling CE with EC is the complete separation of the applied voltage from the separation current to minimize noise.[50] In fact this is a major drawback of using CE with amperometric detection and is perhaps the reason why it has still not been commercialized. The simplest method to overcome this challenge is to ground the cathode. This can be achieved by breaking the capillary to create a small gap such that the ground cathode is placed ahead of the detection cell and the sample reaches the detector by virtue of pressure created by the EOF.[51] Such kind of detection is called off column detection and very often a semipermeable ion exchange membrane is placed between the broken gap to minimize diffusion. Detection can also be achieved using the end column mode where a crack can be introduced on the capillary without complete breakage of the capillary such that the separation current stops at the point of fracture while the analytes are free to move into the detector cell.[50] The working ME is aligned at the end of the detector. Simple amperometric detection is limited to the detection of electroactive compounds only using unmodified electrodes, however a wide array of compounds can be analysed by using different electrode materials and by manipulating

the electrode surface.

CE with EC has been used for the detection of the neurotransmitter dopamine in brain microdialysate samples.[52] In addition microchip capillary electrophoresis has been used for detection of catecholamine and dopamine using carbon nanotube modified working electrodes.[53,54] Kirchhoff et al. have used CE-EC to evaluate the inhibitory properties of several cholineomimitic compounds on the rate of choline uptake by CHT.[55,56]

### 1.9. Chemically Modified Electrodes (CME)

Chemical modification of electrodes refers to various processes of attaching or immobilizing a specific molecule or combination of various chemical species on an electrode surface for deliberate alteration of its chemical and electrochemical properties. Chemical modification results in changes that impart unique properties to the electrode very different from that of an unmodified electrode. CMEs have the versatility of catalyzing specific reactions or chemical recognition of specific molecules that generally cannot be accomplished by unmodified electrodes. CME has immense application in the field of biosensing. Prudent deliberate manipulations of the electrode surface have lead to the development of numerous biosensors and immunosensors for selective detection of the specific analyte of interest. Depending upon the biomaterial assembled different electrical signals such as changes in current, potential, capacitance or measurement of impedance can be employed for detection. Another significant application of CME is understanding the fundamentals of charge transfer processes occurring on electrode surfaces. Such studies are significant for development of energy storage and conservation

devices such as solar cells.

Development of biosensors involves the modification of electrode surface with various enzymes such as oxidases (glucose oxidase, cholesterol oxidase, ChO), dehydrogenase (methanol dehydrogenase), esterase (acetylcholinesterase), peroxidase (horseradish peroxidase) that can recognize specific molecules to generate a product which can undergo an electrochemical reaction. The development of biosensors involves the successful integration of the bioactive material onto the electrode surface. While using enzymes, deposition strategies need to be employed such that the bioactivity of the enzymatic layers is maintained after immobilization. One of the simplest strategies used is simple physical adsorption of enzymes on the electrode surface by coating the electrode layer with a thin film of enzyme.[57] Such non-covalent coupling of enzymes to electrode surfaces mostly involve hydrophobic, hydrophilic or electrostatic interactions between the enzyme interfaces. Although this method maintains most of the enzymatic activity, there is rapid deterioration of electrode performance due to physical loss of enzymes from the electrode surface. Linking enzyme molecules with chemicals such as glutaraldehyde or polyethylene glycol results in the formation of a highly crosslinked covalent polymer which can then be physically adsorbed onto the electrode surface producing a relatively stable biolayer.[58] Integration of enzymes can also be achieved by using affinity complexes such as the affinity interaction between a streptavidin immobilized electrode and a biotinylated enzyme. Since affinity interactions are associated with high association constants they can be manipulated to form stable biolayered structures.[59]

Another strategy is to covalently link the enzymes onto the electrode surface. This is generally achieved by either using metal oxide electrodes that already have surface functional groups for attachment with enzymes or by employing pretreated electrodes. Gold, platinum and carbon electrodes are often treated chemically or electrochemically to generate surface functionalities. Treatment with $O_2$ plasma or $NH_3$ plasma results in the introduction of hydroxyl or amine functional groups on the surface suitable for covalent coupling with enzymes.[59,60] Electrochemical oxidation of metals through silanization can be used to introduce different functionalities such as thiols, esters and amines by using various functionalized silane reagents.[61] Self assembly of amino or carboxylic acid functionalized thiolates especially on Au electrode surfaces enables complementary coupling with the aspartate /glutamate or lysine residues of redox proteins.

The performance of an effective biosensor relies on the efficiency of electron transfer between the redox center of the enzyme and the electrode surface. Although direct electron transfer between the enzyme and electrode is possible, it is usually not a kinetically facile process due to the large distance of separation between the two redox sites. The efficiency of electron transfer is also heavily dependent on the mode of alignment of the enzyme with the electrode surface and configurations where the redox site is easily assessable results in more efficient electron transfers. In such cases artificial redox polymers incorporated with electroactive moieties are utilized to achieve electrical contact between the enzyme and the electrode. A common redox polymer is poly-vinyl pyridine attached to electroactive ferrocene or bipyridinium units. These polymer units are covalently linked to the enzymes and act as molecular wires to facilitate electron transfer processes.

Electrically conductive polymers have also been widely employed to prepare chemically modified electrodes. These polymers are formed from suitable monomers (such as pyrrole, aniline, thiophene) and can be prepared by direct electrodeposition onto the electrode surface. These polymers are conducting due to delocalization of electrons as a result of extended conjugation. The thickness and electrical properties of such polymeric films can be easily controlled by manipulating the electrodeposition conditions. Although not bioactive themselves, these polymers can be employed to entrap various biomolecules on the electrode surface, providing a convenient means of developing stable biosensors.

Effective biosensors have also been developed by coating the electrode surface with inorganic metal catalysts such as transition metal hexacyanometalates. This class of compounds is redox active and has the ability to catalyze the effective electrochemical oxidation and reduction of small molecules such as $O_2$ and $H_2O_2$ which are common by-products of biocatalysed reactions.

### 1.10. Amperometric Biosensors

Amperometric biosensors work on the principle of producing a transducing current as a result of the interaction of a substrate (analyte of interest) with enzymes immobilized on the electrode surface. This type of detection takes advantage of the high specificity of the enzyme-substrate interaction. An amperometric biosensor usually involves electron transfer between the active site of an enzyme immobilized on the

working electrode and the electrode surface. This heterogeneous electron transfer between the enzyme and electrode allows regeneration of enzyme. Oxidase based enzymes are the most common class of enzymes used for amperometric biosensing. This class of enzymes functions by oxidizing their substrate and returning to their original state via electron transfer to molecular oxygen. Hence the final product of their catalysis is the oxidized substrate and a side product, $H_2O_2$. The $H_2O_2$ generated or the oxygen consumed during this chemical process can both serve a way to indirectly quantify the amount of substrate present. However amperometric detection methods based on measurement of amount of $H_2O_2$ generated is preferred due to its ease of detection.

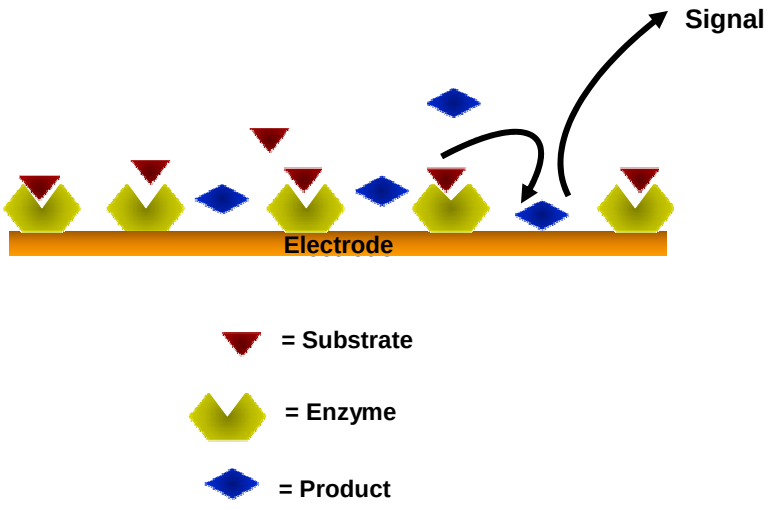


**Figure 1-6**. Mechanism of amperometric detection.

The detection cell consists of a three electrode system comprising a reference electrode, a working electrode and an auxiliary electrode. The electrochemical reaction takes place at the surface of the working electrode that is poised at a fixed potential with respect to the reference electrode. The electrical output from an electron flow caused by the electrochemical reaction that takes place is detected and quantified. The current generated can be mathematically defined by equation 1-2.

$$i = nFADC/\delta \quad (1\text{-}2)$$

where i = current produced, n= number of electrons transferred in the redox process, F= Faraday constant, A = area of electrode in $cm^2$, D = diffusion coefficient of analyte ($cm^2$ /s), C = concentration of the analyte in the bulk solution (mol/ $cm^3$), $\delta$ = thickness of the Nernst diffusion layer (cm).

Amperometric detectors when coupled with CE offer the advantage of high sensitivity that is not limited by the path length, good selectivity towards electroactive compounds and economical instrumentation.[50] Since the working volume of CE is small, MEs are a prudent choice as detector systems.

### 1.11. Microelectrodes

A ME is a small size electrode with dimensions from tens of micrometer to submicrometer.[62] MEs of different geometries can be fabricated such as planar, disk, cylindrical, hemisphere, micro ring, integrated arrays, disk, cylinders and arrays being most commonly used. Commonly used materials are platinum, gold, carbon (fibers) although other materials like nickel, iridium and silver are also used.[63] The simplest method to fabricate a ME is to seal a fine conducting wire into a non-conducting body

(such as glass). During fabrication it is important to ensure a proper seal between the microwire and insulating body for good performance of these electrodes. MEs have certain distinct advantageous properties such as small geometric dimensions, fast response, steady state current response at long time intervals, small diffusion layer, and significantly lower IR drop. These attributes have been primarily investigated by Mark Wightman.[64]

A striking characteristic of MEs is the predominance of non planar diffusion due to their small dimensions. A direct consequence of this is the sigmoidal-shaped cyclic voltammogram obtained at small scan rates in contrast to a peak shaped voltammogram observed at macroelectrodes. The total current response of a ME is contribution from planar and non-planar diffusion. An equation defining the time evolution of current can be obtained as stated in equation 1-3.[63]

$$i = \frac{nFADC}{r} + \frac{nFAD^{1/2}C}{\pi^{1/2}t^{1/2}} \qquad (1\text{-}3)$$

where new terms are r = radius of the electrode, and t = time.

It can be observed that the current response has two distinct terms, a time dependent planar diffusion term and a time independent steady state response due to non planar diffusion. At short time intervals, the thickness of the depleted layer of reactants is much smaller than the dimensions of the electrode and hence mass transfer is predominantly through planar diffusion. During this condition the current response obeys the time dependent Cottrell equation. At longer time intervals mass transfer is mainly dominated by radial or non planar diffusion and the time independent term becomes predominantly significant. In this case the current is limited by the rate of diffusion by the

electroactive species. This steady state current response depends largely on the geometry of the electrode. Cyclidrical MEs also have a large current response but unlike the disc ME, it rarely attains a truly steady state value.

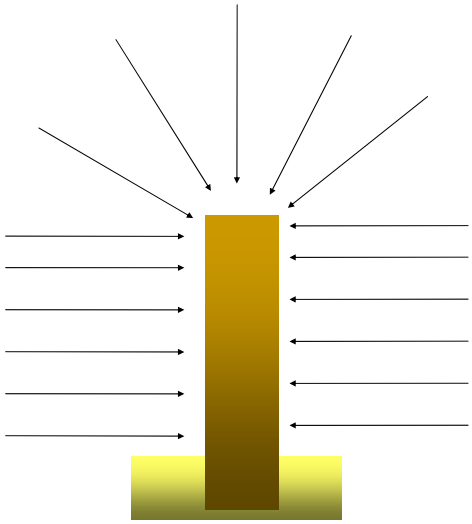

**Figure 1-7**. Mass transport by radial and planar diffusion at a microelectrode surface.

The magnitude of current observed at a ME typically ranges in the pA to nA region.[63] Due to their small size MEs can be used for applications such as small probes in in vivo voltammetry and scanning electrochemical microscopy. Due to its low iR drop they can be used in low conductivity media such as non polar solvents and solutions with low concentrations of supporting electrolytes. Due to their fast response MEs can be used for rapid measurements in fast techniques such as fast scan cyclic voltammetry and spectroelectrochemistry.

### 1.12. Electrochemical Characterization of Chemically Modified Electrodes

Voltammetry comprises all electrochemical techniques based on the measurement of current as a function of potential. Cyclic voltammetry (CV) is a simple yet

versatile technique that can serve as a powerful tool for characterization of various electrode surface modifications.

The excitation signal for CV is a triangular waveform, where the potential is scanned as a function of time from an initial value ($E_i$) to a final value ($E_f$) in the forward scan and back again from $E_f$ to $E_i$ in the reverse scan to complete a cycle. Current generated is the response signal. Figure 1-8 represents a typical CV.

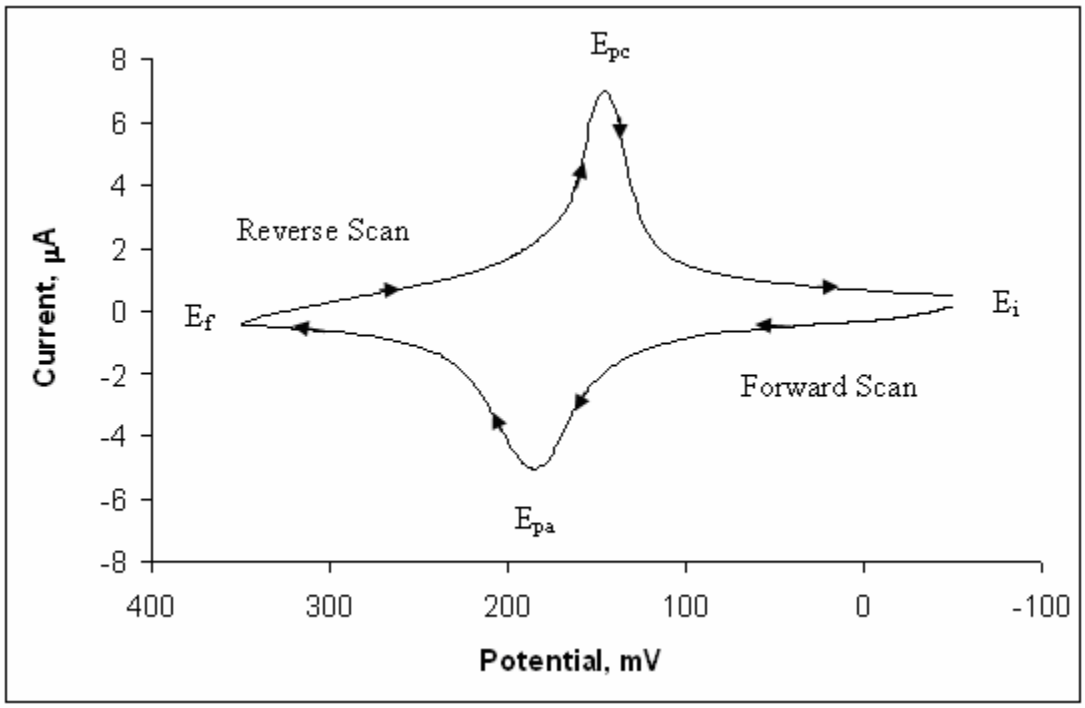


**Figure 1-8**. Typical CV of a fast electron exchange redox couple.

Any electroactive compound whose redox potential lies within the scanned range of potential will undergo an electrochemical reaction corresponding to a change in current with the change being maximum near its redox potential. In this case, a peak shaped waveform is obtained due to the oxidation of the electroactive species in the

forward scan and its consequent reduction in the reverse scan. There are several important parameters of a CV such as anodic peak current ($i_{pa}$), cathodic peak current ($i_{pc}$), anodic peak potential ($E_{pa}$), and cathodic peak potential ($E_{pc}$). A reversible redox couple is a species that can undergo fast electron exchange with the electrode surface. The peak current, ($i_p$), for a reversible species in solution is described by the Randles-Sevick equation :[65]

$$i_p = (2.69 \times 10^5) n^{3/2} A D^{1/2} C \upsilon^{1/2} \quad (1\text{-}4)$$

where n = electron stoichiometry, A = area of electrode ($cm^2$), D = diffusion coefficient ($cm^2$ /s), C = concentration of electroactive species ( $mol/cm^3$ ) and υ = scan rate (V/s or mV/s)

For a reversible redox couple, $i_{pa}/ i_{pc} = 1$, and $\Delta E_p = E_{pa} - E_{pc} \approx 0.059/n$.

However, for surface confined species ideally $\Delta E_p = 0$, (there is no peak to peak splitting) and $i_p$ is proportional to υ.

The nature of the voltammogram obtained depends on the electrochemical behavior of the analyte. Important information such as electron transport properties of mediators and catalysts, electrocatalytic activity of the modified electrode and estimation of surface coverage can be acquired easily from simple voltammograms.

## 1.13. References


1. Araujo, J. A.; Studzinski, C. M.; Milgram, N. W. Further Evidence for the Cholinergic Hypothesis of Aging and Dementia from the Canine Model of Aging. *Prog. Neuropsychopharmacol. Biol. Psychiatry*, **2005,** *29*, 411–422.

2. Sarter, M.; Parikh, V. Choline Transporters Cholinergic Transmission and Cognition. *Nat. Rev. Neurosci.* **2005**, *6,* 48-56.

3. Azalakova, M. H.; Blakely, R. D. The High affinity Choline Transporter: A Critical Protein for Sustaining Cholinergic Signaling as Revealed in Studies of Genetically Altered Mice. *HEP,* **2006,** *175,* 525-544.

4. *http://www.smart-drugs.com*

5. Bartus, R.T.; Dean, R.L.; Beer, B.; Lippa, A.S. The Cholinergic Hypothesis of Geriatric Memory Dysfunctions. *Science,* **1982,** *217,* 408–417.

6. Gualtieri, F. Cholinergic Receptors and Neurodegenerative Diseases. *Pharm. Acta Hevl.* **2000,** *74,* 85–89.

7. Ribeiro, F. M.; Black, S. A. G.; Prado, V. F.; Rylett, R. J.; Ferguson, S. S. G.; Prado, M. A. M. The "Ins" and "Outs" of the High-Affinity Choline Transporter CHT1. *J. Neurochem.* **2006**, *97*, 1-12.

8. Ferguson, S. M.; Blakely, R. D. The Choline Transporter Resurfaces: New Roles for Synaptic Vescicles? *Mol. Interv.* **2004,** *4,* 22-37.

9. Bader, C. R.; Baughman, R. W.; Moore, J. L. Different Time Course of Development for High-Affinity Choline Uptake and Choline Acetyltransferase in the Chick Retina. *Proc. Natl. Acad. Sci. USA,* **1978**, *75,* 2525-2529.

10. Fernstorm, J. D. Effects of the Diet on Brain Function. *Acta Astronaut.* **1981**, *8,* 1035-1042.

11. Zeisel, S. H. Dietery Choline: Biochemistry, Physiology and Pharmacology. *Annu. Rev. Nutr.,* **1981,** *1*, 95-121.

12. Haga, T. Synthesis and Release of [$^{14}$C] Acetylcholine in Synaptosomes. *J. Neurochem.* **1971**, *18*, 781-798.

13. Siman, J. R.; Kuhar, M. J.; High Affinity Choline Uptake: Energy and Ionic Requirements. *J. Neurochem.* **1976**, *27*, 93-99.

14. Yamamura, H. I. Snyder, S. H. Choline. High-affinity Uptake by Rat Brain Synaptosomes. *Science* **1972**, *178,* 626-628.

15. Simon, J. R.; Atwet, S.; Kuhar, M. J. Sodium Dependent High Affinity Choline Uptake: A Regulatory Step in the Synthesis of Acetylcholine. *J. Neurochem.* **1976**, *26,* 909-922.

16. Kuhar, M. J.; Sethy, V. H.; Roth, R. H.; Aghajanian, G. K. Choline: Selective Accumulation by Central Cholinergic Neurons. *J. Neurochem.* **1973,** *20*, 581-593.

17. Raiteri, M.; Marchi, M.; Caviglia, A. M. Studies on a Possible Functional Coupling Between Presynaptic Acetylcholinesterase and High-Affinity Choline Uptake in the Rat Brain. *J. Neurochem*, **1986,** *47*, 1696-1699.

18. Shimon, M.; Egozi, Y.; Kloog,Y.; Sokolovsky, M.; Cohen, S. Vascular Cholinesterases and Choline Uptake in Isolated Rat Forebrain Microvessels : A Possible Link. *J. Neurochem.* **1986**, *46,* 483-488.

19. Okuda, T.; Haga, T. High Affinity Choline Transporter. *Neurochem. Res*. **2003**, *28,* 483-488.

20. Lockman, P. R.; Allen, D. D. The Transport of Choline. *Drug Dev. Ind. Pharm*. **2002**, *28*, 749-771.

21. Sweiry, J. H.; Yudilevich, D. L. Characterization of Choline Transportat Maternal and Fetal Interfaces of the Perfused Guinea-Pig Placenta. *J. Physio.* **1985,** *366,* 251-266.

22. Porter, R. K.; Scott, J. M.; Brand, M. D. Choline Transport into Rat Liver Mitochondria. Characterization and Kinetics of a Specific Transporter. *J. Biol. Chem.* **1992**, *77*, 4417-4419.

23. Ferguson, S. G.; Diksic, M.; Collier, B. Stereospecificity of High- and Low-Affinity Tranport of Choline Analogues into Rat Cortical Synaptosomes. *J. Neurochem.* **1982,** *7*, 749-759.

24. Okuda, T.; Haga, T.; Kanai, Y.; Endou, H.; Ishihara, T.; Katsura, I. Identification and Characterization of the High-Affinity Choline Transporter. *Nat. Neuroscience*, **2000,** *3,* 122-125.

25. Devés, R.; Krupka, R. M. The Binding and Translocation Steps in Transport as Related to Substrate Structure. A Study of the Choline Carrier of Erythrocytes. *Biochim. Biophys. Acta,* **1979,** *557*, 469-485.

26. Batzold, F.; Dehaven, R.; Kuhar, M. J.; Birdsall, N. Inhibition of High Affinity Choline Uptake. Structure Activity Studies. *Biochem. Pharmacol*. **1980**, *29*, 2413-2416.

27. Devés, R.; Krupa, R. M. Evidence for a Two-State Mobile Carrier Mechanism in

Erythrocyte Choline Transport: Effects of Substrate Analogs of Inactivation of the Carrier by N-ethylmalemide. *J. Membrane Biol.* **1981**, *61*, 21-30.

28. Devés, R.; Krupa, R. M. Reaction of Internal Forms of the Choline carrier of Erythrocytes with N-ethylmalemide: Evidence for a Carrier Conformational Change on Complex Formation. *J. Membrane Biol.* **1981**, *63*, 99-103.

29. Jope, S. R. High Affinity Choline Transport and AcetylCoA Production in Brain and their Roles in the Regulation of Acetylcholine Synthesis. *Brain Res. Rev.* **1979**, *1,* 313-344.

30. Haga T.; Noda, H. Choline Uptake in Rat Brain Synaptosomes. *Biochim. Biophys. Acta,* **1973**, *291*, 564-575.

31. Frölich, L.; Dirr, A.; Götz, M. E.; Gsell, W.; Reichmann, H.; Riederer, P.; Maurer, K. Acetylcholine in Human CSF: Methodological Considerations and Levels in Dementia of Alzheimer Type. *J. Neural Transm.*, **1998**, *105*, 961-973.

32. Jäverfalk-Hoyes, E. M.; Bondesson, U.; Westerlund, D.; Andrén, P. E. Simultaneous Analysis of Endogenous Neurotransmitters and Neuropeptides in Brain Tissue Using Capillary Electrophoresis–Microspray-Tandem Mass Spectrometry. *Electrophoresis*, **1999**, *20*, 1527-1532.

33. Quinn, D. M. Acetylcholinesterase: Enzyme Structure, Reaction Dynamics, and Virtual Transition States. *Chem. Rev*. **1987**, *87*, 955-979.

34. Massoulie, J.; Sussman, J.; Bon, S.; Silman, I. Structure and Functions of Acetylcholinesterase and Butyrylcholinesterase. *Prog. Brain Res.* **1993**, *98,* 139-146.

35. *http://www.chem.qmul.ac.uk/iubmb/enzyme/.*

36. Bergman, F.; Segal, R.; Rimon, S. A New Type of Esterase in Hog-Kidney Extract. *Biochem. J.;* **1957**, *67*, 481-486.

37. Aldrige, W. N. Serum Esterases. *Biochem. J*.; **1952**, *53*, 110-117.

38. Shulga, O.; Kirchhoff, J. R. An Acetylcholinesterase Enzyme Electrode Stabilized by an Electrodeposited Gold Nanoparticle Layer. *Electrochem. Commun.* **2007**, *9*, 935-940.

39. Liederer, B. M.; Borchardt, R. T. Enzymes Involved in the Bioconversion of Ester-Based Prodrugs. *J. Pharmaceut. Sci.* **2006,** *95*, 1177-1195.

40. Warshel, A. Electrostatic Origin of the Catalytic Power of Enzymes and the Role of Preorganized Active Sites. *J. Biol. Chem.* **1998**, *273,* 27035-27038.

41. Warshel, A.; Papazyan, A. Computer Simulation of Enzyme Catalysis: Finding Out What has Been Optimized by Evolution. Proc. *Natl. Acad. Sci. USA,* **1998**, *95*, 5950-5955.

42. Berman, H. A.; Nowak, M. W. In Multidisciplinary Approaches to Cholinesterase Function. *Shaffermann, A.; Velan, B. Eds; Plenum Press, New York.* **1992,** 149-156.

43. Soerq, H.; Seidman, S. Acetylcholinesterase-New Roles for an Old Actor. *Nat. Rev. Neurosci*. **2001,** *2*, 294-302.

44. Fan, F.; Germann, M. W.; Gadda, G. Mechanistic Studies of Choline Oxidase with Betaine Aldehyde and Its Isosteric Analogue 3,3-Dimethylbutyraldehyde. *Biochemistry,* **2006,** *45,* 1979-1986.

45. Fan, F.; Gadda, G. On the Catalytic Mechanism of Choline Oxidase, *J. Am. Chem. Soc.* **2005,** *127*, 2067-2074.

46. Budilová, J.; Pazourek, J.; Krásenskỳ, P.; Pospíchal, J. Continuous Mode of Operation for Large Volume Dosing in Analytical Carrier Ampholyte-free Isoelectric Focusing of Proteins Applied to Off-line Detection of Fractions. *J. Sep. Sci.,* **2006**, *29*, 1613-1621.

47. Yang, Y.; Boysen, I. R.; Hearn, M. T. W. Optimization of Field-Amplified Sample Injection for Analysis of Peptides by Capillary Electrophoresis-Mass Spectrometry. *Anal. Chem.* **2006,** *78,* 4752-4758.

48. Sonehara, T.; Kawazoe, H.; Sakai, T.; Ozawa, S.; Anazawa, T.; Irie, T. Ultra-Slim Laminated Capillary Array for High-speed DNA Separation. *Electrophoresis*, **2006**, *27*, 2910-2916.

49. Lamari, F. N.; Gioldassi, X M.; Mitropoulou, T. N.; Karamanos, N. K. Structure Analysis of Lipoglycans and Lipoglycan-Derived Carbohydrates by Capillary Electrophoresis and Mass Spectrometry. *Biomed. Chromatogr*. **2002,** *16*, 116-126.

50. You, T.; Yang, X.; Wang, E. Applications of Microelectrodes in Capillary Electrophoresis /Electrochemical Detection. *Electroanalysis,* **1999**, *11*, 459-464.

51. Wallingford, R. A.; Ewing, A. G. Capillary Zone Electrophoresis with Electrochemical Detection. *Anal. Chem.* **1987**, *59*, 1762-1766.

52. Qian, J.; Wu, W.; Yang, H.; Michael, A. C. An Integrated Decoupler for Capillary Electrophoresis with Electrochemical Detection: Application to Analysis of Brain Microdialysate. *Anal. Chem.* **1999,** *71*, 4486-4492.

53. Vlčková, M.; Schwarz; M. A. Determination of Cationic Neurotransmitters and Metabolites in Brain Homogenates by Microchip Electrophoresis and Carbon

Nanotube-Modified Amperometry. *J. Chromatogr. A,* **2007**, *1142,* 214–221.

54. Pumera, M.; Llopis, X.; Merkoçi, A.; Alegret; S. Microchip Capillary Electrophoresis with a Single-Wall Carbon Nanotube//Gold Electrochemical Detector for Determination of Aminophenols and Neurotransmitters. *Microchim. Acta,* **2006,** *152*, 261–265.

55. Barkhimer, T. V.; Kirchhoff, J. R.; Hudson, R. A.; Messer, W. S. Jr. Classifcation of the Mode of Inhibition of High-Affnity Choline Uptake Using Capillary Electrophoresis with Electrochemical Detection at an Enzyme-Modified Microelectrode. *Anal. Biochem.* **2005**, *339,* 216–222.

56. Cai, S.; Mukherjee, J.; Tillekeratne, L. M.V.; Hudson, R. A.; Kirchhoff, J. R. Inhibition of Choline Transport by Redox-Active Cholinomimetic Bis-Catechol Reagents. *Bioorg. Med. Chem.* **2007**, *15,* 7042–7047.

57. Chen, Z.; Zhang, Y.; Su, Y.; Meng, W.; Xie, Q.; Yao, S. EQCM Studies on Enzymatic Specific Activities of Glucose OxidaseAdsorbed on Au-electroplated and Carbon Nanotubes-Modified Au Electrodes. *Chin. J. Chem. Phys.* **2007***, 23,* 1201-1206.

58. Wise, D. D.; Barkhimer, T. V.; Brault, P. A.; Kirchhoff, J. R.; Messer, W. S.; Hudson, R. A. Internal Standard Method for Measurement of Choline and Acetylcholine by Capillary Elecytrophoresis with Electrochemical Detection. *J. Chromatogr. B***.** **2002**, *775*, 49-56.

59. Willner, I.; Katz, E. Integration of Layered Redox Proteins and Conductive Supports for Bioelectronic Applications. *Angew. Chem. Int. Ed.* **2000,** *39*, 1180-1218.

60. Oyama, N.; Brown, A. P.; Anson, F. Introduction of Amine Functional Groups on Graphite Electrode Surfaces and their Use in the Attachment of Ruthenium (II) to the Electrode Surface. *J. Electroanal. Chem. Interfacial Electrochem.* **1978,** *87*, 435-441.

61. Wrighton, M. S. Surface Functionilazation of Electrodes with Molecular Reagents. *Science,* **1986,** *231,* 32-37.

62. Štulĭk, K.; Amatore, C.; Holub, K.; Mareček, V.; Kutner, W. Microelectrodes, Definitions, Characterizations, and Applications. *Pure Appl. Chem.*, **2000**, *72*, 1483–1492.

63. Forster, R. J. Microelectrodes: New Dimensions in Electrochemistry. *Chem. Soc. Rev.* **1994,** *23*, 289-297.

64. Wightman, R. M. Microvoltammetric Electrodes. *Anal. Chem*. **1981**, *53,* 1125A-1134A.

65. Kissinger, P. T.; Heineman, W. R. Cyclic Voltammetry. *J. Chem. Edu.* **1983,** *60*, 702-706.

# Chapter 2

## Evaluation of Kinetic Parameters and Inhibitory Effects of the High Affinity Choline Uptake Transporter Protein (CHT) using Capillary Electrophoresis with Electrochemical Detection

## 2.1. Introduction

### 2.1.1 Kinetics of CHT Transport

CHT plays a significant role in transport of Ch and intraneuronal synthesis of ACh. Several synthetic analogues have been used to study the relationship between structure, activity and transport properties of Ch carriers.[1] It has been demonstrated that the carrier changes conformation upon binding and several inward and outward facing free and complex conformational states have been proposed.[2] The carrier mechanism of transport using Ch transport inhibitors revealed that dissociation of the carrier substrate complex is rapid with all substrate analogues.[3] Studies elucidating the transport by CHT across the synaptic membrane have shown that the protein bears ligand specificity.[4] This translocation process across the membrane faces competition with structurally similar compounds and the process is saturable.[4] Hence it is logical to define the kinetic parameters of this transporter protein in terms of Michaelis-Menten kinetics.

Michaelis-Menten kinetics considers a single-substrate enzyme catalyzed reaction and gives a mathematical relationship between the initial velocity of the reaction and the substrate concentration. The substrate binds to the enzyme to form a reversible enzyme-substrate complex which dissociates into the free enzyme and a product. The basis of this mathematical model is that equilibrium exists between the enzyme, substrate and enzyme-substrate complex and the dissociation of the complex is the slow step of this process.

$$E + S \underset{k_{-1}}{\overset{k_1}{\rightleftharpoons}} ES \xrightarrow{k_2} E + P \qquad (2\text{-}1)$$

E = enzyme, S = substrate, ES = enzyme-substrate complex, P = product

The constants can be separated from the variables using steady state conditions of chemical kinetics. If an assumption is made that the initial substrate concentration $[S_0]$ is much greater than the initial enzyme concentration, a simplified equation will be obtained:[5]

$$v_0 = \frac{V_{max}[S_0]}{[S_0] + K_m} \qquad (2\text{-}2)$$

Equation (2-2) is known as the Michaelis-Menten equation. $V_{max}$ is the maximum initial velocity of the reaction, $[S_0]$ is the initial substrate concentration, and $K_m$ is the Michaelis-Menten constant. $K_m$ is the value of $S_0$ when the initial velocity is half its maximal value ($v_0 = 1/2V_{max}$)

### 2.1.2. Inhibitors of Choline Uptake Transporters

Since both the CHT and LACHT exhibit substrate selectivity both systems are inhibited by a number of quarternary ammonium analogues. Binding and translocation studies suggest that there is a molecular requirement for a quaternary nitrogen atom and a free hydroxyl group with the optimum distance between the nitrogen-oxygen atoms being approximately 3.26 Å for binding to CHT.[6] Siman et al. have shown that CHT has about 50 fold less affinity for thiocholine than Ch, and substitution of the quaternary N atom with a tertiary N atom results in a five fold decrease in activity.[7]

A CHT inhibitor is a substance that decreases the rate of transport of Ch upon

binding with the protein. Reversible inhibitors bind by noncovalent interactions such as hydrogen bonds, ionic and hydrophobic interactions to form a reversible protein-inhibitor complex and attain an equilibrium resulting in a certain degree of inhibition. Reversible inhibitors can be removed by physical means such as dialysis to restore complete enzymatic activity. Based on the structural specificity of the ligand there are several reversible inhibitors of CHT. Several bisalkyl quaternary nitrogen analogues are good inhibitors of CHT. Hemicholinium is the most potent inhibitor and has an affinity higher than Ch itself.[6] Molecules with a quaternary ammonium group together with a neighboring hydroxyl groups have an effect in inhibiting Ch uptake in synaptosomes probably by producing a Ch analogue-type affinity for cholinergic sites.[8] Holden et al. have also demonstrated that CHT in rat synaptosomes were inhibited by a series of various long chain alkyl compounds with various chain lengths.[9] Reversible inhibitors of CHT can provide valuable understanding of the mechanism of Ch transport across the synaptosamal membrane. Potential information can be obtained regarding chemical structure vs. affinity, and structure vs. rate of transport. These studies can lead to insightful information regarding the nature of the binding sites and its microenvironment and relevance of steric effects on the binding sites.

Reversible inhibitors can be classified into three major categories namely competitive, non-competitive and mixed based on the effects on the kinetic constants of the enzyme they exhibit upon binding. In competitive inhibition the substrate and the inhibitor cannot bind to the enzyme simultaneously. The inhibitor binds to the enzyme to form a dead-end complex preventing the binding of the substrate. Competitive inhibitors most often bear a close structural resemblance to the substrate and hence compete for the

enzyme's catalytic site with the substrate. Since the substrate and inhibitor compete with each other for the enzyme's active site, the degree of inhibition depends upon the inhibitor concentration, substrate concentration and relative affinities of the inhibitor and substrate for the enzyme.

The steady state enzyme kinetics for competitive inhibition yields a modified Michaelis Menten equation:[10]

$$v_0 = \frac{V_{max}[S_0]}{[S_0] + K_m\left(1 + [I_0]/\ K_I\right)} \tag{2-3}$$

where $[I_0]$ is the concentration of the inhibitor. $K_I$ is known as the inhibitor constant and it is the dissociation constant for the equilibrium between the enzyme and the inhibitor. Hence for simple competitive inhibition, the maximum initial velocity remains unchanged but $K_m$ is altered to an apparent value $K'_m$ such that $K'_m = K_m\left(1 + [I_0]/\ K_I\right)$

Uncompetitive inhibitors cannot bind to the free enzyme and they bind exclusively to the enzyme substrate complex. Here the inhibitor and the substrate does not compete with each other for the same binding site, rather the binding of the substrate to the enzyme causes some conformational changes which creates a binding site for the inhibitor. The resultant enzyme-substrate-inhibitor complex is a dead end complex. The derived Michaelis-Menten equation in this case has both $K_m$ and $V_{max}$ altered because of the presence of the inhibitor:[10]

$$v_0 = \frac{\frac{V_{max}}{(1 + [I_0]/ K_I)} .[S_0]}{[S_0] + \frac{K_m}{(1 + [I_0]/ K_I)}} \quad (2\text{-}4)$$

Hence in the presence of an uncompetitive inhibitor, both $V_{max}$ and $K_m$ are decreased by a factor of $1 + [I_0]/ K_I$. $(V'_{max} = V_{max}/1 + [I_0]/ K_I)$, $(K'_m = K_m /(1 + [I_0]/ K_I))$ .

A non-competitive inhibitor binds to a site that is different from the substrate binding site and it can bind both to the free enzyme and the enzyme-substrate complex. Binding of the inhibitor results in the formation of a dead-end complex. In the simplest case of non-competitive inhibition, the inhibitor completely destroys the catalytic property of the enzyme.

Under these conditions, the Michaelis-Menten equation sums up to: [10]

$$v_0 = \frac{\frac{V_{max}}{(1 + [I_0]/ K_I)} .[S_0]}{[S_0] + K_m} \quad (2\text{-}5)$$

In non-competitive inhibition, $K_m$ is unchanged but $V_{max}$ is reduced by a factor of $(1 + [I_0]/ K_I)$.

Mixed inhibition is a subset of non-competitive inhibition. Here the inhibitor can bind both to the free enzyme and the enzyme-substrate complex, however binding of the substrate affects the binding of the inhibitor and vice versa. Although in this kind of inhibition, the inhibitor can bind to the catalytic site of the enzyme, most commonly it binds to an allostearic site causing a conformation change in the enzyme that results in a decrease in affinity of the enzyme for the substrate. There are two inhibitor constants in

this case since there are two cases where the inhibitor can bind to the enzyme.

$$E + I \rightleftharpoons EI \tag{2-6}$$

$$K_i = [E]\,[I]\,/[EI] \tag{2-7}$$

$$ES + I \rightleftharpoons ESI \tag{2-8}$$

$$K_I = [ES]\,[I]\,/[ESI] \tag{2-9}$$

The Michaelis-Menten equation in this case is :[10]

$$v_0 = \frac{\dfrac{V_{max}}{\left(1 + [I_0]/\,K_I\right)}.[S_0]}{[S_0] + K_m\dfrac{\left(1 + [I_0]/\,K_i\right)}{\left(1 + [I_0]/\,K_I\right)}} \tag{2-10}$$

There can be two cases, first when $K_I > K_i$, secondly when $K_I < K_i$. The former is referred to as competitive-non-competitive inhibition, while the latter is referred as non-competitive-uncompetitive inhibition because of the similarity in pattern observed in the Lineweaver-Burk plot with such type of mechanisms.

Apart from these simple modes of inhibition, there can exist other special cases such as partially competitive inhibition, allostearic inhibition and slow-tight inhibition which have more complicated mathematical expressions. Since it difficult to predict the precise mechanism of inhibition from kinetic data, it is a common practice to classify inhibitors into different categories simply based on the parameters obtained from primary and secondary plots irrespective of their actual mechanism of action.

Irreversible inhibitors usually react with the enzyme and cause chemical transformation. They cannot be removed by simple dialysis process.

The focus of this chapter is to study the kinetics of Ch uptake by CHT protein and evaluate the inhibitory parameters of a cholinomimetic compound on CHT utilizing a simple bioassay based on analyte separation by CE and quantitative evaluation by amperometric EC. Mouse synaptosome samples in Kerbs Ringer was used for uptake studies for CHT. The model was based on the fact that CHT activity is dependent on sodium ion gradient and action potential in the neurons increase ACh release from synaptic vescicles resulting in enhancement of CHT activity.

## 2.2. Experimental

### 2.2.1. Materials

Choline oxidase (EC1.1.3.17, Alcaligenes species), acetylcholinesterase (EC 3.1.1.7, Type III from electric eel), choline chloride (>98%), glutaraldehyde (grade I, 25% aqueous solution), and butyrylcholine (BuCh) chloride (>98%) were purchased from Sigma (St. Louis, MO, USA) and stored in a desiccator at -16 °C. N-Tris(hydroxymethyl)methyl-2-aminoethanesulfonic acid (TES) (>99%), bovine serum albumin (BSA) (>98%), and Bradford reagent were also purchased from Sigma and refrigerated at 4 °C. Spin X centrifuge tubes with filter, 2 mL were purchased from Sigma.

N,N′-(2,3-dihydroxybenzyl)-N,N,N′,N′,-tetranethyl-1,6-hexanediaminedibromide (DTH) was synthesized by Gu et al.[11] All other chemicals were of reagent grade and used as received. Hard tempered 25 μm diameter platinum wire (99.95%) was obtained from Goodfellow (Berwyn, PA, USA). Solutions were prepared in distilled and deionized

water purified to a resistivity of 17.5 MΩ cm by a Barnstead B-pure water purification system (Dubuque, IA).

### 2.2.2. Instrumentation

Separation and detection of analytes were conducted using a home-built CE instrument coupled with an EC system.[12] An on-column bare fracture decoupler was used for isolation of the separation current from the detection current. The anode contained in the buffer reservoir was housed inside a plexiglass box with safety interlocks to prevent hazards of electrocution. To minimize contribution from external noise the cathode and the detection cell was placed inside a Faraday cage. A conventional three electrode system was used for detection purposes consisting of a Model RE-4 Ag/AgCl reference electrode (BAS, West Lafayette, IN), a platinum (Pt) auxiliary (counter) electrode and a Pt ME modified with enzymes as the working electrode. The enzyme ME tip was carefully aligned with the capillary outlet to optimize physical contact with the flowing liquid at the end of the capillary and minimize disruption of the enzyme layer. The anode and cathode were connected to a high voltage power supply by high standard cables. A BAS LC-4C amperometric detector interfaced with the electrophoretic system was used for controlling detection potential and monitoring current signal. Data was collected by an IBM P166 MHz computer through an A/D converter and analyzed with P/ACE MDQ Capillary Electrophoresis System Software (Beckman Scientific Instruments, Fullerton, CA). Figure 2-1 represents the schematic of the CE-EC instrument utilized for the experiments.

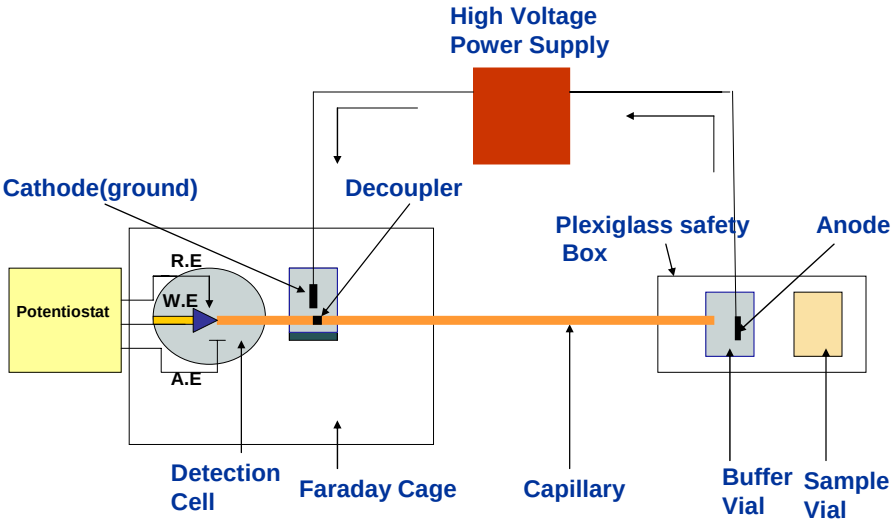


**Figure 2-1.** Schematic of the capillary electrophoresis instrument with electrochemical detection.

### 2.2.3. Methods

#### 2.2.3.1. Preparation of Microelectrodes

25 μm Pt wire was cleaned prior to use. The wires were cleaned first by sonication in a 1:1 (v/v) mixture of deionized water and Micro-90 soap (International Products, Burlington, NJ) for 10 minutes, followed by sonication in 1 M NaOH for the same amount of time. The wires were then thoroughly washed with deionized water. They were then cut into 1 cm pieces, fixed to a ~ 10 cm Cu wire (22 gauge) with colloidal nickel print (Ted Pella, Reddinf CA) and dried in a vertical position for ~ 1 hour. The wires were then housed inside glass capillaries (KIMAX # 34500, 1.5-1.8 by 100

mm) with ~ 0.2 cm of the Pt wire extending from the glass. The glass capillary end containing the Pt wire was sealed with UV glue (UVEXS, CA). The glue was applied by capillary action and allowed to cure under a UV lamp for ~ 3 hours. The capillary end containing the Cu wire was sealed with hot glue. The entire housing was secured with a truncated pipette tip using hot glue. The schematic representation of a ME is depicted in Figure 2-2.

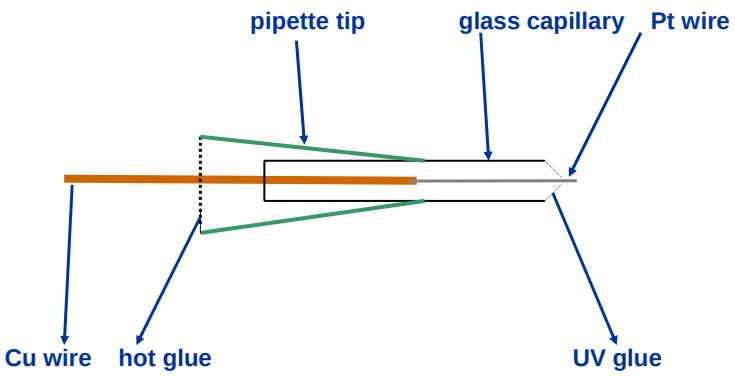


**Figure 2-2.** Schematic representation of a ME.

### 2.2.3.2. Immobilization of Enzymes on Microelectrode Surface

In this study, enzymes were immobilized on the ME surface by a previously developed method.[13] Prior to enzyme immobilization, the electrode surface was cleaned by copious rinsing with deionized water, acetone followed by deionized water again. 0.34 mg (~ 4 units) of ChO was weighed carefully in a conical vial and 7.25 µL AChE

solution (~ 7 units) was added to it. 0.5 µL of 25 % glutaraldehyde solution was added to the enzyme mixture to initiate the cross linking process. During this process the pale yellow solution turned cloudy as the carbonyl groups of glutaraldehyde reacted with the free amine groups of the enzymes to form a cross linked polymer. At this time the Pt ME tip was dipped repeatedly into the enzyme mixture such that the crosslinked polymer physically adsorbed onto the Pt surface. The same solution mixture was used to coat 4-5 electrodes. After immobilization the electrodes were kept at ambient temperature for 30 minutes before use.

**2.2.3.3. Preparation of the Capillary**

80 cm polyimide coated fused silica capillary (I.D. 50 µm, O.D. 350 µm, Polymicro Technologies, Phoenix, AZ, USA) was used for conducting all capillary electrophoretic separations. TES (50 mM, pH 8) was used as the run buffer for all CE separations. Prior to use, the capillary was conditioned with 1 M HCl (10 min, 25 psi) to suppress electroosmotic flow, followed by $H_2O$ (10 min, 25 psi), and finally rinsed with TES (30 min, 25 psi). When not in use the capillary was rinsed and filled with water. The enzyme microelectrode tip was carefully aligned with the capillary outlet by placing both the electrode and the capillary inside a custom made detection cell (Allied Plastics, Toledo, OH, USA).[14] Alignment in this manner optimized physical contact with the flowing liquid at the end of the capillary and minimized disruption of the enzyme layer. To prevent denaturing of the enzymes and damage to the detector electrode, the electrode was aligned to the capillary after conditioning the column. The distance from the decoupler to the capillary outlet was ~ 2.5 cm. Electropherograms were generated by

applying 17 kV separation voltage with a Spellman CZ100R high-voltage power supply (Spellman, Plainview, NY). The separation current during operation ranged from 4 to 20 μA. Samples were injected by pressure injection using high purity argon at 5 psi for 2 s corresponding to an injection volume of ~ 12.5 nL.

#### 2.2.3.4. Calibration Plots

Standard stock solutions of Ch and butyrylcholine (BuCh) were prepared fresh daily and stored in ice. Ch concentrations were analyzed using BuCh as an internal standard. For analysis Ch and BuCh were mixed in 2:1 ratio by volume to give a final concentration of 25 μM of BuCh. Samples were analyzed by CE in triplicate. Calibration plots were generated by plotting the ratio of the peak areas of Ch to the internal standard BuCh versus Ch concentrations ranging from 0.5 to 10 μM.

#### 2.2.3.5. Preparation of Mouse Synaptosomes

Synaptosome preparation was accomplished by the method of Gray and Whittaker as modified by Patel.[15,16] Adult male mice (C57BL6, Harlan Sprague-Dawley, Indianapolis, IN) were sacrificed by cervical dislocation. Their forebrains were removed, rinsed in chilled 0.32 M sucrose at pH 7.4 (adjusted by tris buffer). The tissue was homogenized and suspended in 10 volumes of chilled 0.32 M sucrose. The homogenate was centrifuged at 2,400 rpm for 10 minutes at 4 °C and the pellet was discarded. The supernatant was then centrifuged at 14,000 rpm for 20 minutes and the resultant supernatant was discarded. The pellet was resuspended in sucrose solution and centrifuged for another 20 minutes at 14,000 rpm and the supernatant was discarded. The

resultant pellet was resuspended in 5 volumes Krebs-Ringer phosphate buffer (124 mM NaCl, 5 mM KCl, 1.2 mM $Na_2HPO_4$, 1.2 mM $NaH_2PO_4$, 1.3 mM $MgSO_4$, 0.75 mM $CaCl_2$, 10 mM glucose, aerated with $O_2$ for 2 minutes, adjusted to pH 7.4 by 1 M NaOH ). The schematic of this procedure is representated in Figure 2-3. This resultant solution contained synaptosomes and was used for further experiments. The protein content of the crude synaptosome suspension was measured by the method of Bradford.[11]

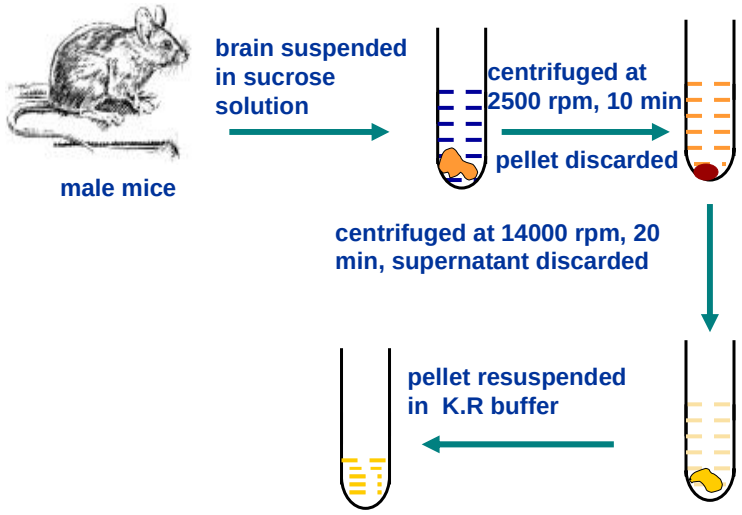


**Figure 2-3.** Schematic of the procedure of preparation of synaptosomes from mice.

### 2.2.3.6. Measurement of Choline Uptake in Synaptosomes

Incubation of synaptosomes was performed at 37 °C using an Isotemp Model 125D Digital Dry Bath Incubator from Fischer Scientific. A range of standard Ch solutions from 1 to 15 µM was used for the studies. Varying concentrations of standard solutions of DTH were prepared ranging from 10 to 3000 µM, which corresponded to a final concentration range of 2.7 to 815.6 µM after addition to the synaptosomal

preparation. 300 µL of synaptosomal solution and 112 µL of stock Ch (or choline and inhibitor, DTH) were equilibrated at 37 °C. Starting from the beginning of incubation (t = 0 min.), subsequent 75 µL aliquots were taken from the resultant solution. Aliquot collection was restricted to the first four minutes to minimize the effect of aging of the synaptosomes. The collected samples were centrifuged at 1000 g for 8 minutes at 4 °C and then stored at -20 °C until analysis. The incubation protocol of synaptosomes with Ch is represented in Figure 2-4.

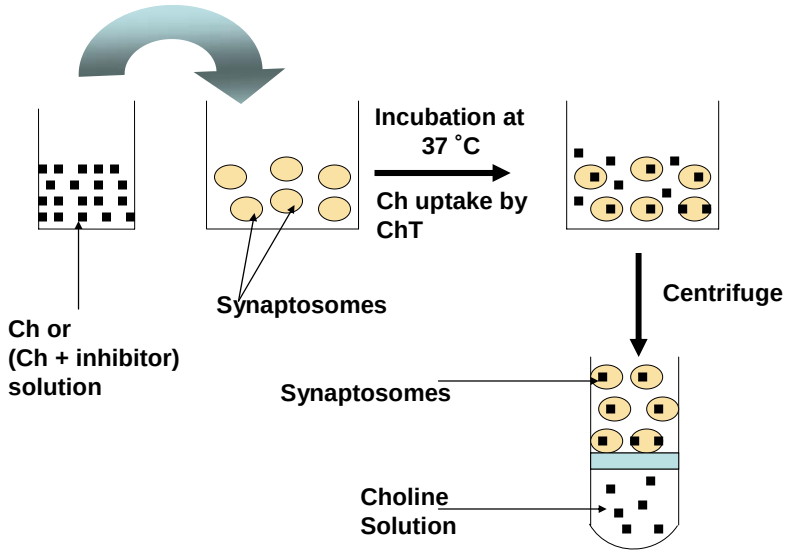


**Figure 2-4.** Schematic of incubation protocol of synaptosomes with Ch solution.

For analysis BuCh solutions were prepared fresh daily and stored in ice. Aliquots of supernatant sample and BuCh were mixed in 2:1 ratio by volume to give a final concentration of 25 µM of BuCh. Samples were analyzed by CE in triplicate.

### 2.2.3.7. Measurement of Protein Concentration

The protein concentration in synaptosome samples were determined by the method

of Bradford. [17] The Bradford assay utilizes Coomassie Brilliant Blue G-250 dye and is based on the principle that there is a shift in absorbance from 465 nm to 595 nm due to binding of the dye with arginine, tryptophan, tyrosine, histidine and phenylalanine residues in proteins. BSA was used for the standard plot. Different concentrations of standard stock solution of BSA were made ranging from 6 to 36 µg/mL and a calibration plot was obtained. The unknown concentration of protein in the sample was determined by the linear equation obtained from the standard plot.

## 2.3. Results and Discussion

### 2.3.1. Electrode Modification with Enzymes

After immobilization of enzymes onto the Pt ME, a change in morphology of the electrode surface was visible to the naked eye. In addition, magnified images of enzyme modified MEs were also visualized by a stereomicroscope. Stereomicroscopic images of unmodified electrodes revealed a well defined metallic surface for the Pt electrode tip. Modification with enzymes formed a translucent porous layer, uniformly coating the electrode surface. This layer was a chemically crosslinked copolymer of AChE and ChO, that was physically adsorbed onto the Pt ME surface. Figures 2-5a-b represents the stereomicroscopic images of bare and modified Pt MEs.

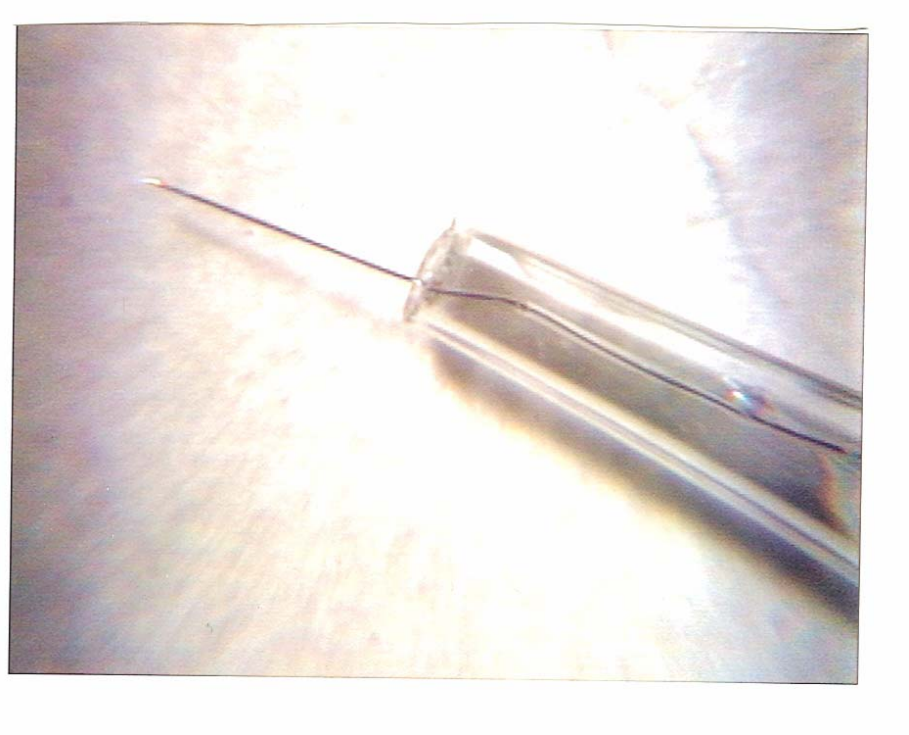

**Figure 2-5a.** Stereomicroscopic image (40x) of a bare Pt ME.

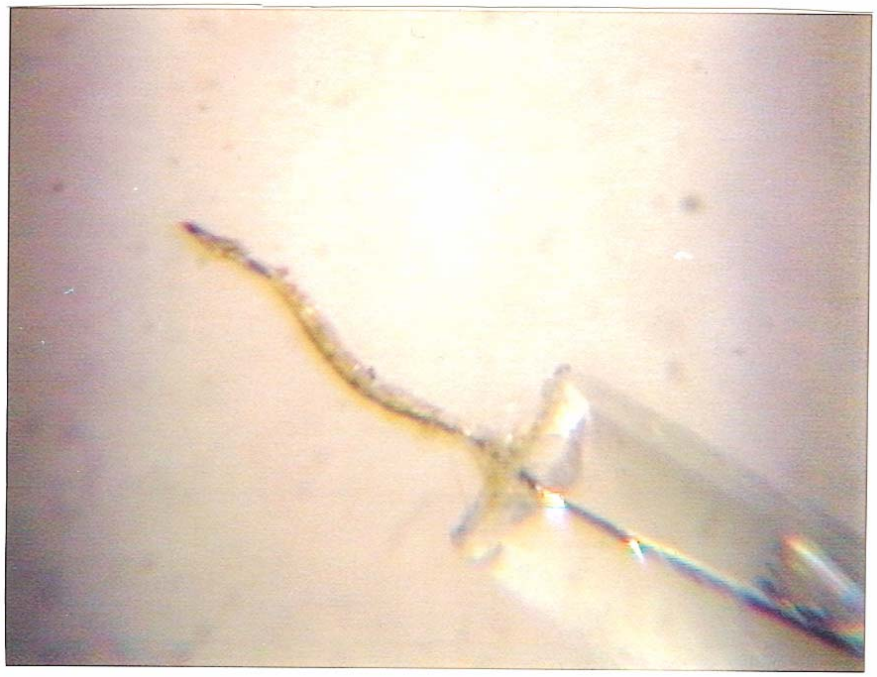

**Figure 2-5b.** Stereomicroscopic image (50x) of an enzyme coated Pt ME.

### 2.3.2. Calibration Plots

Before studying the kinetic aspects of the CHT, calibration plots were generated using the MEs to check the suitability of application of these electrodes towards studies in appropriate concentration ranges. Mixtures of standard stock solutions of Ch (0.5 to 10 μM) and BuCh (held constant at 25 μM) were injected into the CE instrument and electropherograms were generated. Calibration plots were obtained by plotting the ratio of the peak area of Ch to BuCh versus the Ch concentration used. There is a gradual decrease in sensitivity of these electrodes due to physical loss of enzymes from electrode surface as a result of the hydrodynamic conditions of their operation with the CE. Hence to compensate for such loss and to ensure accuracy of measurement BuCh was employed as an internal standard. The stability and performance of these MEs have been studied in great detail by Wise.[14] Electropherograms of standard solutions were injected at a random fashion to minimize systematic error. Measurement for each concentration was performed in triplicate. Three different MEs were used. The response of Ch was linear in the studied concentration range. The sensitivity of the electrodes was determined from the slope of the calibration plots. Sensitivity was different for each electrode. The sensitivity of the electrodes ranged from 0.041 to 0.056 units/μM Ch. Figure 2-6 represents the generated calibration plots.

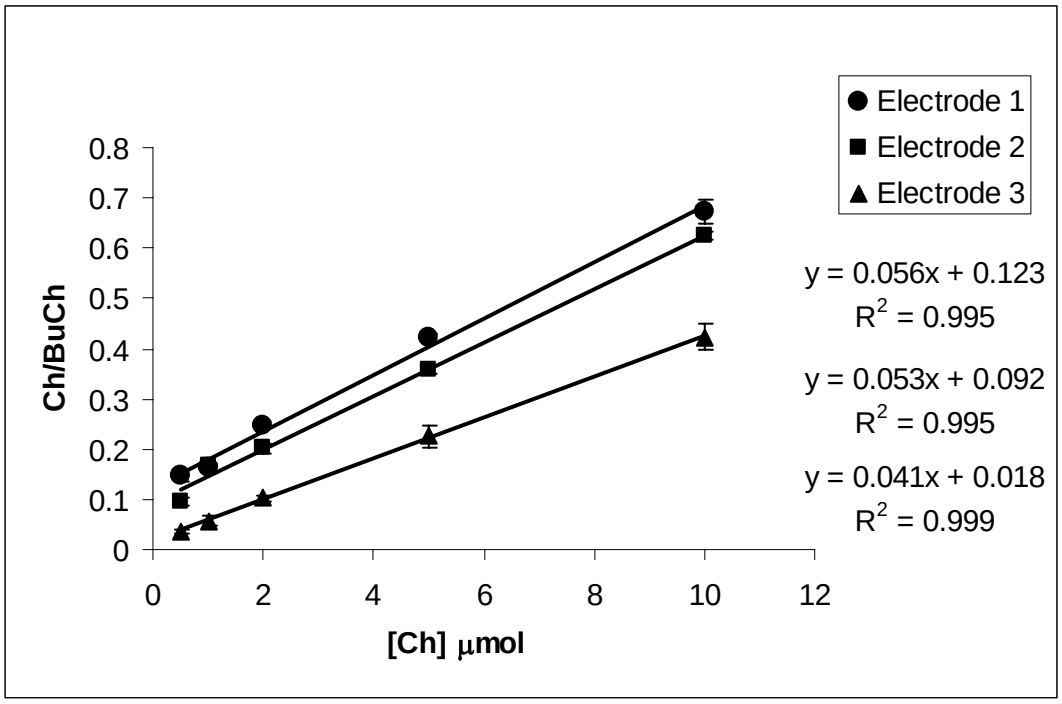


**Figure 2-6**. Calibration plots for Ch from 0.5 to 10 μM using 25 μM of BuCh.

This difference in sensitivity is probably due to the fact that electrodes were manually coated with the enzymes. The enzymes adsorbed onto the electrode surface in a random fashion as the cross linking process was initiated. The alignment of the ME tip with respect to the capillary end is also an important factor in determining the sensitivity of the electrode. A good alignment, where the ME tip is in optimal contact with the capillary outlet results in sharper amperometric peaks. Poor alignments result in broad, weak signals with comparatively poor reproducibility. The slope of the calibration plot depends on the mode of contact of the sensing system with the capillary outlet which is governed by the alignment of the ME with the capillary outlet.

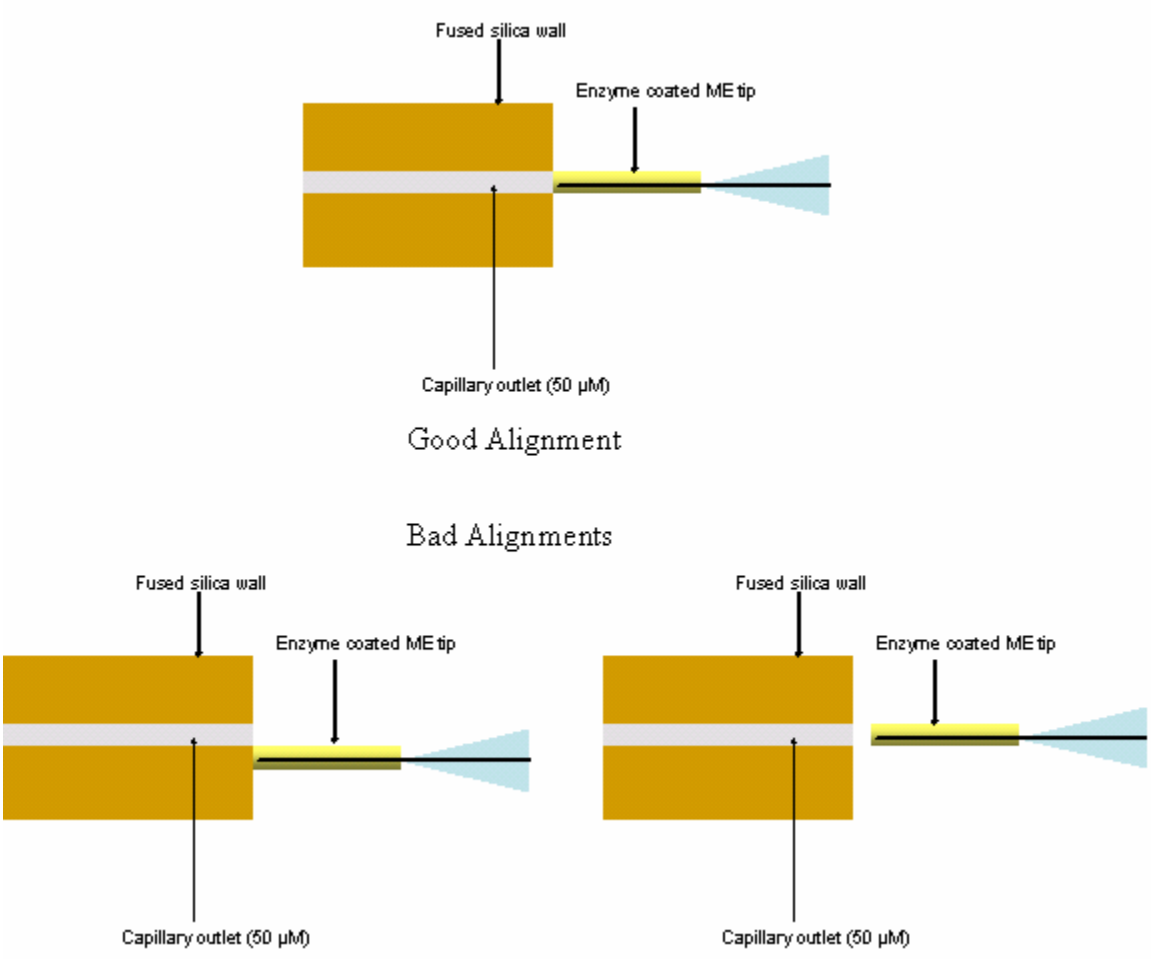


**Figure 2-7.** Various modes of the alignment of the electrode with the capillary outlet. Bad alignment results in decreased sensitivity.

Figures 2-8a-b represents the electropherograms generated by injection of standard solutions of Ch employing BuCh as an internal standard.

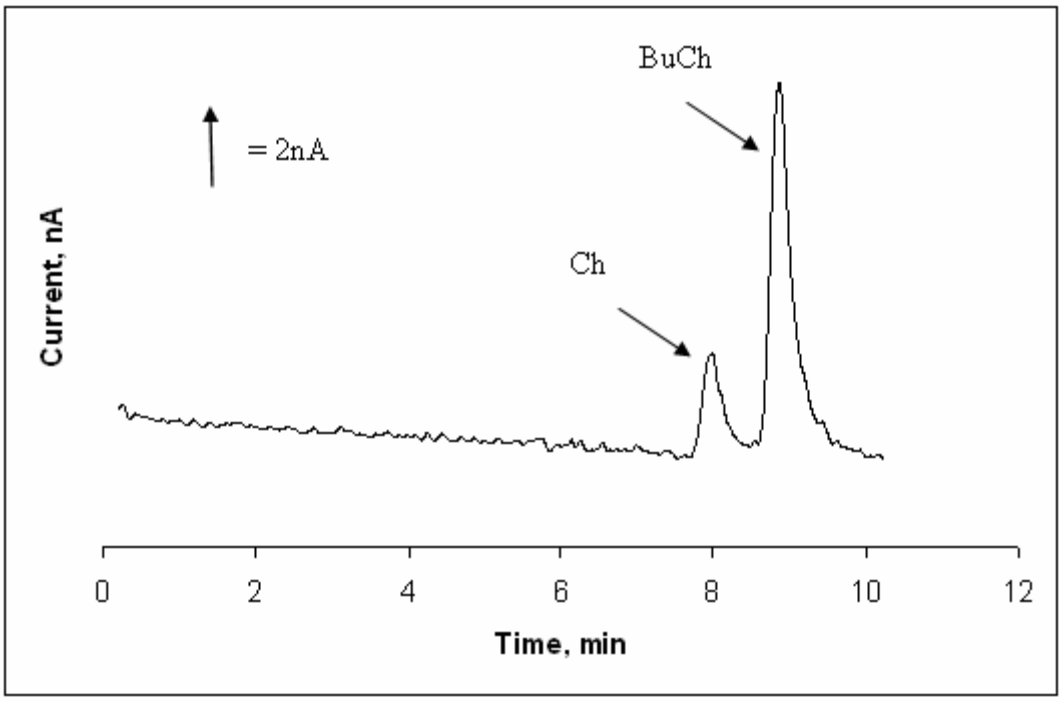


**Figure 2-8a.**

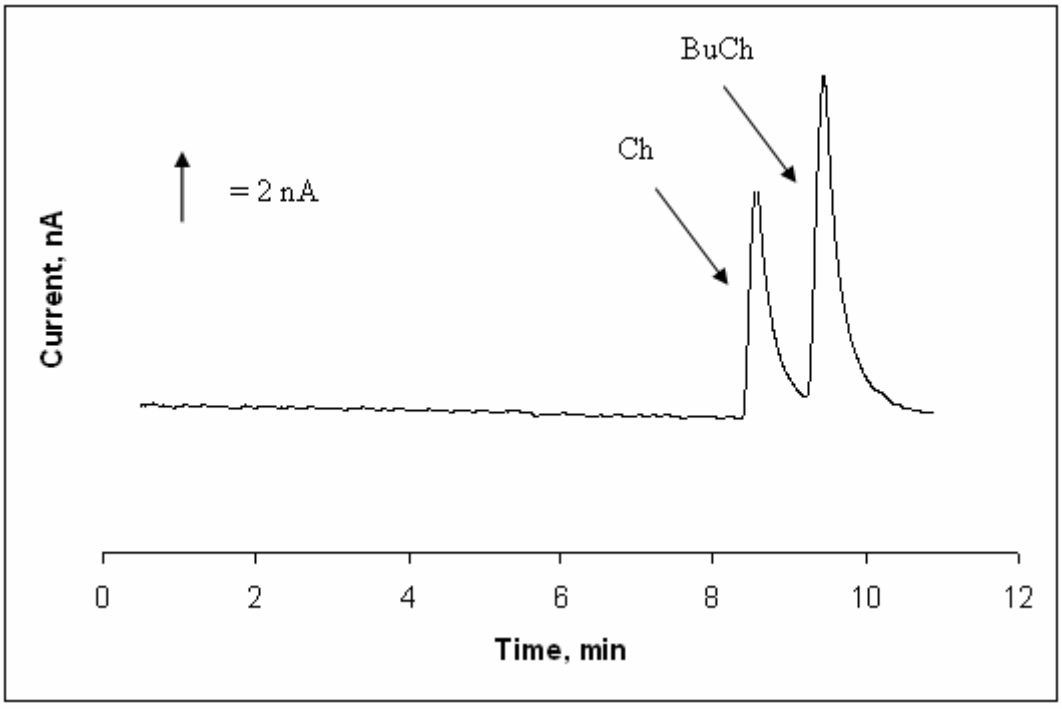


**Figure 2-8b.**

**Figure 2-8.** Electropherograms of standard solution of Ch and BuCh. a: Ch (2 µM), BuCh (25 µM); b: Ch (10 µM) and BuCh (25 µM). Run buffer = 50 mM TES pH 8.0; detection potential = +0.650 V vs. Ag/AgCl; separation voltage = 17 kV.

Electrophoretic separation is governed by the charge to size ratio of the analytes. Ch and BuCh bear unit positive charge, however the functional side chain of BuCh is longer than Ch by 3 carbon atoms. Hence the migration time of Ch is shorter than BuCh.

### 2.3.3. Ch Uptake by Synaptosomes

The uptake of Ch by synaptosome samples were studied for Ch concentrations ranging from 1 to 15 μM. The initial rates of Ch uptake for the first 4 minutes were plotted versus Ch concentrations because of negligible Ch efflux in this time scale.[18] Figure 2-9 represents the response of Ch uptake in synaptosome samples.

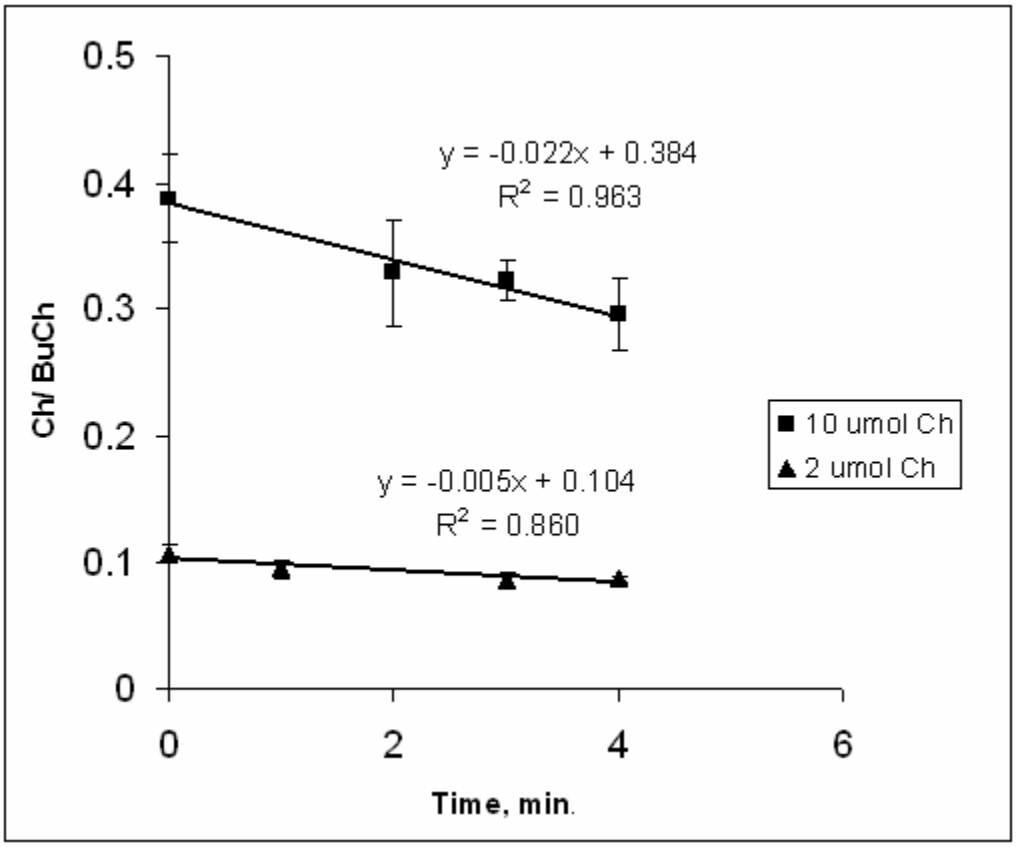


**Figure 2-9.** Ch uptake plot for supernatant sample from synaptosomes incubated with 2 μM (▲) and 10 μM (■) Ch. Protein concentration are 2.4 and 8.1 mg/mL, respectively.

A negative slope was obtained for all concentrations. Since the supernatant Ch solution obtained after centrifugation was analyzed, the Ch that was not taken in during the incubation process was detected. This indicated that the concentration of Ch in the resulting supernatant solution decreased with an increase in incubation time during the time frame of the experiment. Hence, Ch influx increased with increase in incubation time. In order to compare the results from different synaptosomal preparations, the rate of Ch uptake was determined from the slope of the plot normalized by the protein concentration of the synaptosomal preparation. The rate of Ch uptake was found to be directly proportional to the concentration of Ch used during incubation implying that the uptake process is substrate dependent. Figures 2-10a-b represent electropherograms generated from supernatant sample of synaptosome solutions.

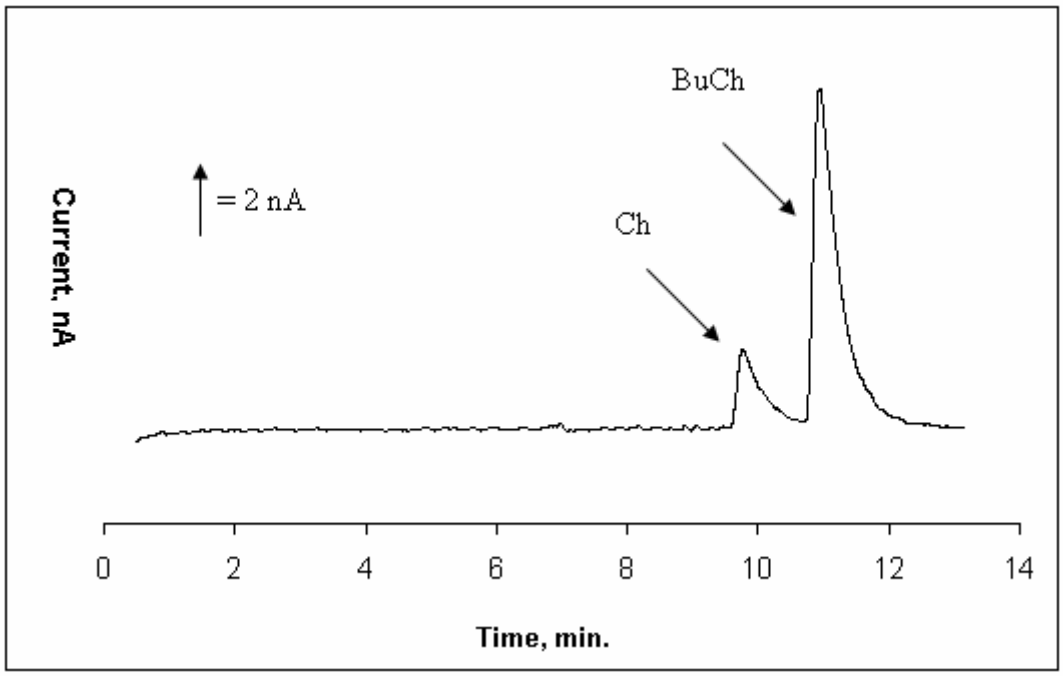


**Figure 2-10a.** Electropherogram of supernatant sample from synaptosomes incubated with 2 μM Ch using 25 μM BuCh for analysis. Run buffer = 50 mM TES; detection potential = +0.650 V vs. Ag/AgCl; separation voltage = 17 kV.

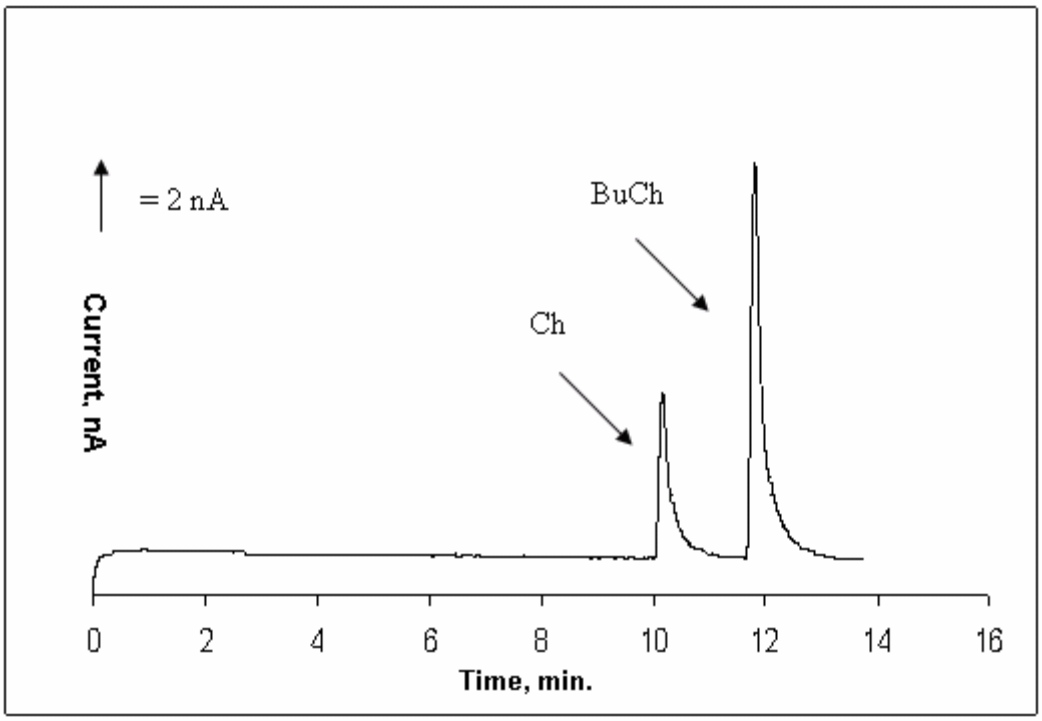


**Figure 2-10b.** Electropherogram of supernatant sample from synaptosomes incubated with 10 µM Ch using 25 µM BuCh for analysis. Run buffer = 50 mM TES; detection potential = +0.650 V vs. Ag/AgCl; separation voltage = 17 kV.

The electropherograms generated from standard Ch solutions, (2-8a-b) and those generated from supernatant samples of incubated synaptosomes (2-10a-b) were indistinguishable. This indicates that either no other electroactive biomolecules were present in the synaptosome preparation or the detection method employed was highly specific and eliminated all possible interferences. It can also be observed that the amperometric signal of electropherogram (2-10b) was sharper than that of (2-8b). This discrepancy could be attributed to the difference in alignment and thickness of enzyme layers on the electrode surface.

### 2.3.4. Protein Concentration

In order to compare results obtained from different synaptosomal preparation, the Bradford dye assay was used to estimate the total protein concentration in synaptosomes.[17] Since the Coomassie Brilliant Blue binds to all proteins; there is no unique method of determining the exclusive CHT concentration. A representative calibration plot for the Bradford assay is depicted in Figure 2-11.

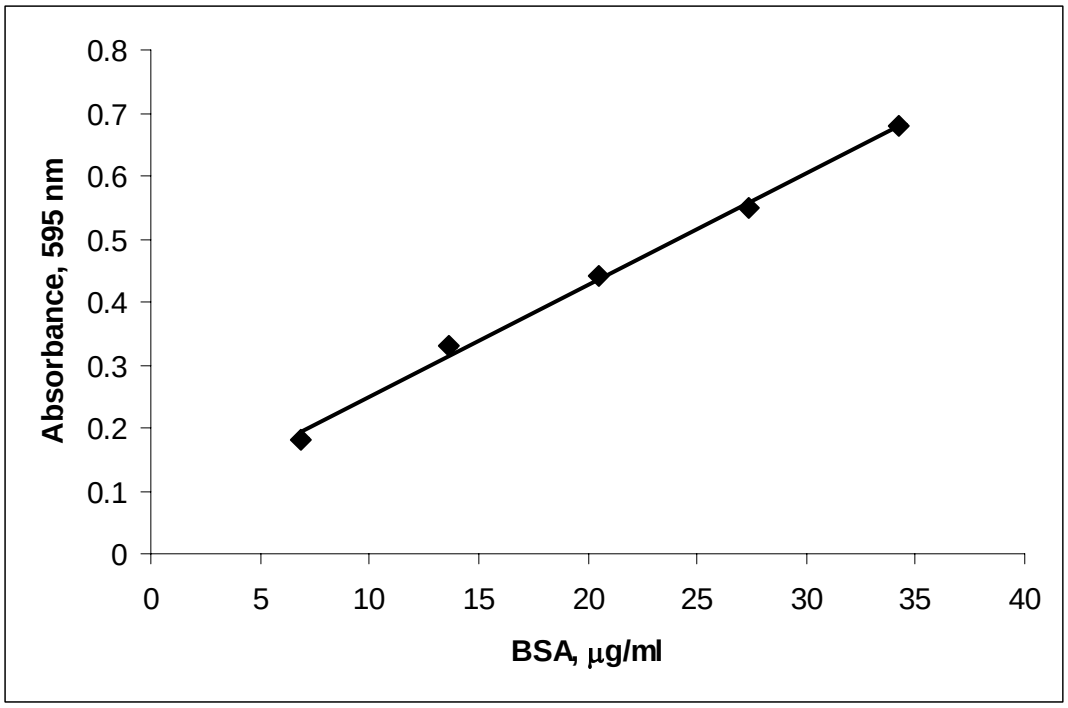


**Figure 2-11.** Representative Bradford assay calibration plot for BSA concentrations from 6 to 36 μg/mL. Error bars are too small to be seen.

### 2.3.5. Evaluation of the Kinetic Parameters of CHT

#### 2.3.5.1. Michaelis-Menten Plot

The initial rates of Ch uptake in synaptosomes were plotted as a function of Ch

concentration and represented in Figure 2-12. An initial increase in rate with increase in substrate concentration was observed for lower Ch concentrations. A saturation of rate of Ch influx was observed at higher substrate concentrations. This indicated that Ch uptake by CHT indeed followed Michaelis-Menten type kinetics. Uptake of Ch in synaptosomes could have been due to both CHT and LACHT since both the proteins are known to be present in brain. However since CHT has a much greater affinity for Ch, low Ch concentrations were used to minimize the contribution from LACHT. The rate of Ch uptake obtained for 15 μM Ch was higher than expected, probably because of substantial multiple uptake mechanisms by CHT, LACHT and non specific adsorption at this concentration. A Ch concentration lower than 1 μM was not utilized as it was challenging to measure such subtle changes. Since peak area ratios of Ch to BuCh were evaluated for determining the uptake rate, the change in peak area ratio (which is proportional to change in Ch concentration) is referred as units.

**Table 2-1.** Normalized Initial Rates of Ch Uptake in Mice Synaptosome Samples

| Ch, μM | Rate of Ch Uptake , units/min. mg protein |
|---|---|
| 1 | $1.63 \pm (0.35) \times 10^{-3}$ |
| 2 | $2.05 \pm (0.19) \times 10^{-3}$ |
| 4 | $2.36 \pm (0.08) \times 10^{-3}$ |
| 6 | $2.52 \pm (0.11) \times 10^{-3}$ |
| 8 | $2.60 \pm (0.14) \times 10^{-3}$ |
| 10 | $2.62 \pm (0.31) \times 10^{-3}$ |
| 15 | $2.95 \pm (0.19) \times 10^{-3}$ |

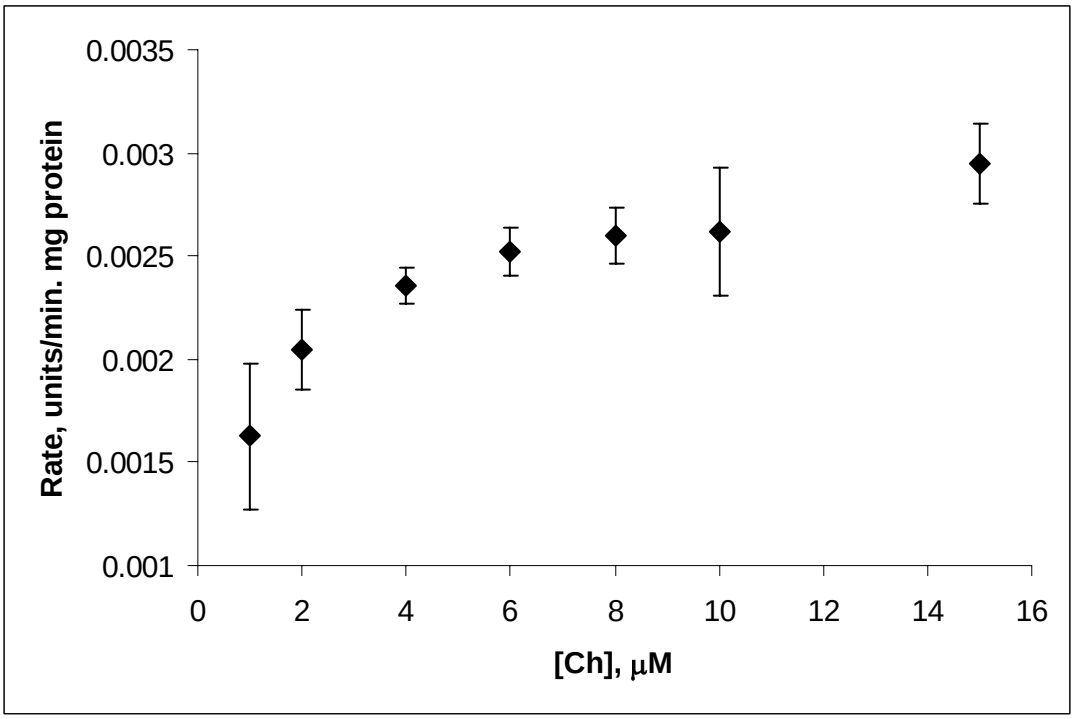


**Figure 2-12.** Michaelis-Menten plot for high affinity uptake of Ch at 37 °C.

### 2.3.5.2. Lineweaver-Burk Plot

Once the Michaelis-Menten plot for CHT was obtained, Lineweaver-Burk plots for CHT were readily generated by plotting 1/rate versus 1/[Ch] as represented by Figure 2-13. A Lineweaver-Burk plot offers a convenient method of calculating the Michaelis constant, but since the reciprocal of the substrate has to be used, values of initial rate obtained from lower substrate concentrations becomes more significant. This is a particular disadvantage as the points on the plot at high substrate concentrations tend to cluster together, and the overall slope becomes heavily dependent on values obtained at lower substrate concentrations where probability of error in measurement is higher. However, a remarkable linear relationship was obtained with $R^2$ value of 0.999. The $K_m$ for CHT calculated from the slope of the plot was 0.79 μM. This value is well within the

range of cited literature value of CHT from other analysis methods, thus demonstrating the reliability of this method.[19] The CHT $K_m$ value established previously using this assay are 0.86 and 1.7 μM.[8,20] These values are in close correlation considering that the reported $K_m$ values for CHT range from 0.5-10 μM.[19]

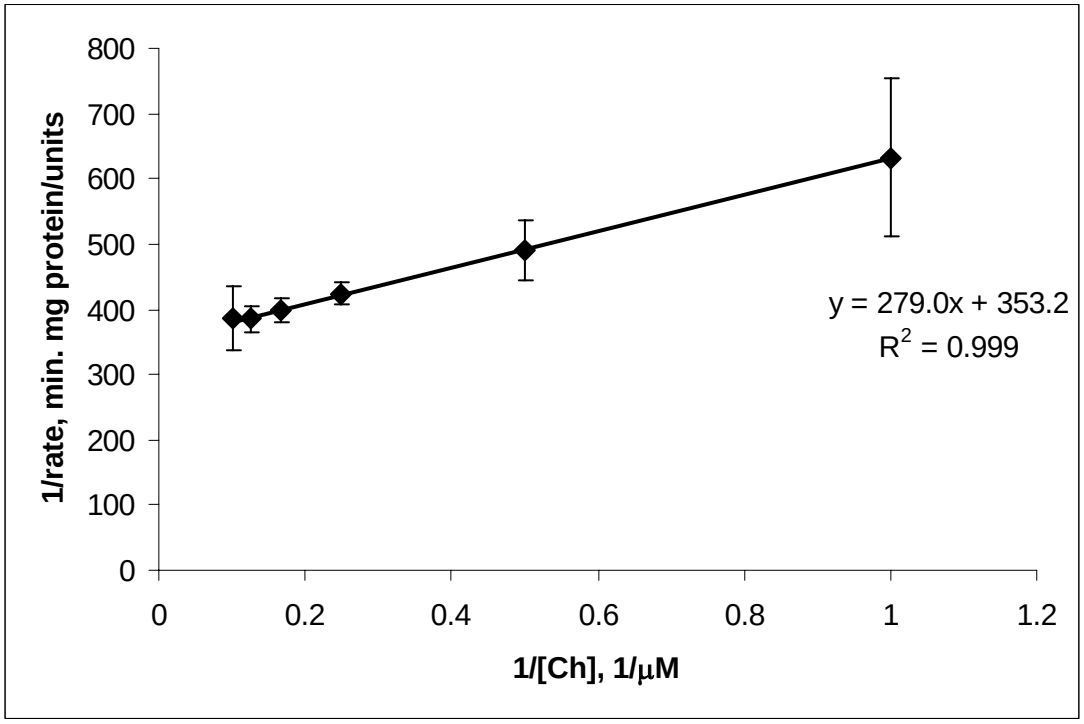


**Figure 2-13.** Lineweaver- Burk plot for high affinity uptake of Ch at 37 °C.

### 2.3.6. Evaluation of the Inhibitory Effects of CHT by N,N´-(2,3-dihydroxybenzyl)-N,N,N´,N´-tetramethyl-1,6-hexanediamine bromide (DTH)

Understanding selective degeneration of cholinergic processes is essential in evaluating degenerative disorders of neuronal dysfunction. Structure activity relationships suggest that the CHT has several points of interaction for which the presence of a quaternary nitrogen atom with a neighboring hydroxyl group is an essential

prerequisite.[21] Studies have shown an increased affinity with an increase in the compound's hydrophobicity.[19]

The structure of DTH is represented in Figure 2-14. As DTH is characterized by two quaternary nitrogen atoms each neighboring a hydroxyl group and separated by a hydrophobic region, the possibility of any inhibition by DTH on Ch uptake was studied to obtain insightful information regarding Ch uptake mechanisms and structure-activity relationships of cholinergic binding sites.

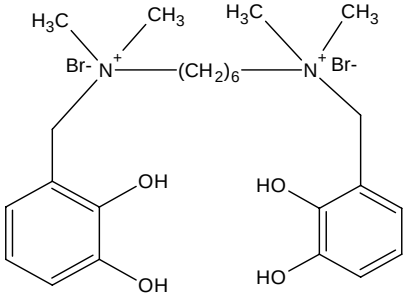


**Figure 2-14.** Structure of DTH

### 2.3.6.1. Dose Response Curve

Concentration dependent inhibition of Ch transport by DTH was established from the dose response curve. The Ch concentration was fixed at 2 μM. The plot of initial rate of Ch uptake versus log [DTH] is represented in Figure 2-15. The $IC_{50}$ value of DTH was evaluated from the plot using Delta Graph version 5 software (Red Rock Software). The dose response curve was fitted to an equation : rate = A - m($10^x$) / ($10^x$ + $10^K$ ) , where x = log (inhibitor), K = log($IC_{50}$), A = extrapolated rate of Ch uptake in the absence of inhibitor, m = A - (lowest rate observed in the presence of inhibitor).

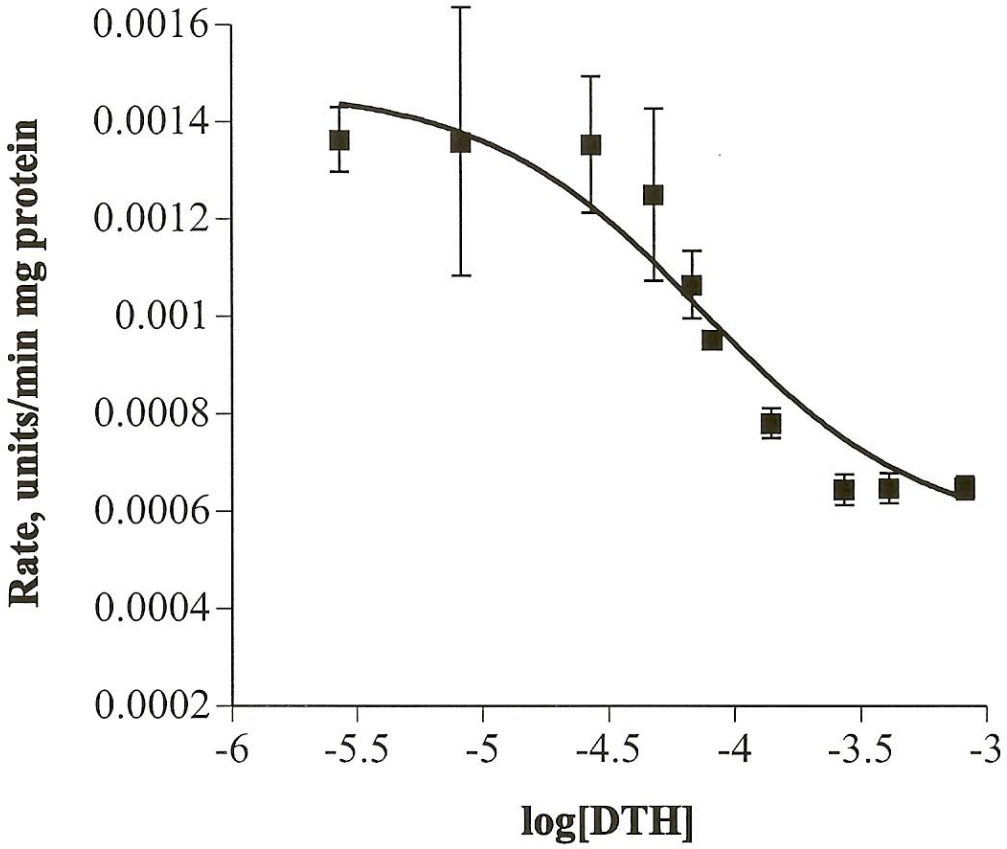


**Figure 2-15.** Plot of the initial rate for Ch uptake corrected for protein concentration at 37 °C versus log [inhibitor] for concentrations of DTH ranging from 2.7 to 815.6 μM. The Ch concentration was fixed at 2 μM. Each data point on the curve is the average rate of Ch uptake determined from three synaptosome preparations, each of which was analyzed in triplicate.

The $IC_{50}$ for DTH was determined to be 76 μM. It is important to note that the rate of Ch uptake does not decrease to zero even at high inhibitor concentrations. This work is complementary to an effort by previous group members to probe the inhibitory effects of various quaternary ammonium catechol based molecules.[8,20] The dose response curve offers the convenience of comparing the relative inhibitor potencies of multiple inhibitors for the same enzyme, but as the $IC_{50}$ values of inhibitors is also dependent on

the concentration of substrate used during the assay, [22] a fixed concentration of Ch was used for all studies for ease of comparison of inhibitor potency based on their structure.

### 2.3.6.2. Multiple Lineweaver Plots for DTH

Once the $IC_{50}$ value for DTH was determined, it was interesting to evaluate the mode of inhibition by this inhibitor. The assay was performed in a similar manner and multiple Lineweaver-Burk plots were generated at several fixed inhibitor concentrations, with the Ch concentration ranging from 2 to 10 μM as represented in Figure 2-16. Addition of DTH caused a change in both $K_m$ and $V_{max}$ which is consistent with a mixed inhibition mechanism. The result obtained is readily understood by the fact that DTH has two quaternary nitrogen atoms with neighboring hydroxyl groups that probably enabled it to interact with the Ch binding site on the protein. The long alkyl chain also probably had some additional interaction with the proposed hydrophobic region in CHT, [19] resulting in mixed inhibition.

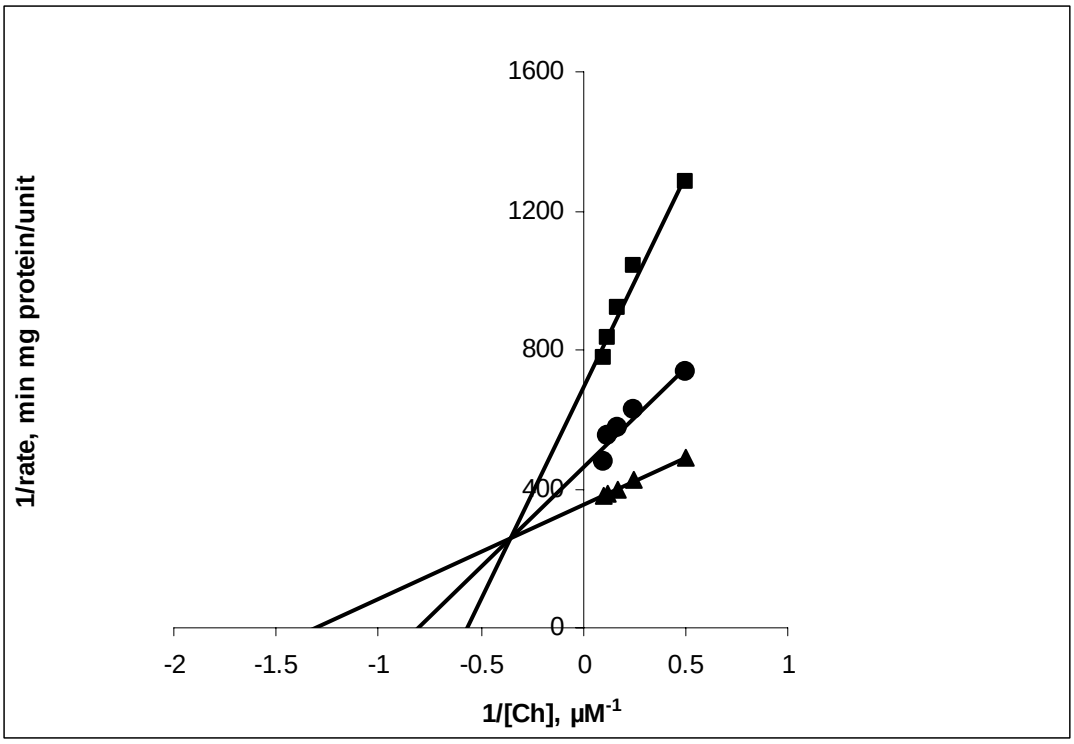


**Figure 2-16.** Double reciprocal plots for the rate of Ch uptake as a function of Ch for three different inhibitor concentrations 0 (▲), 27.2 (●), and 136 (■) μM. Each data point is the average rate of Ch uptake determined from three different synaptosome preparations analyzed in triplicate. Error bars were removed for clarity of presentation. The average error was determined to be 9 %.

### 2.3.6.3. Dixon Plot for DTH

The assay was further used to determine the $K_I$ value of DTH by the method of Dixon.[23] The Ch concentration was held constant at several fixed inhibitor concentrations and Dixon plots were generated by plotting 1/rate of Ch uptake as a function of inhibitor concentrations as shown in Figure 2-17. The point of intersection of the three lines determined the value of $K_I$. The $K_I$ for DTH was calculated to be 73.33 ± 0.62 μM.

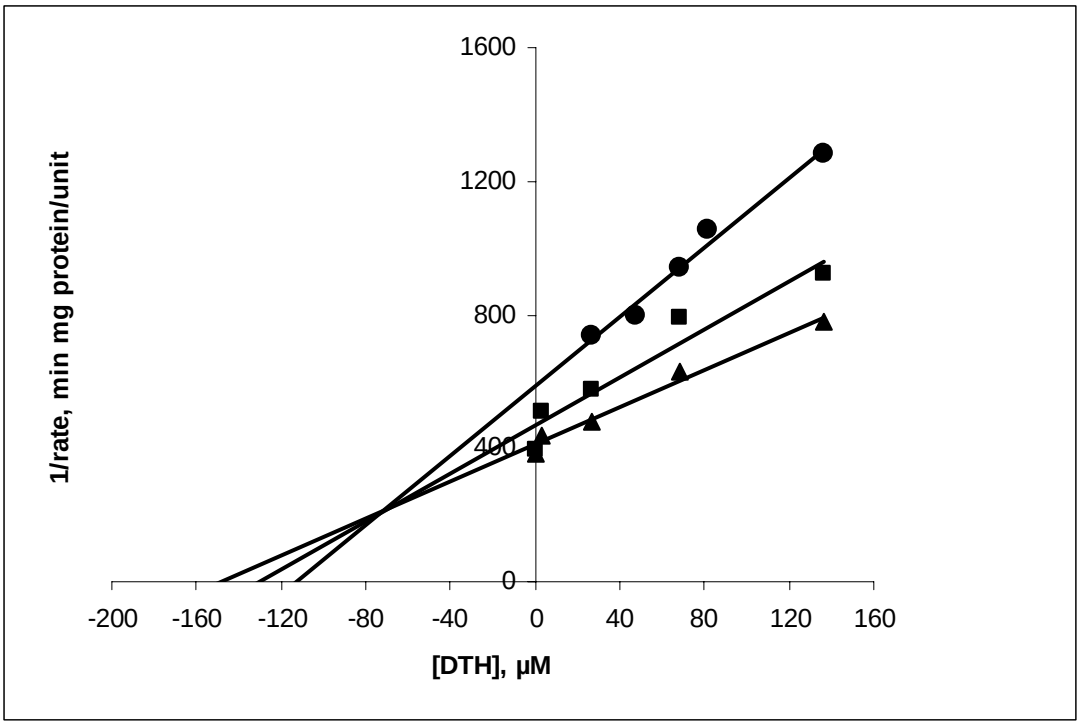


**Figure 2-17.** Dixon plots for the rate of Ch uptake as a function of DTH concentrations for three different Ch concentrations, 2 (●), 6 (■ ), 10 (▲) µM. Each data point on the curve is the average rate of Ch uptake determined from three different synaptosome solutions, each analyzed in triplicate. Error bars were removed for clarity of presentation. The average error for DTH was 7%.

**Table 2-2.** Comparison of Kinetic Parameters of DTH with Other Structurally Close Inhibitor Molecules Evaluated Using the Same Assay.

| | | |
|---|---|---|
| 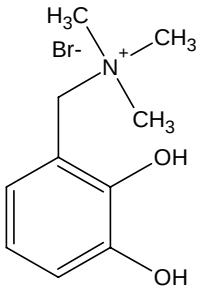 | 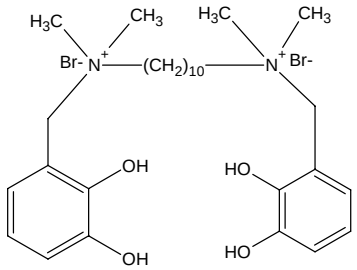 | 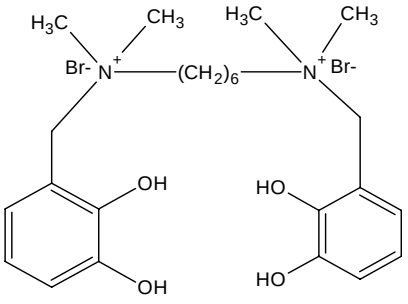 |
| TMC[8]<br>$IC_{50}$ = 28 µM<br>$K_I$ = 17 µM<br>Non Competitive | DTD[20]<br>$IC_{50}$ = 21 µM<br>$K_I$ = 31µM<br>Mixed | DTH<br>$IC_{50}$ = 76 µM<br>$K_I$ = 73 µM<br>Mixed |

In order to elaborate on the kinetic aspects of inhibitory effects of DTH on CHT, the inhibitory parameters of two other cholinomimetic compounds bearing structural analogy with DTH and evaluated using the same assay are compared in Table 2-2.

Comparison of the $IC_{50}$ value of DTH that structurally differs from DTD by an alkyl chain shorter by 4 carbon atom suggest that 21 μM of DTD produced the same degree of inhibition as 76 μM of DTH. TMC which consists of only the catechol analogue without the alkyl chain is a much potent inhibitor. A close look at the $K_I$ and $IC_{50}$ values of DTH and DTD suggest that the difference in their inhibitory effect can be compared as a function of the number of carbon atoms in the alkyl chain. A hypothetical two dimensional binding site as proposed by Lockman and Allen and depicted in Figure 2-18 suggests that there is a hydrophobic domain close to the Ch binding site.[19] A high $K_I$ value of DTH compared to DTD may be logically argued with the fact that the longer alkyl chain of DTD is capable of much stronger hydrophobic interactions in the lipophilic domain of CHT. Hence binding interactions of DTH may be a combination of weak and partial hydrophilic interaction of its catechol and quaternary nitrogen functionality with the Ch binding sites along with weak hydrophobic interactions of its intermediate alkyl chain with the lipophilic domain of the protein. This logic is also consistant with the fact that both DTH and DTD interact with CHT via a mixed inhibition mechanism. TMC on the other hand is a more powerful inhibitor probably because it is capable of unique and stronger interactions with both the hydroxyl bonding region and the methyl interaction region of the quaternary N atom group.

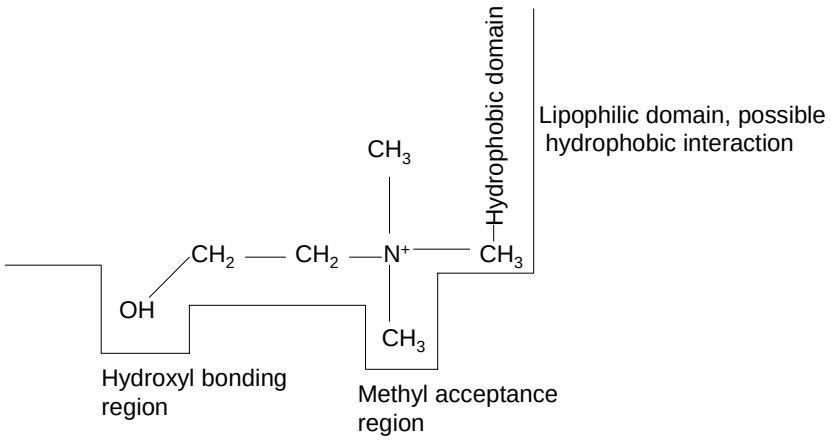


**Figure 2-18.** Theoretical two-dimensional depiction of Ch binding site in CHT.

## 2.4. Conclusions

An indirect electrochemical detection method was utilized to detect Ch and its analogues amperometrically. An in vitro assay utilizing mice synaptosome samples was used to study the initial rate of Ch uptake by CHT and inhibition of this uptake rate by an inhibitor molecule, DTH. The kinetics of these processes were analyzed using CE coupled with EC. $K_m$ for CHT was evaluated to be 0.79 μM. Dose response curves, multiple Lineweaver plots and Dixon plots generated for DTH enabled the calculation of its $IC_{50}$ and $K_I$ values along with determination of its mode of inhibition. The results obtained falls in logical conclusion with previous studies regarding the structural aspects and affinity of CHT and have contributed to relevant understanding of mechanistic aspects of CHT in mice synaptosomes. The findings have further emphasized the role of

a hydrophobic domain adjacent to Ch binding site in the CHT protein.

## 2.5. References


1. Devés R.; Krupka, R. M. The Binding and Translocation Steps in Transport as Related to Substrate Structure: A Study of the Choline Carrier of Erythrocytes. *Biochim. Biophys. Acta*, **1979**, *557*, 469-485.

2. Devés R.; Krupka, R. M. Reaction of Internal Forms of the Choline Carrier of Erythrocytes with N-ethylmalemide : Evidence of a Carrier Conformation Change on Complex Formation. *J. Membrane Biol.* **1981,** *63*, 99-103.

3. Devés, R.; Krupa, R. M. Evidence for a Two-State Mobile Carrier Mechanism in Erythrocyte Choline Transport: Effects of Substrate Analogs of Inactivation of the Carrier by N-ethylmalemide. *J. Membrane Biol.* **1981**, *61*, 21-30.

4. Okuda, T.; Haga, T.; Kanai, Y.; Endou, H.; Ishihara, T.; Katsura, I. Identification and Characterization of the High-affinity Choline Transporter**,** *Nat. Neurosci.* **2000**, *3,* 120-125.

5. Bowden, A. C. Fundamentals of Enzyme Kinetics. Brookfield, Vt., Portland, London. **1995.**

6. Kuhar, M. J.; Murrin, C. L. Sodium-Dependent High Affinity Choline Uptake. *J. Neurochem.* **1978**, *30*, 15-21.

7. Simon J. R.; Mittag, T.; Kuhar, M. J. Inhibition of Synaptosomal Uptake of Choline by Various Choline Analogs. *Biochem. Pharmac*. **1975**, *24*, 1139-1142.

8. Barkhimer, T. V.; Kirchhoff, J. R.; Hudson, R. A.; Messer, W. S. Jr. Classification of the Mode of Inhibition of High-affinity Choline Uptake Using Capillary Electrophoresis with Electrochemical Detection at an Enzyme-Modified Microelectrode. *Anal. Biochem.*, **2005,** *339*, 216-222.

9. Holden, J. T.; Rossier, J. C.; Beaujouan, J. C.; Guyenet, P.; Glowinski, J. Inhibition of High-Affinity Choline Transport in Rat Striatal Synaptosomes by Alkyl Bisquarternary Ammonium Compounds. *Mol. Pharmacol*. **1975,** *11*, 19-27.

10. Palmer, T. Understanding Enzymes. Ellis Horwood, Chichester, West Sussex; Halsted Press, New York; **1985**.

11. Gu,Y.; Lee., H.; Hudson, R. A. Bis-catechol-Substituted Redox-Active Analogs of Hexamethonium and Decamethonium : Stimulated Affinity-Dependent Reactivity through Iron Peroxide Catalysis. *J. Med. Chem*. **1994**, *37*, 4417-4420.

12. Smith, A. R.; Kirchhoff, J. R.; Tillekeratne, L. M. V.; Hudson, R. A. Separation of Negetively Charged Isomeric Quinones in Acidic Solution by Capillary

Electrophoresis with Reductive Electrochemical Detection. *Anal. Commun.,* **1999**, *36*, 371-374.

13. Wise, D. D.; Barkhimer, T. V.; Brault, P. A.; Kirchhoff, J. R.; Messer, W. S. Jr.; Hudson, R. A. *J. Chromatogr. B*. **2002**, *775*, 49-56.

14. Fermier, A. M.; Gostkowski, M. L.; Colon, L. A. Rudimentary Capillary-Electrode Alignment for Capillary Electrophoresis with Electrochemical Detection. *Anal. Chem.* **1996**, *68*, 1661-1664.

15. Gray, E. G; Whittaker, V.P. The Isolation of Nerve Endings from Brain: An ElectronMicroscopic Study of Cell Fragments by Homogenization and Centrifugation. *J. Anat.* **1962**, 96, 79-88.

16. Patel, P. J.; Messer, W. S., Jr.; Hudson, R. A. Inhibition and Inactivation of Presynaptic Cholinergic Markers using Redox-Active Choline Analogs. *J. Med. Chem.* **1993**, *36*, 1893–1901.

17. Bradford, M. M. A Rapid and Sensitive Method for the Quantification of Microgram Quantities of Protein Utilizing the Principle of Protein –Dye Binding. *Anal. Biochem.* **1976**, *72*, 248-254.

18. Barkhimer, T. New Methods for Evaluating Cholinergic Toxicity. *Ph.D. Thesis,* **2004**, 1-138.

19. Lockman, P. R.; Allen, D. D. The Transport of Choline. *Drug Dev. Ind. Pharm*. **2002**, *28*, 749-771.

20. Cai, S. Determination of the Inhibitory Properties of a Cholinomimetic Bis-catechol Decamethonium Analogue on Choline Uptake by Capillary Ele ctrophoresis with Electrochemical Detection. *Masters Thesis*, **2007,** 1-61.

21. Sterling, G. H.; Doukas, P. H.; Ricciardi, Jr. F. J., Biedrzycka, D. W., O'Neill, J. J. Inhibition of High Affinity Choline Uptake and Acetylcholine Systhesis by Quinuclidinyl and Hemicholinium Derivatives. *J. Neurochem.* **1986**, *46*, 1170-1175.

22. R. A. Copeland, Enzymes, A Practical Introduction to Structure Mechanism and Data Analysis, VCH Publishers, New York, **1996**.

23. M. Dixon, E. C. Webb, J. C. R. Thorne, K. F. Tipton, Enzymes, Third Ed., Academic Press, New York San Francisco, **1979.**

# Chapter 3

## Development of a Trienzyme Catalytic Microelectrode Detector for Capillary Electrophoretic Analysis of Cholinergic Neurotransmitters

### 3.1. Introduction

In Chapter 2, the detection and analysis of Ch was described by the amperometric oxidation of $H_2O_2$ on enzyme modified Pt MEs. The oxidation of $H_2O_2$ was achieved using a potential of +0.650 V vs. Ag/AgCl. This method has been used in a broad variety of applications with enzyme immobilized post column reactors coupled with liquid chromatography.[1] The highly sensitive assay scheme allowed the detection of subtle cholinergic changes without interferences. However biological samples very often contain electroactive molecules that can be oxidized non-selectively at the electrode surface. This may result in high levels of non-specific signals and prove to be a disadvantage for certain types of in vivo analysis. Various methods can be adopted to avoid such interferences. One solution is to use a perm selective membrane like Nafion that will only enable the analyte of interest to cross the membrane and interact with the electrode surface. However using perm selective membranes greatly reduces the sensitivity of the electrodes as the analytes have to diffuse through the membrane to reach the sensing surface. Moreover, since capillary electrophoretic analysis requires the use of MEs, complicated modifications of the miniaturized electrode surface is not trivial. Another convenient alternative is to manipulate the detection potential such that only $H_2O_2$ is selectively electrocatalysed in the presence of all other electroactive substances. This can be achieved by using a potential low enough to effectively prevent non specific electrochemical oxidation. Hence an alternative pathway for detection of Ch and ACh would be by selective amperometric reduction of $H_2O_2$ at a lower potential. Unlike $H_2O_2$ oxidation that occurs uncatalysed on the Pt electrode surface, $H_2O_2$ reduction can be catalysed by various catalysts. $H_2O_2$ is a natural substrate for the peroxidase class of

enzymes that can be used for its catalytic reduction.

### 3.1.1. Horseradish Peroxidase

A very common enzyme employed in electrochemical detection of $H_2O_2$ is horseradish peroxidase (HRP). HRP is a generic term for a group of isoenzymes occurring in plants. They are involved in various biological functions such as indole-3-acetic acid metabolism, crosslinking of cell wall polymers, lignification and resistance to infection.[2] HRP C is the most distinct of these iso-enzymes. Its active site is comprised of a heme group and two calcium atoms. The proximal site of the heme group is bonded to a histidine residue while the distal site is unoccupied and is available for $H_2O_2$ binding during enzyme catalysis.[3] The two calcium sites are present in the proximal and distal sites of the heme plane and loss of calcium results in decrease of both enzymatic activity as well as thermal stability.[4] The catalytic mechanism of HRP has been well investigated.[2,5] The iron in the heme group is in the Fe(III) oxidation state during the resting state. The first step of the process involves a 2 $e^-$ catalytic reduction of $H_2O_2$ to yield the first intermediate (compound I). Compound I has a higher oxidation state and is formally two oxidation equivalents higher than the resting state. It consists of an oxoferryl center and a porphyrin based cation radical ($Fe{=}O^{IV+}\ R^{\bullet}$). A first one electron reduction of Compound I by a reducing substrate results in the formation of compound II, a Fe (IV) oxoferryl species ($Fe{=}O^{IV}$). A second one electron reduction returns compound II to its resting state ($Fe^{III}$).[2,5]

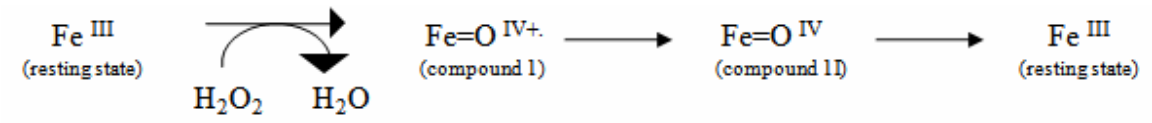


**Scheme 3-1.** Catalytic cycle of HRP

### 3.1.2. Direct and Mediated Electron Transfer in Enzymes

The simplest method for $H_2O_2$ detection is to use an electrode whose surface has been modified with a layer of peroxidase enzymes. If the applied potential is sufficiently negative then current can be generated corresponding to the reduction of $H_2O_2$ and the consequent regeneration of the enzyme at the electrode surface.

According to electron transfer theory, the rate of electron transfer between two species can be mathematically defined by the equation: [6]

$$k_{et} = 10^{13} e^{-\beta(d-3)} e^{-(\Delta G^\circ + \lambda)(\Delta G^\circ + \lambda)/4RT\lambda} \qquad (3\text{-}1)$$

Where $k_{et}$ is the rate of electron transfer between the two species, β is a constant for a particular electron donor-acceptor pair in a specific medium, d is the distance between the donor and the acceptor, $\Delta G^\circ$ is the driving energy of the electron transfer process (determined by the potential difference), λ is the Marcus reorganization energy (which is a qualitative measure of the structural rigidity of the redox species). Marcus has explained that electron transfer will be facile when the structural configuration of the donor acceptor species is such that the reorganization energy required for the ET process is minimized.[7] For example λ is negligible for compositionally identical ions in different oxidation states. Redox couples with a high self exchange rate have small reorganization energy. The rate of ET is higher for an exonergic process where $\Delta G^\circ$ has a negative value. Enzymes being biomacromolecules have their active sites deeply buried within a

three dimensional hydrophobic protein structure. Hence the active sites are often sufficiently far away from the electrode surface which significantly increases the distance of ET. Consequently, most enzymes either do not undergo direct ET with the electrode surface or exhibit a very sluggish rate transfer. Since ET in an enzyme modified electrode system is a direct consequence of the size of the enzymes, small enzymes with small hydrodynamic radius ($r < 23$ Å, such as cytochrome c) have demonstrated electron exchange with electrode surfaces, however enzymes with hydrodynamic radius > 43 Å (glucose oxidase) cannot undergo such electron exchange processes.[8] It is pertinent to mention that although enzymes with favorably small hydrodynamic radii can communicate electrons with the electrode surface, the rate of this process will still heavily depend on the orientation of the adsorbed enzymes. A key factor in developing amperometric sensors is to utilize strategies that reduce the effective ET distance between the sensing surface (enzyme) and the transducer (electrode). In biological systems, the enzymes are often regenerated by small molecules known as cofactors such as FAD and molecular $O_2$. The simplest and most convenient method is to utilize the enzyme's own cosubstrate that can shuttle freely between the enzyme layer and electrode surface. The cofactors can then undergo electrochemical reaction at the electrode to generate a signal. All oxidase enzymes such as ChO, glucose oxidase, lactase oxidase, xanthine oxidase, glutamate oxidase and galactose oxidase use $O_2$ as their mediator and they have been exploited thoroughly for the development of various biosensors.[9-11] Detection of the substrates has been based on either the amount of $O_2$ depleted or amount of $H_2O_2$ generated as a result of the enzymatic catalysis.

A second approach is to replace the enzyme's natural cofactor with a diffusing

redox mediator that can act as an ET shuttle.[12,13] A mediator is a small electroactive molecule that can exchange electrons with the enzyme and undergo facile oxidation-reduction at the electrode surface. A primary requirement for a molecule to act as an electron mediator is that it should exhibit fast ET kinetics with the electrode surface because the mediator will have to compete with the enzyme's natural cofactor (such as molecular oxygen in many cases) which may be present in the reaction medium. Artificial redox mediators commonly used are low molecular weight metal complexes exhibiting reversible electrochemistry such as ferrocene derivatives, metal cyanides, Os and Ru complexes, quinones, etc.[14] In a mediated ET process, the electron hops from the enzyme's prosthetic group to the closest mediator molecule around the microenvironment of the biomolecule and from the mediator to the electrode or vice versa. One of these two electron hopping steps is the rate controlling step of the overall process. ET mediators have been used for several enzyme electrodes such as glucose oxidase, and methanol dehydrogenase. However, mediated ET for ChO has been unsuccessful to date due to the high cofactor specificity of this enzyme.

While using a freely diffusing mediator, it important that the mediator be present in the vicinity of the electrode surface. A common approach to address this issue is by confining the mediators onto the electrode surface by physical entrapment within a polymer matrix such as polyethylene glycol. However, such membranes can slow the response time and decrease the sensitivity of the electrode as the analytes have to diffuse through the membrane to interact with the enzymes. Since these matrices are only partially effective in trapping these small mediator molecules which eventually diffuse through the membrane by virtue of their molecular size and are lost into the solution

leading to a decrease in the catalytic activity of the sensor. However, one distinct advantage of using such membranes is that it can reduce interferences from other electroactive substrates. As an example, enzyme electrodes covered with a negatively charged Nafion membrane can substantially reduce interference from ascorbate, due to the repulsion between negative charges.

As mentioned, a major challenge of entrapment of mediators is the gradual leaching of the mediators from the polymeric membrane resulting in a decrease in response efficiency with time. To enable efficient electron transfer along a polymeric matrix without loss of response, the mediators can be covalently bound to the polymer or to the enzymes themselves.[15] Redox hydrogels are highly hydrophilic charged polymers. Several efficient ET mediators such as ferrocene derivatives or Fe, Ru and Os complexes can be coupled with such hydrogels. Employing a redox polymer is a good method of increasing the efficiency of ET because here the overall process is divided into a series of fast self exchanging electron hopping steps between the mediator itself after the initial rate controlling ET between the enzyme and the mediator. This concept was pioneered by Adam Heller who originally developed the "wired" enzyme system.[16] Heller has extensively studied the bonding of electron relays to enzyme proteins and has established that the electron transfer properties of enzymes can be modified using mediator bound electron relaying polymers.[8] In this system the enzyme itself is modified by covalent attachment of fast ET mediators via spacer chains.[17] Covalent linkage of the mediators to the enzyme system prevents leaching of the mediators from the electrode system, imparting enhanced stability to the sensor.[18] Considerable effort has been devoted in investigating the ET efficiency of various mediators. Commonly used redox relays in

such wired systems are cationic osmium bipyridine complexes contained in a polymeric backbone such as polyvinyl pyridine. The individual polymeric units are further connected to each other by covalent coupling with long chain diepoxides. The result is the formation of a highly crosslinked 3-dimensional network with redox relays in close vicinity to each other and strongly coupled to the enzyme surface. These polymers are known as redox hydrogels because they swell up in an aqueous medium due to repulsion between the positively charged units. These positively charged hydrogels form electrostatic complexes with the enzyme which is essential for the assessibility of the enzyme's deeply buried redox site. ET through the hydrogel is by collisional hopping of electrons between the adjacent redox units along a polymer chain. There is an increase in amplitude of collision between polymeric units when the gels are hydrated which increases the electron-diffusion coefficient (as high as $4 \times 10^{-8}$ $cm^2/s$ )[19] and hence the electrons also hop between adjacent polymeric units. Multiple pathways of ET transfer in these hydrogels impart them with very high current densities. In the absence of such mediators the ET would depend on several hard to control parameters such as the ET distance between the two redox units and the orientation of the enzymes with respect to the electrode surface. Another distinct advantage of employing a redox hydrogel based enzyme sensing system is that the redox potential of the electron relay units can be manipulated to a value close to the redox potential of the enzyme by varying the ligands, thereby minimizing the overpotential for enzyme reduction/oxidation. [17]

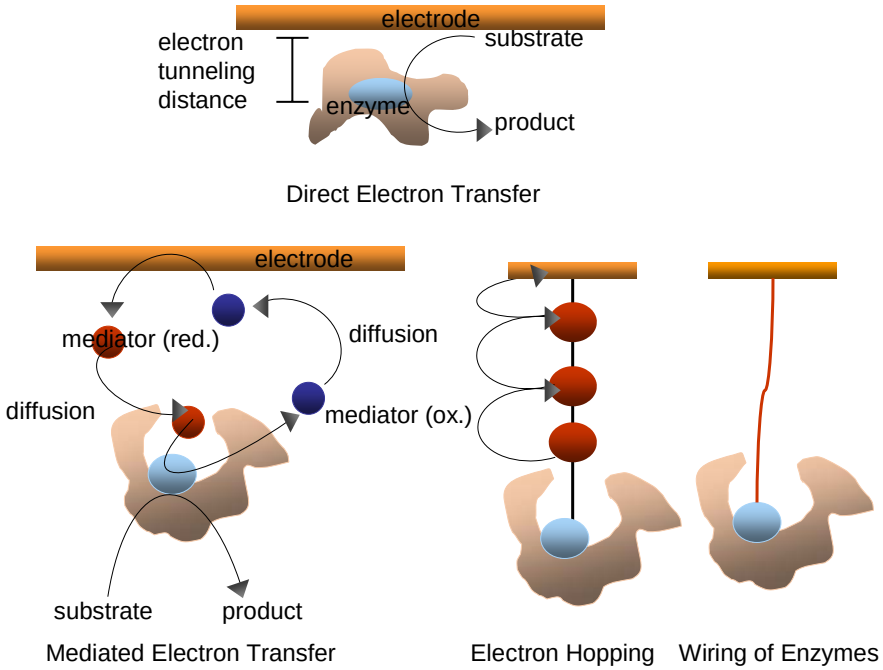


**Figure 3-1.** Schematic of various electron-transfer pathways that can be adopted for amperometric biosensors.

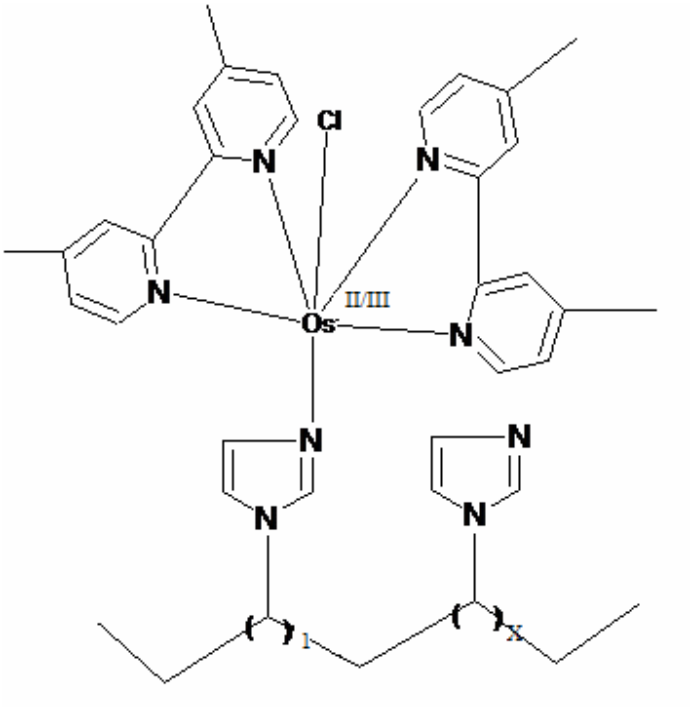


**Figure 3-2.** Structure of a typical redox hydrogel employing an Os center coordinated with bipyridinium units in a polyvinyl imidazole polymer backbone.

As mentioned, although direct electron transfer can occur between HRP and an electrode surface, redox hydrogels have various distinct advantages. In this work, a wired redox polymer film containing HRP enzyme bound to osmium units incorporated in a redox hydrogel (HRP-Os) has been used in conjunction with AChE and ChO to achieve sensitive detection of cholinergic neurotransmitters and their analytes. Figure 3-3 depicts the sequence of events leading to such detection.

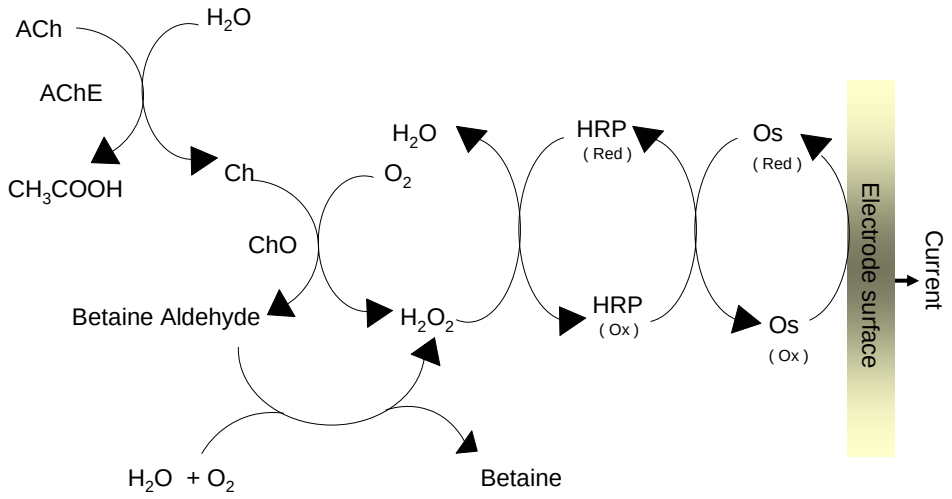


**Figure 3-3.** Depiction of the sequence of events by which an electrochemical signal is generated for the detection of Ch, ACh and BuCh which themselves are not electroactive.

In 1992 Vreeke et al. were the first to use a covalently bound HRP polyvinyl pyridine for the selective reduction of hydrogen peroxide and its consequent amperometric detection.[20] Subsequently Garguilo et al. developed an amperometric sensor for Ch and ACh by coimmobilizing HRP, ChO, AChE in a crosslinked redox polymer on carbon electrodes and were also able to detect in vivo current response upon injection of Ch by microdialysis.[21,22] ACh has also been detected by this scheme by

HPLC using Au ring disk electrode and by flow injection system using solid graphite electrode.[23,24]

## 3.2. Materials and Methods

### 3.2.1. Materials

Acetylcholinesterase (EC 3.1.1.7, type V-S lyophilized powder from *Electrophorus electricus*, > 1070 U/mg of protein), choline oxidase (EC 1.1.3.17, *Alcaligenes* species, 9-18 U/mg), acetylcholine chloride (>99%), choline chloride (>98%), and butyrylcholine chloride (>98%) were purchased from Sigma (St. Louis, MO) and stored in a desiccator at -16 °C. Glutaraldehyde (grade I, 25% aqueous solution) was purchased from Sigma and stored at 4 °C. Horseradish peroxidase redox polymer wired enzyme was purchased from Bioanalytical Systems, Inc. (West Lafayette, IN) and stored at 4 ºC in the dark. *N*-Tris[hydroxymethyl]methyl-2-aminoethane-sulfonic acid (TES) (>99%), was also purchased from Sigma and stored at ambient temperature. Platinum and gold wire (25 $\mu$m in diameter, 99.99%) was obtained from Goodfellow (Berwyn, PA). A Thornel C fiber (7 μm diameter) was obtained from Amoco. All other chemicals were of analytical reagent grade and were used as received. Solutions were prepared with deionized water purified to a resistivity of at least 17 MΩ-cm by a Barnstead B pure water purification system.

### 3.2.2. Instrumentation

All experiments were conducted using a laboratory built capillary electrophoresis

instrument with electrochemical detection which has been previously described in Chapter 2.

### 3.2.3. Methods

#### 3.2.3.1 Preparation of HRP-Os-AChE-ChO Enzyme Electrodes

C, Au and Pt microelectrodes were prepared using the general procedure described in Chapter 2. Au (25 μm), Pt (25 μm) and C fibers (7 μm) were utilized as the electrode material. After fabrication, the tip of the microelectrode was rinsed with acetone, deionized water and finally with acetone. The electrodes were dried at ambient conditions for 10 minutes before immobilization with enzymes.

##### 3.2.3.1.1. Immobilization Methods

Two different methods conveniently referred as single step immobilization and double step immobilization were adopted to study the optimum immobilization conditions.

###### 3.2.3.1.1.1. Single Step Immobilization Method

A single layer immobilization method was used. The ratio of HRP-Os, AChE and ChO, to be used were optimized. Only Pt MEs were used for this purpose. 0.6 mg of ChO (~ 6 units) was carefully weighed in a conical vial and 4 μL of AChE (~ 25 units) was added to it. After the enzymes were mixed thoroughly 4 μL of the HRP-Os mixture was added to the vial along with 0.5 μL of glutaraldehyde solution. The ME tips were gently

dipped into the resultant solution and slowly rotated until a thin layer of enzymes were immobilized onto its surface. The solution was further used to coat 3-4 additional electrodes. Before use the electrodes were dried at ambient temperature for ~ 1 hour.

#### 3.2.3.1.1.2. Double Step Immobilization Method

The tip of the ME was bent into a loop and 0.5 µL of the HRP-polymer solution was added onto it. The electrode was dried for 30 minutes in an inverted position at ambient temperature. This immobilization step was repeated twice. The resultant electrodes were gently dipped into a 7 µL aqueous solution containing 6 units of ChO, 25 units of AChE and 0.5 µL of 25 % glutaraldehyde solution. The enzymes were physically adsorbed onto the electrode surface as crosslinking occured. This solution was used to coat 3-4 additional electrodes. Before use, the electrodes were dried at ambient temperature for ~ 1 hour. The double step immobilization method was adapted to coat C fiber, Pt and Au MEs.

### 3.2.3.2. Separation of Ch, ACh and BuCh

Varying lengths (85 -145 cm) of polyimide coated fused-silica capillary with i.d. 50 µM and o.d. of 350 µM (Polymicro Technologies, Phoenix,AZ, USA) was used to optimize separation conditions of the analytes. Electropherograms were generated by applying voltages from 9 to 20 kV. Phosphate buffer (20 mM, pH 7.0) and TES buffer (50 mM, varying pH : 6.1 -8.0) were prepared following standard buffer prepration procedures and used as run buffers. All standard solutions of Ch, ACh and BuCh were prepared fresh daily in deionized water and stored in ice.

#### 3.2.3.3. Linear Range of HRP-Os-AChE-ChO Au MEs

The linear range for Ch and ACh with HRO-Os-AChE-ChO Au MEs were studied using optimized electrophoretic separation conditions. Varying concentrations of standard solutions of Ch and ACh were prepared from 2 to 2000 μM. The concentration of BuCh was held constant at 200 μM for all analyses.

#### 3.2.3.4. Stability of HRP-Os-AChE-ChO Au MEs

Au MEs were modified with enzymes following the double step immobilization method and their operational and storage stability were studied.

##### 3.2.3.4.1. Operational Stability of the Modified Au MEs

After enzyme modification, Au MEs were carefully aligned with the already conditioned capillary and fixed in the configured position using electrical liquid tape. Standard stock solutions of Ch, ACh and BuCh were prepared daily and mixed in 1:1:1 ratio corresponding to a final concentration of 500 μM. Electropherograms were continuously collected for the first 24 hours and then for ~ 8 hours every 12-15 hours until the electrode performance severely deteriorated and negligible response was obtained.

## 3.3. Results and Discussion

### 3.3.1. Immobilization of Enzymes

The key focus of developing stable and sensitive enzyme based biosensors is the integration of these biomolecules onto the electrode surface under conditions that will

deliver optimum output. Hence two strategic immobilization steps were considered. The single step immobilization method involved cumulative integration of the enzymes (AChE and ChO) and HRP-Os redox polymer units simultaneously onto the electrode surface. The double step immobilization method was based on simple adsorption of the redox polymer onto the electrode surface followed by simultaneously crosslinking of the chemically more compatible enzymes on it. The method of immobilization is an important factor in biosensor development because the sensitivity and stability of the sensor depend upon the microenvironment of the immobilized enzymes.

#### 3.3.1.1. Single Step Immobilization Method

After immobilization of enzymes employing the single step method, the detection capability of the electrode system was evaluated by injecting a standard Ch solution into the capillary. The amperometric response was recorded at various potentials to generate a current-potential voltammogram. Figure 3-4 represents the voltammetric response of the electrode. A sigmoid hydrodynamic voltammogram was obtained with maximum limiting current at +600 mV vs Ag/AgCl. A limiting current at a high oxidizing potential indicated that the amperometric response generated by this biosensor was due to direct uncatalysed electrochemical oxidation of $H_2O_2$ formed by enzymatic transformation of Ch. Hence, under this condition of immobilization, ChO retained its enzymatic activity; however the HRP-Os hydrogel system was catalytically inactive. Direct crosslinking of the HRP-Os redox hydrogel polymer with AChE and ChO using glutaraldehyde may have caused denaturation of the HRP-enzyme polymer system. Since the HRP-Os polymer system is a positively charged hydrophilic 3-dimensional polymer,

glutaraldehyde may have caused severe cross linking among the already crosslinked highly branched side chains. This may have resulted in disruption of the 3-dimensional unit that consequently posed great hindrance in the charge transfer process. This basis is further supported by the fact that the polymer solution precipitated upon the addition of glutaraldehyde or ChO indicating a disruption of its electrostatic nature upon such additions. It is pertinent to mention that HRP, ChO, AChE and Os-polyvinyl imidazole polymer have been successfully coimmobilized by crosslinking with polyethyleneglycol diglycidyl ether (PEGDGE).[24] In this case the longer PEGDGE chain enabled the formation of effective electron transfer relays.

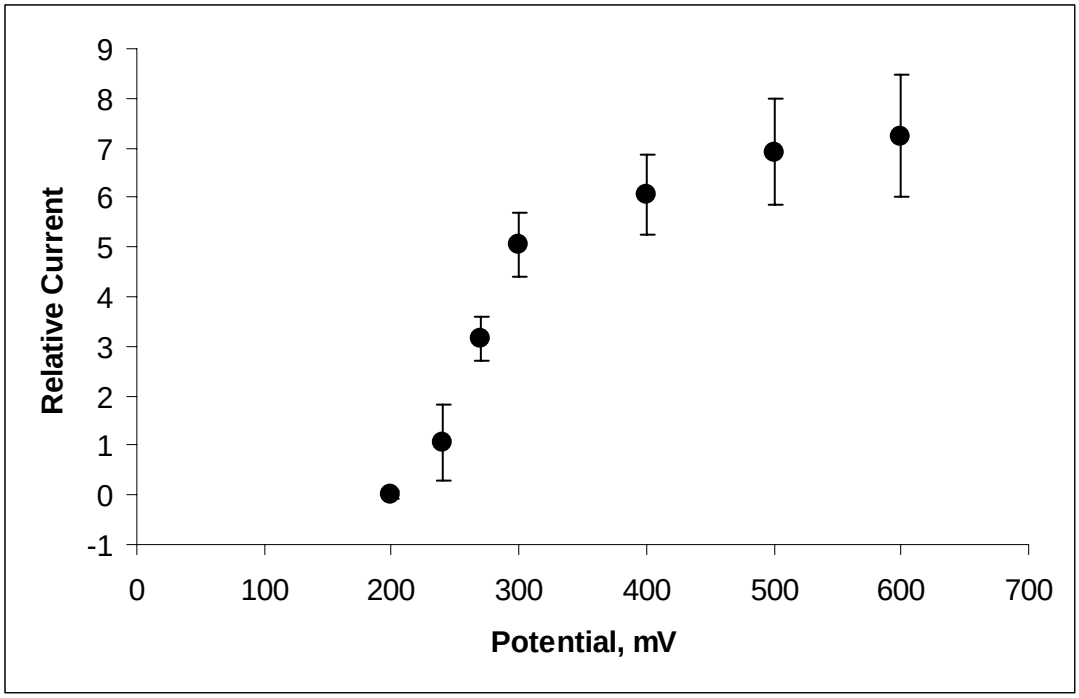


**Figure 3-4.** Current-Potential plot of a HRP-AChE-ChO ME using single step immobilization method. Ordinate depicts the relative peak current for injection of 100 μM Ch at different potentials. Current peak of Ch at 240 mV is defined as 1. Each data point is the average response of 3 different random injections of Ch.

### 3.3.1.2. Double Step Immobilization Method

In the double immobilization method first the HRP-Os polymer unit was allowed to adsorb onto the electrode surface in the absence of any other enzyme system or crosslinking agent. This method was expected to keep the HRP units properly wired as minimal disruption of its physical/chemical characteristics were expected to occur by mere physical adsorption. ChO and AChE were then simultaneously crosslinked onto its surface to yield a trienzyme system. Efforts were made to generate hydrodynamic voltammograms with this modification. The magnitude of current generated was comparatively constant between -200 to +400 mV. It decreased beyond -300 mV and +500 mV. This indicated that $H_2O_2$ was being effectively electrocatalysed by the HRO-Os system, and there was a range of potential at which this electrode system could be operated. The effectiveness of immobilization by this method was further supported by CV studies.

Figure 3-5 compares the CV of a bare Pt ME and CV of a Pt ME supporting a layer of the HRP-Os cross linked redox polymer in phosphate buffer. The peak shaped voltammogram for the coated ME corresponds to the oxidation of $Os^{II}$ ($E_a$ = 423 mV) in the anodic scan towards positive potential and the reduction of $Os^{III}$ to $Os^{II}$ in the reverse scan ($E_c$ = 354 mV).

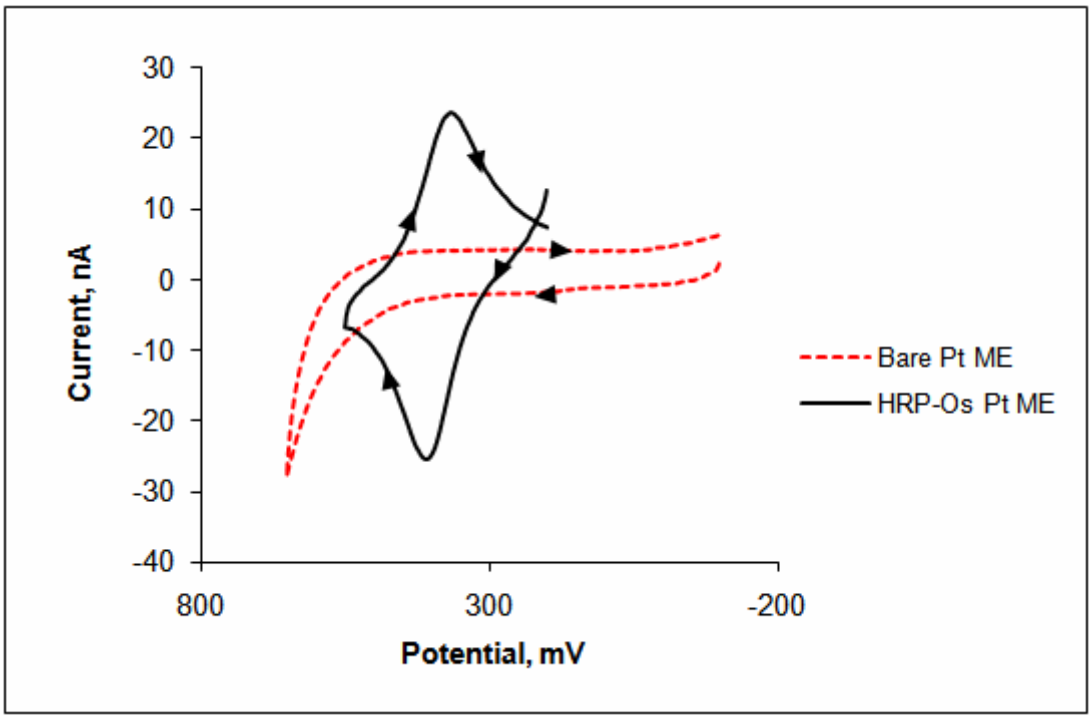


**Figure 3-5.** Comparison of CVs of bare and HRP-Os redox polymer modified Pt ME in 20 mM phosphate buffer, pH 7.0. Scan rate = 20 mV/s. Arrows indicate direction of scan.

Figure 3-6 compares the CVs of Pt MEs modified with ChO and AChE and ME modified with all the three enzymes using double step immobilization. As expected, a Pt ME bearing crosslinked ChO and AChE was not electroactive. In contrast, ME modified with double step immobilization yielded a peak shaped voltammogram for both anodic and cathodic scans corresponding to oxidation of $Os^{II}$ to $Os^{III}$ ($E_a$ = 430 mV) and its reduction again from $Os^{III}$ to $Os^{II}$ ($E_c$ = 370 mV) in the reverse scan. The HRO-Os-AChE-ChO Pt ME CV showed typical characteristics of a surface confined reversible redox species characterized by sharp anodic and cathodic peak currents.

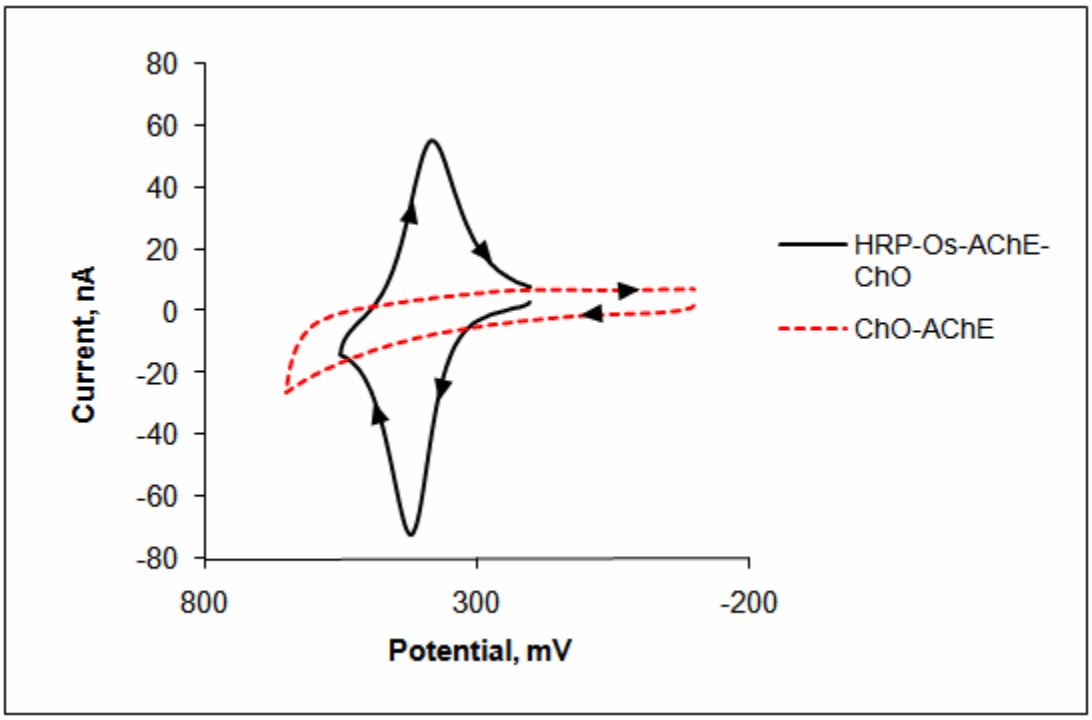


**Figure 3-6.** Comparison of CVs of Pt ME modified with ChO-AChE and Pt ME modified with HRP-Os-AChE-ChO using double step immobilization method. Electrolyte solution = 20 mM phosphate buffer, pH 7.0; scan rate = 20 mV/s. Arrows indicate direction of scan.

### 3.3.2. Choice of Electrode Material

Since multienzyme sensors were being developed in this work, it was important to select a suitable electrode material. One of the challenges of employing modified ME is controlled modification of the miniature surface. Therefore initial experiments were performed by fabricating MEs using common electrode materials such as C fiber, Pt and Au.

#### 3.3.2.1. Carbon fiber ME

C MEs were fabricated using 7 µM C fibers. Owing to its small dimension, it was difficult to modify the fiber surface with the HRP-Os polymer system by simple physical

adsorption. Moreover the fabricated electrodes were too fragile to be aligned to the capillary outlet and broke easily. Although various types of C electrodes have been used for the detection of Ch and ACh,[21,22,25] not all strategies of making enzyme-modified microelectrodes are adaptable to CE.

### 3.3.2.2. Pt ME

Pt MEs were investigated for suitability of application to development of sensors. The double step immobilization method appeared compatible with Pt. However, the HRP-Os polymer solution adsorbed weakly on the Pt surface, in spite of efforts of repeated coating. This posed a significant hindrance to development of the sensor with respect to aspects of long term stability and sensitivity. The overall current response to Ch and ACh was low, compared with Pt enzyme electrodes modified with only ChO and AChE. The detection limit was high (100 fmol) emphasizing the need to look for an alternate electrode material.

### 3.3.2.3. Au ME

The focus of the search of suitable electrode material was to utilize something that would enable moderately stable binding of the HRP-Os polymer onto its surface only by physical adsorption and allow alignment with the capillary outlet without breakage. Au MEs were used as an alternative. Au is known to have an affinity for thiols. Numerous studies have proven to form self assembled layers of various thiols on Au surfaces.[26-28] Hence, Au was considered as an alternative material because of possibility of its bonding with cysteine moieties present in the horseradish peroxidase enzyme. The HRP-Os

polymer exhibited comparatively superior adherence to the Au surface. The Au electrodes were operated at constant potential of +0.10 V vs Ag/AgCl.

The sensitivity of the resultant electrodes is governed by the ratio of the different enzymes used, the thickness of the enzyme layer, method of immobilization and mode of alignment with the capillary outlet.

### 3.3.3. Separation of Ch, ACh and BuCh

After the immobilization process was optimized, the resolution ability and detection capacity of the Au ME system was investigated using CE-EC. An 80 cm polyimide silica capillary was initially employed to achieve separation, a dimension previously used for analysis of cholinergic assays. Varying separation potentials ranging from 9 -20 kV are applied to achieve separation, but baseline resolution of Ch, ACh and BuCh was difficult even at low analyte concentrations. The amperometric signal resulted in broad current peaks. This is probably due to the fact that a bilayer system was used that increased the diffusion distance of generated $H_2O_2$ resulting in significant peak broadening and hence poor resolution.

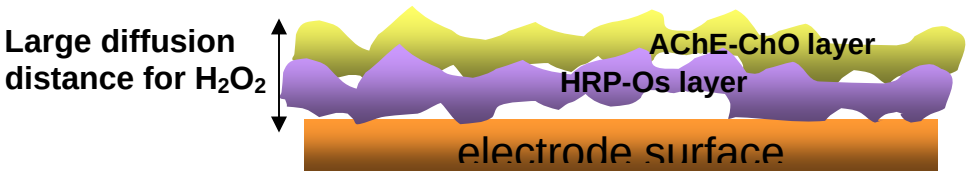


**Figure 3-7.** Schematic of larger diffusion pathway for $H_2O_2$ in a bilayer system.

Convenient alternatives to manipulate separation conditions in CE are by controlling the separation potential and manipulating buffer compositions such as pH and

ionic strength. A low buffer pH would cause protonation of the silanol groups resulting in decreased electrosmotic flow. Lower EOF would allow sufficient time for the analytes to separate along the capillary column. Various run buffer solutions [phosphate buffer (20 mM) pH 7.0, TES buffer (50 mM) pH 6.4, 6.7, 7.1 and 8.0] were used for electrophoretic separation. pH lower that 6.4 was not used as relatively acidic conditions would destroy the enzymes on the electrode surface. Although subtle improvement in resolution was observed, complete peak separation was not achieved even at low pH where the electroosmotic flow of the system is expected to be smaller. The electropherograms of Ch, ACh and BuCh for various pH are depicted in Figure 3-8.

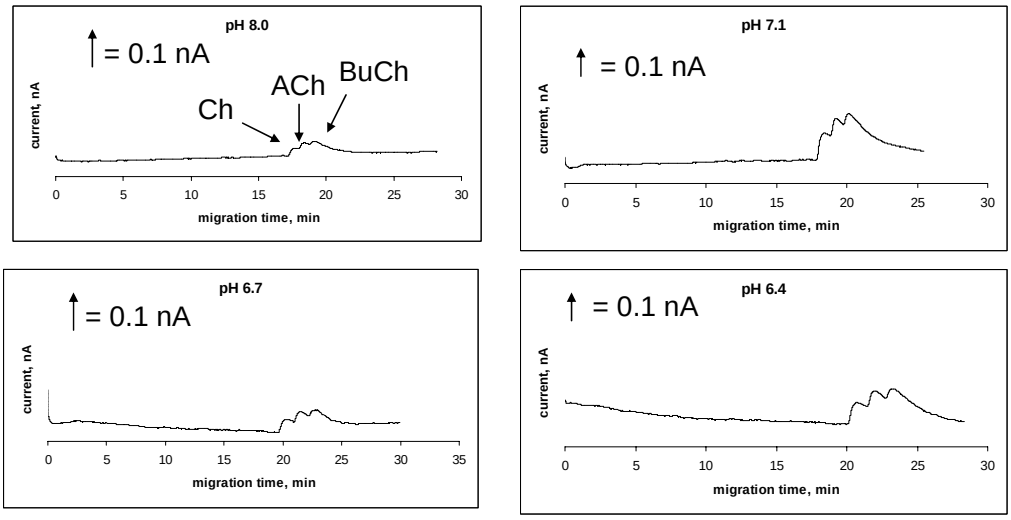


**Figure 3-8.** Electropherograms of a mixture of 10 μM solution of Ch, ACh and BuCh using 50 mM TES run buffer at pH 8.0, pH 7.1, pH 6.7, pH 6.4. Separation potential = 9 kV. Detection potential = +0.10 V vs. Ag/AgCl.

Since manipulating potential and buffer composition did not allow complete baseline resolution, the length of the silica capillary was increased from 80 cm to 145 cm. Due to the increase in length, migration time of the analytes were greatly compromised, however it lead to efficient baseline resolution for Ch, ACh and BuCh. Figure 3-9a-d. depicts elctropherograms obtained for various analyte concentrations. 50 mM TES buffer, pH 8.0 was used for all separation as a basic pH buffer would augment the longevity of enzyme modified MEs.

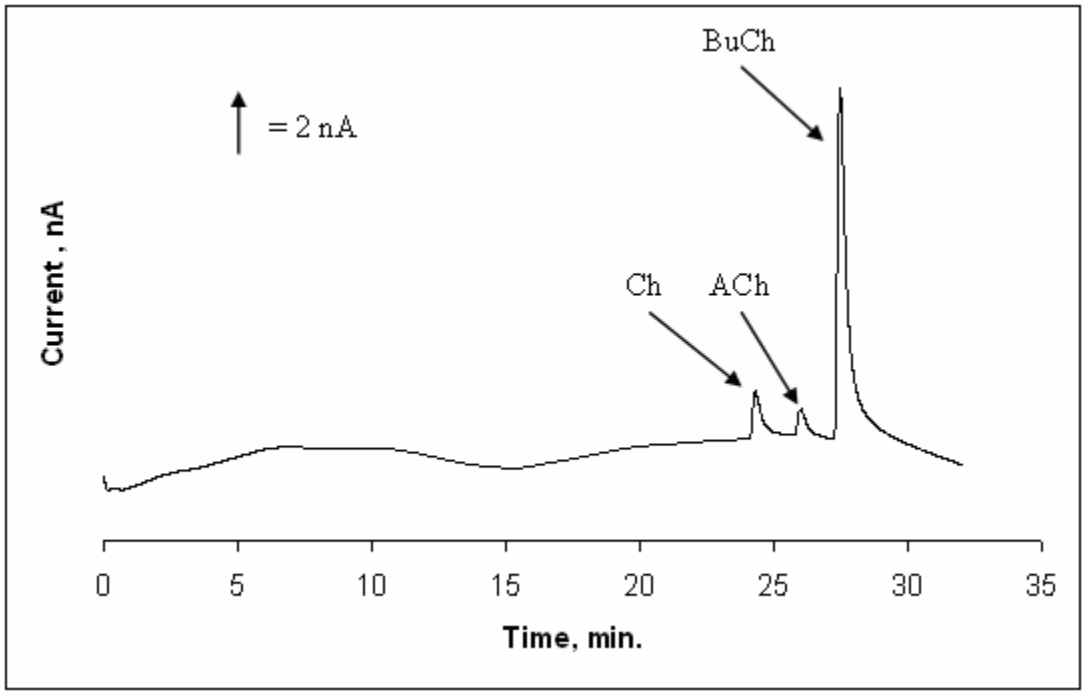


**Figure 3-9a.**

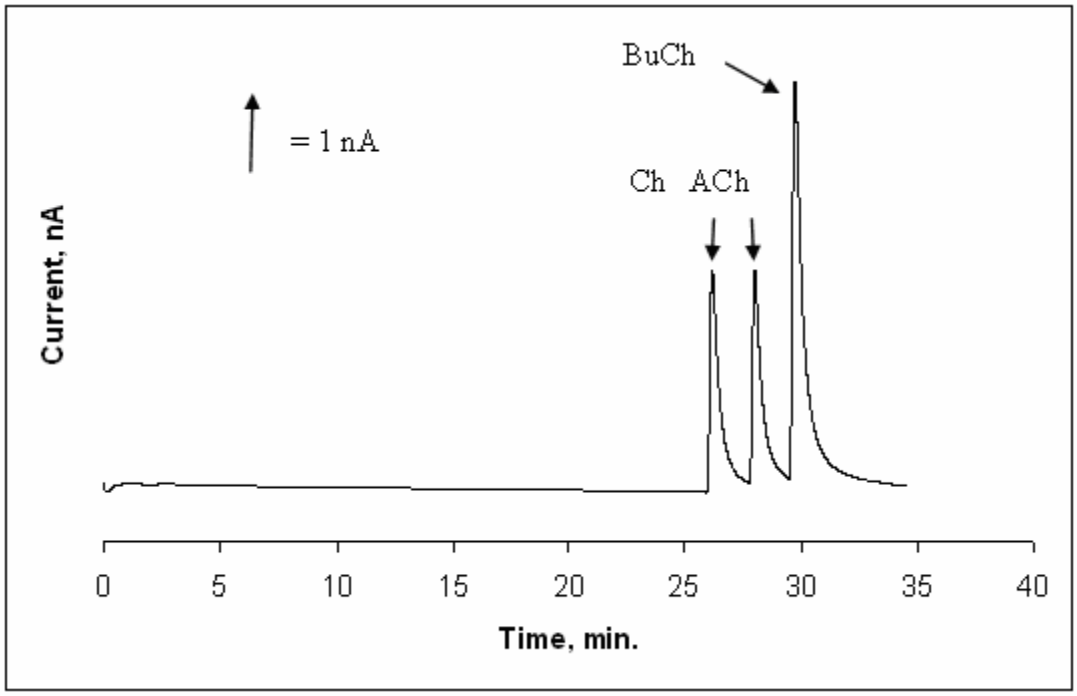


**Figure 3-9b.**

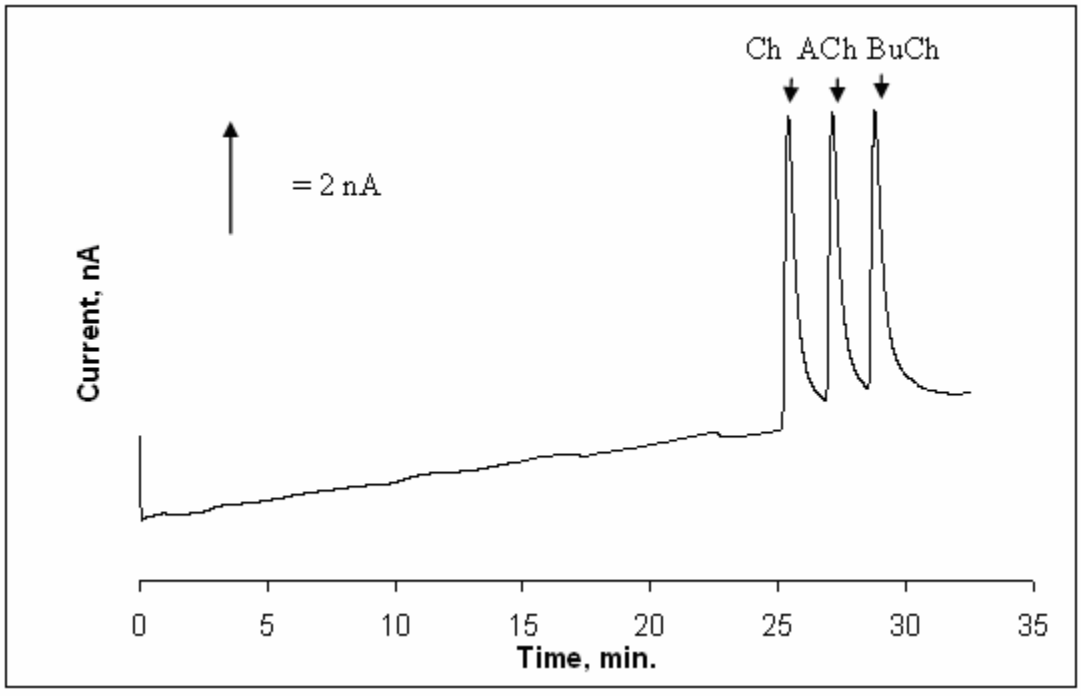


**Figure 3-9c.**

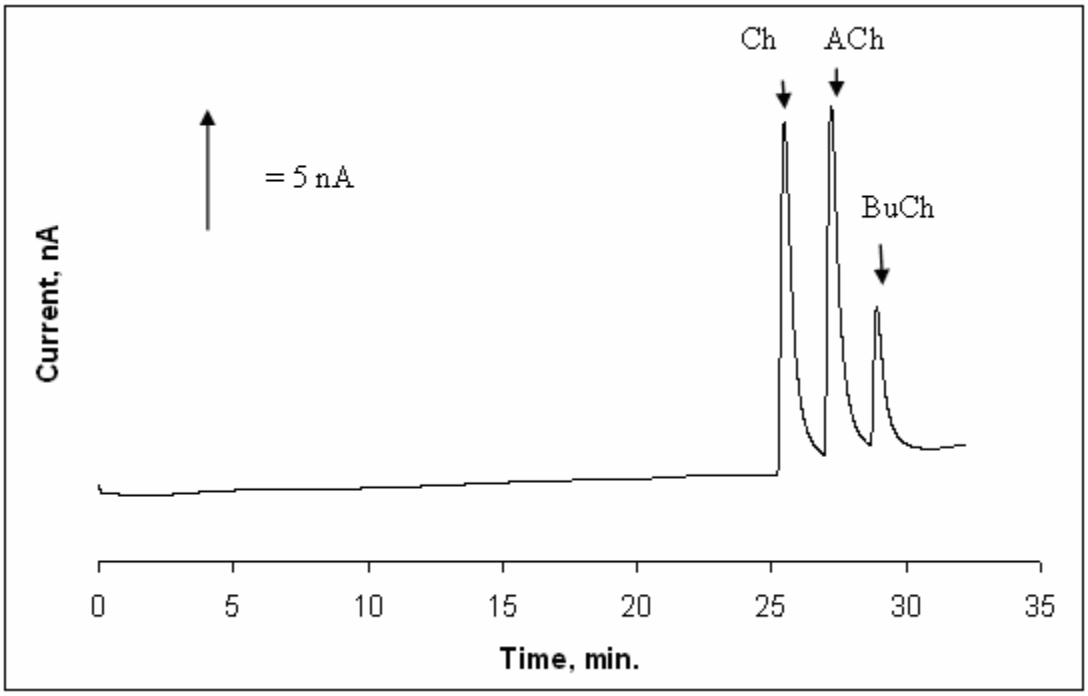


**Figure 3-9d.**

**Figure 3-9a-d.** Electropherograms of mixtures of 3-9a.: 10 µM Ch, 10 µM ACh , 200 µM BuCh; 3-9b: 75 µM Ch, 75 µM ACh, 200 µM BuCh; 3-9c.: 200 µM Ch, 200 µM ACh, 200 µM BuCh; 3-9d: 500 µM Ch, 500 µM ACh, 200 µM BuCh using a HRP-AChE-ChO modified Au ME. Run buffer, 50 mM TES, pH 8.0; separation voltage +17 kV; detection potential +0.10 V vs. Ag/AgCl.

### 3.3.4. Range of Linearity of HRP-Os-AChE-ChO ME

The linear range for Ch and ACh were studied. Calibration plots were generated by plotting the ratio of the peak areas of either analyte (Ch and ACh) to that of internal standard (BuCh) which was held constant at 200 µM. As enzymes on the electrode surface obeyed Michaelis-Menten kinetics, large injection volumes resulted in a limiting value of the current signal beyond 1000 µM. The current response showed considerable deviation from linearity due to saturation of the catalytic sites on the electrode surface. Hence a low volume of injection of ~ 0.8 nL was employed for the HRP-AChE-ChO Au ME which yielded a good linear response from 2 µM to a high concentration of 2000 µM

for both Ch and ACh. Three different electrodes were examined. The $R^2$ values ranged from 0.997 to 0.999 for Ch and from 0.996 to 0.999 for ACh. Concentrations beyond 2000 μM were not examined, as very high concentrations could cause overloading of the column and inefficient separations. Also, since in vivo concentrations of cholinergic neurotransmitters are in the sub-micromolar to micromolar range, studies of lower concentration ranges are more important for biological applications. Figures 3-10a-b and 3-11a-b depicts calibration plots for Ch and ACh, respectively, for three different electrodes. Each data point indicates the average of triplicate measurements for Ch and ACh.

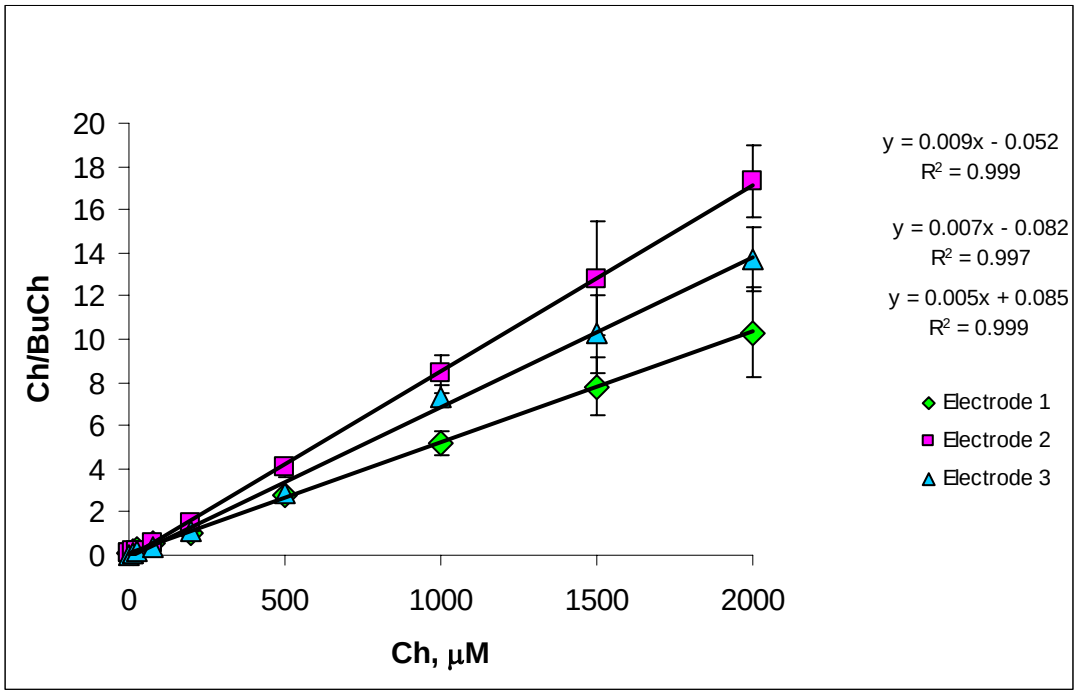


**Figure 3-10a.** Calibration plots for Ch from 2-2000 μM for 3 different HRP-AChE-ChO Au MEs.

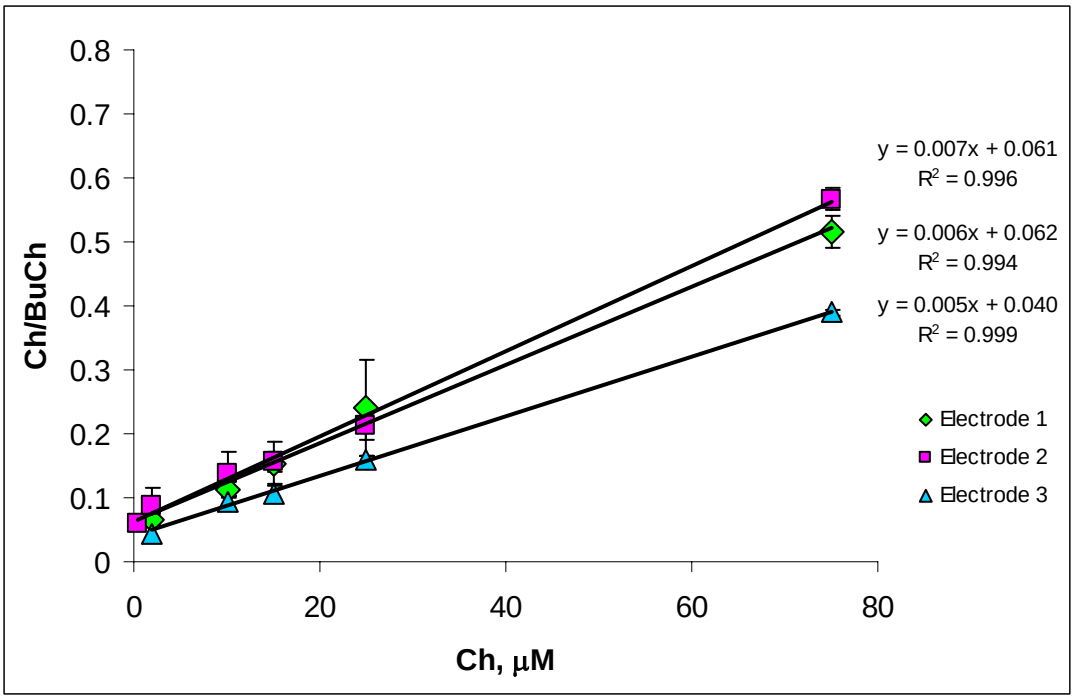


**Figure 3-10b.** Calibration plots for Ch from 2-75 µM for 3 different HRP-AChE-ChO Au MEs.

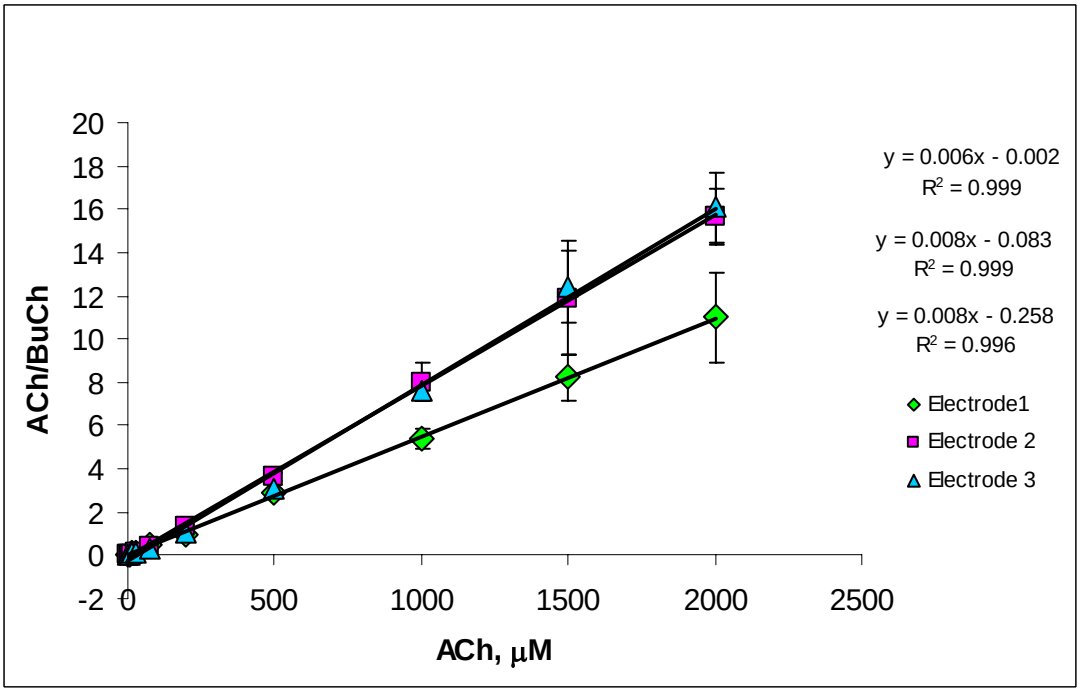


**Figure 3-11a.** Calibration plots for ACh from 2-2000 µM for 3 different HRP-AChE-ChO Au MEs.

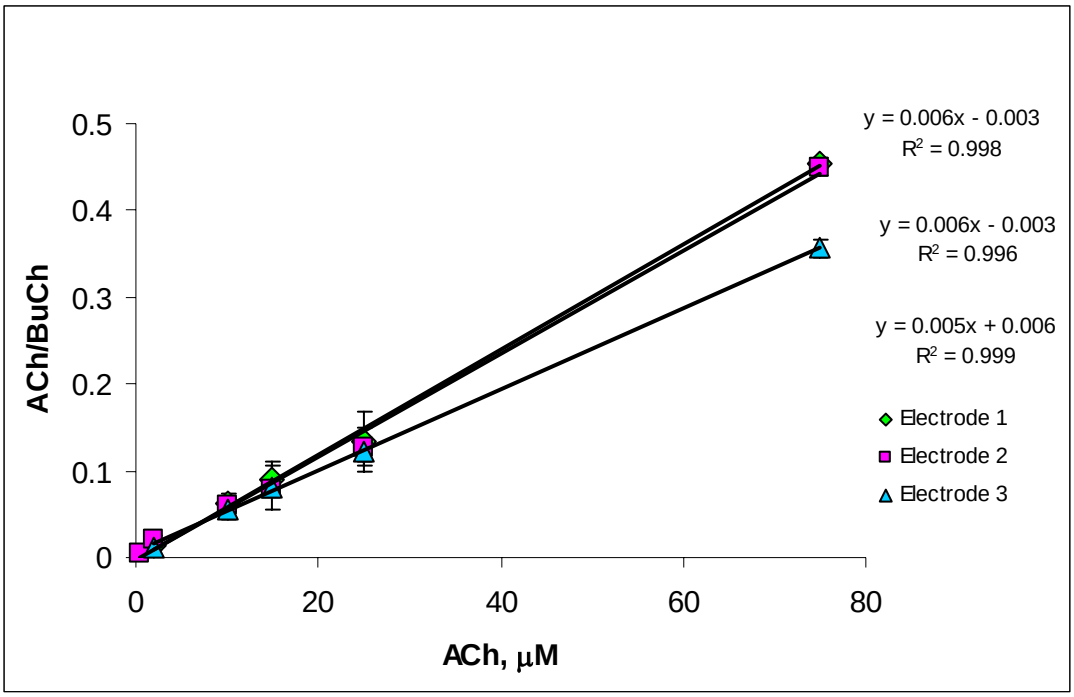


**Figure 3-11b.** Calibration plots for ACh from 2-75 μM for 3 different HRP-AChE-ChO Au MEs.

The sensitivity of the electrodes was calculated from the slope of the calibration plots of the different electrodes. The sensitivity of Ch varied from 0.005 to 0.009 units /μM Ch, while that of ACh varied from 0.006 to 0.008 units/μM ACh for the HRP-AChE-ChO Au ME. This variation in sensitivity is due to the fact that the enzymes are randomly adsorbed onto the electrode surface during the crosslinking process. The sensitivity of the electrodes is also dependent on the mode of alignment of the electrode with the capillary outlet. The reproducibility of these electrodes depend on hard to control parameters such as specific activity of the surface confined enzymes, the quantity of enzymes immobilized, the exact ratio of the enzymes immobilized, thickness of the enzyme film and variation in amperometric response of the manually fabricated MEs.

Careful observation of the calibration plot for Ch at lower concentrations

(3-10b) indicates that the concentration of Ch does not drop to zero if extrapolated to zero Ch concentration. This indicates the presence of endogeneous Ch in the standard stock solution. This may be attributed to the fact that both ACh and BuCh undergoes slow hydrolysis to Ch or because the purity of commercially available BuCh is only 98%. Extrapolation of ACh calibration plot (3-11b) to zero ACh concentration does not indicate the presence of any endogeneous ACh. This observation further emphasizes the sensitivity of the method employed. It can also be observed that the sensitivity of the same electrode is different for Ch and ACh indicating that their individual response to the enzyme modified electrodes are different.

### 3.3.5. Limit of Detection of HRP-Os-AChE-ChO Au ME

The limit of detection refers to the lowest concentration of the analyte which can be detected with sufficient accuracy and most often corresponds to a signal: noise ratio of > 2:1. After successful baseline resolution of the analytes and evaluation of individual electrode sensitivity, the limit of detection for Ch, ACh and BuCh were determined. Since CE allows injection of very low volumes of sample, a 0.1 μM solution of Ch, ACh and BuCh was injected at 5 psi for 0.1 s which corresponded to an injection volume of 0.38 nL. A detection limit of 0.1 μM for Ch, ACh, and BuCh was achieved that corresponded to a mass detection limit of 38 amol at a signal to noise ratio > 3:1. Figure 3-12 depicts the electropherogram of a mixture of 38 amol of Ch, ACh, and BuCh. Since the sample concentration and volume used was low, a high separation potential of 20 kV was applied to achieve shorter migration times.

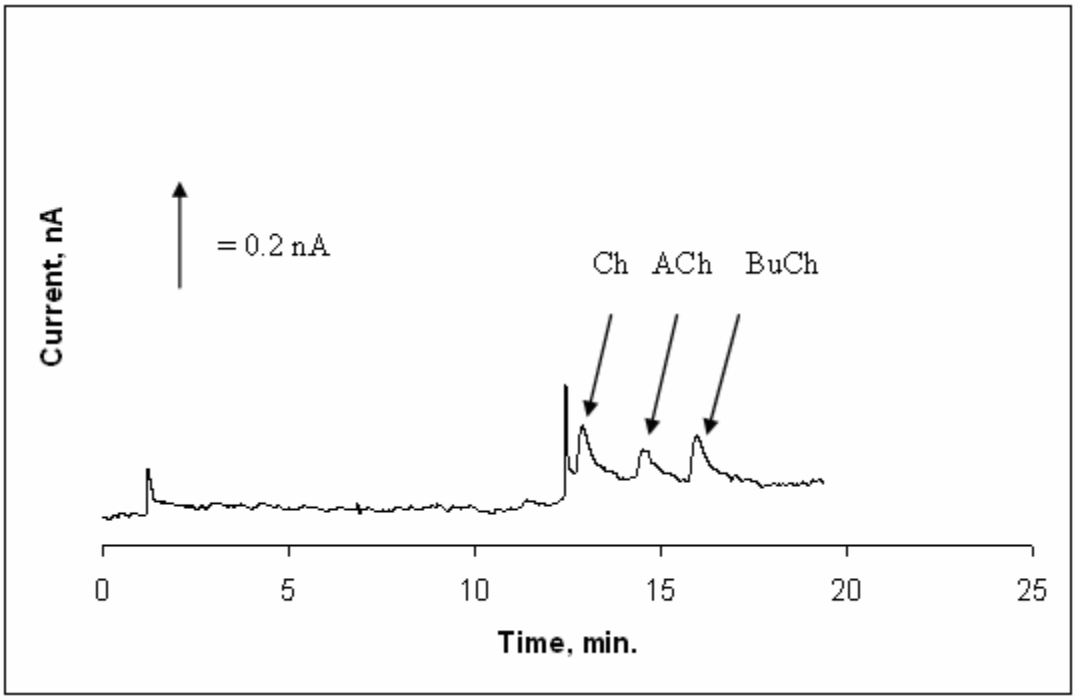


**Figure 3-12.** Electropherogram of a mixture containing 38 amol Ch, ACh, and BuCh detected by a HRP-AChE-ChO Au ME. Run buffer = 50 mM TES, pH 8.0; separation voltage = +20 kV; detection potential = +0.10 V vs. Ag/AgCl.

The limit of detection of a previous method by Kirchhoff et al. using a Pt ME crosslinked with ChO and AChE was 25 fmol for ACh and 100 amol for Ch.[29,30] Yamamoto et al. had developed a osmium-peroxidase redox polymer modified gold ring-disk electrode in compliance with HPLC for detection of ACh with a detection limit of 3 fmol.[23] Larsson et al. has also developed a three enzyme sensor using graphite electrodes for ACh detection, with a detection limit of 0.3 μM.[24] This low detection limit clearly demonstrates the advantage of extraordinary sensitivity of capillary electrophoresis coupled with the selectivity of enzyme modified electrode.

### 3.3.6. Stability of HRP-Os-AChE-ChO Au ME

The operational and storage stability of these ME systems were evaluated. Operational stability indicates the performance of the electrodes when being used continuously, while storage stability is an indication of the duration for which the electrodes can be stored under suitable condition before actually being used.

#### 3.3.6.1. Operational Stability of the Electrodes

One of the challenges of using enzyme modified microelectrodes for CE is that the electrodes are operated under hydrodynamic conditions. Hence, there is a gradual loss of sensitivity due the washing away of enzymes from the electrode surface. Loss of sensitivity also results due to decrease in enzymatic activity as a result of fouling of the electrode surface. The operational stability of these electrode systems was therefore studied. The amperometric response for Ch and ACh was monitored both as a function of time and number of runs, the starting time of the first run being t = 0. The electrodes showed good performance for at least more that 40 runs for a period of ~ 72 hours. An average electrode could be operated for approximately 63 runs for about 83 hours. Since samples were injected using a semiautomatic method, and extremely small sample volumes were used, the absolute peak area of the analytes could not be used as a standard for evaluating the operational stability of the electrodes. However, for the HRP-AChE-ChO system there was an average decrease of current peak area of Ch by 8 % during the first 10 hours of operation, which dramatically decreased to 48 % after 24 hours of continuous usage. The corresponding decrease of ACh peak area was 4 % and 47 %, respectively. The use of an internal standard enabled evaluation of the current response of Ch and ACh as a function the ratio of their respective peak areas. This effectively

compensated for any loss of sensitivity due to fouling/loss of enzymes on the electrode surface along with discrepancies resulting from the semiautomatic injection method used. Hence, a fairly stable electrode response was observed for both Ch and ACh. Figures 3-13. and 3-14. depict the operational stability of three different electrodes in response to Ch and ACh as a function of the number of runs. Figure 3-15 and 3-16 indicates the response towards Ch and ACh respectively as a function of time in hours.

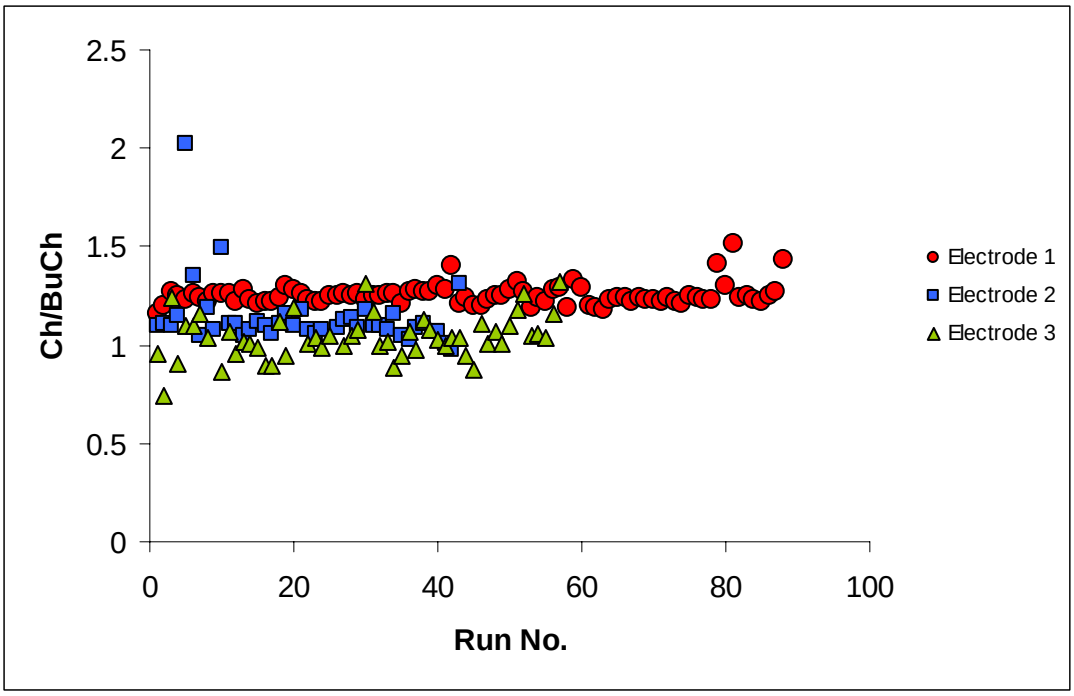


**Figure 3-13.** Operational stability of three different HRP-AChE-ChO Au MEs indicated by peak area ratio of Ch/BuCh as a function of number of runs.

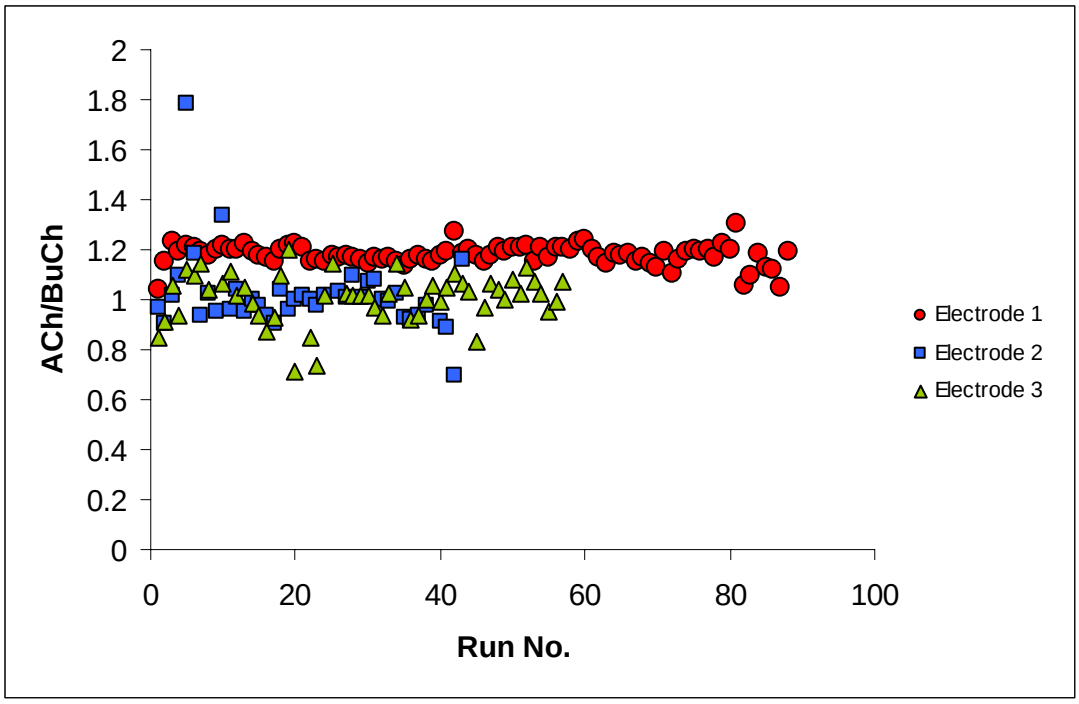


**Figure 3-14.** Operational stability of three different HRP-AChE-ChO Au MEs indicated by peak area ratio of ACh/BuCh as a function of number of runs.

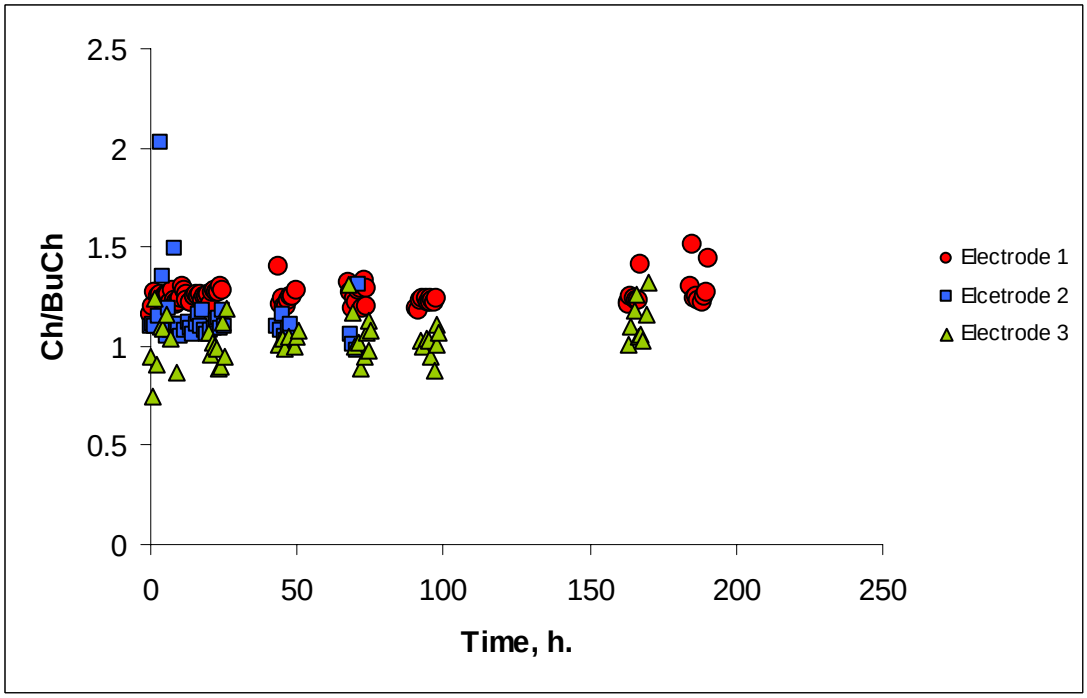


**Figure 3-15.** Operational stability of three different HRP-AChE-ChO Au MEs indicated by peak area ratio of Ch/BuCh as a function of time measured in hours.

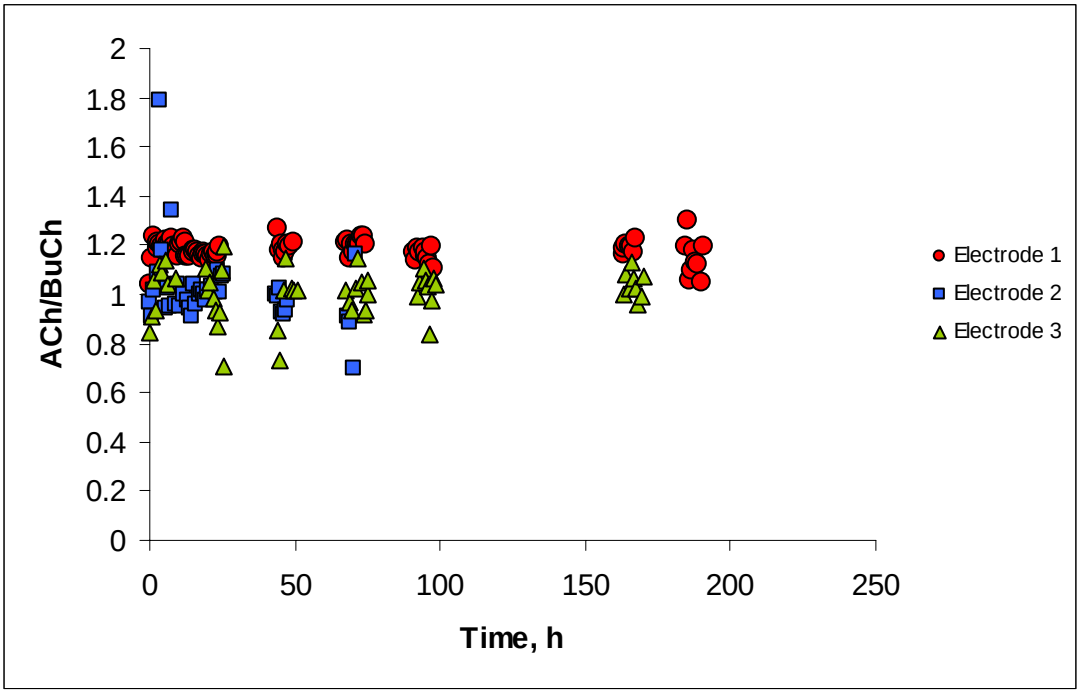


**Figure 3-16.** Operational stability of three different HRP-AChE-ChOAu MEs indicated by peak area ratio of ACh/BuCh as a function of time measured in hours.

As can be seen from Figures 3-13 to 3-16 electrode 1 had exceptionally good performance, while electrode 2 had a relatively poor performance. Since the performance would vary for each electrode, probably most electrodes would have an average performance of the three electrodes. It can also be concluded that the response of an electrode follows the same trend for both Ch and ACh i.e., an electrode with a stable response for Ch is expected to exhibit similar trend for ACh and vice versa. This is due to the fact that the detection of both these molecules is governed by the same set of enzymes.

It can be noted that run number 5 and 10 for electrode number 2 had an erratic value for both Ch and ACh. The ratios are fairly consistent before and after this run. This characteristic value is attributed to adsorption of air bubbles onto the electrode surface

which significantly alters the performance properties. Formation of air bubbles is a common problem encountered with CE-EC and at such a situation the air bubble has to be removed manually prior to further continuation of the experiment.

Although the capillary was rinsed after every run, the column was not conditioned for the entire duration of experiment, as conditioning with HCl would destroy the electrode enzyme layer. Hence, in spite of good analytical performance of the electrode sometimes erratic peak area ratios are also obtained due to variation in degrees of baseline resolution of the analytes. This happens as a result of gradual changes occurring inside the capillary after repeated runs which ultimately affect the resultant EOF.

It is pertinent to mention that accurate quantification of analytes without using an internal standard can sometimes be achieved by attachment of enzymes on the electrode surface through covalent linkage. However this approach has certain disadvantages because electrode performance under this condition heavily depend on the orientation of enzymes with respect to the electrode surface. Covalent modifications also may result in a decrease in overall enzymatic activity due to distortion of the enzymatic structure.

### 3.3.6.2. Storage Stability of the Developed Electrodes

After immobilization with enzymes, electrodes were dried at ambient temperature for ~ 1 hour and then stored at -20 °C until used. Under this storage condition, the electrode performance was excellent for the first 2-3 days and good for up to one week. Weak amperometric signals were only obtained after 7-10 days. Electrode activity was retained for a maximum of two weeks.

### 3.4. Conclusions

The focus of this effort was to extend microelectrode techniques for capillary electrophoretic systems for the detection of Ch and ACh, two important substances playing a pivotal role in mammalian neurochemistry. Catalytic redox polymer microelectrode systems were developed. These sensors when coupled to CE enabled efficient separation of the neurotransmitters. The response of these electrodes varied in sensitivity indicating the necessity for calibration for quantitative studies, but once calibrated would provide a reliable method for cholinergic analysis. The electrodes exhibited good overall performance and seemed suitable for analysis of biological samples containing low endogenous levels of Ch and ACh. Development of these catalytic redox polymer microelectrodes has hence proved to be an integral aspect of cholinergic analysis as broad linear range and low detection limits were also achieved.

## 3.5. References


1. Potter, P. E.; Meek, J. L.; Neff, N. H. Acetylcholine and Choline in Neuronal Tissue Measured by HPLC with Electrochemical Detection. *J Neurochem.* **1983,** *41*, 88-94.

2. Vetich, N. C. Horseradish Peroxidase: A Modern View of a Classic Enzyme. *Phytochemistry*, **2004**, *65*, 249-259.

3. Veitch, C.; Smith, A. T. Horseradish Peroxidase, *Adv. Inorg. Chem*. **2001**, *51*, 107-162.

4. Haschke, R. H.; Friedhoff, J. M. Calcium-related Properties of Horseradish Peroxidase. *Biochem. Biophys. Res. Commun.* **1978,** *80*, 1039-1042.

5. Gajhede, M.; Schuller, D. J.; Henriksen, A.; Smith, A. T.; Poulos, T. L. Crystal Structure of Horseradish Peroxidase C at 2.15 Å Resolution. *Nat. Struct. Biol.* **1997**, *4*, 1032 – 1038.

6. Marcus, R. A.; Sutin, N. Electron Transfers in Chemistry and Biology. *Biochim. Biophys. Acta.* **1985***, 811,* 265-322.

7. Marcus, R. A. Electron Transfer Reactions in Chemistry: Theory and Experiment. Nobel Lecture, December 8, **1992**.

8. Heller, A. Electrical Wiring of Redox Enzymes. *Acc. Chem. Res.* **1990**, *23*, 128-134.

9. Woderer, S.; Henninger, N.; Garthe, C.; Kloetzer, H. M.; Hajnsek, M.; Kamecke, U.; Gretz, N.; Kraenzlin, B; Pill, J. Continous Glucose Monitoring in Interstitial Fluid Using Glucose Oxidase Based Sensor Compared to Establish Blood glucose Measurements in Rats. *Anal. Chim. Acta*, **2007**, *581*, 7-12.

10. Kuwahara, T.; Meguro, M.; Osaka, T. Amperometric Acetylcholine Sensor Based on Bienzyme Immobilized by Polyion Compels on the Electrodeposited Platinum. *Chem. Sensors,* **2000**, *16*, 100-102.

11. Sato, N.; Okuma, H. Amperometric Simultaneous Sensing System for D-glucose and L-Lactate Based on Enzyme Modified Bilayer Electrodes. *Anal. Chim. Acta*, **2006,** *565*, 250-254.

12. Cass, A. E. G.; Davis, G.; Francis, G. D.; Hill, H. A. O.; Aston, W. J.; Higgins, I. J.; Plotkin, E. V.; Scott, L. D. L.; Turner, A. P. F. Ferrocene-Mediated Enzyme electrode for Amperometric Detection of Glucose. *Anal Chem*. **1984,** 56, 667-671.

13. Kulys, J. J.; Samalius, A. S.; Svirmickas, G. J. S. Electron Exchange Between Enzyme Active Center and Organic Metal. *FEBS Lett.* **1980,** *114*, 7-10.

14. Habermüller, K.; Mosbach, M.; Schuhmann, W. Electron-Transfer Mechanisms in Amperometric Biosensors. *Frensenius J. Anal. Chem*. **2000**, *366*, 560-568.

15. Heller, A. Electrical Wiring of Enzymes. *Acc. Chem. Res*. **1993**, *23*, 128-134.

16. Heller, A. Amperometric Biosensors. *Curr. Opin. Biotechnol*. **1996**, *7*, 50-54.

17. Degani, Y.; Heller, A. Direct Electrical Communication between Chemically Modified Enzymes and Metal Electrodes. Methods for Bonding Electron Transfer Relays to Glucose Oxidase and D-Amino Acid Oxidase. *J. Am. Chem. Soc.* **1988**, *110,* 2615-2620.

18. Willner, I.; Katz, E. Integration of Layered Redox Proteins and Conductive Supports for Bioelectronic Applications. *Angew. Chem. Int. Ed.* **2000**, *39*, 1118-1218.

19. Aoki, A.; Rajagopalan, R.; Heller, A. Effect of Quarternization on Electron Diffusion Coefficients for Redox Hydrogels based on Poly(4 vinyl pyridine). *J. Phys. Chem.* **1995**, *99*, 5102-5110.

20. Vreeke, M.; Maidan, R.; Heller, A. Hydrogen Peroxide and β -Nicotinamide Adenine Dinucleotide Sensing Amperometric Electrodes Based on Electrical Connection of Horseradish Peroxidase Redox Centers to Electrodes through a Three-Dimensional Electron Relaying Polymer Network. *Anal. Chem.* **1992**, *64,* 3004-3090.

21. Garguilo, M. G.; Huynh, N.; Proctor, A.; Michael, A. C. Amperometric Sensors for Peroxide, Choline, and Acetylcholine Based on Electron Transfer between Horseradish Peroxidase and a Redox Polymer. *Anal Chem.* **1993,** *65,* 523-528.

22. Garguilo, M. G.; Michael, A. C. An Enzyme-Modified Microelectrode That Detects Choline Injected Locally into Brain Tissue. *J. Am. Chem. Soc*. **1993**, *115*, 12218-12219.

23. Yamamoto, K.; Sato, K.; Chikuma, T.;Kato, T. A Highly Sensitive and Stable Detection of Acetylcholine by HPLC-Osmium-Horseradish Peroxidase Redox Polymer Electrode Coated on a Gold Radial Flow Ring Disk. *Anal. Chim. Acta*, **2004**, *521*, 209–213.

24. Larsson, N.; Ruzgas, T.; Gorton, L.; Kokaia, M.; Kissinger, P. Design and Development of an Amperometric Biosensor for Acetylcholine Determination in Brain Microdialysates. *Electrochim. Acta,* **1998**, *43*, 3541 – 3554.

25. Garguilo, M. G.; Micheal, A. C. Enzyme Modified Electrodes for Peroxide Choline and Acetylcholine. *Trends Anal. Chem*. **1995**, *14,* 164-169.

26. Alvarado, R. J.; Mukherjee, J.; Pacsial, E. J.; Alexander, D.; Raymo, F. M. Self

Assembling Bipyridinium Multilayers. *J. Phys. Chem. B.* **2005,** *109*, 6164-6173.

27. Kauz, N. A.; Kandel, A. S. Alkanethiols/Au (111) Self Assembled Monolayers Contain Gold Adatoms: Scanning Tunneling Microscopy before and After Reaction with Atomic Hydrogen. *J. Am. Chem. Soc.* **2008**, *130*, 6908-6909.

28. Sun, Y.; Liu, Y.; Feng, C. A Comparative Studies of Immunosensors Based on Self-Assembled Monolayers Formed from here Different Sulfides. *Lanzhou Dax. Xuebao Zir. Kex.* **2007,** *30*, 207-209.

29. Wise, D. D.; Barkhimer, T. V.; Brault, P.-A.; Kirchhoff, J. R., ; Messer, W. S., Jr.; Hudson, R. A. J. Internal Standard Method for the Measurement of Choline and Acetylcholine by Capillary Electrophoresis with Electrochemical Detection. *J. Chromatogr. B,* **2002,** *775*, 49–56.

30. By decreasing the internal standard concentration to 25 μM, the mass detection limit for Ch was reduced to 100 amol.

# Chapter 4

## Development of an Artificial Peroxidase Based Bienzyme Microelectrode Detector for Capillary Electrophoresis

## 4.1. Introduction

Peroxidases covalently bound to redox mediators can effectively catalyse the reduction of $H_2O_2$, its natural substrate. Although these redox relay bound peroxidases allow efficient electron transfer to detect peroxides with sufficient sensitivity, they are very often limited by shortcomings of moderately high unit costs and weak binding to electrode surfaces. The catalytic function of HRP can be substituted by various synthetic electron mediators that can act as electrochemical transducers for $H_2O_2$. The application of transition metal catalysts for reduction of $H_2O_2$ has been a matter of interest.[1,2] These catalysts are a class of mixed valance metal hexacyanometallate compounds. They have the general formula $M_k^A[M^B(CN)_6]_l$ where A and B are different oxidation numbers of the transition metal whereas k and l are the respective stoichiometry.[3] Prussian Blue (PB) is one such compound with interesting electrochemical and magnetic properties. PB also exhibits an interesting property of electrochromism where the catalyst changes color depending upon its redox state.

PB, also known as "artificial peroxidase" has strong preferential catalytic properties for the electroreduction of $H_2O_2$.[4] This effective catalytic activity towards the reduction of $H_2O_2$ has been exploited for use in several novel biosensors.[5,6] In addition several analogues of PB namely ferric ruthenocyanide (Ruthenium Purple), palladium hexacyanoferrate, chromium hexacyanoferrate, and cupric hexacyanoferrate have also demonstrated flexible catalytic electrochemistry.[1]

### 4.1.1. Structure of Prussian Blue

PB (ferric ferricyanide $Fe_4^{III}[Fe^{II}(CN)_6]_3$ or iron(III)hexacyanoferrate(II)) is one of

the oldest coordination compounds reported in the literature. Numerous data gathered from characterization techniques such as X-ray diffraction, photoelectron spectroscopy, magnetic susceptibility and infrared spectroscopy have confirmed that this coordination compound is an iron (III) salt of hexacyanoferrate (II) and the presence of other alkali metals do not affect the oxidation state of these iron ions.[7] Keggin and Miles first reported the structure of PB based on powder diffraction pattern studies.[8] They have distinguished between two forms of PB, a soluble form ($KFe^{III}Fe^{II}(CN)_6$) and an insoluble form ($Fe_4^{III}(Fe^{II}(CN)_6)_3$). The insoluble form differs from the soluble form in the aspect of having excess Fe(III) ions, that have replaced the $K^+$ ions. These names do not refer to the real solubility of the compounds in water, but is only an indication of the ease with which potassium salts can be peptized. In reality both forms are highly insoluble in water. According to Keggin and Miles, the soluble form, $KFe^{III}Fe^{II}(CN)_6$ is formed in the presence of excess of potassium ions in solution, whereas the insoluble form lacks $K^+$ ions. The soluble form has a cubic structure where the Fe(II) and Fe(III) ions are located on the face centered cubic lattice. The Fe(II) ions are surrounded by C atoms, whereas Fe(III) ions are octahedrally surrounded by N atoms. The $K^+$ ions are believed to occupy the interstitial sites. The structure of insoluble PB has also been investigated through electron and neutron diffraction measurement studies by several researchers namely Ludi et al.,[9] Herren et al.,[10] and Buser et al.[11] with some basic differences from the soluble structure proposed by Keggin and Miles. The determined structure of insoluble PB is comparatively more disordered, with one fourth of the ferrocyanide sites unoccupied and no Fe(III) ions in the interstitial sites. The presence of 14-16 water molecules has also been detected. Some of them occupy the vacant nitrogen

sites from the ferrocyanide vacancies, while the others are uncoordinated and occupy the interstitial sites. Mossbauer and infrared studies have established that PB is a ferric ferricyanide with the weak field Fe(III) ions coordinated to N atoms and strong field Fe(II) ions coordinated to C atoms.[3] However it is important to remember that the structure of PB greatly depends on the experimental procedure and materials used for synthesis and hence PB can be designated as the generic terminology for a class of ferrocyanide compounds with variable stoichiometry. These transition metal hexacyanides have a three-dimensional crosslinked polymeric network characterized by low density, variable stoichiometry and are very similar to crosslinked organic polymers. PB is known to be like zeolites in nature, they readily exchange Group I cations in solution and allow the free diffusion of low molecular weight molecules like $O_2$ and $H_2O_2$ through their three-dimensional crystal structure.[3,12]

### 4.1.2. Electrochemistry of PB

PB or ferric ferricyanide $Fe_4^{III}[Fe^{II}(CN)_6]_3$ can be formed by deposition from an aqueous solution of $FeCl_3$ and $K_3Fe(CN)_6$ either spontaneously or under the influence of a constant potential.[13] Neff was the first to report the successful electrodeposition of thin films of PB on Pt foil electrode and the electrochemical oxidation and reduction properties.[14] The film prepared from a solution containing equimolar amounts of $FeCl_3.6H_2O$ and $K_3Fe(CN)_6$ was bright blue in color during the anodic sweep and turned colorless on the cathodic sweep. He attributed this reaction to the reduction of colored PB into a colorless form named Everitt's salt or Prussian White (PW). The electrochemistry of PB has been further investigated by several other researchers. Itaya et al. have reported

the electrodeposition of PB on various types of electrodes such as Pt, glassy carbon, and tin oxide ($SnO_2$).[15] His investigation revealed that the amount of PB electrodeposited could be varied by controlling certain experimental parameters such as electrode potential, electrolysis time and solution concentration. The cathodic and anodic voltammogram waveform observed were attributed to the reduction of Fe(III) ions to Fe(II) ions and the reoxidation of Fe(II) ions to Fe(III) ions respectively. Figure 4-1 depicts the reversible CV of PB which is a significant feature for its electroanalytical applications. The electrochemistry of PB has been thoroughly investigated by various researchers.[16-18] Since PB forms cross linked polymer films on the electrode surface, it has posed severe challenges for accurate structure characterization. The uncertainty in its three-dimensional structure has also lead to several contradictions related to the stoichiometry of the electrochemical reaction on the electrode surface and its exact mechanism of catalysis. Ellis et al. have proposed the following electrochemical reaction for soluble PB:[12]

$$KFe^{III}Fe^{II}(CN)_6 + K^+ + e^- \rightleftharpoons K_2Fe^{II}Fe^{II}(CN)_6$$

Prussian Blue (PB) Prussian White (PW or Everitt Salt)

However, Itaya et al. have proposed another reaction scheme based on the reaction of insoluble PB :[11]

$$Fe_4^{III}[Fe^{II}(CN)_6]_3 + 4K^+ + 4e^- \rightleftharpoons K_4Fe_4^{II}[Fe^{II}(CN)_6]_3$$

Prussian Blue (PB) Prussian White (PW or Everitt Salt)

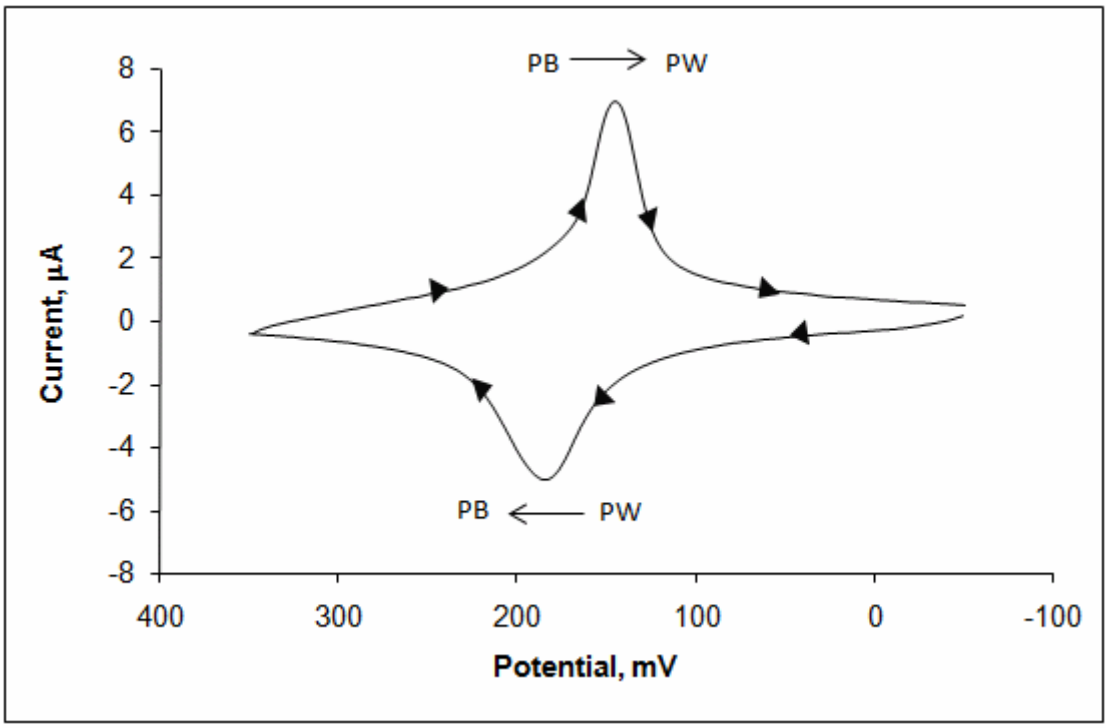


**Figure 4-1.** CV depicting the electrochemical oxidation and reduction of PB on a Pt ME. Electrolyte solution = 0.1 M KCl/HCl; scan rate = 40 mV/s; initial potential = -50 mV; switching potential = +350 mV. Arrows indicate direction of scan.

The reduced form of PB (PW) exhibits catalytic effect towards the reduction of $H_2O_2$. Hence, PB has been used as a transducer for $H_2O_2$ in several electrochemical sensors. $H_2O_2$ has been detected using PB based microelectrode and nanoelectrode array, as well as electrode modified with dendrimetric PB.[19-22] The fast electron transfer rate coupled with a low detection potential has made PB an attractive mediator for $H_2O_2$ reduction in various biosensors.

However in spite of the catalytic activity of PB as a transducer for $H_2O_2$ not much effort has been invested towards the quantification and analysis of cholinergic neurotransmitters using PB. Wu et al. have obtained a patent for detection of ACh using PB-gold nanoparticle modified electrodes.[23] Carlo et al. have developed a PB based sensor for detection of pesticides based on esterase inhibition.[24] Ricci et al. have

developed PB modified conducuting polymer nanotubules and PB based screen printed electrodes immobilized with various enzymes for detection of their respective substrates.[25] In this chapter, the ability of PB modified ME coordinated with cholinergic enzymes as detectors for capillary electrophoresis has been evaluated and the performance characteristics of these electrodes studied. Figure 4-2 depicts the sequence of events expected to occur at the electrode surface utilizing PB as a transducer for cholinergic detection.

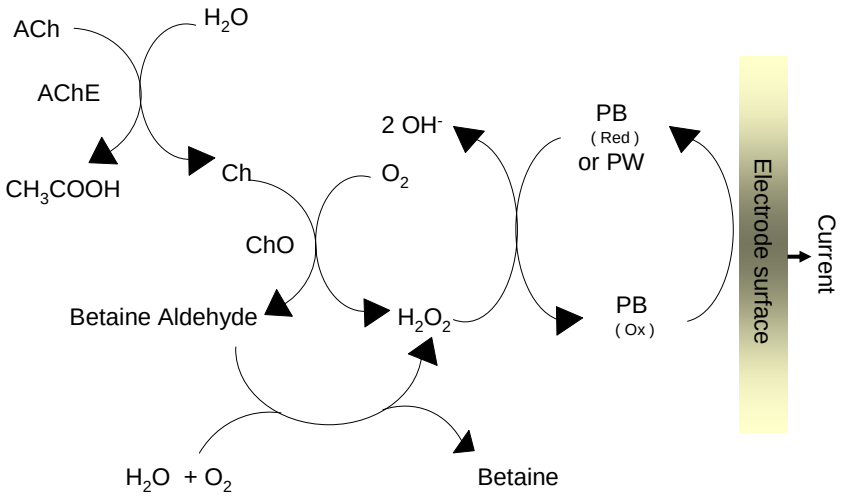


**Figure 4-2.** Depiction of the sequence of events by which an electrochemical signal is generated for the detection of Ch, ACh and BuCh using a PB-modified enzyme electrode.

## 4.2. Material and Methods

### 4.2.1. Materials

Acetylcholinesterase (EC 3.1.1.7, type V-S from *Electrophorus electricus*, > 1070 U/mg of protein), choline oxidase (EC 1.1.3.17, *Alcaligenes* species, 9-18 U/mg), acetylcholine chloride (>99%), choline chloride (>98%), and butyrylcholine chloride (>98%) were purchased from Sigma (St. Louis, MO) and stored in a desiccator at -16 °C. Glutaraldehyde (grade I, 25% aqueous solution) was purchased from Sigma and stored at 4 °C. *N*-Tris[hydroxymethyl]methyl-2-aminoethane-sulfonic acid (TES) (>99%), iron (III) chloride (97%) and potassium hexacyanoferrate (III) (≥ 99.9%) were also purchased from Sigma and stored at ambient temperature. Platinum wire (25 $\mu$m in diameter, 99.99%) was obtained from Goodfellow (Berwyn, PA). All other chemicals were of analytical reagent grade and were used as received. Solutions were prepared with distilled deionized water purified to a resistivity of at least 17 MΩ-cm by a Barnstead B pure water purification system.

### 4.2.2. Instrumentation

All experiments were conducted using a laboratory built capillary electrophoresis instrument with the electrochemical detection method that has been previously described in Chapter 2.

### 4.2.3. Methods

#### 4.2.3.1 Preparation of PB-AChE-ChO Enzyme Electrodes

##### 4.2.3.1.1. Preparation of ME

Pt MEs were prepared using the general procedure described in Chapter 2. In the case of thermal deposition processes, the electrodes were housed inside a truncated plastic pipette tip after heat treatment as the plastic and hot glue would melt at elevated temperature. Before any chemical modification, the ME tip was rinsed with acetone, deionized water and finally with acetone. The electrodes were then dried at ambient conditions for 10 minutes.

##### 4.2.3.1.2. Deposition of PB on ME Surface

The surface of the Pt MEs was modified using an electrodeposition method and two different approaches to thermal deposition techniques.

###### 4.2.3.1.2.1. Thermal Deposition Method: Spontaneous Film Formation

PB films have been prepared by placing equimolar solutions of $FeCl_3$/ $K_3[Fe(CN)_6]$ onto the working electrode.[25] Hence, analogous literature methods were adopted and 1:1 molar ratio of 2 mM, 4 mM, and 8 mM $FeCl_3$/ $K_3[Fe(CN)_6]$ in 0.1 M HCl/KCl aqueous solution was mixed together in a 25 mL beaker. The tip of the Pt ME was dipped into the solution and rotated manually for ~ 10 minutes. The electrodes were handled carefully and allowed to cure in an oven at 80-100 ºC for at least 12 hours.

PB is known to form spontaneously on metal surfaces. Since the small surface of the Pt ME posed a hindrance to the deposition process, alternately ~ 2 mL of the solution was placed on an Al foil and the electrode tip was rubbed against it for ~ 10 minutes. The electrodes were then cured under the same conditions.

The resulting PB film was then activated following modified procedure of Karyakin et al. where the films were cycled repeatedly between -0.50 to + 0.35 V vs Ag/AgCl at 40 mV/s in 0.1 M KCl/HCl solution until a stable voltammogram was obtained. [19,26] The Pt surface was rinsed with copious amount of deionized $H_2O$ to remove any traces of acid that can destroy enzymes. A solution of 1:1 4 mM $FeCl_3$/ $K_3[Fe(CN)_6]$ was also prepared in various concentrations of HCl/KCl solution for optimization studies. If not used immediately, the electrodes were stored at ambient temperature in the dark. Enzyme modification of the electrode surface was performed by gently dipping the electrode into a 7 μL aqueous solution containing 6 units of ChO, 25 units of AChE and 0.5 μL of 25 % aqueous glutaraldehyde solution.

#### 4.2.3.1.2.2. Thermal Deposition Method: Slow Film Formation

Neff had demonstrated a method of preparing PB films by simply immersing a cathodized Pt electrode in a solution of ferric ferricyanide for a certain period of time.[14] Hence, a similar procedure was used where 1:1 molar ratio of $FeCl_3$/ $K_3[Fe(CN)_6]$ were prepared in 0.1 M HCl/KCl aqueous solution in concentrations ranging from 4 to 25 mM. The Pt MEs were dipped into unstirred solution and allowed to grow for ~ 72 h in dark. During this time a thin layer of catalyst formed on the surface of the Pt metal and grew with time. The electrodes were then washed with deionized water and cured in an oven at

~ 80-100 ºC for ~ 12 h. The PB film formed was similarly activated by repeated cyclic voltammetry scans and enzyme modification method identical to Section 4.2.3.1.2.1.

#### 4.2.3.1.2.3. Electrochemical Deposition Method

PB films were electrochemically deposited on Pt MEs following generalized literature procedures with modifications.[2,19] Various concentrations of 1:1 molar ratio of $FeCl_3$/ $K_3[Fe(CN)_6]$ ranging from 2 to 50 mM were prepared in 0.1 M HCl/KCl aqueous electrolyte solution. PB was deposited at constant potential of +0.4 V vs Ag/AgCl for 180 s. The film was activated by cycling between -0.50 to +0.35 V vs Ag/AgCl at 40 mV/s in fresh 0.1 M KCl/HCl solution until a stable voltammogram was obtained (approximately 20 sweeps, 10 cycles). The electrodes were thoroughly washed with deionized water and further modified with AChE/ChO by chemical crosslinking with glutaraldehyde using a 7 µL aqueous solution containing 6 units of ChO, 25 units of AChE and 0.5 µL of 25 % aqueous glutaraldehyde solution.

### 4.2.3.2. Determination of Optimum Operational Potential

The optimum operational potential was determined by injecting a standard Ch solution into the capillary and observing the generated electropherogram. Because pure Ch solution was used, separation was not necessary; hence the analyte solution was allowed to pass through the capillary by applying pressure.

### 4.2.3.3. Separation of Ch, ACh and BuCh

A 145 cm polyimide coated fused-silica capillary with i.d. 50 µM and o.d. of 350

μM (Polymicro Technologies, Phoenix,AZ, USA) was used for the optimized separation. Electropherograms were generated by applying varying voltages from 9 to 20 kV. TES buffer (50 mM, pH, 8.0) was used as the separation buffer. Phosphate buffer (20 mM, pH, 7.0) was used in the detection cell. All standard solutions of Ch, ACh and BuCh were prepared fresh daily in deionized water and stored in ice.

#### 4.2.3.4. Linear Range of PB-AChE-ChO PB MEs

The linear range for Ch and ACh with PB-AChE-ChO Pt MEs were studied using optimized electrophoretic separation conditions. Varying concentrations of standard solutions of Ch and ACh were prepared from 10 to 2000 μM. The concentration of BuCh was held constant at 200 μM for all analyses.

#### 4.2.3.5. Stability of PB-AChE-ChO Pt MEs

The electrode surface was electrodeposited with PB film and then immobilized with enzymes. Operational and storage stability of these chemically modified electrodes were studied.

##### 4.2.3.5.1. Operational Stability of the Modified Au MEs

Modified Pt MEs were carefully aligned with the already conditioned capillary and fixed in the configured position using liquid electrical tape. Standard stock solutions of Ch, ACh and BuCh were prepared daily and mixed in 1:1:1 ratio corresponding to a final concentration of 500 μM. Electropherograms were continuously collected for the first 24 hours and then for ~ 8 hours every 12-15 hours until the electrode performance severely deteriorated and negligible response was obtained.

## 4.3. Results and Discussion

### 4.3.1. Deposition of PB on Pt MEs

#### 4.3.1. 1. Thermal Deposition

PB is known to form spontaneously on a variety of surfaces that are simply in contact with acidic $FeCl_3$ /$K_3[Fe(CN)_6]$ solution. This property of formation of PB was utilized to form catalytic films on Pt MEs.

##### 4.3.1.1.1. Spontaneous Film Formation

PB-AChE-ChO Pt MEs were prepared by a spontaneous film formation thermal deposition method. The basis of this method was that the small Pt surface would act as a substrate for PB deposition. In theory rotation of the Pt tip in the $FeCl_3$ /$K_3[Fe(CN)_6]$ solution and rubbing Pt wire against the Al foil would enhance the reaction and lead to more deposition yielding a catalytic film of sufficient thickness. Under these conditions, an electroactive layer of PB catalyst was formed on the electrode surface under all circumstances. However, the catalytic activity of these films was very low. The catalytic activity was estimated from their CVs. Catalytic activity was also evaluated by further modification of the electrodes with ChO and AChE followed by testing for the detection of Ch. Figure 4-3 depicts the CVs of the PB modified films. The voltammograms were broad with low cathodic and anodic peak currents. Different concentrations of HCl/KCl were used to evaluate the effect of concentration of acid and salt on PB deposition. The best films were formed using 0.1 M HCl/KCl solution. Although more PB was formed using 0.5 M and 1 M HCl/KCl, most of it remained suspended in solution and did not

adhere to the Pt ME surface.

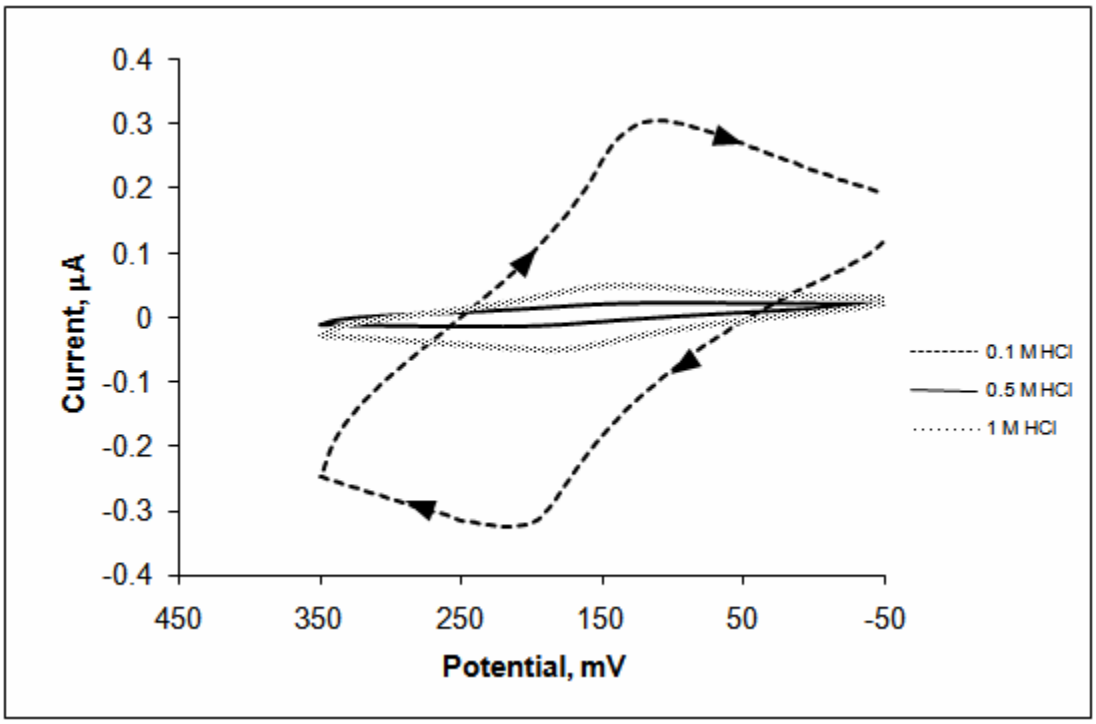


**Figure 4-3.** CVs of Pt MEs modified by PB deposition by spontaneous film formation method employing 4 mM 1:1 $FeCl_3/K_3[Fe(CN)_6$ in a solution containing varying amounts of HCl and KCl. Scan rate = 40 mV/s; initial potential = -50 mV; switching potential = +350 mV; Arrows indicate direction of scan.

#### 4.3.1.1.2. Slow Flim Formation

Since films developed by the spontaneous deposition method did not result in good sensitivity, a new method of depositing PB films onto the electrode surface was developed. The basis of developing this method was that the Pt MEs would be in contact with a solution of $K_3[Fe(CN)_6]$ and $FeCl_3$ and the Pt metal itself would act as a substrate for film formation. The PB films would be allowed to grow on the Pt surface undisturbed and a reaction would occur between $K_3[Fe(CN)_6]$ and $FeCl_3$ in a stoichiometric amount. The system would be left for relatively long time to obtain a catalytic film of sufficient

thickness. The properties of the film would be governed by deposition conditions such as deposition time and concentration of $K_3[Fe(CN)_6]$ and $FeCl_3$ used.

A 0.1 M KCl/HCl solution was used for all concentrations since the best films were formed by the spontaneous deposition method. 4 mM, 8 mM, 15 mM, 25 mM of 1:1 $K_3[Fe(CN)_6]/FeCl_3$ solutions were prepared. Concentrations lower that 4 mM were not used because adequate film formation may not occur at low concentrations. Figure 4-4 compares the CV of films formed using 4 mM, 8 mM, 15 mM and 25 mM concentrations. The CVs correspond to the oxidation of PW to PB in the positive scan as the potential is sweeped towards more positive values. In the reverse negative scan as the potential is sweeped from + 350 mV to -100 mV, oxidized PB is reduced again to yield PW.

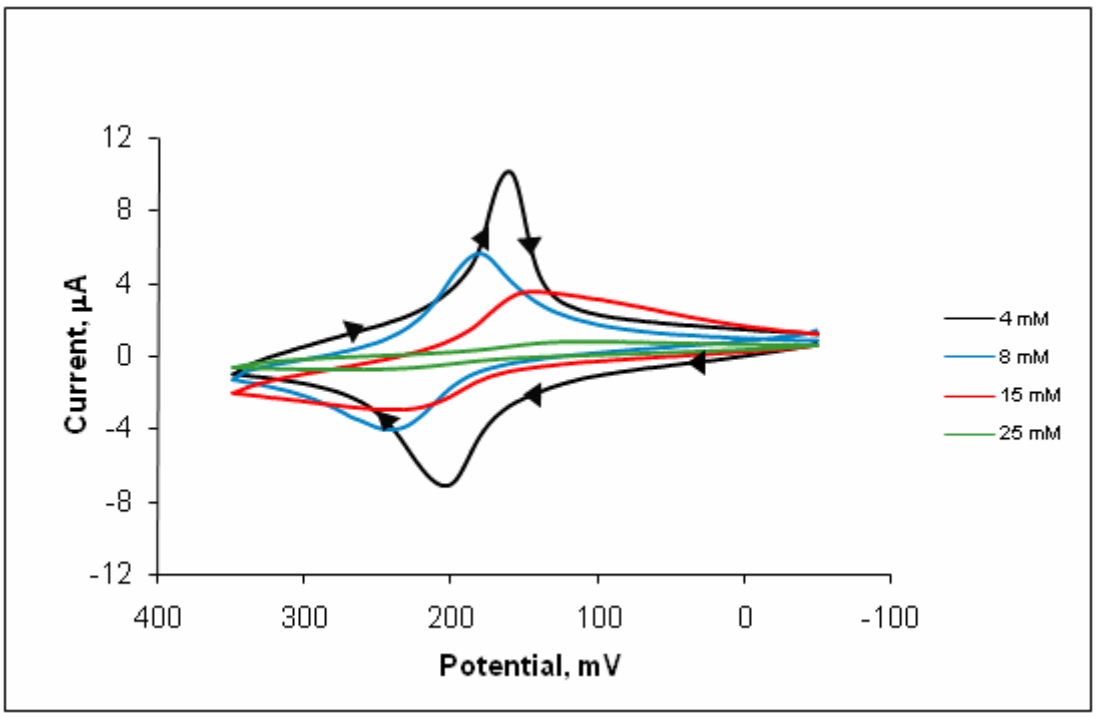


**Figure 4-4.** CVs of Pt MEs modified with varying concentrations of 1:1 $K_3[Fe(CN)_6]$ : $FeCl_3$ in 0.1 M KCl/HCl solution deposited by slow film formation method. Scan rate = 40 mV/s; initial potential = -50 mV; switching potential = +350 mV. Arrows indicate direction of scan.

As predicted, it was observed that the activity of the deposited PB were a function of concentration of $K_3[Fe(CN)_6]$ and $FeCl_3$ used. By varying the solution concentration it was possible to change the thickness of the film formed. Film thickness was proportional to the solution concentration and could be easily visually distinguished. At concentrations above 8 mM, thick amorphous lumps were formed on the electrode surface. However in spite of thicker films being formed at higher concentrations, optimum catalyst formation occurred at 4 mM concentration.

After PB deposition and thermal curing, the catalyst was activated by repeated potential cycling until a stable voltammogram was obtained. As the films grew in thickness, probably only the lower layers could be activated rendering most of the deposited catalyst ineffective.

**Table 4-1**. Comparison of $i_p$ and $E_p$ of Pt MEs Modified with Varying Concentrations of 1:1 $K_3[Fe(CN)_6]$ : $FeCl_3$ Deposited by Slow Film Formation Method.

| Concentration of $K_3[Fe(CN)_6]$, $FeCl_3$ (mM) | $i_{pa}$ (μA) | $i_{pc}$ (μA) | $E_{pa}$ (mV) | $E_{pc}$ (mV) | $\Delta E_p$ (mV) |
|---|---|---|---|---|---|
| 4 | - 5.16 | + 6.50 | + 204 | + 162 | 42 |
| 8 | - 3.41 | + 4.09 | + 241 | + 183 | 58 |
| 15 | - 2.02 | + 2.37 | + 233 | + 151 | 82 |
| 25 | - 0.39 | + 0.33 | + 246 | + 129 | 117 |

Table 4-1 compares the different voltammetric parameters of Pt MEs deposited using varying concentrations of $K_3[Fe(CN)_6]$ and $FeCl_3$. The cathodic and anodic peak currents were largest for 4 mM solution and decreased dramatically with increase in reactant concentration in the growing solution. It can be observed that the peak potential separation also increased progressively with an increase in $K_3[Fe(CN)_6]/FeCl_3$

concentration. As the concentration increased the peaks assumed a less symmetric nature indicating a shift from reversible towards a quasireversible electrochemical process.

It is pertinent to mention that varying the deposition time would probably have been an alternative method for manipulating the catalyst deposition condition. A smaller deposition time for higher concentrations may have resulted in more active catalyst formation. However such experiments were not conducted as it would result in too many variables and difficult choice of optimized conditions.

#### 4.3.1.2. Electrodeposition Method

The ability to form PB flims by an electrodeposition method on MEs was also investigated. Electrodeposition is a convenient method of electrocatalyst formation as the amount of catalyst deposited, thickness of film and electrochemical properties of the PB layer can be controlled very easily by controlling simple parameters such as deposition potential, deposition time and type of electrode material.[15] Under the influence of a constant potential, PB films were spontaneously electrodeposited onto the Pt MEs by the reduction of ferric ions in the presence of ferricyanide. An electrodeposition time of 180 s was selected as the optimum time as increasing the time of deposition beyond this point did not increase the surface coverage of catalytic films as determined by CV. Smaller deposition times resulted in lower currents. Figure 4-5 shows the coulometric behavior of a Pt ME in a solution of $K_3[Fe(CN)_6]$ and $FeCl_3$ as a function of time. The total charge can be calculated from the resulting current.

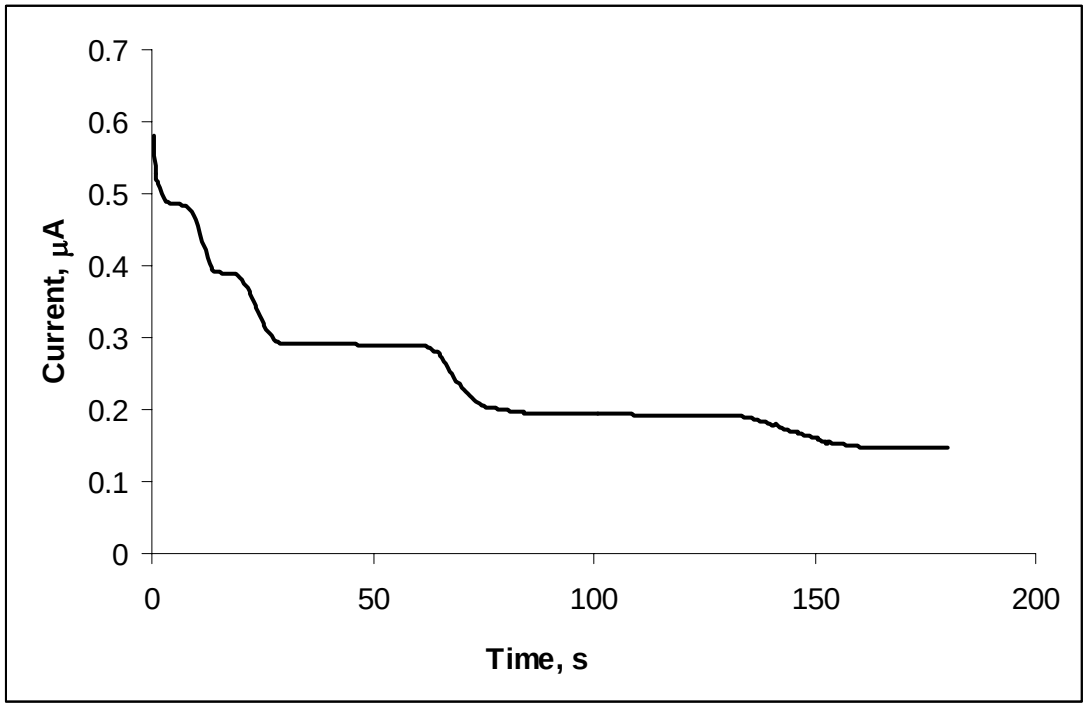


**Figure 4-5.** A typical potentiostatic deposition of PB on Pt ME prepared from 1:1, 4 mM $K_3[Fe(CN)_6]$ : $FeCl_3$ in 0.1M KCl / HCl solution . The response of change in current is monitored as a function of time. Applied potential = 400 mV vs. Ag/AgCl; deposition time = 180 s.

Total charge for this deposition was 43.44 μC. The average charge for potentiometric deposition for the same time range for 6 different electrodes wes calculated to be 40.17 ± 4.3 μC. Assuming a 4 ET process, the total amount of PB deposited is 112.6 pmoles. Since the exact surface area of the ME was unknown, the thickness of the deposited film could not be calculated. However, estimated coverage for a 1 mm long cylindrical ME is 1.43 nmol/$mm^{2.}$

In order to evaluate the optimum concentration of $K_3[Fe(CN)_6]$ : $FeCl_3$, various concentrations ranging from 2 to 50 μM of a 1:1 solution of $K_3[Fe(CN)_6]/FeCl_3$ were examined.

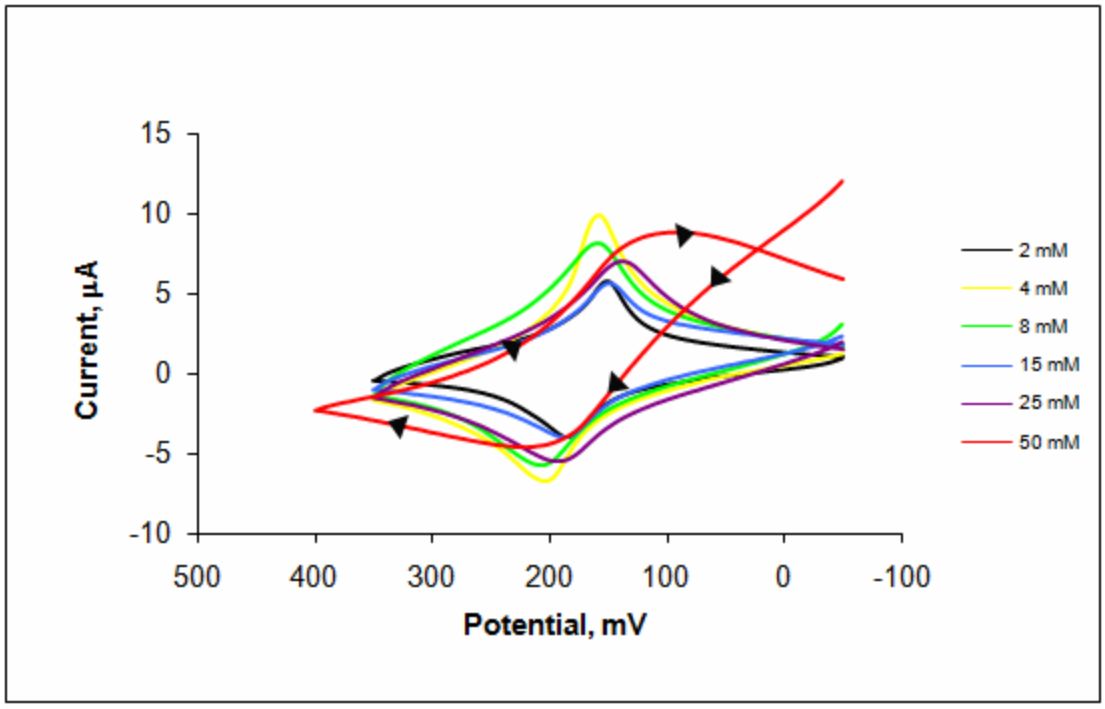


**Figure 4-6.** Representation of CVs of PB electrodeposited for 180 s on Pt MEs prepared from varying concentrations of $K_3[Fe(CN)_6]/FeCl_3$ in 0.1M KCl/HCl solution. Scan rate = 40 mV/s; initial potential = 50 mV; switching potential = +350 mV. Arrows indicate direction of scan.

CVs of the PB electrodes prepared from varying concentrations of $K_3[Fe(CN)_6]/FeCl_3$ revealed that the characteristics of the deposited catalyst was dependent on the solution concentration used for film preparation. Table 4-2 compares the voltammetric characteristics of the modified Pt electrodes.

**Table 4-2.** Comparison of $i_p$ and $E_p$ of PB Films Formed on Pt MEs by Electrodeposition from Varying Concentrations of 1:1 $K_3[Fe(CN)_6]$ : $FeCl_3$ in 0.1 M KCl/HCl Solution.

| Concentration (mM) | $i_{pa}$ (µA) | $i_{pc}$ (µA) | $E_{pa}$ (mV) | $E_{pc}$ (mV) | $\Delta E_p$ (mV) |
|---|---|---|---|---|---|
| 2 | - 2.79 | + 2.59 | + 184 | + 152 | 32 |
| 4 | - 4.60 | + 6.04 | + 203 | + 159 | 44 |
| 8 | - 2.96 | + 2.88 | + 203 | + 163 | 40 |
| 15 | - 2.38 | + 2.32 | + 185 | + 151 | 34 |
| 25 | - 1.93 | + 2.24 | + 185 | + 143 | 42 |
| 50 | - 0.80 | + 1.10 | + 94 | + 209 | 115 |

Increasing the solution concentration from 2 to 4 mM resulted in larger cathodic and anodic peak currents. This was probably because higher concentrations resulted in more catalyst deposition. However the current dropped beyond 4 mM progressively from 4 mM to 50 mM. The quality of the PB catalyst deposited can be judged by the sharpness of voltammetric oxidation and reduction peaks. At very high concentration the peak currents decreased significantly, the cathodic and anodic peaks were broad and very spread out with large peak to peak splitting values; indicating film thickness beyond the optimum conditions. More symmetrical voltammograms were observed at lower salt concentrations, indicating facile reversible reduction and oxidation of the PB polymer catalyst under such conditions.

After preparation of PB films by employing any of the above methods, the modified electrode was activated by repeated cycling between a suitable potential range.[19,26] This process caused oxidation of PW to PB in the positive scan and reduction of PB to PW during the negative scan along with incorporation of $K^+$ ions into its lattice structure. This repeated cycling of oxidation and reduction activated the catalyst. Figure 4-7 and 4-8 depicts the CV of a particular PB modified Pt ME prepared by electrodeposition process, for the first 10 and next 10 scans, respectively. With repeated cycling, the cathodic and anodic peak currents increased in magnitude until limiting values were obtained indicating that the film was fully activated.

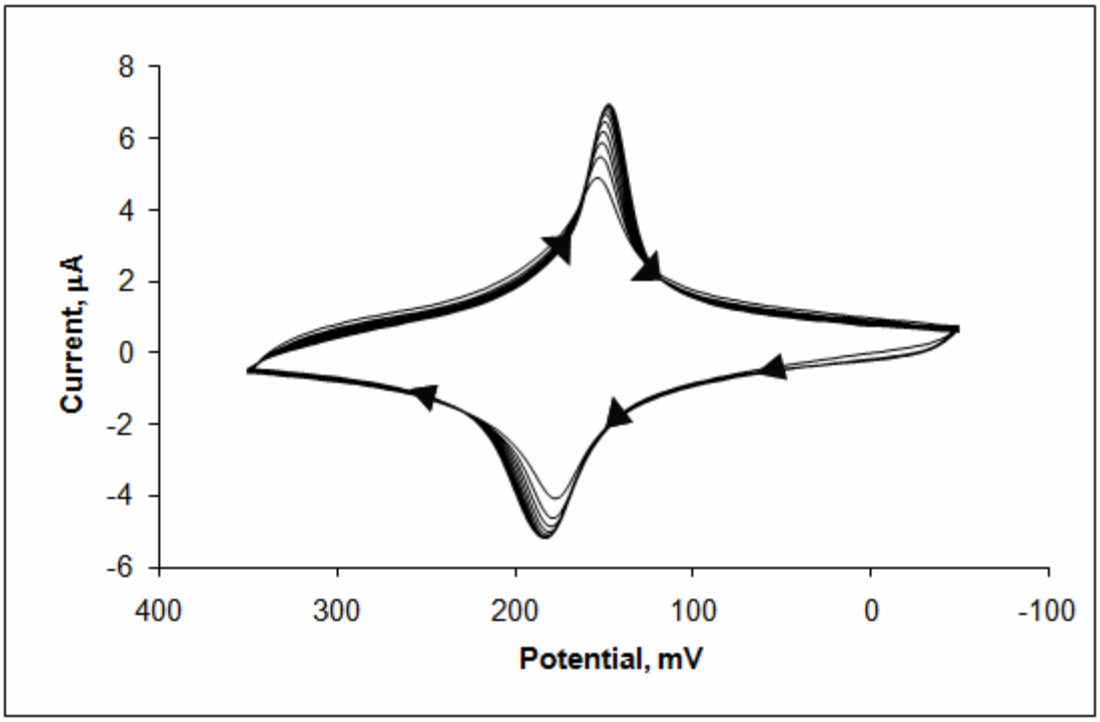


**Figure 4-7.** Representation of first 10 CV scans of PB electrodeposited on Pt ME prepared from 4 mM $K_3[Fe(CN)_6]/FeCl_3$ in 0.1 M KCl/HCl solution. Scan rate = 40 mV/s; initial potential = -50 mV. Arrows indicate direction of scan.

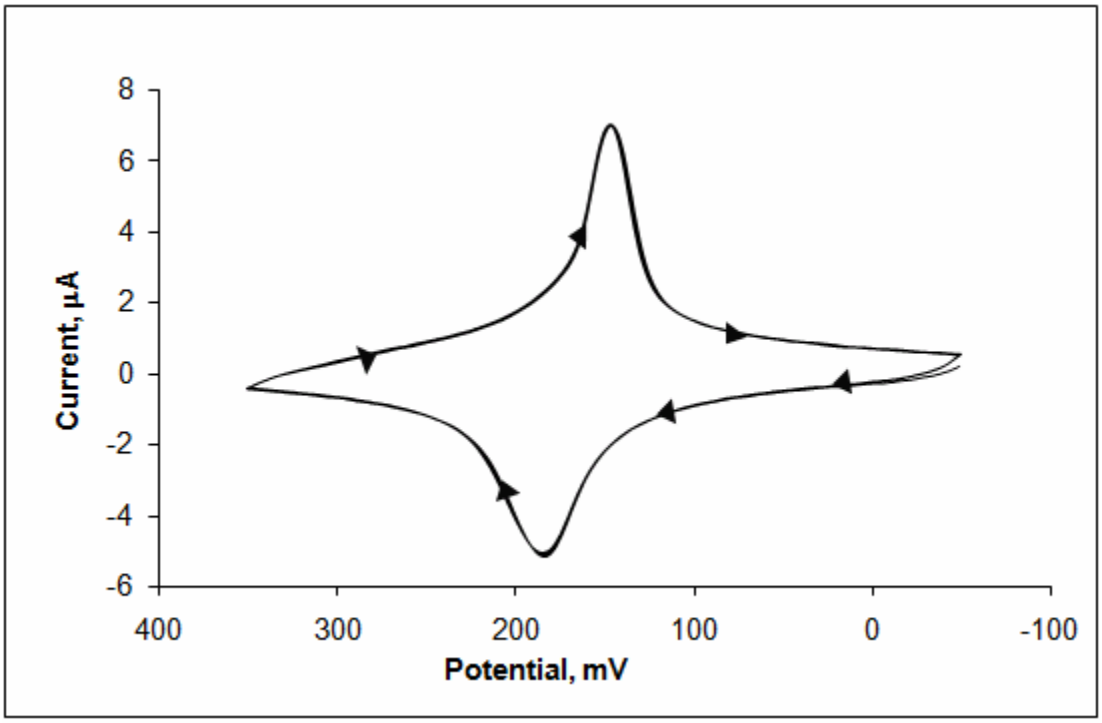


**Figure 4-8.** Representation of next 10 CV scans of the same PB modified Pt ME in 0.1M KCl/HCl solution depicting a stable voltammogram. Scan rate = 40 mV/s; initial potential = -50 mV; switching potential = 350 mV; Arrows indicate direction of scan.

In this particular case the magnitude of $i_{pc}$ increased by 2.3 µA while $i_{pa}$ increased by 1 µA. Figure 4-9 compares the CVs of PB-Pt MEs prepared from various method of deposition. PB films developed from slow film formation thermal deposition and electrodeposition processes yielded comparable results. PB films formed by electrodeposition were used for further studies because of its ease of preparation and more reproducible film characteristics.

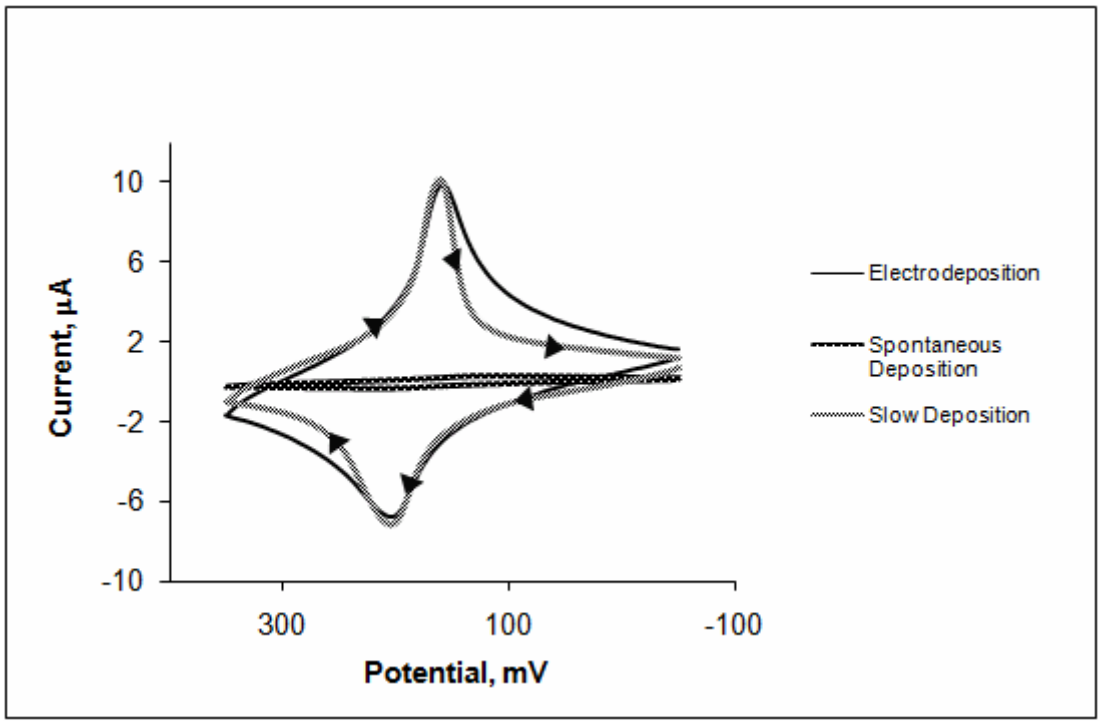


**Figure 4-9.** Comparison of CVs of PB modified Pt MEs prepared from 4 mM solution of $K_3[Fe(CN)_6]/FeCl_3$ in 0.1 M KCl/HCl by electrodeposition, spontaneous thermal deposition and slow thermal deposition method. Scan rate = 40 mV/; initial potential = -50 mV; switching potential = + 350 mV. Arrows indicate direction of scan.

### 4.3.2. Determination of Operational Potential

Once the optimum method of deposition of PB was determined, the optimum operational potential of the PB-AChE-ChO Pt MEs were determined. Figure 4-10 shows electropherograms obtained by injection of pure Ch at different potentials. As only pure

Ch was injected, the analyte was allowed to pass through the column without application of voltage.

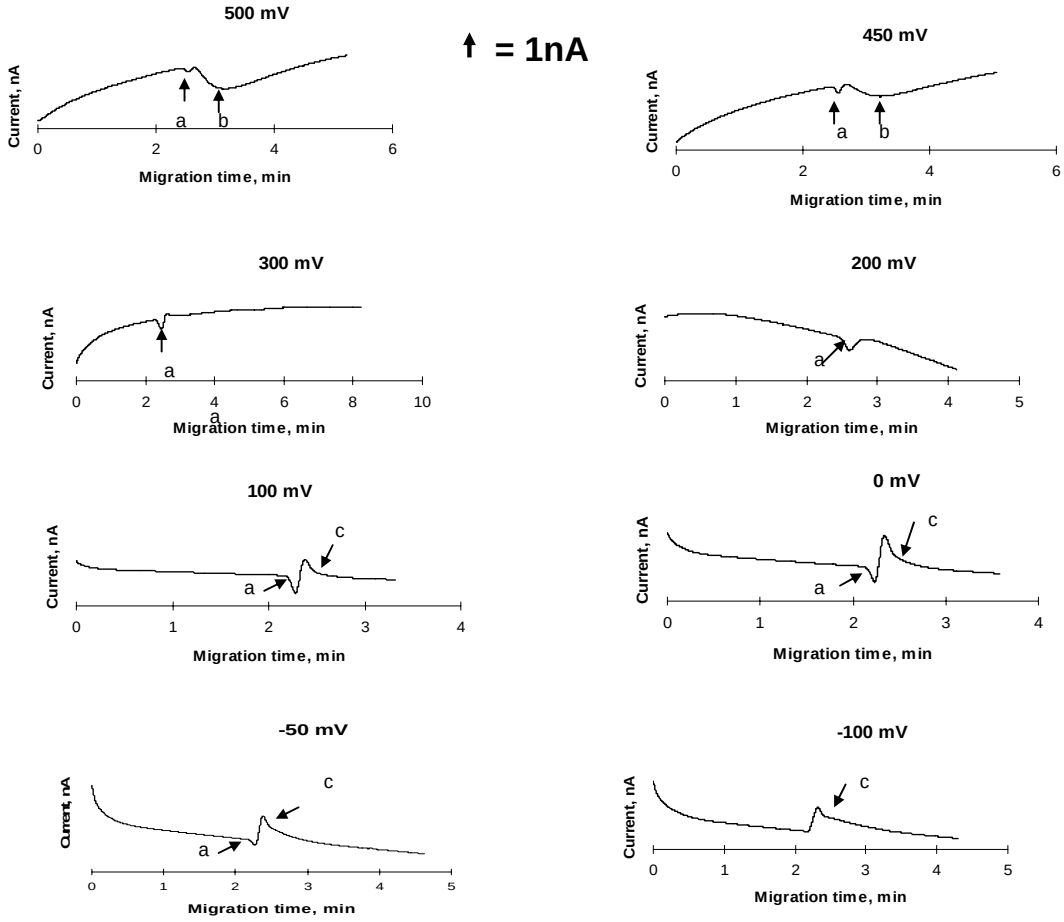


**Figure 4-10.** Depiction of amperometric response of a PB-AChE-ChO modified electrode to the injection of standard solution of Ch at various potentials vs. Ag/AgCl .

As mentioned, the reduced form of PB (PW) is known to have catalytic effects towards reduction of $H_2O_2$ while the oxidized form PB is known to have catalytic effects towards the oxidation of $H_2O_2$.[12] Inverted peaks indicate current generated at the electrode surface by electrochemical oxidation, while upright peaks indicate current generated because of any electrochemical reduction occurring at the electrode surface.

At 500 mV two peaks namely peak-a and peak-b were observed. Peak-a represents the electrochemical regeneration of PB on the electrode surface after catalytic oxidation of $H_2O_2$. Peak-b is a result of uncatalysed oxidation of $H_2O_2$ on the Pt ME. The broadness of peak-b is an indication of the fact that $H_2O_2$ had to diffuse through layers of catalyst to reach the electrode surface. At 450 mV, as the potential became less positive, the magnitude of peak-b decreased significantly. At 300 mV the applied potential was not oxidizing enough to permit the uncatalysed oxidation of $H_2O_2$, however PB catalysed electrochemical oxidation still occured. The magnitude of peak-a is slightly larger probably due to the absence of any other competing reactions. At 200 mV peak-a became distinct. When the potential was further lowered to 100 mV, an additional current peak namely peak-c was generated. Peak-c represents the electrochemical regeneration of PB at the Pt ME as a result of catalytic electrochemical reduction of $H_2O_2$. As the potential was held at relatively more negative values, (0 mV and -50 mV), peak-c appeared more prominent, while current peak-a became less significant. This is because lower potentials favored reduction processes. Finally at -100 mV, only peak-c was generated due to the electrochemical reduction of $H_2O_2$ by PB. The fact that peak-b indeed represented uncatalysed electrochemical oxidation of $H_2O_2$ is further supported by the fact that similar peaks are observed in Pt-AChE-ChO electrodes not modified with PB. Injection of blank buffer solution or distilled water did not result in any current peaks, supporting the fact that peak-a and peak-c were generated as a result of PB catalysed electrochemical oxidation and reduction of $H_2O_2$ and not due unspecific catalysis of PB towards oxidation or reduction of $O_2$ or other small electroactive molecules.

This dual nature of transduction of $H_2O_2$ by catalytic oxidation and reduction of

PB is further supported by the CVs (figure 4-1). At 500 mV the predominant form of the catalyst would be the oxidized form (PB), a good catalyst towards oxidation of $H_2O_2$ . As the detection potential is set towards more negative values, the ratio of the oxidized form of catalyst (PB) to its reduced form (PW) would change as dictated by the Nernst equation. At -100 mV the potential is sufficiently negative for only PW to exist, that would solely catalyze the reduction of $H_2O_2$ and would be regenerated by its own reduction at the Pt surface. Cheng et. al have also developed a PB based amperometric sensor for glucose where they have demonstrated a dual mode detection scheme for $H_2O_2$ at different potentials.[27]

In order to avoid multiple electropherograms generated for a single substrate due to multiple modes of detection, it is important to operate the electrochemical sensor at a potential where only one mechanism of catalysis would be predominant. Hence the Pt MEs were operated at -100 mV vs Ag/AgCl. This potential seemed a practical choice as it was sufficiently negative to prevent interferences from biologically active species. Hence electropherograms generated at -100 mV represents the quantitative enzymatic conversion of Ch, ACh and BuCh to $H_2O_2$ and its electrochemical reduction .

### 4.3.3. Separation of Ch, ACh and BuCh

The ability of the PB-AChE-ChO electrodes to amperometrically detect cholinergic molecules when coupled with capillary electrophoretic separations were evaluated. Fused silica capillary of 145 cm length was used to achieve separation. 50 mM TES, pH 8.0 was utilized for all separations and 20 mM phosphate buffer, pH 7.0 was used in the detector cell. Figure 4-11a-d depicts electropherograms generated by the

injection of various concentrations of Ch and ACh, holding the BuCh concentration constant at 200 μM.

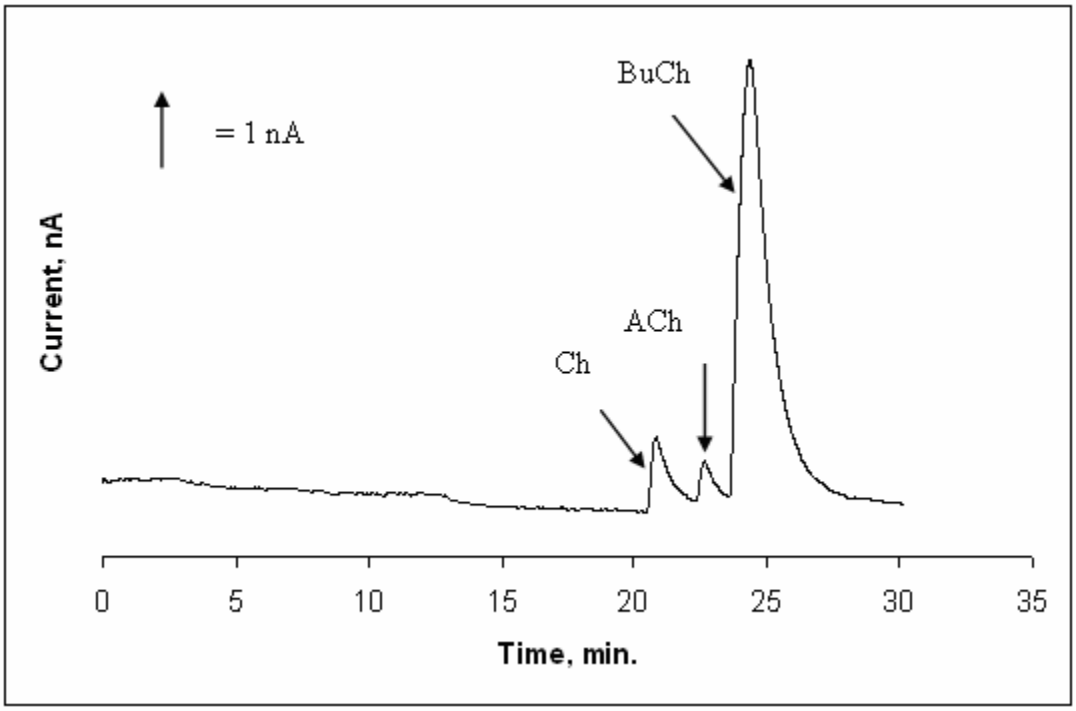


**Figure 4-11a.**

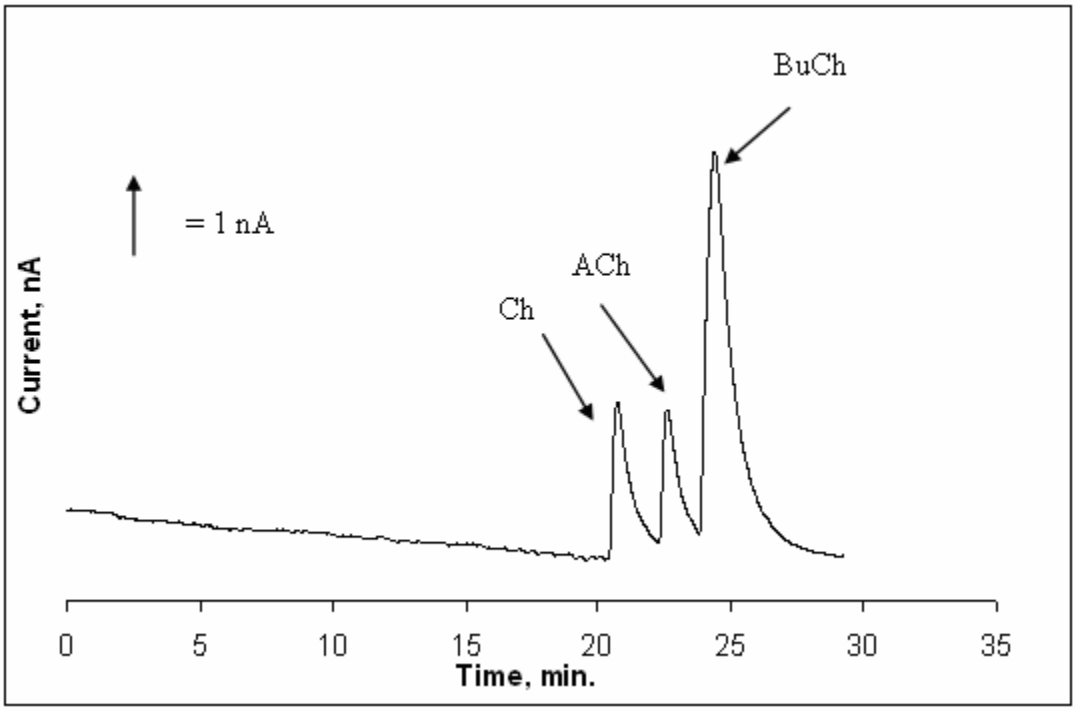


**Figure 4-11b.**

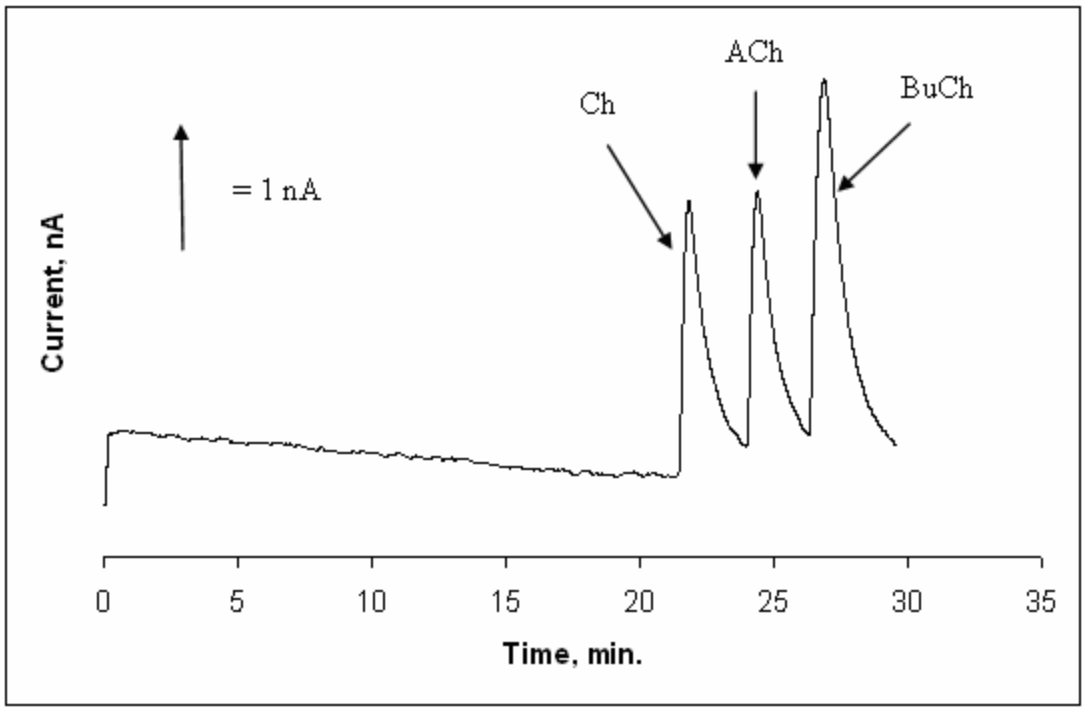


**Figure 4-11c.**

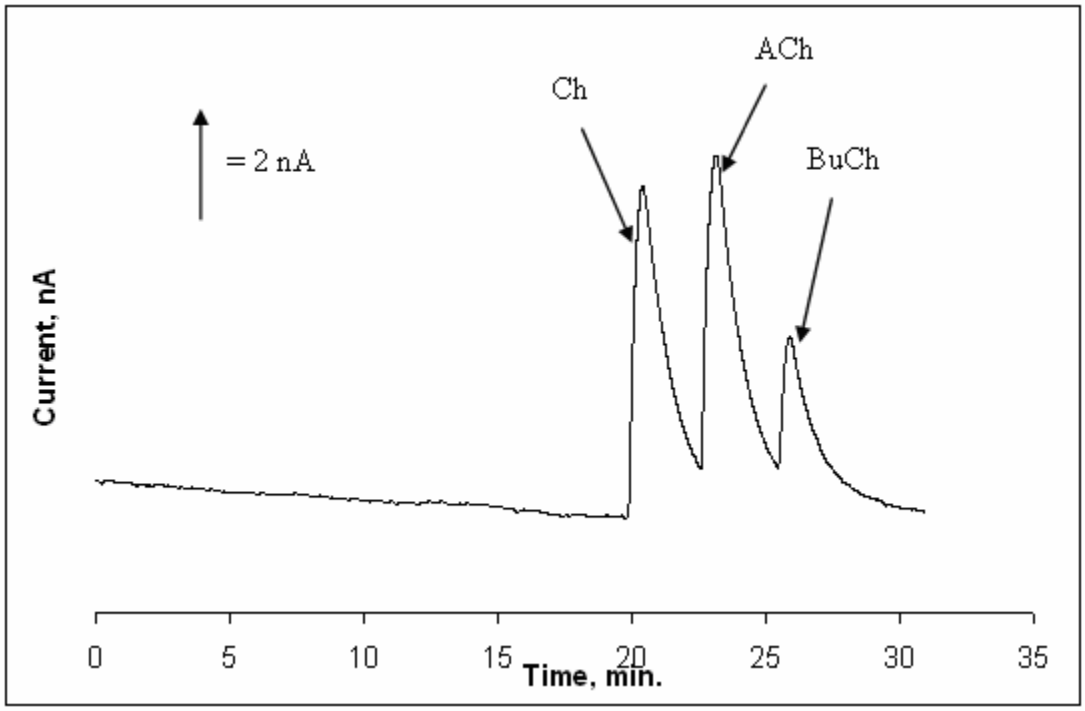


**Figure 4-11d.**

**Figure 4-11.** Electropherograms of mixtures of (a) 15 µM Ch, 15 µM ACh, 200 µM BuCh; (b) 75 µM Ch, 75 µM ACh, 200 µM BuCh; (c) 200 µM Ch, 200 µM ACh , 200 µM BuCh; (d) 1000 µM Ch, 1000 µM ACh, 200 µM BuCh using a PB-AChE-ChO modified Pt ME. Run buffer, 50 mM TES, pH 8.0; separation voltage +17 kV; detection potential - 0.10 V vs. Ag/AgCl.

Ch, ACh and BuCh were successfully detected using this new electrode system. Also satisfactory baseline resolution was achieved. However the amperometric signal yielded broad current peaks for PB-AChE-ChO MEs under all circumstances as compared with HRP-Os-AChE-ChO ME system (efforts were made to coat the PB-Pt MEs with very thin layers of AChE and ChO). Since the same capillary length and decoupler was used for both systems, peak broadening could not attributed to electrophoretic separation conditions such as longitudinal diffusion of the analytes along the capillary. This comparatively broad analyte signal as compared with the HRO-Os-AChE-ChO system may be attributed a lower catalytic conversion rate of the PB metal catalyst. As the response time is related to the rate of electron transfer to the electrode, a slower conversion rate of $H_2O_2$ transduction would result in longer response time, hence broader signals.

### 4.3.4. Limit of Detection

As successful separation and detection of Ch, ACh and BuCh was achieved, it was interesting to evaluate the sensitivity of the PB-AChE-ChO electrode systems by investigating the limit of detection of these electrodes. A mass detection limit of 9.5 fmol for Ch, ACh and BuCh was obtained by injecting ~ 1.9 nL of 5 μM mixture of the analytes. A concentration detection limit of 1 μM was obtained by injecting 38 nL of 1 μM mixture of Ch, ACh and BuCh. Figures 4-12 and 4-13 represents the corresponding electropherograms depicting the detection limits.

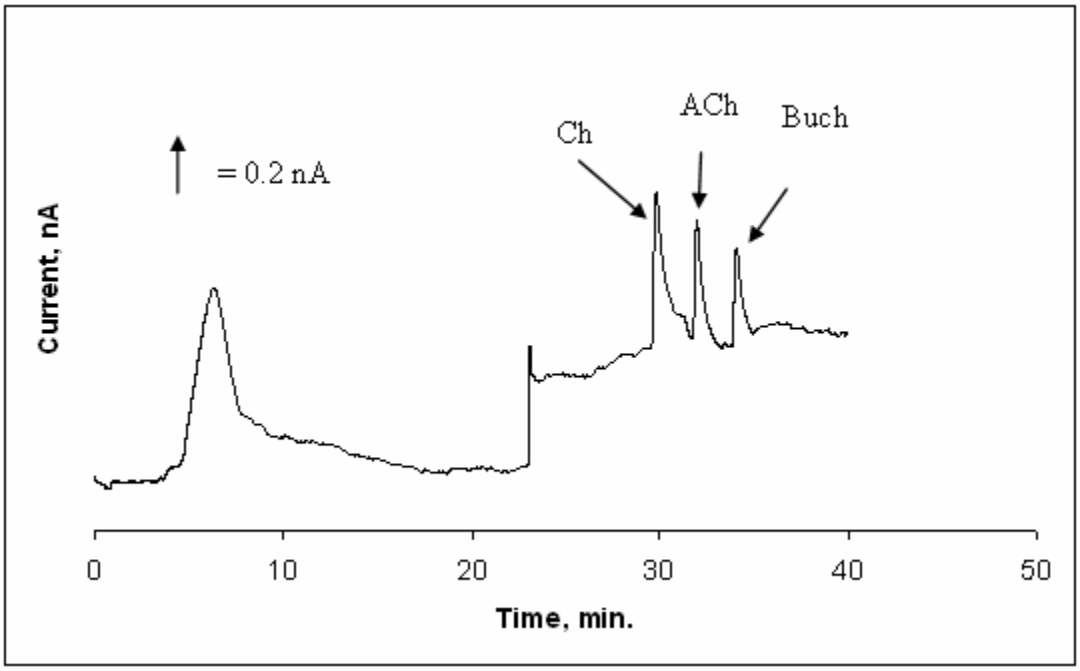


**Figure 4-12.** Electropherogram of a mixture containing 9.2 fmol Ch, ACh, and BuCh detected by a PB-AChE-ChO Pt ME. Separation potential = 10 kV; volume of injection = ~ 1.2 nL of 5 μM mixture of Ch, ACh and BuCh; detection potential = - 0.10 V vs. Ag/AgCl.

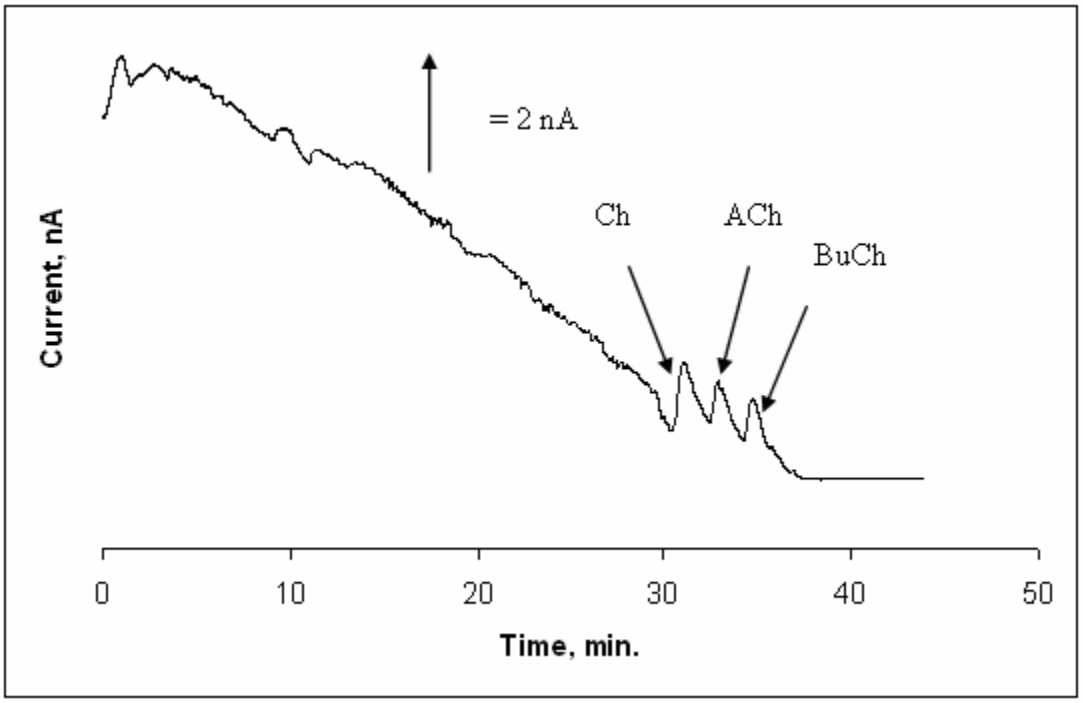


**Figure 4-13.** Electropherogram of a mixture containing 1 μM Ch, ACh, BuCh detected by a PB-AChE-ChO Pt ME. Separation potential = 10 kV; volume of injection = ~ 38 nL of 1 μM mixture of Ch, ACh and BuCh; detection potential = - 0.10 V vs. Ag/AgCl.

An interesting observation from Figure 4-12 is that although the same concentration of Ch, ACh and BuCh was injected into the capillary, their amperometric response was noticeably different. The current peak was largest for Ch and smallest for BuCh. One possible explanation is that ACh and BuCh both can undergo slow hydrolysis to yield Ch that would result in a larger amperometric signal of the latter. However, another plausible explanation would be adsorption of analytes onto the capillary wall. The inner wall of the capillary bears a negative charge due to the ionized silanol groups. During the process of electrophoretic separation, the positively charged analytes can be electrostatically attracted to the negative charge on the capillary, resulting in smaller analyte response signal. The longest migration time of BuCh coupled with the low applied potential may have allowed it to interact with the silanol groups sufficiently long to produce visible reduction in response signal. This nature of discriminatory signal has been observed several times at low analyte concentrations. Figure 4-14 represents an electropherogram of Ch, ACh and BuCh generated utilizing the same standard solution and electrode as 4-12 except with a higher injection volume.

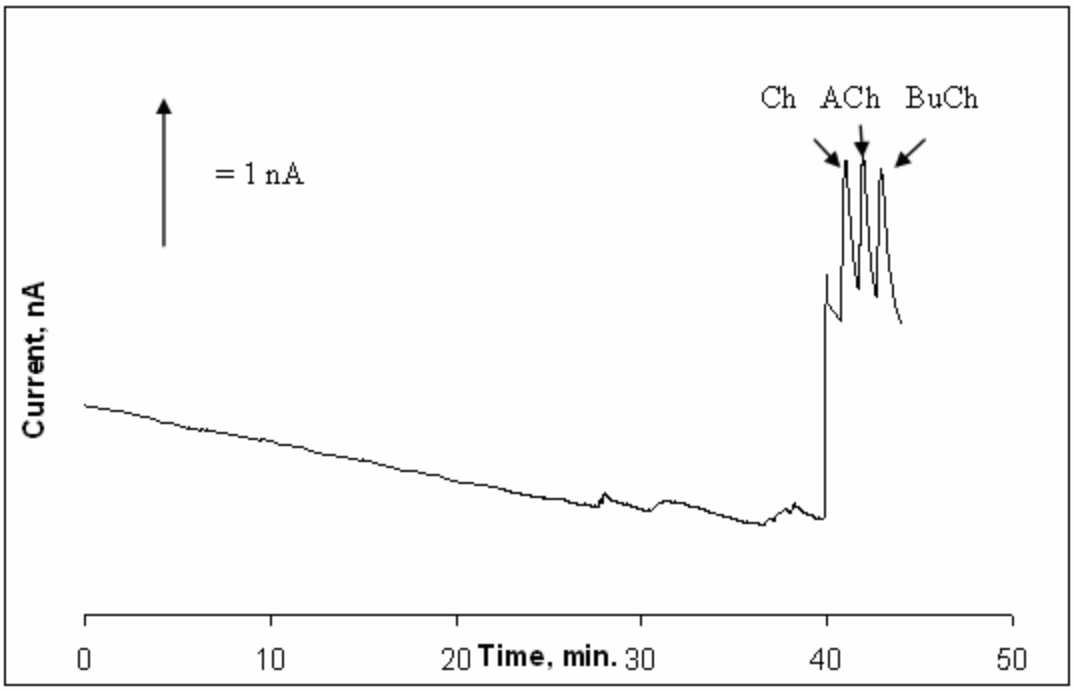


**Figure 4-14**. Electropherogram of a mixture containing 5 μM of Ch, ACh and BuCh detected by a PB-AChE-ChO Pt ME. Separation potential = 10 kV; volume of injection = ~ 38 nL; detection potential = - 0.10 V vs. Ag/AgCl.

At a larger injection volume this discriminatory signal becomes less predominant thereby eliminating the possibility of hydrolysis of ACh and BuCh.

Both the mass and concentration detection limit of PB-AChE-ChO ME were larger than that obtained by the HRP-Os-AChE-ChO system. One significant difference in both the systems is that the former involved the integration of a transition metal catalyst of purely inorganic nature with biological enzyme systems while the latter involved the integration of metal centered organic redox polymers with enzyme systems. Although the performance of the Os-redox polymer hydrogel is very sensitive to the ionic strength and pH of the buffer electrolyte, it has significantly good performance at physiological or basic pH (the optimum pH range for AChE and ChO).[28] A significant challenge of using a combination of inorganic PB with macromolecular enzymes is that

PB is unstable at high pH under basic or neutral conditions,[13] whereas the optimal catalytic ability of the enzymes ChO and AChE are at physiological pH. A complex array of factors play an important part for optimal functioning of these integrated electrodes. Such optimization becomes more complicated with the increase in number of catalysts in the sensing system and broad variation in their chemical nature.

### 4.3.5. Linear Range

The linear operational range of these microelectrodes for Ch and ACh from 10 to 2000 μM was studied. An injection volume of 38 nL was used due to the comparatively lower sensitivity of this electrode system. Figures 4-15a-b and 4-16a-b represents the response of Ch and ACh to three different PB-AChE-ChO Pt MEs. BuCh was used as an internal standard. A good linear relationship was observed for all the electrodes. The $R^2$ values for Ch ranged from 0.994 to 0.999, while that of ACh ranged from 0.995 to 0.999. Concentrations beyond 2000 μM were not examined, as very high concentrations causes overloading of the column and inefficient separation of the analytes. Concentrations less than 10 μM were not evaluated as the response of these electrodes was more variable at lower concentrations.

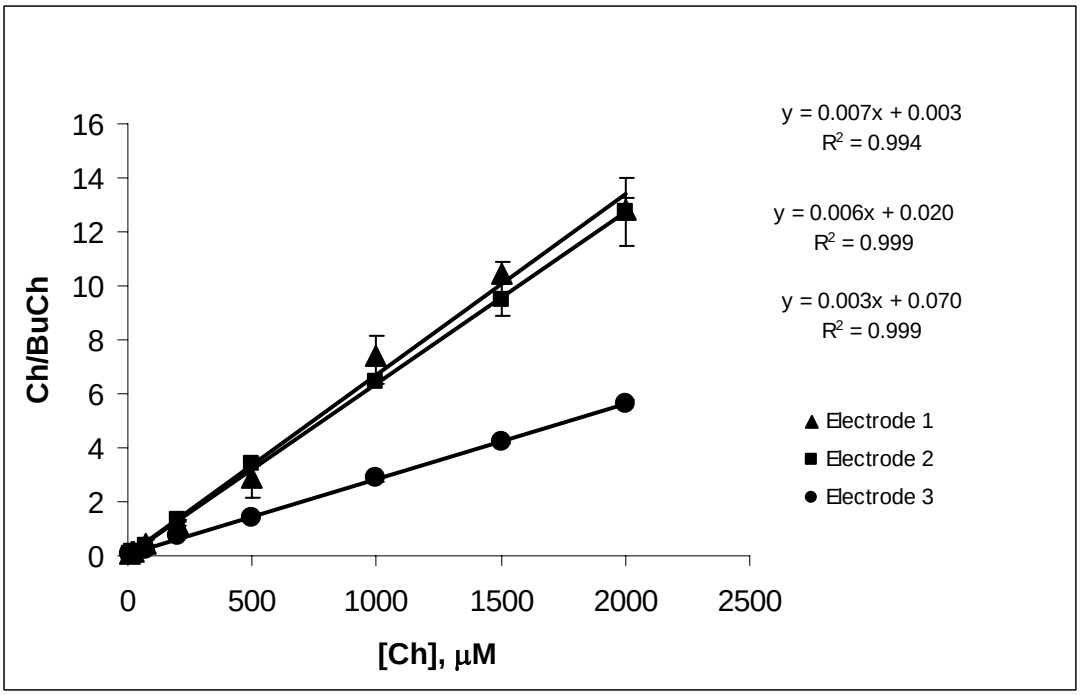


**Figure 4-15a.** Calibration plots for Ch from 10-2000 µM for 3 different PB-AChE-ChO Pt MEs. Error bars for electrode 3 are too small to be seen.

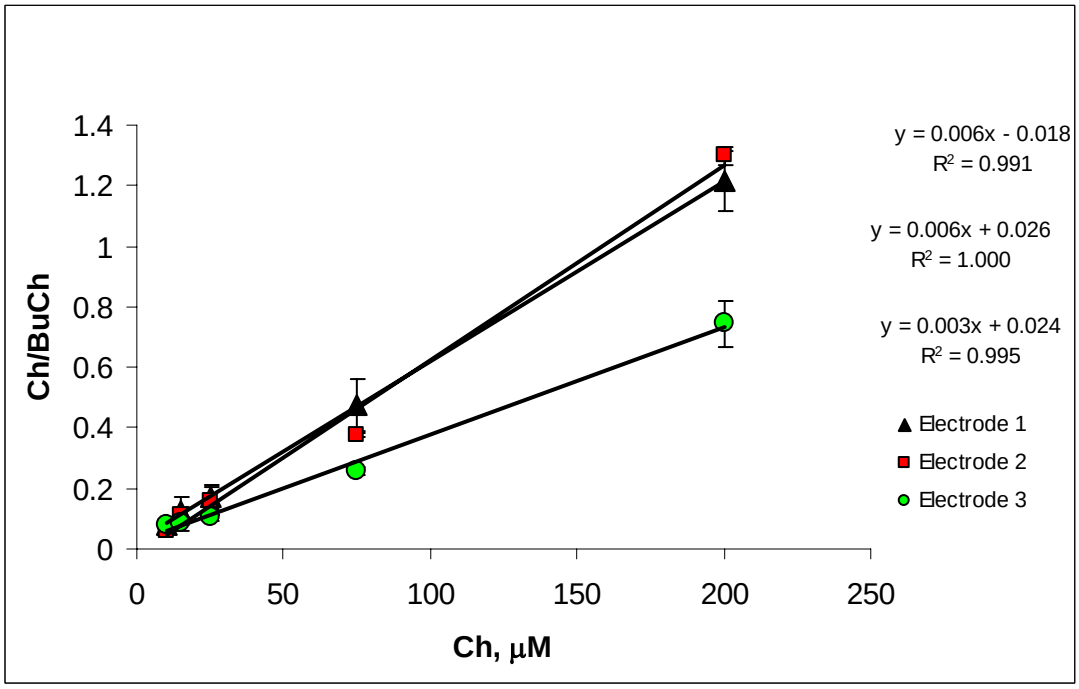


**Figure 4-15b.** Calibration plots for Ch from 10-200 µM for the 3 PB-AChE-ChO Pt MEs.

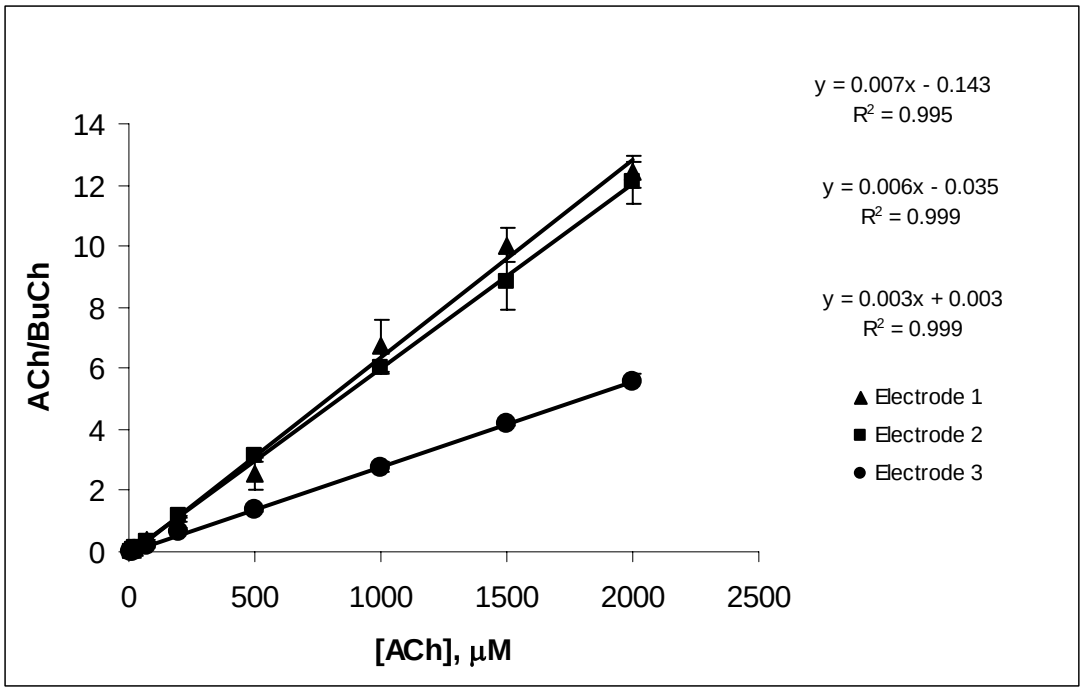


**Figure 4-16a.** Calibration plots for ACh from 10-2000 µM for 3 different PB-AChE-ChO Pt MEs. Error bars for electrode 3 are too small to be seen.

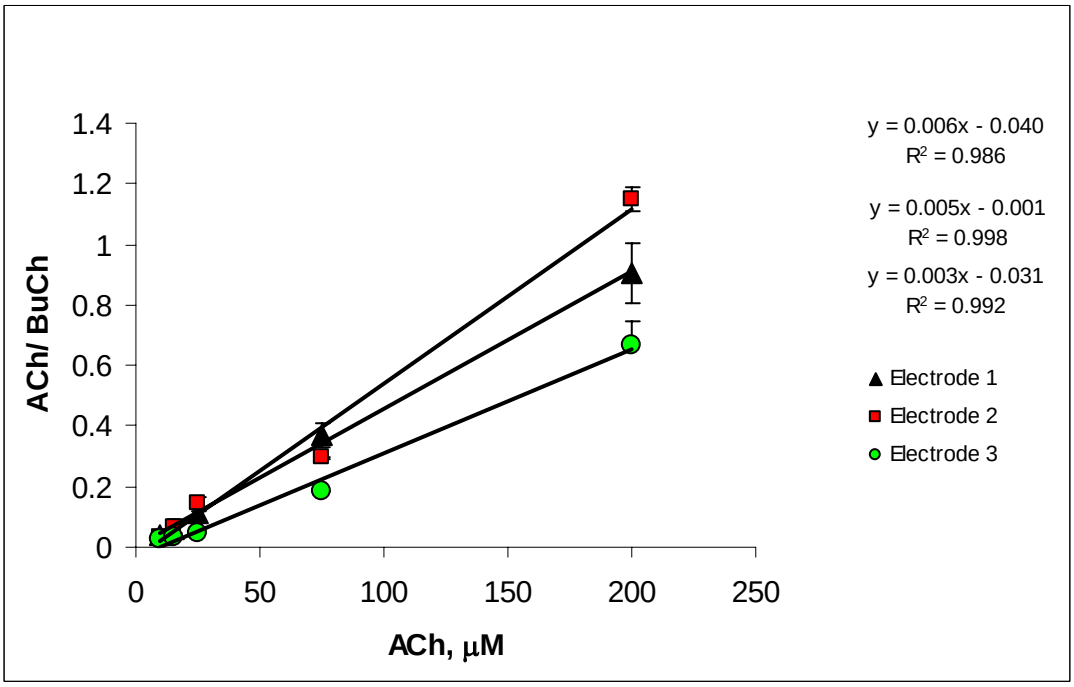


**Figure 4-16b.** Calibration plots for ACh from 10-200 µM for the 3 PB-AChE-ChO Pt MEs.

However, in this case, in spite of a high injection volume, a limiting value of current response was not obtained at even higher concentrations. This may be attributed

to the comparatively low sensitivity of PB as a transducer for $H_2O_2$ than the HRP-Os polymer redox hydrogel utilized previously. Hence the overall response of the sensor could have been governed by the catalytic response of the PB layer. The transduction of $H_2O_2$ by PB could have been the slow, rate limiting step of the overall process.

The sensitivity of PB-AChE-ChO modified Pt MEs was also studied. As previously mentioned in Chapter 3, the sensitivity of these electrodes are determined from the slope of the calibration plots. The calibration plots were generated by plotting the ratio of the peak areas of either analyte (Ch and ACh) to that of internal standard (BuCh) which was held constant at 200 μM. The sensitivity of Ch and ACh were similar and ranged from 0.003 to 0.007 unit/μM.

As specified, the predominant cause of variation in sensitivity of the enzyme modified electrode was due to the fact that the enzymes are randomly adsorbed onto the electrode surface during the crosslinking process. This yields different relative proportions of various enzymes on each electrode that also differ significantly in orientation. However, in this case the variation in sensitivity can also be attributed to the PB catalyst layer involved in detection. As observed, the nature of the catalyst is sensitive to the deposition method and thickness of the PB film. Holding the deposition time and potential constant is expected to produce uniform results, however the area of the manually fabricated Pt MEs varied slightly from each other. This variation in overall electrode surface area may have possibly lead to slight variations in film thickness which would result in variation of the catalytic properties of the PB layer. It can be observed that the sensitivity of electrode 1 and 2 are very similar, while that of electrode 3 is significantly different. In spite of this variation in sensitivity, electrode 3 demonstrates a

good linear range, indicating that these electrodes can be reliably used for quantification purposes after calibration.

### 4.3.6. Stability of the Developed PB-AChE-ChO Pt MEs

#### 4.3.6.1 Operational Stability of PB Modified Electrodes

The stability of any biosensor depends on its design. As various efforts had been made to optimize the development conditions, it was interesting to observe the performance characteristics of these electrodes. The performance of the PB-AChE-ChO Pt MEs were evaluated by investigating their operational stability. The amperometric response for Ch and ACh was monitored both as a function of time and number of runs, the starting time of the first run being t = 0. Figures 4-17 and 4-18 represent the response of Ch and ACh respectively as a function of number of runs. Figures 4-19 and 4-20 indicate the response of Ch and ACh respectively as a function of time monitored in hours.

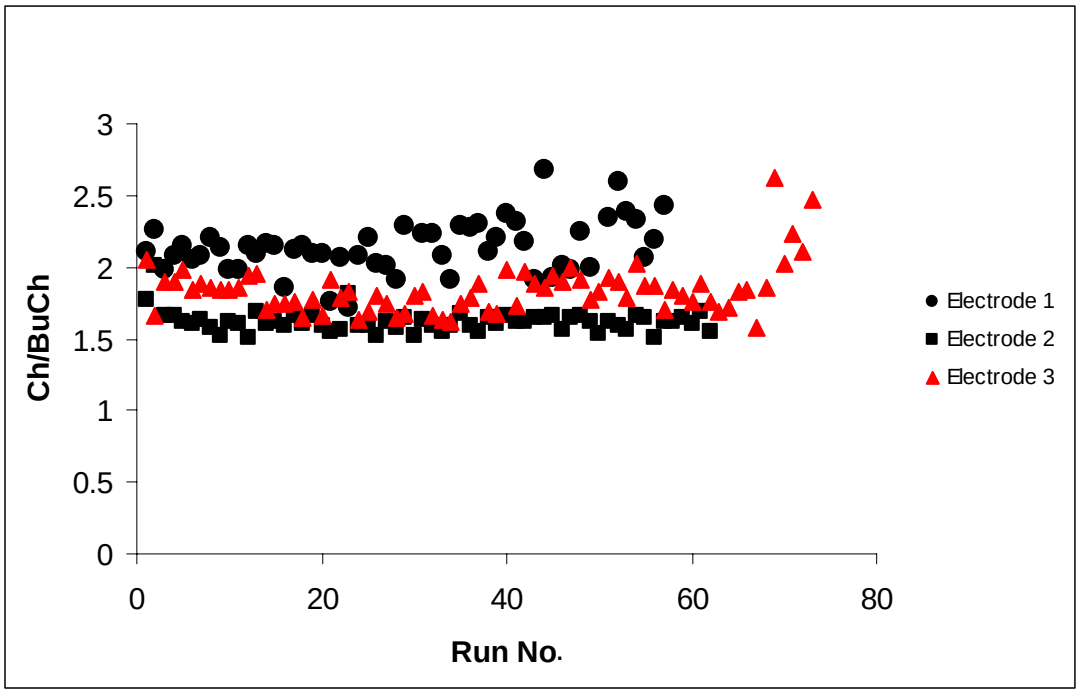


**Figure 4-17.** Operational stability of three different PB-AChE-ChO Pt MEs indicated by peak area ratio of Ch/BuCh as a function of number of runs.

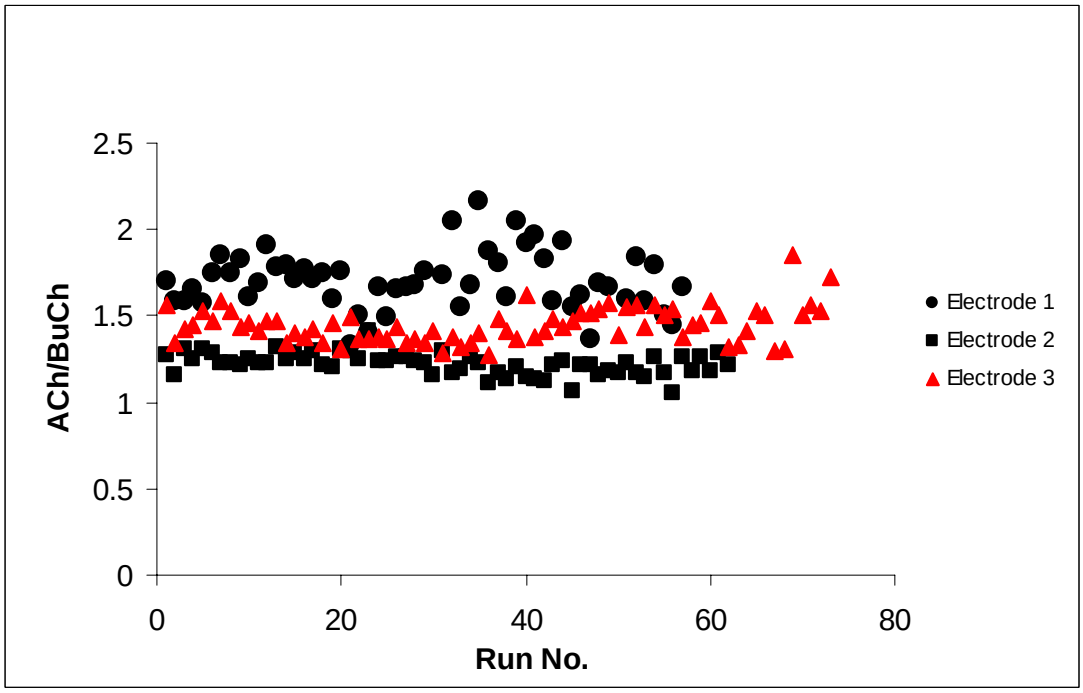


**Figure 4-18.** Operational stability of three different PB-AChE-ChO Pt MEs indicated by peak area ratio of ACh/BuCh as a function of number of runs.

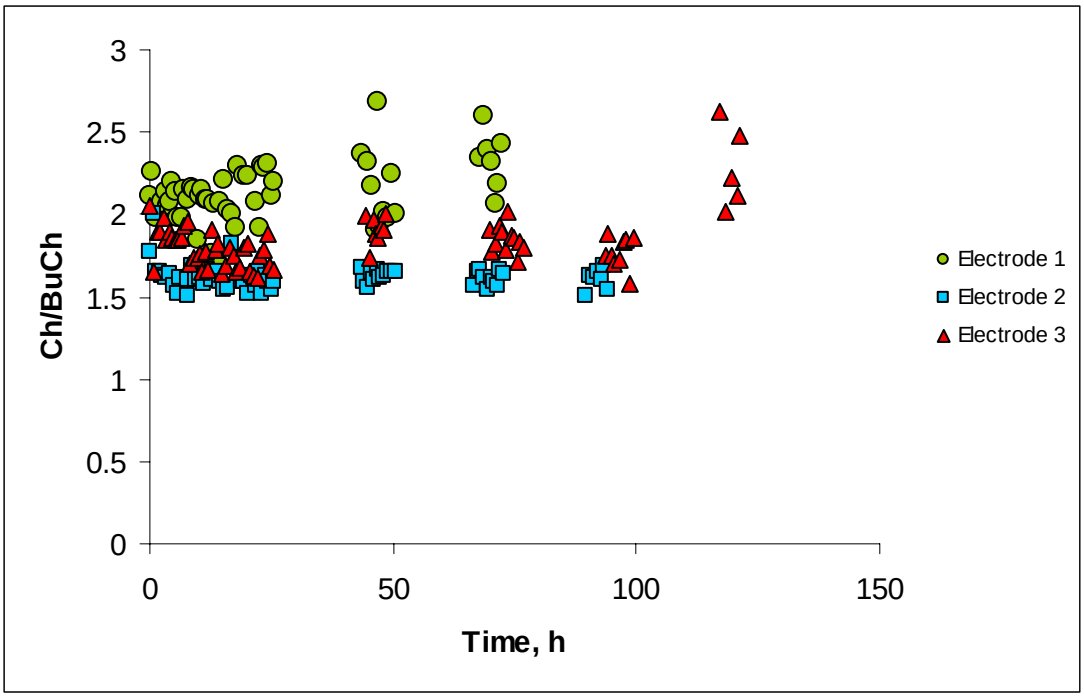


**Figure 4-19.** Operational stability of 3 different PB-AChE-ChO MEs in response to Ch as a function of time.

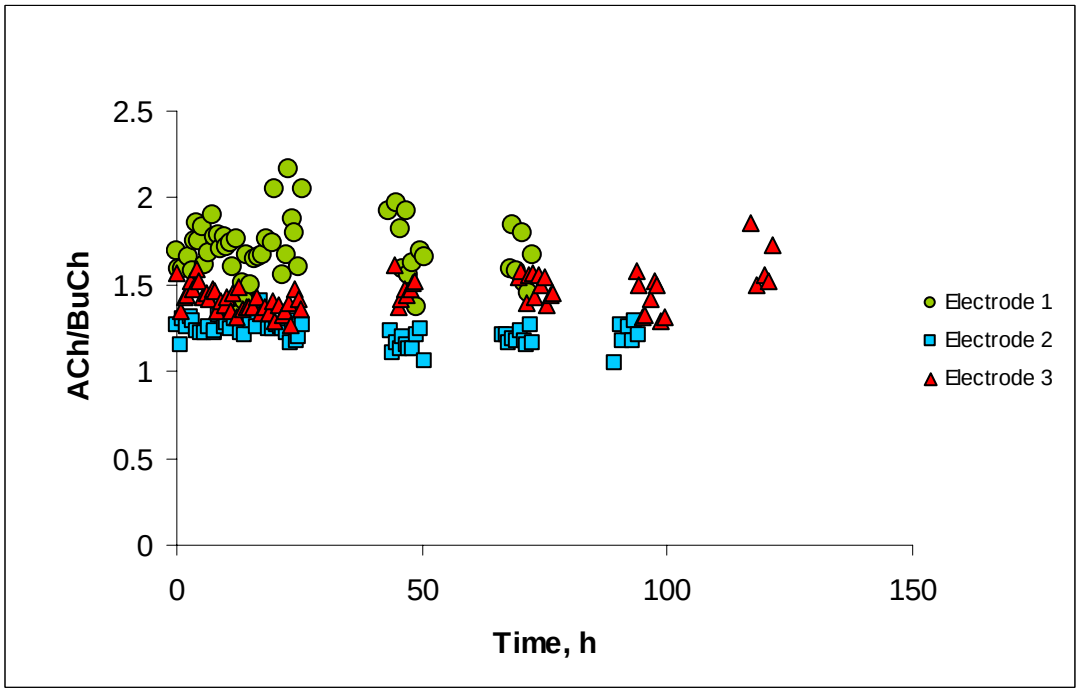


**Figure 4-20.** Operational stability of 3 different PB-AChE-ChO MEs in response to ACh as a function of time.

The PB-AChE-ChO Pt MEs showed an average drop of 14% for both peak areas of Ch and ACh after 10 hours of operation, which further decreased by 46% and 40 % for Ch and ACh respectively after 24 hours of usage. This diminishing response was likely due to the decrease in sensor sensitivity as a result of loss of enzymes from the electrode surface as well as decrease in overall catalytic activity as a result of constant usage and fouling. The use of an internal standard enabled to evaluate the current response of Ch and ACh as a function the ratio of their respective peak areas. This compensated for any loss of sensitivity along with discrepancies resulting from the semiautomatic injection method. In general the electrodes were good for about 60 runs for both Ch and ACh. The response of electrode 2 was most stable, while that of electrode 1 was most variable. Although the maximum runs for electrode 3 was 73, it can be observed that the electrode performance severely deteriorated after 60 runs.

As mentioned, one of the challenges of integrating inorganic catalysts with biomolecules is that they have markedly different stability conditions. The poor stability of PB films has always been a challenge for practical applications as sensors. It has been proposed that the reduced form of PB (PW) is thermodynamically unstable.[13] Also the kinetics of PB catalysis operated in a neutral media produces $OH^-$ ions that causes dissolution of the inorganic crystal.[13] A neutral pH was used as electrolyte for the detection cell, that resulted in slow gradual loss of catalytic activity which was severely reflected after a significant number of runs. However, the PB-AChE-ChO Pt MEs could be operated for at least 72 hours.The operational stability for PB based biosensors reported by Curulli et al. under a flow system was 60 hours.[6] Karyakin et al. have reported an operational stability for 20 hours.[13,26]

#### 4.3.6.2. Storage Stability of PB Modified Electrodes

Once electrodeposited with PB, the electrodes could be stored at ambient temperature in darkness for at least one month with no deterioration of catalytic activity. After modification with enzymes, the electrodes were stored at – 20 °C. The electrodes were catalytically active for up to one week. Around 90% loss of activity was observed after a week.

## 4.4. Conclusions

New methods of modification of ME surfaces with PB were developed. Coupling of PB modified Pt MEs with enzymes ChO and AChE enabled quantitative detection of Ch, ACh and BuCh. The behavior of the PB-AChE-ChO sensor towards the electrochemical reduction of $H_2O_2$ was characterized. Under the conditions of deposition, the developed PB catalyst was selective to the electrochemical oxidation and reduction of $H_2O_2$ in the presence of $O_2$. A linear calibration range extending over three orders of magnitude was obtained for both Ch and ACh. Although stability conditions of the transition metal catalyst and biomacromolecules were remarkably different, synergistic effects between these systems were achieved as demonstrated by good operational performance of these electrodes.

## 4.5. References


1. Tian, F.; Llaudet, E.; Dale, N. Ruthenium Purple-Mediated Microelectrode Biosensors Based on Sol-Gel Film. *Anal. Chem*. **2007,** *79*, 6760-6766.

2. Karyakin, A. A.; Karyakina, E. E.; Gorton L. The Electrocatalytic Activity of Prussian Blue in Hydrogen Peroxide Reduction Studied Using a Wall-jet Electrode with Continous Flow. *J. Electroanal. Chem.* **1998,** *456*, 97-104.

3. Itaya, K.; Uchida, I.; Neff, V. D. Electrochemistry of Polynuclear Transition Metal Cyanides: Prussian Blue and Its Analogues. *Acc. Chem. Res*. **1986**, *19*, 162-168.

4. Karyakin, A. A.; Karyakina, E.E.; Gorton, L. Amperometric Biosensor for Glutamate Using Prussian Blue Based "Artificial Peroxidase" as a Transducer for Hydrogen Peroxide. *Anal. Chem*. **2000**, *72*, 1720-1723.

5. Zou, Y.; Sun, L.X.; Xu, F. Biosensors Based on Polyaniline-Prussian Blue Multiwalled Carbon Nanotubes Hybrid Composites. *Biosens. Bioelectron.* **2007**, *22*, 2669-2674.

6. Curulli, A.; Valentini, F.; Orlanduci S.; Terranova, M. L.; Palleschi, G. Pt based Enzyme Electrode Probes Assembled with Prussian Blue and Conducting Polymer Nanostructures. *Biosens. Bioelectron.* **2004**, *20,* 1223–1232.

7. Karyakin, A. A. Prussian Blue and it's Analogues: Electrochemistry and Analytical Applications. *Electroanalysis*, **2001**, *13*, 813-819.

8. Keggin, J. F.; Miles, F. D. Structures and Formulas of the Prussian Blues and Related Compounds. *Nature*, **1936,** *137,* 577-578.

9. Ludi, A.; Gudel, H. U. Structural Chemistry of Polynuclear Transition Metal Cyanides. *Struct. Bond*. **1973**, *14*, 1-22.

10. Herren, F.; Fisher, P.; Ludi, A.; Halg, W. Neutron Diffraction Study of Prussian Blue, $Fe_4[Fe(CN)_6]_3xH_2O$. Location of Water Molecules and Long-Range Magnetic Order. *Inorg. Chem*. **1980**, *19*, 956-959.

11. Buser, H. J.; Schwarzenbach, D.; Petter, W.; Ludi, A. The Crystal Structure of Prussian Blue: $Fe_4[Fe(CN)_6]_3xH_2O$. *Inorg. Chem*. **1977**, *16*, 2704-2710.

12. Ricci, F.; Palleschi, G. Sensor and Biosensor Preparation, Optimization and Applications of Prussian Blue Modified Electrodes. *Biosens. Bioelectron.* **2005,** *21*, 389-407.

13. Karyakin, A. A.; Karyakina, E.E. Electroanalytical Applications of Prussian Blue and

its Analogs. *Russ. Chem. Bull.* , **2001,** *50,* 1811-1817.

14. Neff, V.D. Electrochemical Oxidation and Reduction of Thin Films of Prussian Blue *J. Electrochem. Soc*., **1978**, *125*, 886-887.

15. Itaya, K.; Haruo, A.; Shinobu, T. Electrochemistry of Prussian Blue Modified Electrodes: An Electrochemical Preparation Method. *J. Electrochem. Soc*., **1982**, *129*, 1498-1500.

16. Ellis, D.; Eckhoff, M.; Neff, V.D. Electrochromism in the Mixedvalence Hexacyanides. 1. Voltammetric and Spectral Studies of the Oxidation and Reduction of Thin Films of Prussian Blue. *J. Phys. Chem.* **1981**, *85*, 1225–1231.

17. Rajan, K.P., Neff, V.D. Electrochromism in the Mixed Valence Hexacyanides. 2. Kinetics of the Reduction of Ruthenium Purple and Prussian Blue. *J. Phys. Chem.* **1982**, *86*, 4361–4368.

18. Ohzuku, T., Sawai, K., Hurai, T. On a Homogeneous Electrochemical Reaction of Prussian Blue/Everitt's Salt System. *J. Electrochem. Soc*. **1985,** *132*, 2828–2834.

19. Puganova, E. A.; Karyakin A. A. New Materials Based on Nanostructured Prussian Blue for Development of Hydrogen Peroxide Sensors. *Sens. Actuators,* **2005,** *109,* 167–170.

20. Karyakin, A. A.; Puganova, E. A.; Budashov, I. A.; Kurochkin, I. N.; Karyakina, E. E.; Levchenko, V. A.; Matveyenko, V. N.; Varfolomeyev, S. D. Prussian Blue Based Nanoelectrode Arrays for $H_2O_2$ Detection. *Anal. Chem.* **2004**, *76*, 474-478.

21. Pan D.; Chen J.; Nie L.; Tao W.; Yao S. Amperometric Glucose Biosensor Based on Immobilization of Glucose Oxidase in Electropolymerized *o*-aminophenol Film at Prussian blue-Modified Platinum Electrode. *Electrochim. Acta*, **2004**, *49*, 795–801.

22. Bustos, E. B.; Chapman, T. W.; Rodríguez-Valadez, F.; Godínez, L. A. Amperometric Detection of $H_2O_2$ Using Gold Electrodes Modified with Starburst PAMAM Dendrimers and Prussian Blue. *Electroanalysis,* **2006**, *18*, 2092 – 2098.

23. Wu, H. C.; Li, C.; Shih, H. C.; Chang, F. L.; Linbi, X. Agrochemical Detection Method and Bio-Microsensor. *Kokai Tokkyo Koho.* **2007**

24. Carlo, M. D.; Pepe, A.; Mascini, M.; Gregorio, M. D.; Visconti, A.; Compagnone D. Determining Pirimiphos-Methyl in Durum Wheat Samples Using an Acetylcholinesterase Inhibition Assay. *Anal Bioanal Chem.* **2005,** *381*, 1367–1372.

25. Ricci, F.; Amine, A, Palleschi, G.; Moscone, D. Prusian Blue Based Screen Printed Biosensors with Improved Characterisitcs of Long- Term Lifetime and pH Stability. *Biosens. Bioelectron.* **2003**, *18*, 165-174.

26. Karyakin, A. A.; Karyakina, E. E. Prussian Blue Based "Artificial Peroxidase" as a Transducer for Hydrogen Peroxide Detection. Applications to Biosensors. *Sens. Actuators B,* **1999**, *57*, 268-273.

27. Zhang, N.; Wilkop, T.; Lee S.; Cheng, Q. Bi-functionalization of a Patterened Prussian Blue Array for Amperometric Measurement of Glucose via Two Integrated Detection Schemes. *Analyst*, **2007,** *132*, 164-172.

28. Heller, A. Electrical Wiring of Redox Enzymes. *Acc. Chem. Res*. **1990**, *23*, 128-134.

# Chapter 5

## Real Time Amperometric Detection of Thiols Using a Pyrroloquinoline Quinone Coenzyme Incorporated Conductiong Polymer Electrode

## 5.1. Introduction

In the previous Chapters, AChE was used to effectively catalyze the hydrolysis of ACh and BuCh as a part of their electrochemical detection scheme. The remarkable catalytic power of this enzyme can be further utilized to generate a variety of products that serve as important markers in biological and chemical processes. Acetylthiocholine (ASCh) is one such substrate of hydrolysis by AChE. The product of its hydrolysis is thiocholine (SCh). SCh is an invaluable marker because it is the hydrolysis product of various other thioesters. In addition, SCh has traditionally been used for measuring cholinesterase activity by detection of its free thiol group via a spectrophotometric method known as Ellman's assay.[1] The toxicity of nerve gases and organopesticides are based on alteration of cholinergic activity via inhibition of AChE.[2] Traditional methods of detection of these toxins have been based on simple chemical reactions or antigen-antibody interactions.[3] Recently, various electrochemical methods have been developed for the detection of pesticides with SCh as the chemical marker.[3,4]

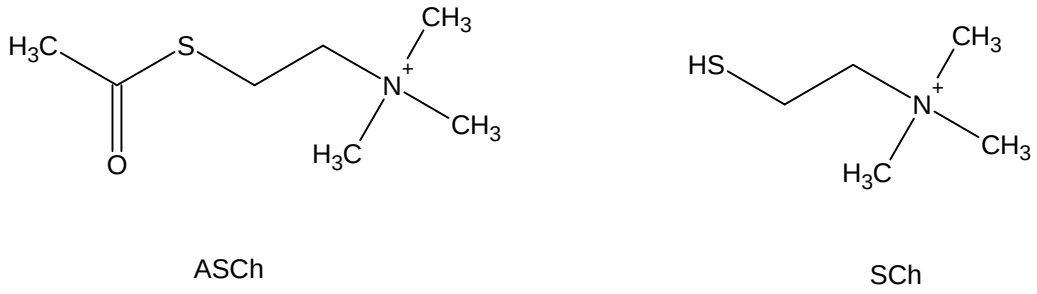


**Figure 5-1.** Structures of Acetylthiocholine and Thiocholine

### 5.1.1. Electrochemistry of Thiocholine

Unlike Ch, which is not electroactive, thiols such as SCh can undergo electrochemical oxidation at certain electrode surfaces to form disulfides. However, most often this electrochemical reaction is sluggish due to slow electron exchange with the electrode and require large positive overpotentials leading to challenges for its detection. Hence modification of the electrode with an ET mediator is an alternative for obtaining better activity for SCh detection. Various approaches to this concept have been employed such as incorporation of electroactive inorganic catalysts and novel materials like carbon nanotubes.[5, 6]

In this study, detection of SCh has been investigated by employing a biological redox cofactor, pyrroloquinoline quinone (PQQ) as an ET mediator incorporated in a conducting matrix.

### 5.1.2. Pyrroloquinoline Quinone

PQQ is a redox cofactor in many proteins. PQQ was first discovered by Hauge as a novel prosthetic group in glucose dehydrogenase enzyme of bacterium anitratum.[7] Most of the enzymes with PQQ as the cofactor are oxidoreductase enzymes such as methanol dehydrogenase, alcohol dehydrogenase, etc. that are present in bacterial microorganisms. Various other enzymes such as amine oxidase, lysil oxidase, galactose oxidase and nitrile hydratase have also been reported to utilize PQQ as the prosthetic group.[8] Like most quinones, PQQ undergoes a two electron reduction/oxidation at the electrode surface. Figure 5-2 depicts the redox reaction of PQQ.

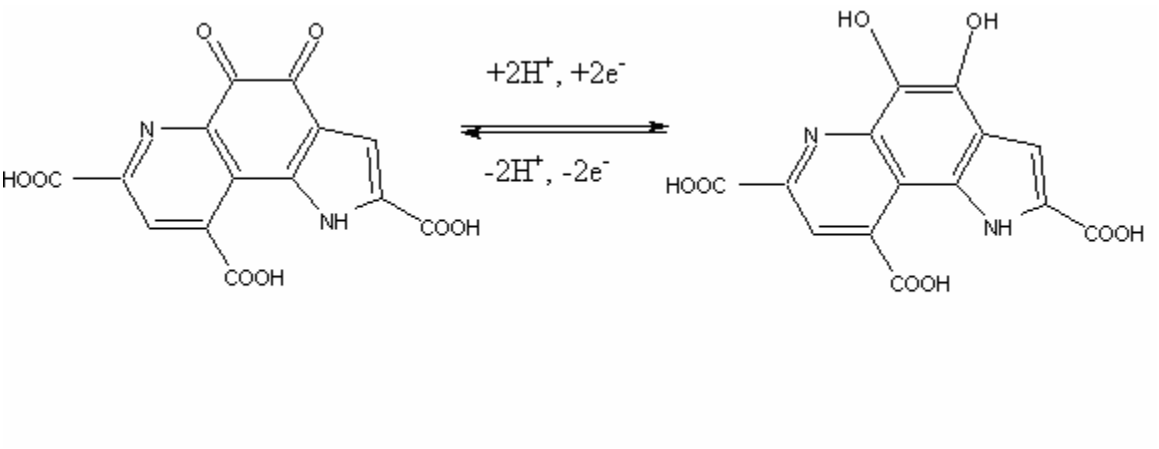


**Figure 5-2.** Electrochemical redox reaction of PQQ.

The electrochemisty of PQQ on various types of electrodes has been thoroughly investigated by Shinohara et. al.[8] CV of PQQ at a Pt electrode yielded cathodic (reduction) peak, $i_{pc}$, at -180 mV (vs. Ag/AgCl) and an anodic (oxidation) peak, $i_{pa}$, around +180 mV. The anodic peak area was much smaller than the cathodic peak area with $\Delta E_p$ > 350 mV, indicating irreversible electron transfer between PQQ moiety and the Pt electrode surface. CV of PQQ using Au electrode was also irreversible, with a negligible anodic peak area and a small cathodic peak around -400 mV. In case of glassy carbon (GC) electrode cathodic and anodic peaks were observed with $\Delta E_p$ around 250 mV. Hence, reversible oxidation and reduction of PQQ was not observed at any type of electrode surface probably due to inefficient ET between the PQQ moiety and electrode surface. However the electrochemistry of PQQ incorporated inside a conducting polymer was completely different. CV of PQQ entrapped inside a polymeric membrane had all the attributes of a reversible redox couple i.e., $\Delta E_p$ ~ 40 mV and cathodic peak area/anodic peak area ~1.[8] Hence the conducting matrix facilitated the ET process by acting as a molecular wire through electrical connection of the PQQ redox center and the electrode

surface. Facile electron transfer in the PQQ polymer system is probably achieved through electron hopping mechanism where the electron hops between several adjacent redox centers and reaches the electrode surface. Electron hopping reduces the overall ET distance through several faster ET steps via the covalently bound redox polymers.

Kano et al. have extensively studied the pH dependent voltammetric characteristics of PQQ at a hanging drop mercury electrode. They have observed reversible CVs under neutral, basic and acidic pH conditions that have been ascribed to a two-step one electron redox reaction of the o-quinone moeity of the PQQ coenzyme.[9,10]

### 5.1.3. Pyrrole and Polypyrrole

Pyrrole (Py) is a five membered heterocyclic aromatic compound occurring naturally such as in porphyrins of heme proteins and in chlorophyll. Py can be polymerized to form polypyrrole (PPy), an interesting class of conducting polymers. Polymerization can be initiated by chemical or electrochemical means, the later being more efficient. Electrochemical polymerization of Py can be executed by holding the potential constant (potentiostatic) or by passing a constant current (galvanostatic).[11]

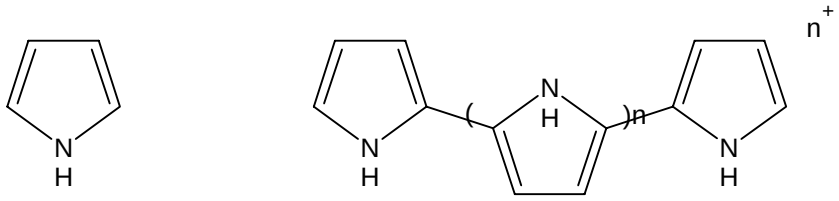


**Figure 5-3.** Chemical structures of Py and PPy.

Although extensive work has been done to understand the mechanism of polymerization, it is still a controversial subject. No single mechanism has been universally accepted, a major challenge being the rapidity of the reaction process. There are a number of proposed mechanisms for the initiation step. The mechanism proposed by Diaz et al. is most widely accepted where the initiation step involves the formation of a radical cation.[12] Kim et al. have proposed the formation of an initial active intermediate by the loss of 2 electrons and a proton from a Py molecule.[13] Another mechanism has been proposed by Pletcher et al. where the radical cation formed reacts with a neutral molecule to form a cation dimer as opposed to Diaz's mechanism where two radical cations dimerize to form a dihydrogen dication.[14] The electropolymerization of pyrrole has been studied using EQCM by Reynolds et al where they have observed three different stages of polymerization where the number of electrons involved are different.[15] There are myriad of factors which can influence the actual mechanism of electropolymerization such as the nature of solvent and electrolyte, pH and temperature of the reaction.[11] The choice of solvent and electrolyte is an important parameter in the polymerization process since both species should be electrochemically stable at the applied potential and the reaction medium should be conducting. The applied potential needs to be higher that the oxidation potential of the monomer. Electropolymerization of Py can be carried out in aqueous solution as it has a relatively low oxidation potential as opposed to other molecules such as thiophene or benzene. According to the well acclaimed mechanism proposed by Diaz et al. the initial species formed is a radical cation.[12] This radical monomer may react with other monomers to form a conjugated system of oligomers. The oxidation potential of the resulting oligomeric units is lower than the monomer as a result

of this extended conjugation. In addition, the anion also has a significant contribution (hydrophobic or hydrophilic characteristics) to the quality of polymer produced.

### 5.1.4. Characteristics of PQQ Incorporated PPy Film

The sensitivity and detection ability of PQQ incorporated with PPy would depend on various factors such as thickness of the polymeric film and amount of PQQ added. The thickness of the PPy membrane is critical for the stability and efficient performance of the PQQ-PPy sensor. A thin membrane may not be very efficient in entrapping the small molecule effectively resulting in leaching of PQQ from the sensor surface. Very thick membranes on the other hand may be efficient in holding the PQQ molecules, but the catalyst may be deeply trapped inside the membrane and may not be easily assessible for interaction with the analyte to be detected. This may result in a slow irreversible amperometric response. The thickness of the PQQ-PPy film can be controlled easily during the process of electropolymerization of pyrrole by controlling the charge passed through the polymer. Various aspects of the PQQ-PPy sensor optimization such as polymerization potential and polymer thickness have been studied in details in the Kirchhoff laboratory by Inoue et al.[16] It was determined that a film of 125 nm thickness deposited at 630 mV on GC electrodes produced optimum sensor performance.[16]The charge corresponding to this thickness is 100 $mC/cm^2$.[8]

A myriad of biosensors have been designed for the detection of SCh. The basis of most of these sensors are detection schemes based on various modes of immobilized AChE such as direct adsorption, covalent bonding with the electrode or based on interactions with carbon nanotubes.[17-19] The major limitation of these sensors is loss of

enzymatic activity due to leaching of enzymes from the electrode surface. In addition incorporation of AChE onto the sensor surface limits the versatility of the sensor due to its inability to distinguish between amperometric signal generated from ASCh and SCh. In this study a biosensor scheme is designed for the detection of the hydrolysis product of ASCh electrochemically without incorporation of any AChE onto the electrode surface. Figure 5-4 represents the schematic of electrode design and SCh detection pathway.

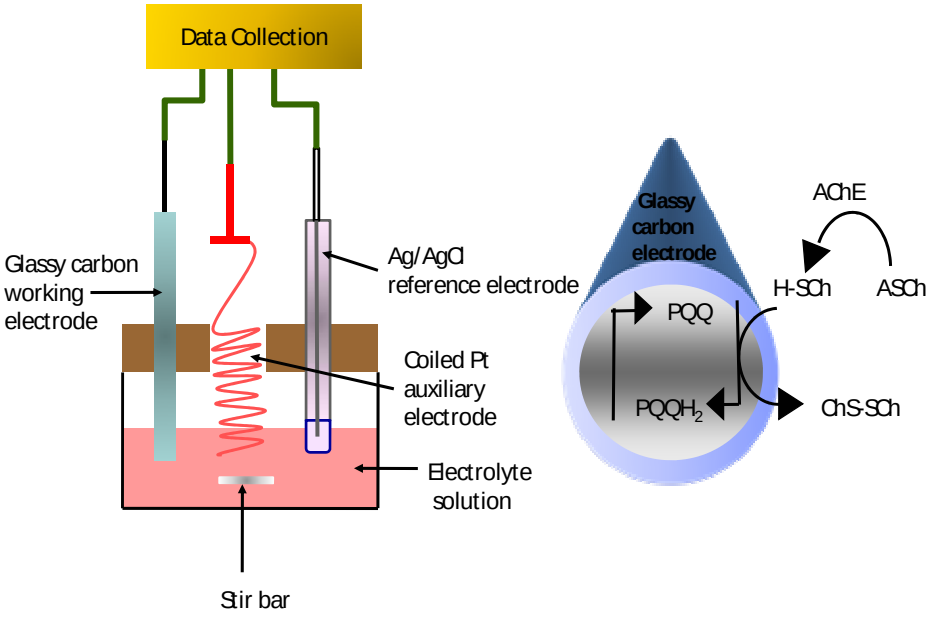


**Figure 5-4.** Detection scheme for SCh at a PQQ incorporated PPy modified electrode.

## 5.2 Materials and Methods

### 5.2.1 Materials

Acetylcholinesterse (AChE) (EC 3.1.1.7, from human erythrocytes, in aqueous 20 mM HEPES, pH 8.0 containing 0.1% Triton X -100., 930 units /mg protein), Pyrroloquinoline quinone (PQQ) ~98%, and acetylthiocholine chloride (ASCh) ≥99%

were purchased from Sigma Aldrich (St. Louis, MO, USA) and stored in a dessicator at -20 ºC. Pyrrole (≥ 98%), was purchased from Sigma (St. Louis, MO, USA) and refrigerated at 4 °C. Pyrrole was refluxed with $CaH_2$ for 1 hour under Ar and distilled every day before use. Carbofuran was also purchased from Sigma and stored at ambient temperature. All other chemicals were of reagent grade and used as received. Solutions were prepared in distilled and deionized water purified to a resistivity of 17.5 MΩ cm by a Barnstead B-pure water purification system (Dubuque, IA). Alumina polishing gamal was purchased from Fisher, while microcloth polishing pads were purchased from Buehler.

### 5.2.2. Apparatus

Electrochemical studies were performed in a single compartment cell equipped with a conventional 3 electrode system comprising of a Ag/AgCl reference electrode (BAS), a coiled Pt auxillary electrode and a glassy carbon electrode (BAS, 3mm diameter) working electrode. High purity Ar gas was used for deoxygenating the electrolyte solution. All experiments were conducted using a BAS interfaced with a computer for data collection.

### 5.2.3. Methods

#### 5.2.3.1 Preparation of the Electrocatalytic Electrode

The PQQ modified GC electrode was prepared by thoroughly cleaning the GC electrode surface followed by incorporation of PQQ within a polypyrrole matrix by an

electropolymerization method.

#### 5.2.3.1.1. Cleaning Procedure

Prior to use, the GC electrode was polished with alumina polishing gamal, rinsed thoroughly in deionized water and then sonicated (Branson Model 1210 ultrasonic cleaner, Danbury, CT) in deionized water for 5 minutes. The electrode surface was further pretreated by repeated cycling (approximately 20 cycles) in 1 M $H_2SO_4$ between 0-2200 mV. The electrode was polished again in alumina and cleaned by sonication.

#### 5.2.3.1.2. Preparation of PPy Modified Electrode

Electropolymerization of Py was conducted following a previously established procedure where the authors had investigated the optimum polymerization conditions.[16] A conventional 3-electrode system was used. 1 mL of aqueous 0.1 M KCl solution was deoxygenated for 15 minutes using high purity Ar. 7 µL of freshly distilled Py was injected into this solution contained in an electrochemical cell. A potential of 630 mV was applied. The electropolymerization was allowed to occur on the GC electrode surface in an inert atmosphere under hydrodynamic conditions to obtain a final thickness of 125 nm. For PPy films incorporating $Cl^-$ counterions, a charge of 100 mC/cm$^2$ produces a 125 nm thick film.[10]

#### 5.2.3.1.3. Preparation of PQQ Entrapped Polypyrrole Modified Electrode

The PQQ modified PPy electrode was prepared in a similar manner. 0.5 mg of PQQ was weighed carefully and suspended in 1.0 mL of 0.1 M aqueous KCl . A few

drops (~ 50 μL) of 0.1 M KOH were added to dissolve the PQQ. A pale red solution was obtained. The solution was bubbled with Ar for 15 minutes and 7 μL of freshly distilled Py was added. Electropolymerization of Py in the presence of PQQ was achieved by utilizing the same electrodeposition conditions as 5.2.3.1.2. During this process as the polymer was formed, it adsorbed onto the GC surface trapping the PQQ molecules and resulting in a catalyst entrapped conducting polymer system.

#### 5.2.3.2. Generation of SCh

SCh was generated from ASCh by the enzymatic hydrolysis by AChE. 1.5 mL (2:1 v/v phosphate buffer pH 8.0: water) of a 12.5 mM stock solution of ASCh was prepared. The solution was purged with Ar for 20 minutes, 3 μL of AChE (0.45 units) was added to it and the resultant solution was stirred under Ar for 1.5 hours to assure complete hydrolysis. The hydrolysed ASCh solution was then diluted to appropriate concentrations and used for experiments.

#### 5.2.3.3. Electrochemical Measurements at the PPy/ PQQ-PPy Modified Electrode

All electrochemical measurements were conducted under hydrodynamic conditions in an inert atmosphere using phosphate buffer solution, pH 8.0 as the electrolyte. Prior to any measurement the electrolyte solution was purged with Ar for 15 minutes. All experiments were conducted utilizing PQQ-PPy modified GC electrodes, except for control experiments where a bare or PPy modified GC electrode was used.

#### 5.2.3.3.1. Generation of Hydrodynamic Voltammogram for SCh

The optimum operational potential for the detection of SCh was evaluated. 30 µL of 12.5 mM hydrolysed ASCh solution was injected into 3.0 mL of phosphate buffer electrolyte using a gas tight syringe. The detection potential was varied between +100 to +800 mV vs Ag/AgCl. The amperometric response generated at each potential upon the addition of hydrolysed ASCh was monitored. Response at each potential was measured in triplicate at random.

#### 5.2.3.3.2. Amperometric Detection of Enzymatically Generated SCh

Amperometrc detection was conducted at 500 mV vs Ag/AgCl. 3 mL of phosphate buffer electrolyte (pH 8.0) was deoxygenated for 15 minutes. After obtaining a stable baseline 30 µL of hydrolyzed ASCh solution of appropriate concentration was added and the current generated was monitored.

#### 5.2.3.3.3. Real Time Monitoring of Enzymatic Hydrolysis of ASCh

Hydrodynamic voltammograms for real time monitoring of enzymatic hydrolysis of ASCh were generated at 500 mV. The appropriate concentration of ASCh was added in phosphate buffer pH 8.0 and the resultant mixture was stirred under an inert atmosphere. After a stable baseline was obtained 1 µL of AChE (0.15 units) was added to the resultant solution. Hydrodynamic voltammograms for blank experiments were generated under identical conditions except that the working electrode was modified by electropolymerization with Py only without any PQQ in the electrolyte.

#### 5.2.3.3.4. Detection of Carbofuran

A 20 mM standard stock solution of carbofuran was prepared in 9:1 v/v (water: ethanol) mixture. Standard ASCh solution was added to 1 mL phosphate buffer solution. After a stable baseline was obtained at 500 mV, AChE was added to the resultant solution to obtain a limiting current value. Then appropriate amount of carbofuran solution was added and the change in current was monitored as a function of time.

## 5.3. Results and Discussion

### 5.3.1. Electropolymerization of Pyrrole

Electropolymerization of Py on a GC electrode was allowed to occur coulometrically at +630 mV. The process was monitored by observing the resultant current (charge). Figure 5-5 depicts a typical amperometric response during the electropolymerization process. There was an initial sharp increase in current followed by more gradual and steady change. As the polymerization process was initiated, the oligomer being more conjugated than the monomer was more conducting which resulted in an increase in current. The initial sharp rise may be attributed partially to non-faradaic activity but the increasing conductivity of the oligomer has a substantial contribution. The polymerization process in the presence of PQQ exhibited the same amperometric behavior. In this case, the PQQ anion being present in the solution was incorporated along with PPy onto the GC conductive support like a dopant. After the polymerization process, visible changes were noticible on the GC electrode surface. A deep gray color was observed for polymerization with PPy and a reddish tint was observed when PQQ

was incorporated.

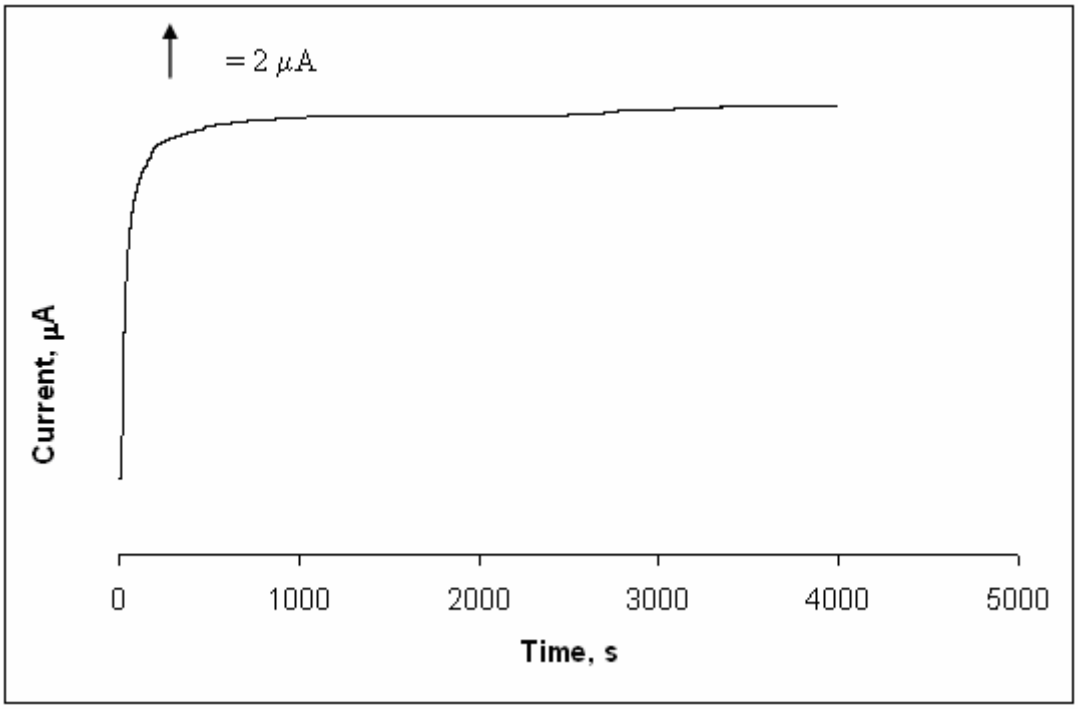


**Figure 5-5.** Real time amperometric response for electrodeposition of Py on GC surface at +630 mV vs. Ag/AgCl.

### 5.3.2. Cyclic Voltammetry

The primary basis to adopt a PQQ entrapped PPy sensor was to detect SCh catalytically by electrochemical transformation of PQQ. Hence prior to any experimentation, it was important to evaluate the electrochemical interactions of SCh with GC electrode in the absence of PQQ. Bare GC and PPy modified GC electrodes were employed for these experiments. Figure 5-6 compares the CVs of SCh at bare GC and PPy modified GC at 500 mV/s. SCh underwent slow quasireversible oxidation and reduction at an unmodified GC electrode corresponding to its oxidation to disulfide around +560 mV and reduction to SCh again at around -640 mV. The CV peaks were reduced in size, drawn out and had widely separated peak potentials. This low current

was due to the slow ET of SCh at the electrode surface. However, after modification of the electrode surface with PPy, both anodic and cathodic peaks disappeared. Hence SCh had weak electrochemical interactions with a GC electrode with large overpotential; however the PPy layer prevented the observatiob of any direct electrochemical reactions of SCh at the electrode surface.

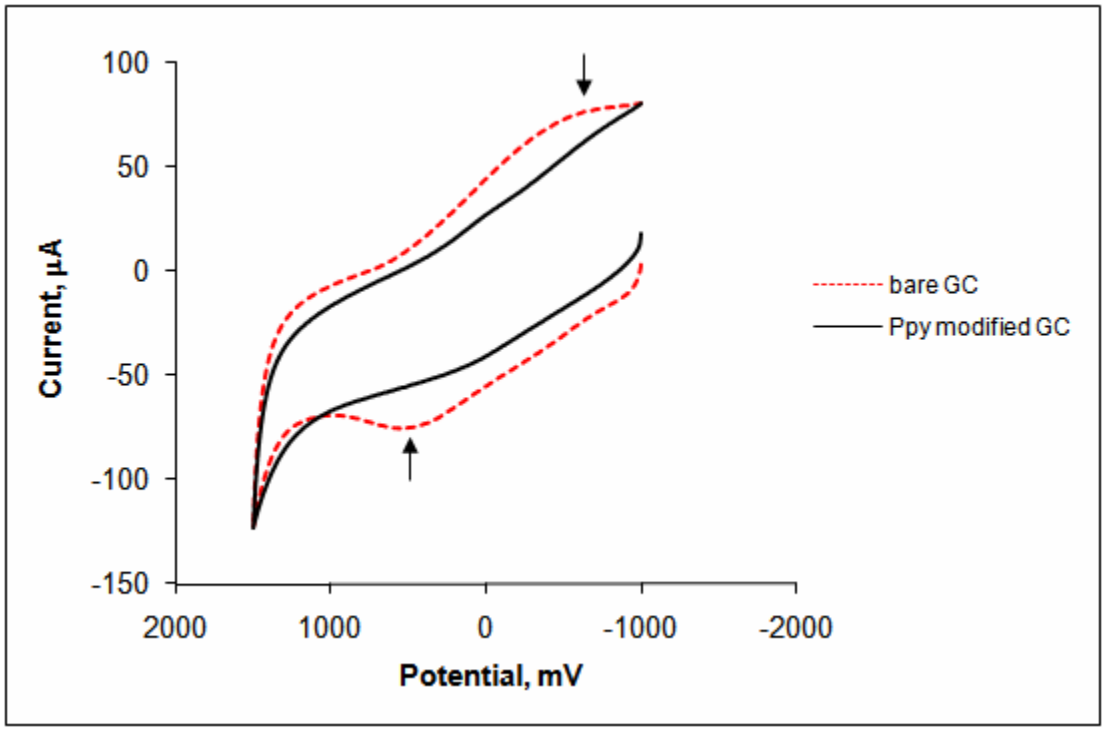


**Figure 5-6.** CVs of 0.25 mM hydrolysed ASCh solution in phosphate buffer pH 8.0 at bare and PPy modified GC electrode. Scan rate: 500 mV/s.

### 5.3.3. Hydrodynamic Voltammogram for Determination of Optimum Potential

In order to determine the optimum operational potential of the PQQ sensor, a hydrodynamic voltammogram for SCh was generated by plotting the observed current vs applied detection potential. A sigmoidal curve was obtained as depicted in Figure 5-7. The amperometric response was negligible at lower potentials, it increased sharply around +400 mV and a limiting value was obtained at +600 mV. An operational potential

of +500 mV was selected because a stable baseline with minimal noise and sufficient amperometric response was observed at this potential.

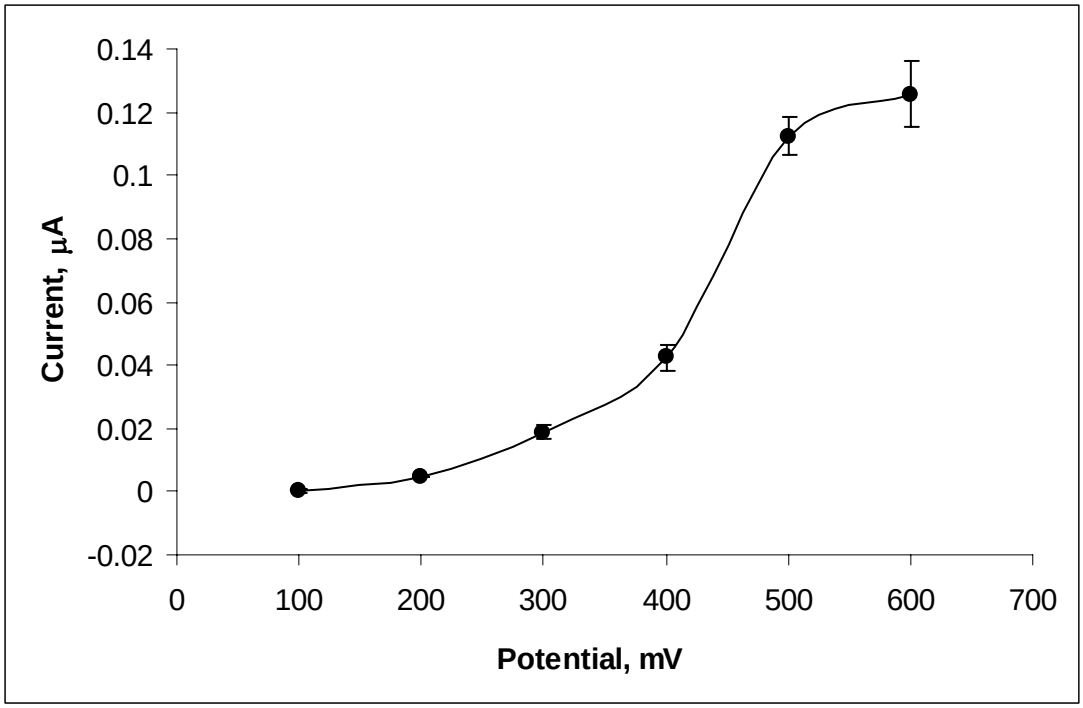


**Figure 5-7.** Hydrodynamic voltammogram for 0.125 mM hydrolysed ASCh at various potentials at a PQQ-PPy modified GC electrode. Each point is the average of three trials.

### 5.3.4. Amperometric Response of Enzymatic Product SCh

Amperometric detection of SCh was conducted at 500 mV utilizing a PQQ incorporated PPy modified GC electrode. In order to compare the detection capacity and sensitivity of the catalyst, suitable control experiments were also designed where detection of SCh was performed at a PPy modified electrode without any incorporated catalyst.

### 5.3.5. Amperometric Response of SCh at a PQQ-PPy Modified Electrode

Various concentrations of 30 µL hydrolysed ASCh were injected into 3 mL

phosphate buffer solution. At all studied concentrations the PQQ-PPy GC responded favorably and an increase in amperometric current was observed upon the injection. The response was due to current generated as a result of regeneration of PQQ at the GC surface after catalysis of the oxidation of SCh. The increase in current was proportional to the initial concentration of ASCh hydrolysed. A fast response time of 11 to 27 s was achieved for all concentrations. The sensor reached a steady state quickly at lower concentrations. Figure 5-8a-c compares the response of a PQQ-PPy sensor to several injections of various concentrations of hydrolysed ASCh. The sensor performance was more reproducible at lower concentrations.

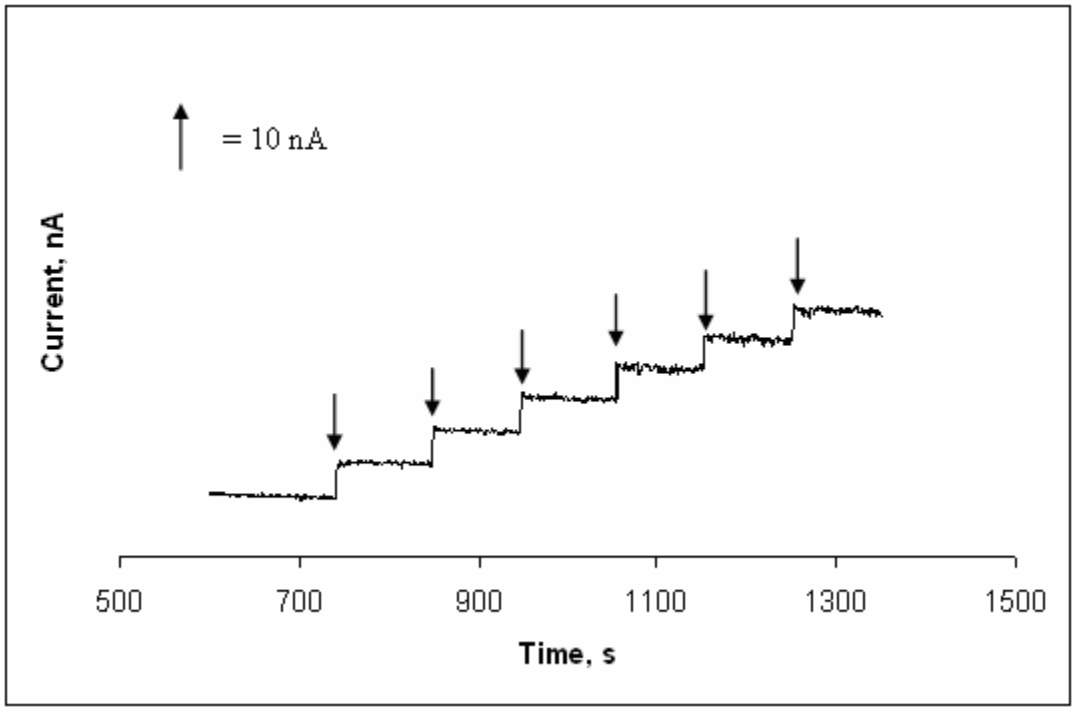


**Figure 5-8a.** Amperometric response of SCh generated after enzymatic hydrolysis of ASCh. (30 µL of hydrolyzed 0.125 mM ASCh was injected to a 3 mL phosphate buffer at pH 8.0). Arrows represent points of injection.

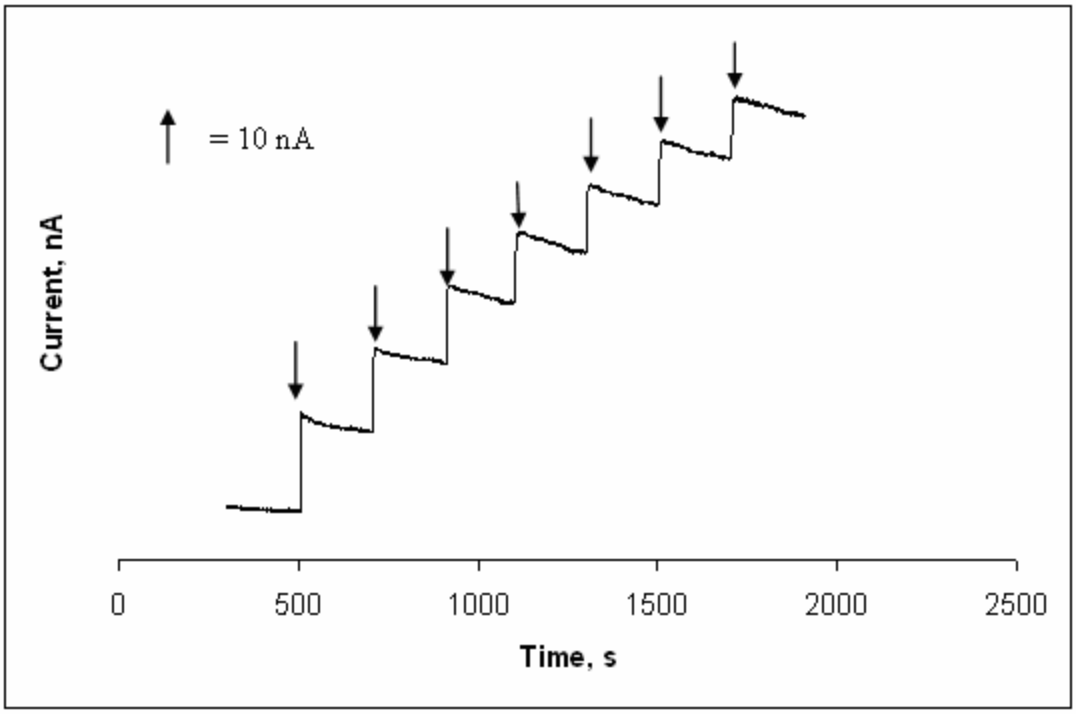


**Figure 5-8b.** Amperometric response of SCh generated after enzymatic hydrolysis of ASCh. (30 µL of hydrolyzed 1.25 mM ASCh was injected to a 3 mL phosphate buffer at pH 8.0). Arrows represent points of injection.

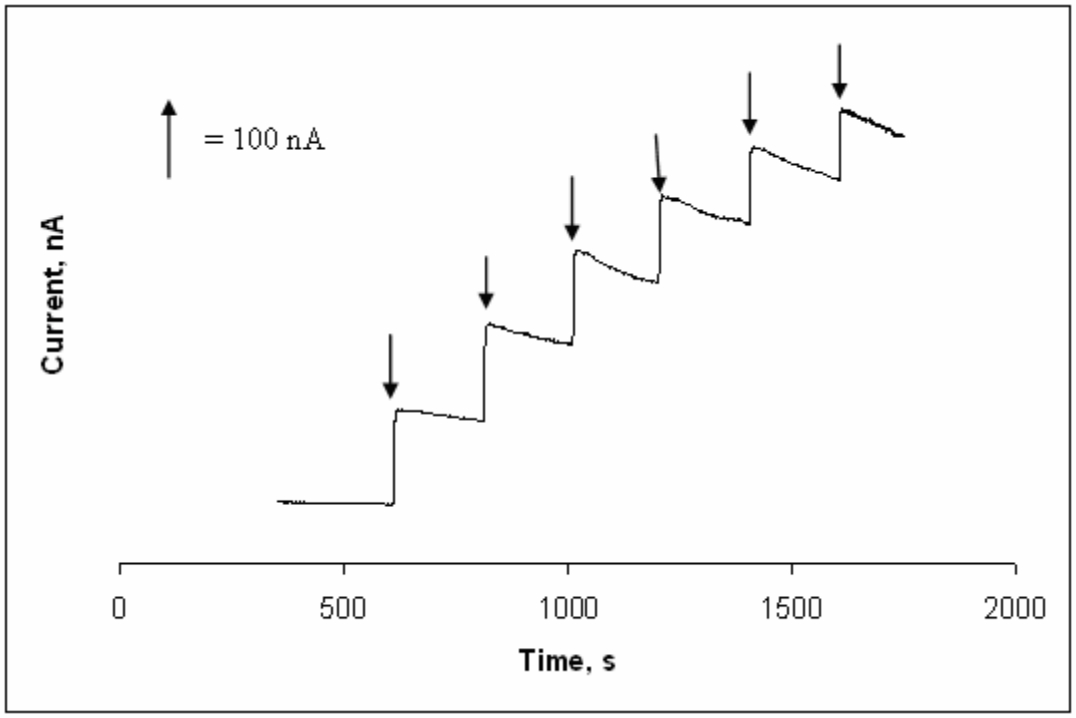


**Figure 5-8c.** Amperometric response of SCh generated after enzymatic hydrolysis of ASCh. (30 µL of hydrolyzed 12.5 mM ASCh was injected to a 3 mL phosphate buffer at pH 8.0) . Arrows represent points of injection.

**Table 5-1**. Comparison of the Temporal and Amperometric Response of a PQQ-PPy GC Electrode to Injections of Various Concentrations of Hydrolysed ASCh.

| Concentration of injected hydrolysed ASCh (mM) | Final concentration of hydrolysed ASCh in solution (μM) | Average response time before attaining limiting current (s) | Average limiting current (nA) |
|---|---|---|---|
| 12.5 | 123.8 | 22.5 ± 1.4 | 107.6 ± 14.4 |
| 1.25 | 12.38 | 27.1 ± 5.8 | 13.1 ± 2.7 |
| 0.125 | 1.238 | 11.2 ± 1.7 | 4.9 ± 0.3 |

**Table 5-2.** Comparison of the Amperometric Response of Various Concentrations of Hydrolysed ASCh as a Function of Injection Number.

| Injection number | 123.8 μM ASCh | 12.38 μM ASCh | 1.238 μM ASCh |
|---|---|---|---|
| | Limiting Current (nA) | Limiting Current (nA) | Limiting Current (nA) |
| 1 | 114 | 18.1 | 5.3 |
| 2 | 121 | 14.2 | 5.0 |
| 3 | 122 | 14.2 | 4.6 |
| 4 | 104 | 12.4 | 5.2 |
| 5 | 97 | 12.1 | 4.9 |
| 6 | 86 | 10.1 | 4.5 |

Table 5-1 compares the temporal response and average limiting current for various SCh concentrations. The amperometric response of the PQQ-PPy modified electrode was comparatively more reproducible at lower SCh concentrations. Table 5-2 compares the sensor response upon successive analyte injections. At moderate and high

SCh concentrations, a decay in amperometric response was observed with progressive injections. This decrease in signal is attributed to fouling of the electrode surface by SCh. Fouling is caused due to adsorption of thiols onto the electrode surface. The magnitude of this damage depends upon various factors such as nature of thiol group, electrode material and detection pH.[20,21] The decrease in the limiting current value was more prominent with an increase in the number of injections as the total concentration of SCh in the electrochemical solution increased. Various thiols and disulfides such as disulfiram, cysteamine and cystamine are notorious for fouling electrode surfaces.[20,21] This commonly observed phenomenon and has profound implications on sensor performance. However, this PQQ-PPy electrode system seemed suitable for monitoring lower SCh concentrations.

### 5.3.6. Amperometric Response of SCh at a PPy Modified Electrode

In order to evaluate the sensitivity of the PQQ-PPy GC sensor, the amperometric response of hydrolysed ASCh was compared at the same working potential at a PPy GC electrode. Solutions of 0.125 to 12.5 mM hydrolysed ASCh were employed for such studies. 30 μL of respective concentrations of hydrolysed ASCh were injected and the change in current was monitored. Figure 5-9a-b depicts the amperometric response at the control electrode. The PPy GC electrode exhibited no visible amperometric response upon injection of 0.125 and 1.25 mM hydrolysed ASCh. However, at a higher analyte concentration of 12.5 mM, a detectable change in current was observed upon every injection. The average current was 30.2 ± 6.9 nA. This response was almost 4 times smaller than at a catalyst modified electrode.

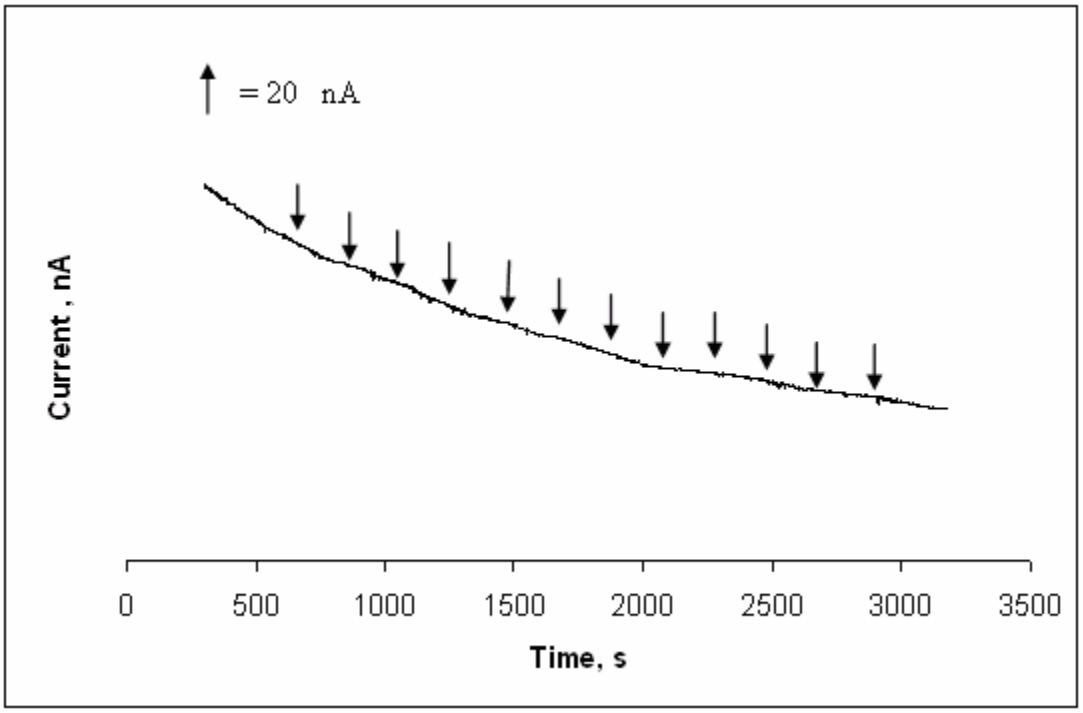


**Figure 5-9a.** Amperometric response of SCh generated after hydrolysis of ASCh by AChE at a PPy modified GC electrode. (30 µL of hydrolysed 1.25 mM ASCh was injected to 3.0 mL phosphate buffer of pH 8.0). Arrows represent points of injection.

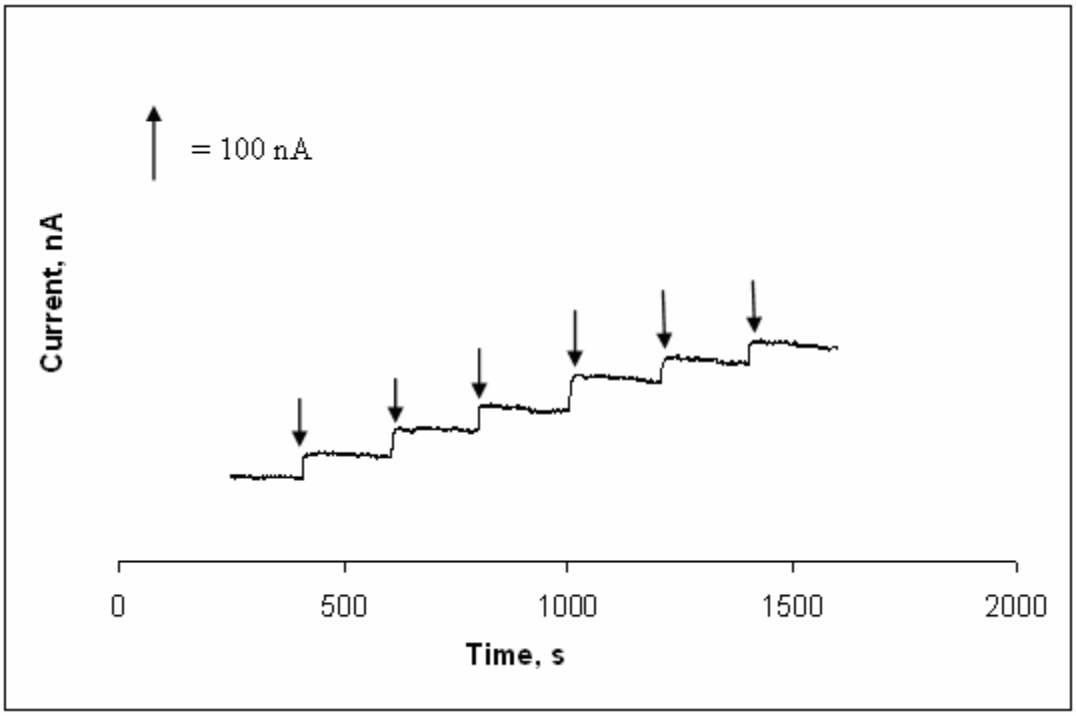


**Figure 5-9b.** Amperometric response of SCh generated after hydrolysis of ASCh by AChE at a PPy modified GC electrode. (30 µL of hydrolysed 12.5 mM ASCh was injected to 3.0 mL phosphate buffer of pH 8.0). Arrows represent points of injection.

In the presence of PQQ, the oxidation of SCh occurred efficiently and electrochemical changes even at low concentrations were observed. In the absence of PQQ, amperometric response was observed only at high analyte concentrations due to the slow, direct uncatalysed oxidation of SCh to disulfide at the electrode surface. However, this reaction being electrochemically sluggish, the amperometric response was much smaller. Hence incorporation of a quinone redox catalyst at a GC surface, greatly improved the sensitivity for detection of SCh.

### 5.3.7. Real Time Monitoring of Enzymatic Hydrolysis at the PQQ-PPy Electrode

The catalytic activity of AChE and PQQ was further exploited to observe real time amperometric changes from catalytic generation and oxidation of SCh in situ. Figures 5-10a-b represents the various chronoamperograms generated.

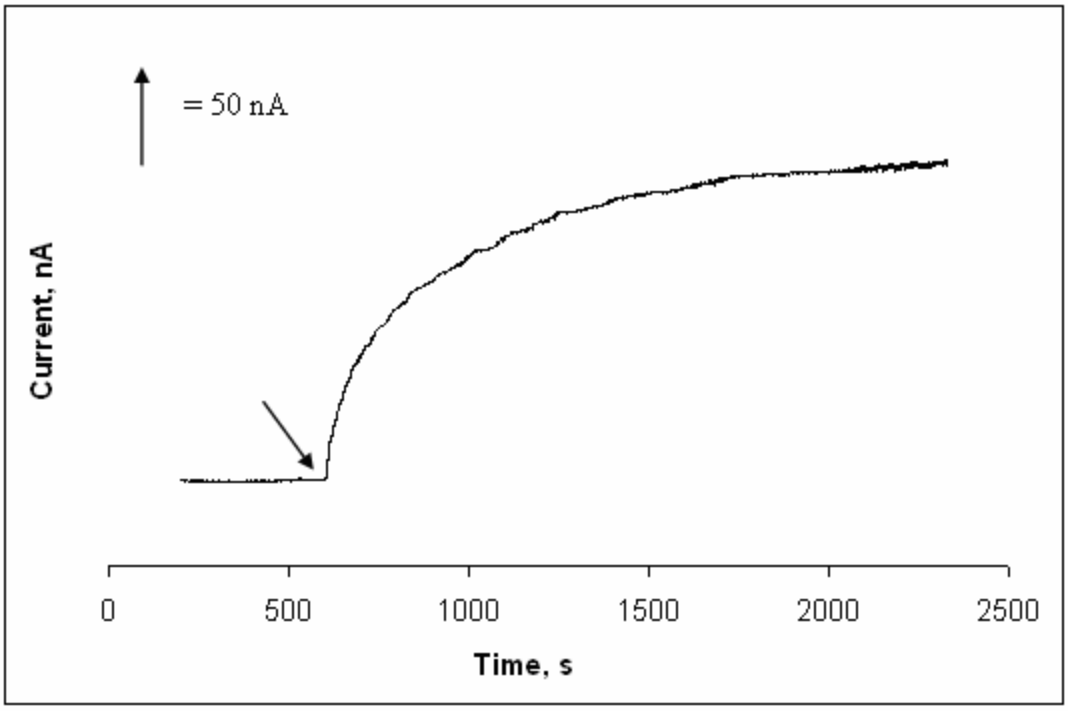


**Figure 5-10a.** Hydrodynamic chronoamperogram at a PQQ-PPy-modified GC electrode upon the addition of 1 µL of AChE to a solution containing 1.25 mM ASCh in 3000 µL of phosphate buffer solution. Arrow indicates point of injection of AChE.

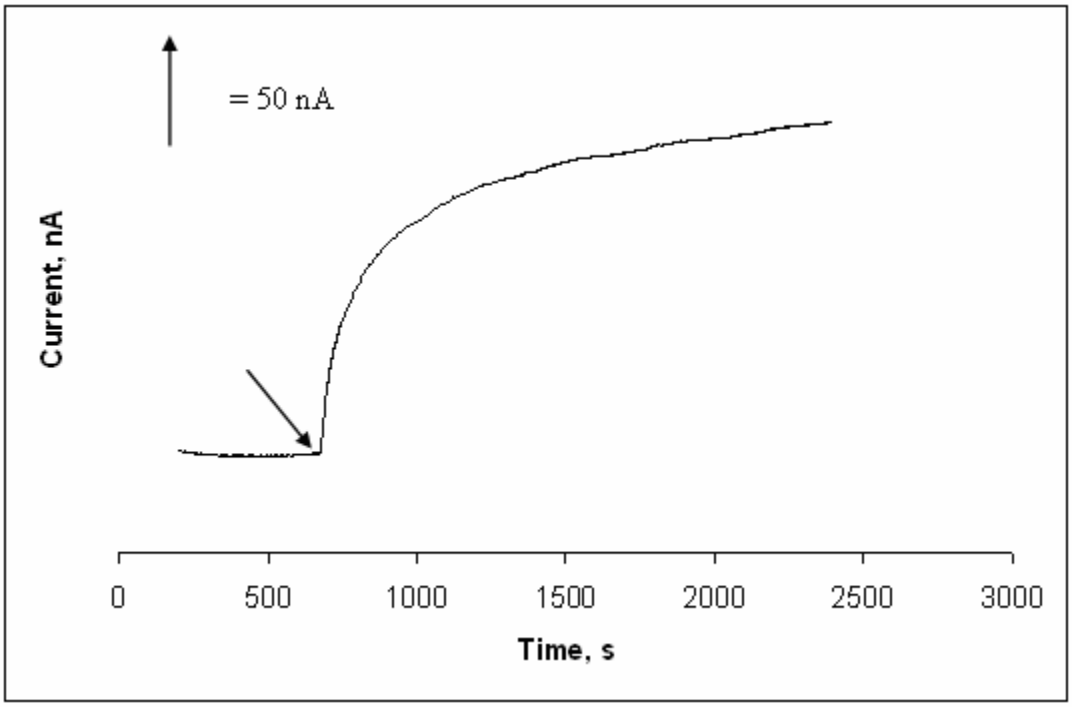


**Figure 5-10b**. Hydrodynamic chronoamperogram at a PQQ-PPy-modified GC electrode upon the addition of 1 μL of AChE to a solution containing 2.89 mM of ASCh in 1300 μL of phosphate buffer solution. Arrow indicates point of injection of AChE.

An immediate change in current was observed after the addition of AChE into the electrolyte solution containing ASCh. The addition of AChE caused rapid enzymatic hydrolysis of ASCh to SCh. SCh generated in situ was consequently oxidized to disulfide by PQQ which was further generated at the electrode. The current reached a maximum limiting value. The fast enzyme kinetics of AChE coupled with the catalytic power of PQQ enabled real time detection of SCh generated in situ. This observation emphasizes the fact that this amperometric detection method can not only form a basis for detection of thiols, but also can be developed into a potential assay for evaluating the enzymatic activity of AChE.

A steady state current of 158 nA was obtained for both chronoamperograms,

however the initial increase in current was much steeper for 5-10b that contained a higher concentration of ASCh. The same value of steady state current indicates saturation of either or both the catalysts.

### 5.3.8. Real Time Monitoring of Enzymatic Hydrolysis at PPy GC Electrode

Suitable control experiments were conducted to further emphasize the catalytic activity of PQQ and the sensitivity of the developed method. For these experiments, GC working electrodes were prepared without the entrapped catalyst. Real time amperometric measurements were conducted under identical conditions.

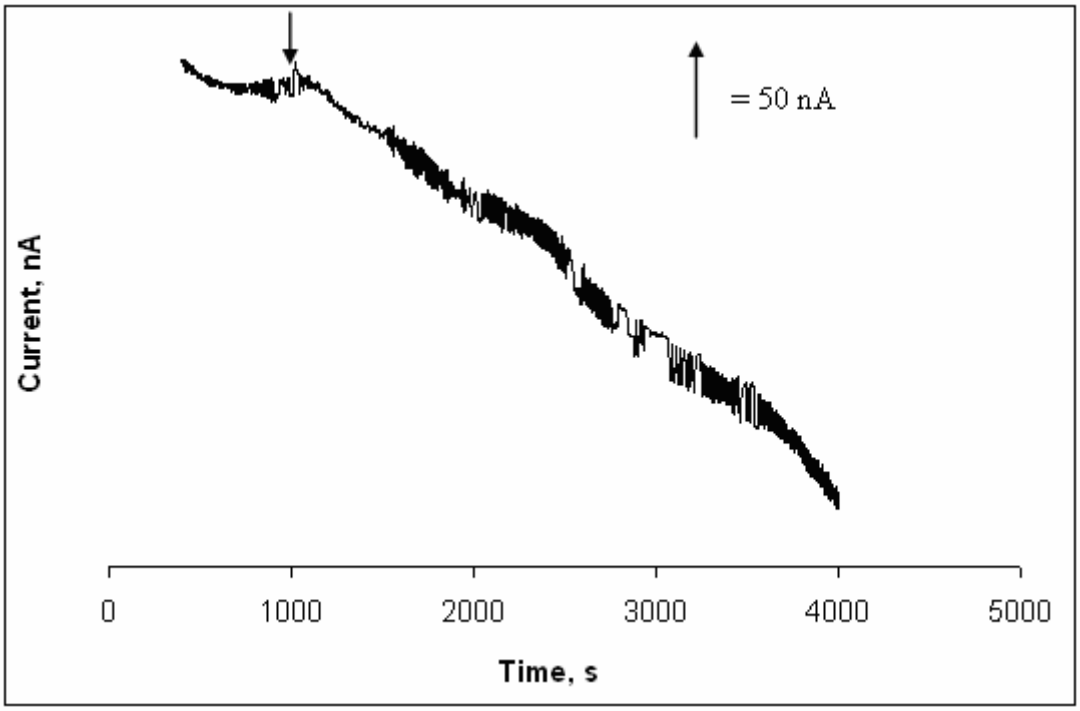


**Figure 5-11a.** Hydrodynamic chronoamperogram at a PPy-modified GC electrode upon the addition of 1 µL of AChE to a solution containing 1.25 mM ASCh in 3000 µL of phosphate buffer solution. Arrow indicates point of injection of AChE.

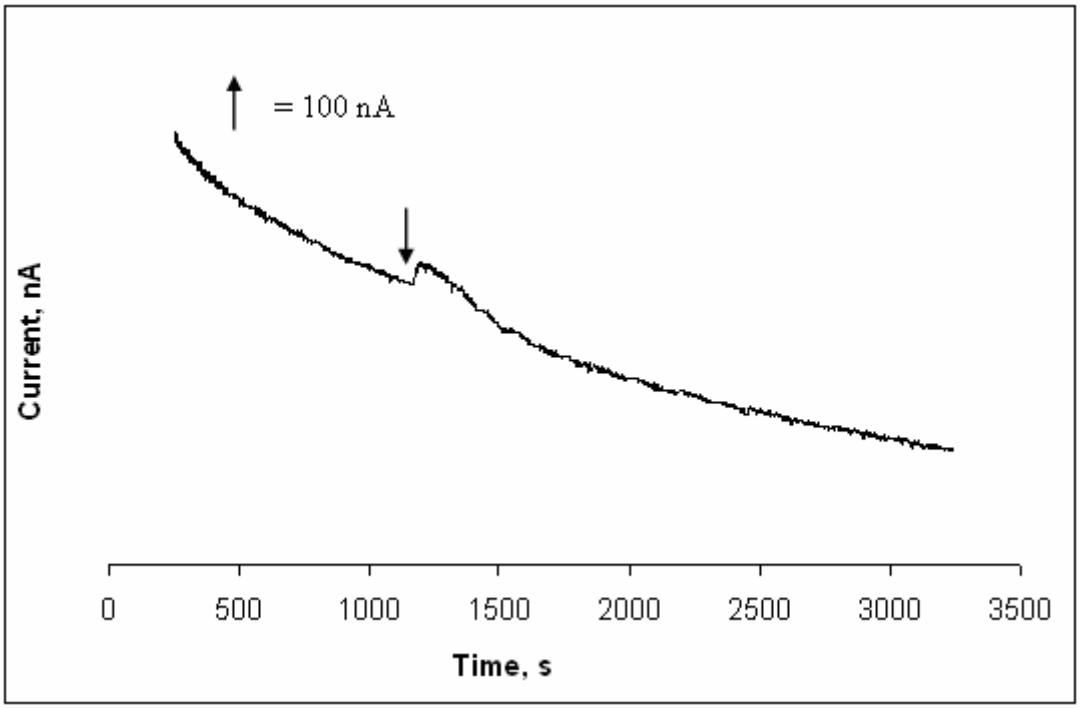


**Figure 5-11b.** Hydrodynamic chronoamperogram at a PPy-modified GC electrode upon the addition of 1 µL of AChE to a solution containing 2.89 mM of ASCh in 1300 µL of phosphate buffer solution. Arrow indicates point of injection of AChE.

Hydrodynamic chronoamperograms generated for SCh in the absence of PQQ showed no observable current change for a solution containing 1.25 mM ASCh (Figure 5-11a). A small limiting current of 18.4 nA was observed upon injection of AChE to 2.89 mM of ASCh solution (Figure 5-11b). This current generated was almost 9 times smaller in magnitude compared to the corresponding PQQ-PPy electrode. The rate of generation of SCh was the same in the absence of PQQ; however the current generated in this case was solely due to the direct oxidation of SCh at the GC surface emphasizing the slow electrochemical oxidation process of SCh in the absence of catalyst.

### 5.3.9. Effect of Addition of Cabofuran

As mentioned before, AChE belongs to class B esterase and is inhibited by organic pesticides such as organophosphates and carbamates.[22] Carbofuran is an N-Me

carbamate insecticide that inhibits AChE reversibly. The versatility of the PQQ-PPy-GC sensor was further exploited by evaluating its ability to detect carbofuran in real time. For these experiments, initially 1 µL of AChE was employed. However, the inhibitory effect of carbofuran was difficult to monitor because the resultant concentration of AChE in the solution was too low. Hence higher volumes of AChE were injected for further studies. After a steady current was obtained, carbofuran solution was added into the phosphate buffer electrolyte containing AChE. Addition of carbofuran caused inhibition of AChE activity resulting in decrease in limiting current. The drop in current was dependent upon the initial concentration of AChE present in solution for the same concentration of carbofuran. Figures 5-12a-b represents the amperometric response of the various events occurring as a result of addition of AChE and carbofuran.

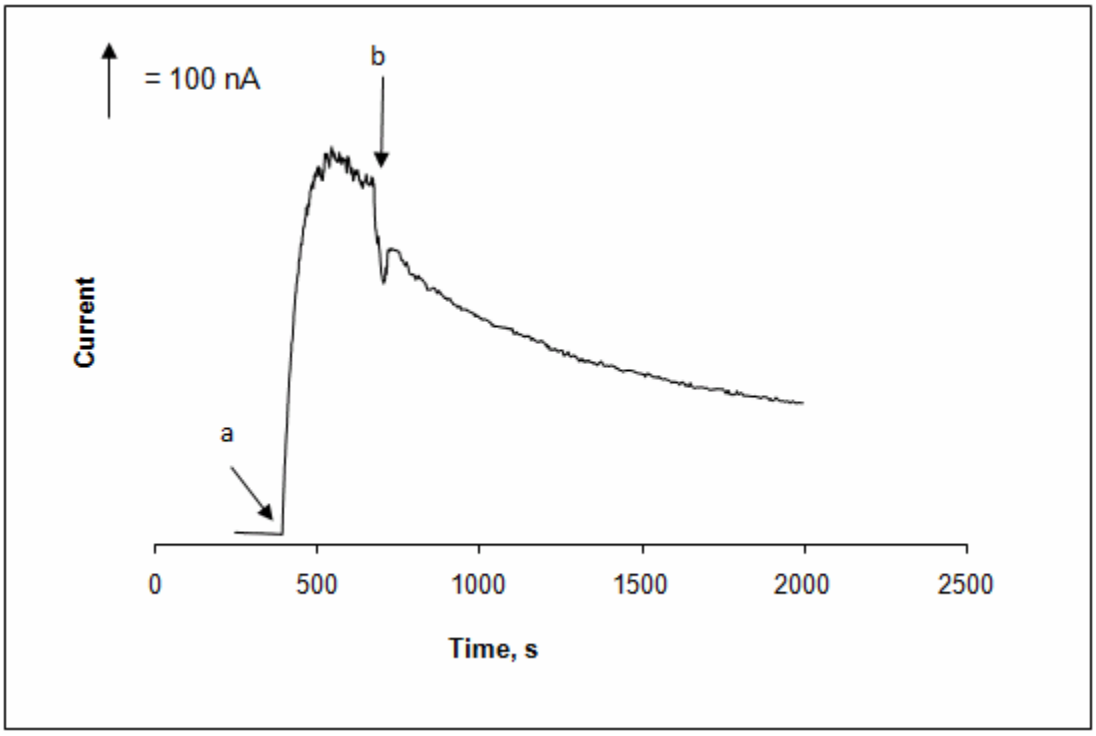


**Figure 5-12a.** Amperometric response of PQQ/PPy electrode containing 0.245 mM ASCh in 1020 µL of phosphate buffer solution. (a) after the injection of 5 µL (0.75 units) of AChE; (b) after injection of 50 µL of 20 mM carbofuran. Arrows indicate points of injection of AChE and carbofuran respectively.

Figure 5-12a indicates a remarkable rise in current upon addition of 5 µL (0.75 units) of AChE. A limiting current of 360 nA was obtained. The steady state current decreased by 15 nA due to the fouling activity of generated SCh. Upon the addition of carbofuran, a small sharp decrease in current of 97 nA was observed corresponding to 28.12% inhibition. This drop in current was due to a decrease in the rate of generation of SCh as a result of inhibition of AChE by carbofuran. With time, progressive decay in current was observed that may be attributed to both inhibition of esterase activity by carbofuran as well as surface passivation of the electrode as a result of fouling by SCh generated in situ.

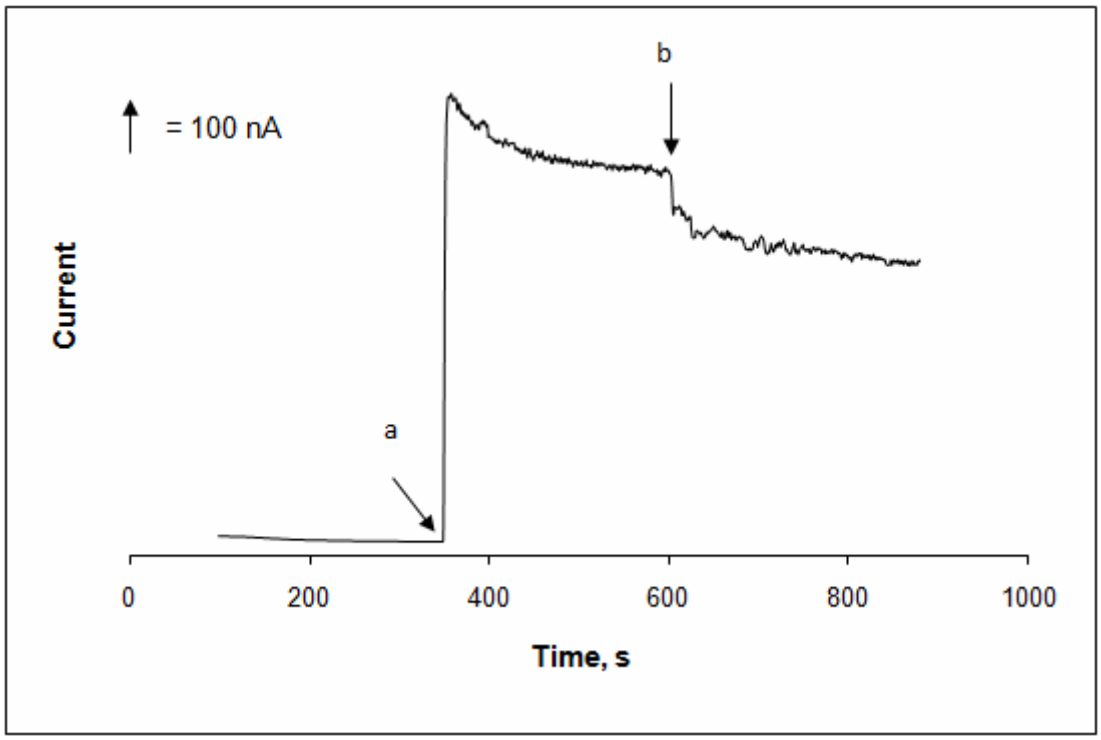


**Figure 5-12b.** Amperometric response of PQQ/PPy electrode containing 0.245 mM ASCh in 1020 µL of phosphate buffer solution. (a) after the injection of 15 µL (2.25 units) of AChE; (b) after injection of 50 µL of 20 mM carbofuran. Arrows indicate points of injection of AChE and carbofuran respectively.

Figure 5-12b indicates the response of the amperometric sensor in presence of 15

μL (2.25 units) of AChE. As a higher concentration of enzyme was used, the limiting current obtained was even higher corresponding to a value of 555 nA. In this case the steady state current decreased by 128 nA as a result of more pronounced passivation by SCh. Carbofuran was injected into the solution after allowing the current to decay for a sufficient time interval. Injection of this AChE inhibitor caused a sharp decrease in current of 95 nA magnitude corresponding to 22.24% inhibition.

Hence, the degree of inhibition by carbofuran depended on the initial amount of enzyme (AChE) present. Further studies also indicated that for same concentration of AChE, the degree of inhibition was directly related to the concentration of carbofuran injected. It is pertinent to mention that because the enzyme (AChE) is present in extremely low concentration in solution, direct quantitative evaluation of inhibition activity is challenging in this case as compared to SCh sensors with AChE immobilized (hence preconcentrated) onto the electrode surface. Another interesting fact is that the sensitivity of the assay would also depend upon the appropriate cholinesterase used. As an example it was determined that inhibitory effect of organophosphates (OP) towards *Drosophila melanogaster* AChE was most prominent.[19] A better detection limit for OP pesticides was obtained with *Drosophila melanogaster* AChE as compared with AChE derived from *Electropharus electricus*. However, in the practical world the choice is restricted to the availability of such enzymes from the manufacturers.

### 5.4. Conclusions

An amperometric method was developed for the detection of SCh by coupling a fast enzymatic hydrolysis process with a sensitive electrochemical detection scheme utilizing

a PQQ-PPy modified GC electrode. Well defined current peaks proportional to the concentration of hydrolysed ASCh were obtained for various concentrations. The sensitivity of the assay allowed real time detection of SCh, the electroactive enzymatic product of AChE. In addition to real time monitoring of ASCh hydrolysis, the inhibition of this hydrolysis process was also observed by addition of carbofuran, a carbamate pesticide. The limiting current obtained for real time ASCh hydrolysis was dependent upon the concentration of ASCh and AChE.

The developed method had various distinct advantages. Incorporation of PQQ catalyst allowed more sensitive detection of SCh at a GC electrode. A common problem of leaching of enzymes from an electrode surface was averted as AChE was not immobilized to the sensor surface. The detection scheme was proven to be very versatile as it achieved sensitive detection of both SCh and ASCh. It could also be used to monitor the enzymatic activity of AChE and presence of a carbamate pesticide. Hence, if developed further, the PQQ based sensor could act as a platform for estimation of AChE activity and detection of organophosphate and organocarbamate pesticides.

## 5.5. References


1. Šinko, G.; Čalić, M.; Bosak, A.; Kovarik, Z. Limitation of the Ellman Method: Cholinesterase Activity Measurement in the Presence of Oximes. *Anal. Biochem.* **2007**, *370*, 223–227.

2. Jiri, B. Organophosphates/Nerve Agent Poisoning: Mechanism of Action, Diagnosis, Prophylaxis and Treatment. *Adv. Clin. Chem.* **2004**, *38*, 151-216.

3. Akira, N.; Manami, N. Simple Detection of Organophosphates in Biological Materials. *Jpn. J. Tox.* **2008**, *21*, 141-143.

4. Li, X; Xie, Z; Min, H; Xian, Y; Jin, L. Amperometric Biosensor Based on Immobilization Acetylcholinesterase on Manganese Porphyrin Nanoparticles for Detection of Trichlorfon with Flow-Injection Analysis System. *Electroanalysis*, **2007**, *19*, 2251-2257.

5. Long, Y.; Zhang, Y.; Honglan, Q.; Zhang, C. Organophosphorous Electrochemical Biosensors Based on Incorporation of Acetylcholinesterase on Gold Nanoparticles. *Yaowo Fenxi Zazhi*, **2006**, *26*, 1702-1705.

6. Liu, G.; Riechers, S.L.; Mellen, M. C.; Lin, Y. Sensitive Electrochemical Detection of Enzymatically Generated Thiocholine at Carbon Nanotube Modified Glassy Carbon Electrode. *Electrochem. Comm*. **2005**, *7*, 1163–1169.

7. Hauge, J.G. Glucose Dehydrogenase of Bacterium Anitratum: An Enzyme with a Novel Prosthetic Group. *J. Biol. Chem*. **1964,** *239,* 3630-3639.

8. Shinohara, H.; Khan, G. F.; Ikariyama, Y.; Aizawa, M. Electrochemical Oxidation and Reduction of PQQ Using a Conducting Polypyrrole-coated Electrode. *J. Electroanal. Chem.* **1991**, *304,* 75-84.

9. Kano, K.; Mori, K.; Uno, B.; Kubota, T.; Ikeda, T.; Senda, M. Voltammetric and Spectroscopic Studies of Pyrroloquinoline Quinone Coenzyme Under Neutral and Basic Conditions. *J. Electroanal. Chem.* **1990,** *23,* 227-238.

10. Kano, K.; Mori, K.; Uno, B.; Kubota, T.; Ikeda, T.; Senda, M. Voltammetric Determination of Acid Dissociation Constants of Pyrroloquinoline Quinone and its Reduced Form Under Acidic Conditions. *J. Electroanal. Chem.* **1990**, *24*, 193-201.

11. Sadki, S.; Schottland, P.; Brodie, N. Sabouraud, G. The Mechanisms of Pyrrole Electropolymerization. *Chem. Soc. Rev*. **2000,** *29*, 283-293.

12. Genies, E. M.; Bidan, G.; Diaz, A. F. Spectroelectrochemical Study of Polypyrrole Films. *J. Electroanal. Chem.* **1983**, *149*, 101-113.

13. Kim, K. J.; Song, H. S.; Kim, J. D.; Chon, J. K. Mechanism of Electropolymerization of Pyrrole in Acidic Aqueous Solutions. *Bull. Korean Chem. Soc.* **1988**, *9*, 248-251.

14. Asavapiriyanout, S.; Chandler, G. K.; Gunawardena, G. A.; Pletcher, D. J. The Electrodeposition of Polypyrrole Films from Aqueous Solutions. *Electroanal. Chem.* **1984,** *177,* 229-244.

15. Baker, C. K.; Reynolds, J. R. A Quartz Microbalance Study of the Electrosynthesis of Polypyrrole. *J. Electroanal. Chem.* **1988***, 25*, 307-322.

16. Inoue, T.; Kirchhoff, J. R. Electrochemical Detection of Thiols with a Coenzyme Pyrroloquinoline Quinone Modified Electrode. *Anal Chem.* **2000**, *72*, 5755-5760.

17. Lin, Y; Lu, F; Wang, J Disposable Carbon Nanotube Modified Screen-Printed Biosensor for Amperometric Detection of Organophosphorus Pesticides and Nerve Agents. *Electroanalysis*, **2004**, *16,* 145-149.

18. Joshi, K.; Tang, J.; Haddon, R.; Wang, J.; Chen, W.; Mulchandani, A. A Dual Amperometric/Potentioametric FIA-Based Biosensor for the Distinctive Detection of Organophosphoros Pesticides. *Electroanalysis* **2005**, *17*, 54-58.

19. Liu, G.; Lin, Y. Biosensor Based on Self-Assembling Acetylcholinesterase on Carbon Nanotubes for Flow Injection /Amperometric Detection of Organophosphate Pesticides and Nerve Agents. *Anal. Chem.* **2006,** *78*, 835-843.

20. Mairesse-Ducarmois, C. A.; Patriarche, G. J.; Vandenbalck, J. L. Contribution to the Electrochemistry of Thiols and Disulfides. Part IV. A.C., D.C., and Differential Pulse Polarography and Cyclic Voltammetry of Disulfiram. *Anal. Chim. Acta,* **1976**, *84*, 47-52.

21. Mairesse-Ducarmois, C. A.; Vandenbalck, J. L.; Patriarche, G. J. Contribution to the Electrochemistry of Thiols and Disulfides. Part VI. A.C., D.C., and Differential Pulse Polarography of Cysteamine and Cystamine. *Anal. Chim. Acta*, **1977**, *90*, 103-110.

22. Tõngu, V. Acetylcholinesterase: Mechanism of Catalysis and Inhibition. *Curr. Med. Chem.* **2001**, *1,* 155-170.

# Chapter 6

# General Conclusions

## 6.1. General Conclusions

The focus of this work has been to develop analytical strategies for selective and sensitive detection of cholinergic molecules. A sensitive analytical method coupling CE separations with EC was applied to monitor subtle changes in the concentration of cholinergic molecules.

CE-EC was used to study transport kinetics of the CHT protein in mouse synaptosome samples. The assay was further extended to evaluate the inhibitory effect of a cholinomimetic compound, DTH, on Ch transport by CHT. Comparison of the inhibitory effects of DTH with other structurally close inhibitor molecules assayed using the same method revealed that a quaternary nitrogen atom coupled with neighboring hydroxyl groups is a prerequisite for strong interactions with CHT transporter. Kinetic studies also emphasized the significance of a long alkyl chain for more potent inhibitory effect, indicating possibility of hydrophobic interactions of inhibitors with CHT.

CE-EC methods for cholinergic analysis were further extended to develop two tricatalytic microelectrode enzyme sensors for CE. These sensors were comprised of the cholinergic enzymes AChE and ChO incorporated with the natural peroxidase enzyme (HRP) and the artificial peroxidase catalyst (PB) respectively. The general motive for venturing into more complicated systems was to be able to use a lower detection potential. A low detection potential is essential for reduction of interference signal from other easily oxidizable biological species such as ascorbic acid, uric acid, catechols and dopamine which are common constituents of biological matrices.[1] Another goal was to attain sensitivity and detection levels suitable for monitoring endogeneous concentrations of Ch and ACh.

The PB-AChE-ChO ME sensor allowed the use of a low operational potential of -100 mV vs. Ag/AgCl while a detection potential of + 100 mV was employed for the HRP-Os-AChE-ChO Au ME. Both electrode systems were operated at much lower potentials compared to the bienzyme system (operated at + 650 mV vs. Ag/AgCl), which was comprised of only AChE and ChO due to the transduction of $H_2O_2$ reduction by the peroxidase catalysts as opposed to uncatalysed oxidation of $H_2O_2$ at a Pt ME with the AChE-ChO sensor. Efficient separation of Ch, ACh and BuCh with a linear range extending upto three orders of magnitude was obtained for both HRP-Os-AChE-ChO and PB-AChE-ChO MEs. However, the peak current response for the PB-AChE-ChO system was comparatively broader which may be attributed to slower catalytic conversion of $H_2O_2$ by PB. The HRP-Os-AChE-ChO electrode exhibited maximum sensitivity to Ch and ACh injection because the HRP-Os redox hydrogel was characterized by very high current densities due to fast mediated ET pathways. So a remarkable detection limit of 38 amol was obtained for Ch and ACh. The detection limits for ACh by PB-AChE-ChO and AChE-ChO were comparable and were three orders of magnitude higher than that obtained from the trienzyme system. Both HRP-Os-AChE-ChO and PB-AChE-ChO MEs exhibited good performance when operated under hydrodynamic conditions, however the PB-AChE-ChO system was comparatively less stable because of the thermodynamic instability of PB in neutral and basic pH conditions.[2] In general, the mode of operation and ease of fabrication was most feasible with the bienzyme system which also exhibited sufficient sensitivity for monitoring endogeneous Ch concentrations.[3] Immobilization techniques for the trienzyme system was most challenging as it was critical to maintain the bioactivity of all three enzyme as well as the catalytic effectiveness of the highly

sensitive redox hydrogel polymer, but this sensor seemed most promising for monitoring very low concentrations of the neurotransmitters.

Furthermore a thiol specific sensor developed by Inoue et al.[4] was employed for detection of SCh, an important biomarker. The sensor system which comprised of PQQ catalyst entrapped within a polymeric matrix had exhibited excellent sensitivity towards the detection of biologically important thiols such as cysteine and glutathione.[4] The detection scheme allowed real time monitoring of enzymatic hydrolysis of ASCh by AChE and detection of carbofuran by inhibition of the hydrolysis process. The advantage of this assay was that AChE was not bound to the sensing electrode surface, hence the stability and lifetime of the sensor was independent of fouling or leaching of enzyme. The sensor design scheme also opened the possibility of monitoring irreversible AChE inhibitors such as organophosphates and nerve agents, as regeneration of the enzyme was not required in this independent functioning module.

Detection of various biologically important thiols such as cysteine and mercaptoethanol are also been pursued using self assembled electrocatalytic molecular wires.

## 6.2. References

1. Ali, S. R; Parajuli, R. R.; Ma, Y.; Balogun, Y.; He, H. Interference of Ascorbic Acid in the Sensitive Detection of Dopamine by a Nonoxidative Sensing Approach. *J. Phys. Chem. B,* **2007,** *42,* 12275 -12281.

2. Karyakin, A. A.; Karyakina, E.E. Electroanalytical Applications of Prussian Blue and its Analogs. *Russ. Chem. Bull. ,* **2001,** *50,* 1811-1817.

3. Barkhimer, T. New Methods for Evaluating Cholinergic Toxicity. *Ph.D. Thesis,* **2004**, 1-138.

4. Inoue, T.; Kirchhoff, J. R. Electrochemical Detection of Thiols with a Coenzyme Pyrroloquinoline Quinone Modified Electrode. *Anal Chem.* **2000**, *72*, 5755-5760.